MODEL SCALE EXPERIMENT AND FULL-SCALE NUMERICAL SIMULATIONS OF GEOTHERMAL PILES FOR COOLING DOMINATED CLIMATE

A Dissertation

by

MOHAMMADREZA KESHAVARZ

Submitted to the Office of Graduate and Professional Studies of
Texas A&M University
in partial fulfillment of the requirements for the degree of

DOCTOR OF PHILOSOPHY

Chair of Committee,	Jean-Louis Briaud
Committee Members,	Marcelo Sanchez
	Charles Aubeny
	Charles Culp
Head of Department,	Robin Autenrieth

December 2018

Major Subject: Civil Engineering

ABSTRACT

The objective of this research is to investigate the soil behavior surrounding a typical full-scale pile foundation of a large building under cyclic thermal loading from the application of geothermal foundation technology in a high plastic clay with shrink-swell problems. The current state of knowledge on the application of energy foundations has been challenged by potential users in the U.S.; specifically, in the southern regions with the high demand of cooling loads for their buildings. The key outcome of this study should provide preliminary answers to the uncertainties about the implementation of a full-scale geothermal foundation system.

The focus will be on the effect of geothermal foundation on soil behavior including short and long-term foundation movement, distortion, and soil thermal pollution. First, the research background including current published literatures in the form of journal papers, manuals, and government issued guidelines and incentives are presented.

Then, the performance of the modified full-scale geothermal pile under the Liberal Arts and Humanities (LAAH) building at the Texas A&M University campus, College Station, Texas, is analyzed. Findings of the LAAH building's system showed the propagation of thermal flux from the energy pile to the surrounding soil mass.

The third step discusses the design and execution of a model-scale laboratory test. This test includes running long-term mechanical and cyclic thermal loading on a compacted native clay soil. Extensive long-term creep (i.e. over 24 hrs.), shrink-swell, and heat propagation testing was done. The water content sampling results showed that cyclic thermal loading will not have major effect on the shrink-swell concern within the soil. Creep movement results showed that the "n" value is increased by heating process compared to the mechanical loading only. The cooling cycle poses a lesser threat in changing the "n" value comparing to the heating.

The fourth step includes numerical simulation work by using one of the most common numerical simulation software in Geotechnical Engineering, FLAC3D v.6.0. First, the mechanical model calibration for FLAC3D was done by the load tests performed by Briaud (1999). Then, series of sensitivity analysis was performed to design the proper numerical structure script for the more complicated and complex problems. After the sensitivity analysis part, the thermal, fluid, and mechanical modules were calibrated coupled with the data published by Akrouch et al. (2014).

Then, the hypothetical study on a typical $30 \times 30m$ foundation footprint with various affecting parameters was done. We called this part "design recommendation" study. This aimed to propose some preliminary design guidelines for the engineers who deal with the challenges of designing a thermo-active foundation under a super structure. According to the findings, the thermal pollution of a full-scale geothermal pile system is affected mainly by pile spacing. Pile length found to be the factor with most impact on the productivity level of the system toward meeting the thermal load demand. Additionally, it was found that a gap between the surface of the load bearing soil and structural slab prevents development of large tension loads in the piles.

As a test to our findings in the design recommendation part, the LAAH building was used as a case history to demonstrate its performance and pile-foundation behavior for a two-year cyclic operation of full-scale geothermal foundation system. Finally, for the economic analysis work, several operational guidelines were recommended based on the findings in the numerical simulation section and existing literatures.

DEDICATION

I'd like to dedicate this work to my mom (Akram), dad (Majid), and two beautiful sisters (Shohreh and Shiva), my aunt (khale Mina), and my uncles (Dae Akbar and Amoo Sadegh), who's their endless love and support pushed me through the tough journey of my PhD in U.S.

ACKNOWLEDGMENTS

Throughout the course of this research work, I've been absolutely blessed to work with the greatest mentor and advisor in Geotechnical Engineering field, Prof. Jean-Louis Briaud. I've learnt not only technical side of my major, but also great life lessons such as toughness, resilience, patience, and staying focused on my goals from Prof. Briaud. Without him this journey would not be possible for one single day. For all the greatness you taught me Prof. Briaud, I will be forever thankful.

I'd like to extend my great appreciation to a person who changed me and helped me shaping my research work, Augusto Lucarelli. I would not have been able to finish my PhD research without Augusto Lucarelli and his endless support regardless of time and his super busy work schedule. He dedicated his time and outstanding knowledge to me for more than 2 years, almost every day. He worked with me to teach me and help preparing one of the most complicated numerical simulation models ever assembled in Geotechnical Engineering field in the capacity of a PhD student. His dedication above and beyond what was asked for left me with only one message in my life, which is to be helpful and humble. I can't say thank you enough to you my friend. I'd like to also thank Itasca Consulting Group Inc. for providing the access to FLAC3D for free during my PhD work.

I'd like to greatly appreciate and thank the Texas A&M Transportation Institute (TTI) team at RELLIS campus for providing me unlimited time, resources, and support to conduct my experiment. I'd like to thank specifically Matt Robinson, Ken Reeves, and Gary Gerke for their support and help.

I'd like to greatly thank my dear committee member, Dr. Marcelo Sanchez. He is not only a great example to look up, but also a great friend who has been supportive of my work in

any way he could. I'd like to thank Prof. Charles Culp and Charles Aubeny for serving on my advisory committee and giving me helpful advice during my preliminary defense.

Finally, I'd like to extend my appreciation to my dear friend Sahar Eshghjoo who supported me through all the tough times. Also, I'd like to thank Mohsen Mahdavi, Pooyan Razi, Anahita Goudarzi, Mohammad Mahdavi, Bahman Torkamandi, and Soheil Sohrabi for their support toward me.

CONTRIBUTORS AND FUNDING SOURCES

Contributors

This work was supported by a dissertation committee consisting of Professor Jean-Louis Briaud [advisor - chair], Professor Marcelo Sanchez [member] of the Zachry Department of Civil Engineering, Professor Charles Aubeny [member] of the Zachry Department of Civil Engineering, and Professor Charles Culp of Department of Architecture.

All work for the dissertation was completed by the student, in collaboration with Mr. Augusto Lucarelli from Itasca Consulting Group Inc. through IEP program and Mr. Matt Robinson from Texas A&M Transportation Institute (TTI) at TAMU RELLIS campus.

Funding Sources

Graduate study was supported by Spencer J. Buchanan Chair of Zachry Department of Civil Engineering, Texas A&M University Energy Institute, and Texas A&M University System Chancellor's office Area 41 Initiative.

NOMENCLATURE

α_w	Free water thermal expansion coefficient
ω	Soil water content
W_t	Soil total weight
W_s	Soil dry weight
$\dot{\varepsilon}_{vol.}^{mech}$	Average mechanical volumetric strain
V_t	Soil total volume
V_0	Soil initial volume
n_{relax}	Relaxation “n” value
n	Creep “n” value
L	Applied measured load
L_0	Applied initial load
S	Measured pile top displacement
S_0	Measured initial pile top displacement
ρ	Soil density
$\frac{d\dot{u}_i}{dt}$	Strain rate or velocity
σ_{ij}	Total stress tensor
g_i	Gravitational acceleration
ΔF	SEL thermal axial force increment
E	SEL Young’s modulus
A	SEL cross sectional area

α	SEL linear thermal expansion coefficient
ΔT	Temperature change
Δp	Mean pressure
K	Soil bulk modulus
G	Soil shear modulus
$s_{i,j}$	Soil deviator stress tensor
Δe_v^e	Soil volumetric elastic strain
$e_{i,j}$	Soil deviator elastic strain
υ	Poisson's ratio
E_{ur}	Young's unload-reloading modulus
E_{50}	Initial stiffness at 50% strain
$P_{c,ini}$	Initial hardening parameter
OCR	Soil over consolidation ratio
$\tilde{q}_{ini}$	Initial shear stress
p_{ini}	Volumetric stress
$\Delta\gamma_v$	Volumetric hardening parameter
$\Delta\varepsilon_v^p$	Volumetric plastic strain increment
$\lambda\left(W/m°C\right)$	Soil thermal conductivity
$c_v\left(J/kg°C\right)$	Soil specific heat
$\alpha\left(1/°C\right)$	Soil thermal volumetric expansion coefficient

TABLE OF CONTENTS

Page

LIST OF FIGURES

Page

LIST OF TABLES

Page

1. INTRODUCTION

1.1 History

According to Johnston et al. (2011), the very first application of geothermal energy was in the central French town of Chaudes-Aigues in the 14th century. Gilbert and Jaudin (1999) reported that the geothermal system used in Chaudes-Aigues district was to provide hot water for 150 homes. This system includes $5km$ of pipelines from five different sources in form of springs. Gilbert and Jaudin (1999) also reported that the houses which were built on these springs will also be able to benefit from this source of energy toward floor heating.

Geothermal foundation application has been recently picked up significant attention in US for cooling and heating purposes of the buildings. Briaud (2013) stated that the temperature gradient in the earth changes and could vary from $15^{\circ}C$ per km over the first $100km$ of depth. This indicates the fact that the deep foundation application would be a good source of constant temperature zone to be used for geothermal system. The effect of this system on the energy saving and consequently the reduction in billing costs, created a great motivation for clients to use it. However, the common practice in studying the behavior of the heat exchanger pile for design phase is currently limited to applying large safety factors to make sure that the design would cover all the thermal effects. The implementation of geothermal piles in cooling dominated regions in U.S. such as Texas with problematic soil profile such as high plastic clay has been challenged by potential owners regarding its unknown impacts on soil-foundation behavior both in short and long term. This research provides practical guidelines and recommendation toward design of a full-scale geothermal pile system for cooling dominated climate.

1.1 Conventional HVAC Systems for Buildings

The HVAC term denotes to the heating, ventilation, and air-conditioning equipment being used for heating and cooling of buildings. The air conditioning or cooling mode is achieved by cooling and dehumidifying the air when it passes over a cold coil surface. Finned surfaces are assigned to surfaces in heat transfer process, which have surfaces extended from objects to increase the heat transfer rate to or from the surrounding environment. The indoor coil represents an air-to-liquid heat exchanger containing tubes, which passes the liquid. Two type of HVAC equipment might be used with its proper liquid: direct expansion (DX) or chilled water (CW). In case of DX system, for cooling mode the air absorbed from warm environment is passed over the cold refrigerant liquid and warms it.

The vapor gas resulting from heating up the by the warm air is pumped to the compressor. The compressor would compress the vapor gas to very high pressure and high temperature. This highly compressed and hot gas is pumped to outside unit to reject the heat of the gas. Then the warm and high-pressure gas is pumped to an expansion device, converting it to cold and low-pressure liquid. This is transferred to the cooling coil and the entire process is repeated (Figure 1.1a and Figure 1.1b).

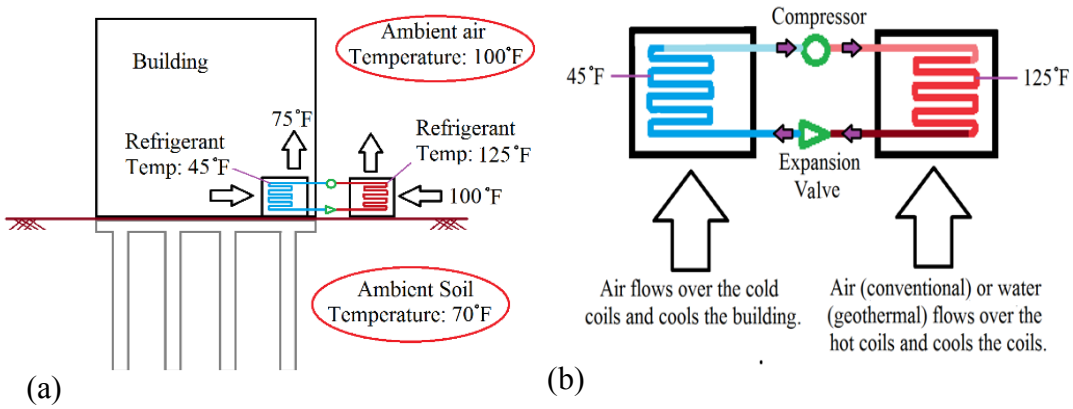

Figure 1.1. (a) Conventional HVAC system; (b) Air conditioning mode.

1.2 Geothermal Foundation System

The geothermal foundation system is a renewable energy source improving the efficiency of the conventional HVAC systems. Since the ground has a constant temperature throughout a year, it acts as a heat source in winter and heat sink in summer providing an environmentally friendly and renewable source of heat exchange for a geothermal foundation HVAC system. According to Environment Protection Agency (EPA) and U.S. Department of Energy (DoE), the geothermal systems considered to be one of the most environmentally friendly, energy and costly effective methods to reduce electricity consumption. Any deep foundation structure is constantly in contact with the surrounding soil. The geothermal foundation system uses the earth natural heat transfer capacity to warm or cool the heat carrying fluid (HCF) circulating inside the loops embedded in piles.

Any geothermal system regardless of the installation method has three major components:

1. The ground loop connections, which carry the HCF causing the heat, transfer between fluid and earth. This part acts as a replacement for the heat rejection in outside unit of conventional HVAC in cooling mode.
2. The heat pump to transfer the heat or cool between the HVAC system and ground loop.
3. Distribution system to circulate either warm or cool air inside the building.

For heating operation, the geothermal system pumps the cold HCF inside the high-density polyethylene (HDPE) pipes. Since the ground temperature is higher than the HCF, the HCF temperature rises by transferring heat from the ground to HCF (at this time ground acts as a

heat source) and then circulates back to the heat pump to get passed over the coil for sending out warm air (Figure 1.2). the cooling mode, reverse of the heating process happens.

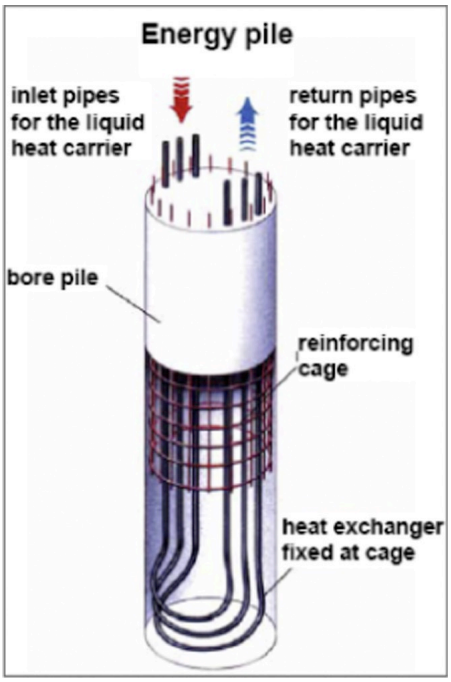

Figure 1.2. Typical energy pile installation schematic (Morrone et al., 2014)

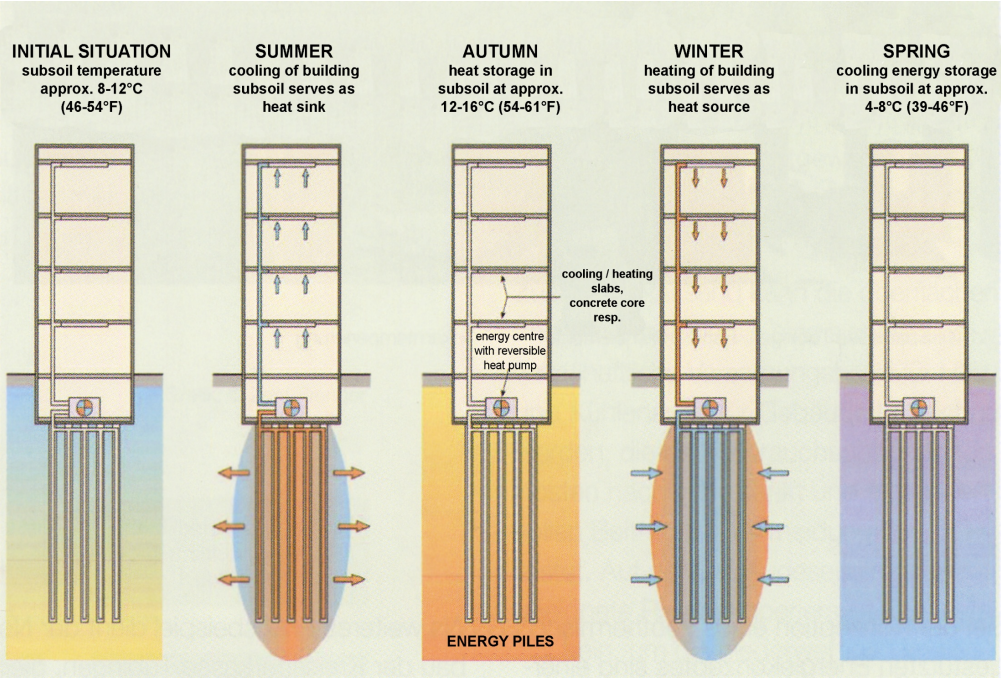

Figure 1.3. Seasonal geothermal foundation operation schematics during a year.

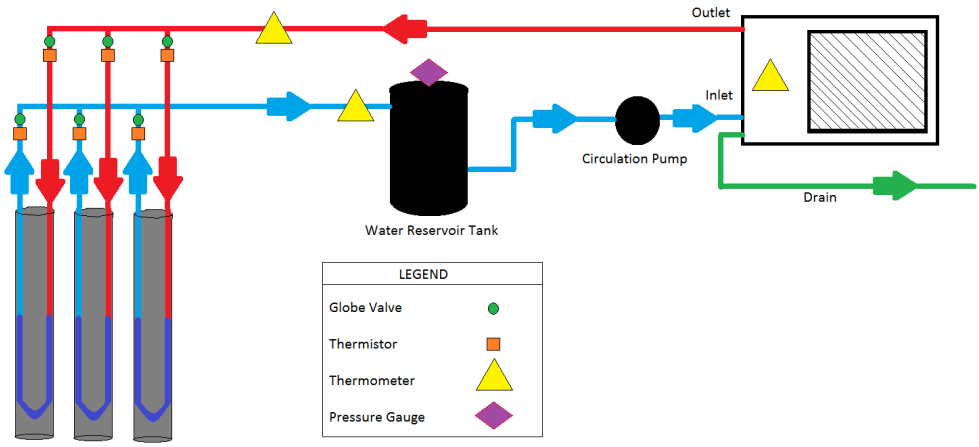

Figure 1.4. Schematic of the geothermal foundation system installed at Liberal Arts Building

Figure 1.3 demonstrates the fundamental concept of using constant earth temperature profile within the depth of pile foundation for geothermal foundation system. Throughout one-year cycle, the ambient air temperature changes considerably comparing to the earth temperature.

Figure 1.4 shows the components of an existing geothermal foundation system under LAAH building at TAMU College Station campus.

1.3 Energy Saving Contributions by Energy Pile

The most of electricity usage of a conventional HVAC system is to provide the power for compressor to compress or expand the refrigerant liquid in the system for heating and cooling of a building (McCartney et al. 2010). This powering frequency depends on the outside temperature and the level of effectiveness of the thermal insulation of the building. If we consider the highly efficient insulation for the building, then the outside temperature would be primary cause of the high or low frequency of compressor power up.

On the other hand, the geothermal foundation system by using the constant temperature of the ground as either heat source or sink, would reduce the frequency at which the compressor needed to be powered up. This would eventually lead into the reduction in electricity bills and saving energy. McCartney et al. (2010) defined this improvement to the HVAC system as the goal of a geothermal system. Regardless of energy saving goals of geothermal systems, since the ground loops are placed inside the foundation, which are designed anyway, the installation of ground loops becomes very low (McCartney et al. 2010). This advantage would be another great motivation for clients to consider the energy efficient geothermal foundation for cooling and heating of buildings.

1.4 Economic Benefits

The economic benefits from application of geothermal foundation systems have been briefly stated in several researchers including Brandl 2006; Bourne-Web et al. 2009; McCartney 2011; Bouazza and Adam 2012.

1.5 Research Goals

The application of geothermal foundation will not come without any concerns and questions by the owners. The additional thermal loading coupled with mechanical forces on the foundation, induces unknown stresses and deformations in the soil, pile, and soil-pile interactions. The challenges facing the application of geothermal foundation system can be categorized into three subjects as discussed in the following sections.

1.5.1 Building-Foundation Behavior

The cyclic thermal effect on the soil's ultimate bearing capacity in a full-scale problem is the most critical factor when it comes to design a thermo-active deep foundation. As the soil contracts (i.e. during building cooling operational mode) or compresses (i.e. during building heating operational mode), the confining effective stress profile, modulus, and pore pressure changes in which result in change of the ultimate bearing capacity of the designed pile group. This variation needs to be carefully analyzed and recognized to provide a safe design for both short term (i.e. undrained) and long term (i.e. drained) application of the energy pile system.

Another important issue to point out, is the effect of cyclic thermal loading on any possible differential settlements between soil, soil-pile foundation, and soil-pile-building global system. Any changes to the effective stresses within the soil either caused by excessive heating or accumulative pore pressure, will have a direct impact on the amount of additional settlement by the energy pile application.

The stress distribution in pile structural elements has direct relationship with the down drag and movement of pile embedded in soil. The heating and cooling cycle will cause the pile to contract or compress in the dominating vertical direction. This vertical movement will create a point within the pile structural element called the null point in which the axial force changes

from compression to tension. These cyclic variations should be studied for short-term and long-term performance of the system.

1.5.2 Soil Thermal Pollution and System Efficiency

Imposing cyclic thermal loads will change the temperature ambiance inside the soil profile. Consequently, it will impact the heat transfer capacity of the energy pile system. The duration of operation, heating or cooling schedule, seasonal needs, number of active piles, pile spacing, pile length, and soil thermal properties are among the most important parameters when it comes to the heat transfer and efficiency of the energy pile system concerns. The thermal pollution within the foundation and its surrounding soil mass, drop or gain in the heat transfer capacity, and overheating of the soil will be the key issues to be addressed by this research effort.

1.5.3 Economic Analysis

A brief overview on the economic analysis and cost-benefit breakdown of some case histories collected from various sources will be presented.

The following sections will demonstrate the research background and existing literatures, experimental testing details, numerical simulation work to propose the design considerations and case history analysis, and finally the economic study based on the existing resources.

2. RESEARCH BACKGROUND

2.1 Introduction

Currently, there are two developing practices regarding the application of geothermal capabilities of earth in heating or cooling any structures; Enhanced Geothermal System (EGS), and Ground Source Heat Pump (GSHP). The EGS comprises of the engineering or enhancement efforts toward making an impermeable undisturbed rock much more permeable. This kind of geothermal system would only be applicable in case of deep injection drilling, ranging from 4 to 5 km. Johnston et al. (2011) meniotned the fact that one of the major unknowns and uncertanities of the EGS is its possible contribution to future energy balance.

On the other hand, the GSHP method benefits from the heat transfer capacity of the soil beneath the foundaiton. In this method the heat carrying fluid (HCF), the ground would absorb heat or cold flux from the HCF which are running through the loops of pipes. As demonstrated in the Figure 2.1 and Figure 2.2, the geothermal system loops can be placed along with the pile construction process.

One of the current challenges for geothermal foundation application is to identify its impact on soil behavior specifically clays. The condition of cyclic thermal loading which means heating-cooling for each year and having the effect of saturated or unsaturated zone along with the shrink-swell problems in fat clays introduces new uncertainties to the feasiblity of this system in super structures and industrial projects.

Figure 2.1. Geothermal loops inside the cage of an auger cast pile (Akrouch, 2013)

Figure 2.2. Geothermal piles installation (Akrouch, 2013)

In the following two sections, the existing experimental and numerical work published in literature is presented.

2.2 Existing Experimental Work

From Campanella and Mitchell (1969), Naik (1986) stated that the volume and pore water pressure in saturated soils would change with temperature variations (Figure 2.3). Campanella and Mitchell (1969) conducted a series of drained triaxial tests, which showed that considerable permanent compressions (volume decrease) were observed during initial temperature increase. Biot (1956) first introduced the concept of thermoelasticity theory and thermoelastic potential derived from free energy concept. Additionally, Biot (1956) introduced the irreversible thermodynamics of an elastic porous medium by dissipation functions, which then has a quadratic proportionality with the time rate of the flow through the elastic porous medium. Biot's work opened the possibilities of considering the thermal effects on soil medium although the elasticity concept might not be a proper consideration for clay soils with high plasticity and shrink-swell properties.

Campanella and Mitchell (1969) data showed that the increase in temperature under drained condition during a constant effective stress and imposing cooling load would have the same result on soil behavior as in the case of over-consolidated soil with the pressure increase followed by unloading. Naik (1969) also reported that Noble and Demirel (1969) observed the fact that the higher consolidation temperature goes, the higher shear strength can get. However, for a consolidation ratio at given temperature, the shear strength goes down with the increase in temperature.

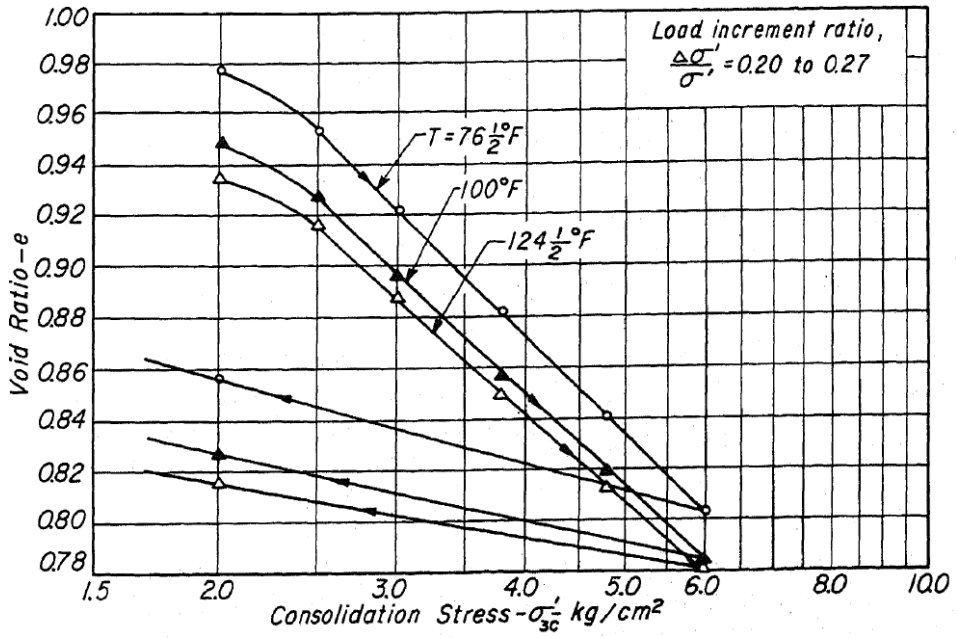

Figure 2.3. Isotropic consolidation for saturated illite (Campanella and Mitchell, 1968)

Noble and Demirel (1969) investigated the effect of temperature variations on the maximum shearing strength and creep behavior of remolded and statically compacted high plastic clay and low plastic silt (Figure 2.4and Figure 2.5). Both of the samples were tested by means of direct shear test in a temperature-controlled condition. According to Noble and Demirel (1969) in clay soils, the temperature variations affect the water density and viscosity and consequently the double layer diffusion, which has significant influence on soil strength. Noble and Demirel (1969) concluded that the creep tests have a linear relationship between the log of deformation rate and shear stress. They also suggested that the coefficient relating deformation rate and shear stress for silt is about three times larger than clays due to the specific surface differences between silt and clay.

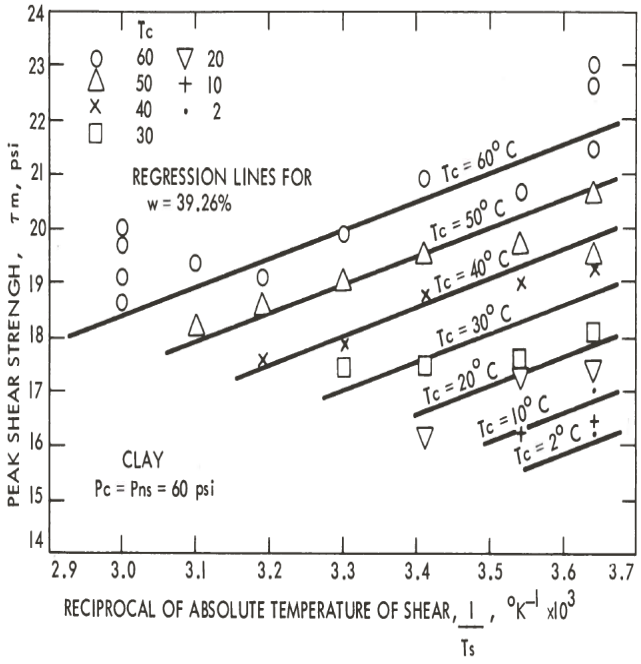

Figure 2.4. Shear strength vs. applied absolute temperature (Noble and Demirel, 1969)

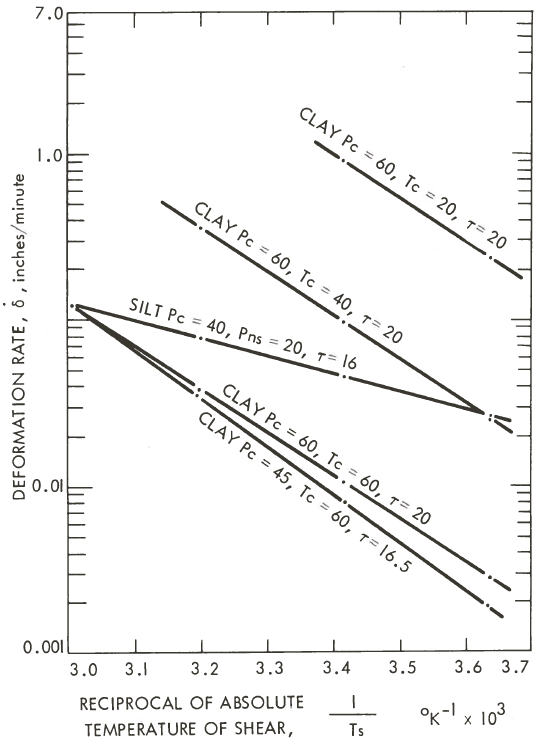

Figure 2.5. Strain rate variation with shear temperature (Noble and Demirel, 1969)

Paaswell (1969) analyzed the temperature profile that develops in soil in which the temperature would change at one boundary surface (Figure 2.6). Passwell (1969) studied the temperature profile distribution and moisture content variations in both unsaturated and saturated soil. Results showed Paaswell (1969) that the temperature profile provides a relationship between surface temperature and moisture content variations for transient temperature condition. Additionally, the heat conduction theory proved to be simulating accurately the temperature profiles by the assumption of sample homogeneity.

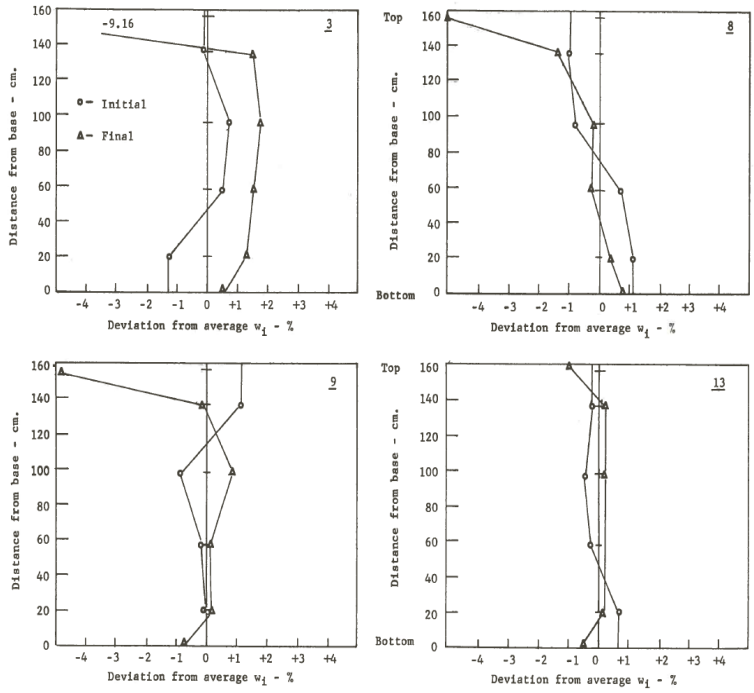

Figure 2.6. Initial and final water content profiles for different samples (Paaswell, 1969)

Plum et al. (1969) studied the effect of thermal loading on two cohesive soil's compressibility and pore water pressure; one was a fractionated illitic soil with high LL and one a glacial lake clay from Newfield, New York. They observed that in a cohesive soil during heating condition the soil compressibility increases at low applied stress with decrease in volume.

They further concluded that this volume decrease is proportional to the OCR ratio such that if OCR increases the volume change decreases. However, Plum et al. (1969) found that during soil's cooling mode behavior is as if it were an over-consolidated soil (Figure 2.7). The secondary consolidation changes significantly by cooling and slightly by heating. Plum et al. (1969) showed that excess pore water pressure caused by thermal loading during an undrained triaxial test is related to pre-consolidation stress of the soil (Figure 2.8 and Figure 2.9).

Palciauskas and Domenico (1982) studied the low permeability with high thermal conductivity formations with the general use for nuclear waste disposal sites. They discuss the parameters that make these formations to be an ideal selection to dispose nuclear waste with respect to their undrained behavior within the fractured rock.

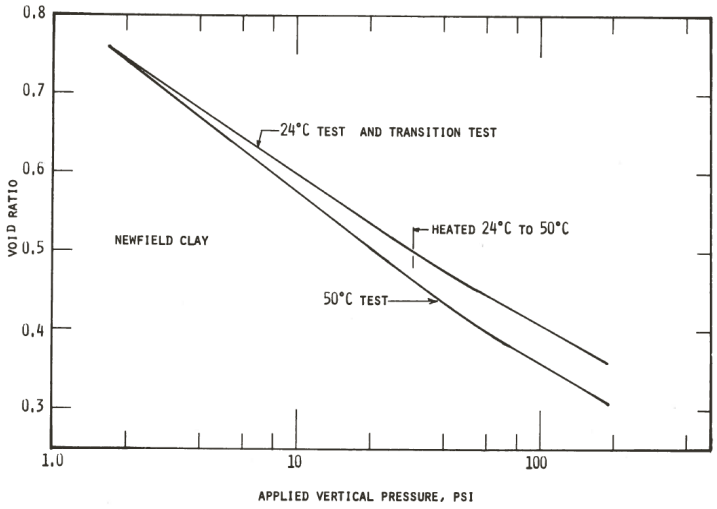

Figure 2.7. Void ratio vs. stress from consolidation test on Newfield clay (Plum et al., 1969)

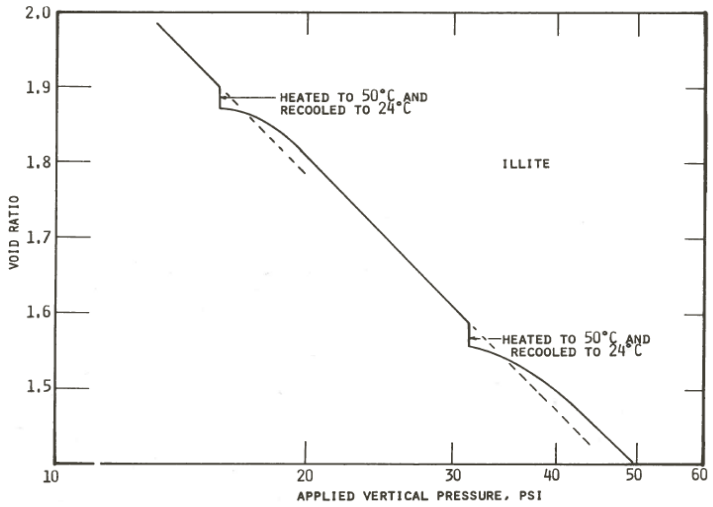

Figure 2.8. Heating and cooling effect on void ratio vs. the applied vertical (Plum et al., 1969)

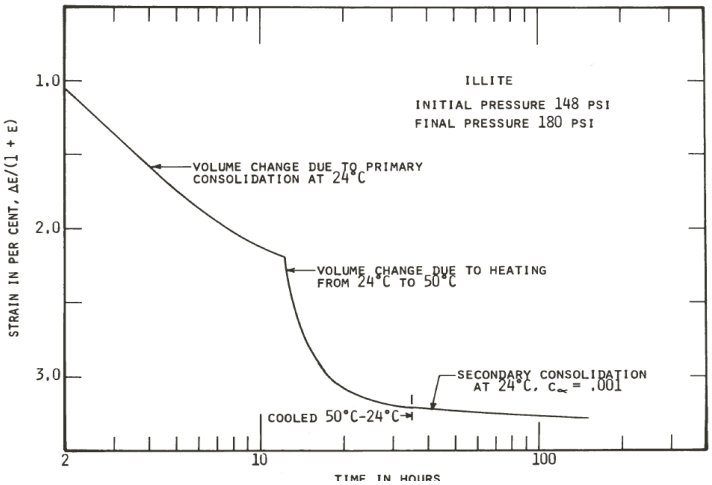

Figure 2.9. Secondary consolidation during heating and cooling of illite (Plum et al., 1969)

Evans et al. (1984) made modifications to the triaxial test cell to study the effect of hazardous and toxic wastes and temperature variations on the soil permeability. They used a spiral plastic tube surrounding the sample inside the triaxial cell, which have the water with constant temperature running through. A submerged pump inside a constant temperature water bath circulates this HCF. It would act as an agent changing the temperature on sample in cell.

They measured the undrained shear strength of samples. Furthermore, in order to accommodate the ASTM standard requirements, water content, Atterberg limits, and grain size distribution of samples were measured.

According to Naik (1986) there were several reports demonstrating the fact that heating can significantly affect the physico-chemical behavior of clay mineral structure. Naik (1986) presented a series of hazardous and toxic waste permeants and heat influence on the shear properties of clay including the Atterberg limits, grain size distribution, water content, and undrained shear strength. Results showed that in saturated condition, the water content would increase with the temperature increase while shear strength decreases. Agar et al. (1986) presented the thermal expansion and thermally induced pore pressure relationship for oil sand for temperature range of 20-300°C. The undrained thermal expansion coefficient presented by Agar et al. (1986) was derived from the undrained heating testing condition.

Hueckel and Baldi (1990) investigated the thermomechanical behavior of three saturated clays for drained and undrained conditions. For drained elastic behavior, the heating and cooling loading cycle has strong effect on soil strength and its consolidation condition in which it is NC or OC. There would be hardening due to thermoplastic strain to compensate for the softening in NC clay under constant imposed stress.

Hueckel and Baldi (1990) also reported that in the undrained condition the pore water pressure increases which eventually leads to reduction of effective stress and failing of the clay. Hueckel and Pellegrini (1992) and Bai and Abousleiman (1997) studied the effect of coupling and decoupling between thermal and mechanical loading and hydraulic pore fluid flow for 1D consolidation application. They mainly focused on the possibility of decoupling parameters from a fully coupled thermo-hydro-mechanical model for practical applications.

Abu-Hamdeh and Reeder (2000) studied the thermal conductivity variations with bulk density, water content, salt concentration, and organic matter through laboratory experiments. The thermal conductivity was reported to be measured by single probe method for sand, sandy loam, loam, and clay loam. They concluded that for both sand and clay soil the thermal conductivity would increase by water content increases (Figure 2.10 and Figure 2.11).

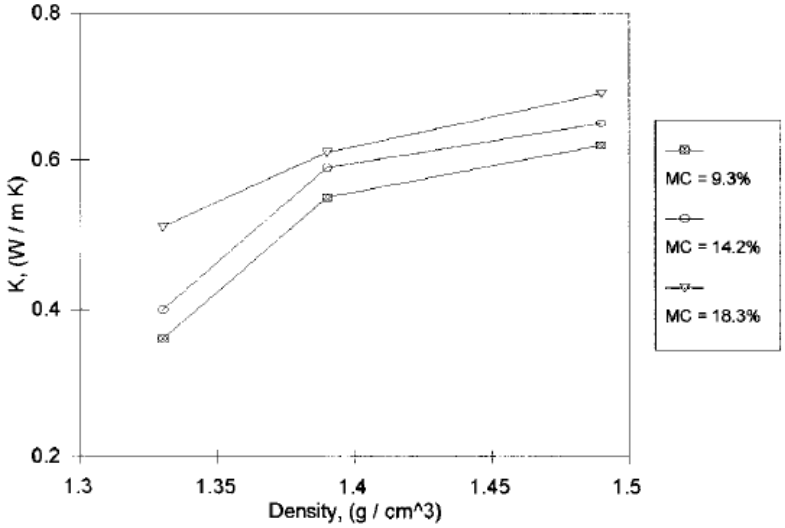

Figure 2.10. Thermal conductivity vs. density for clay loam (Abu-Hamdeh and Reeder, 2000)

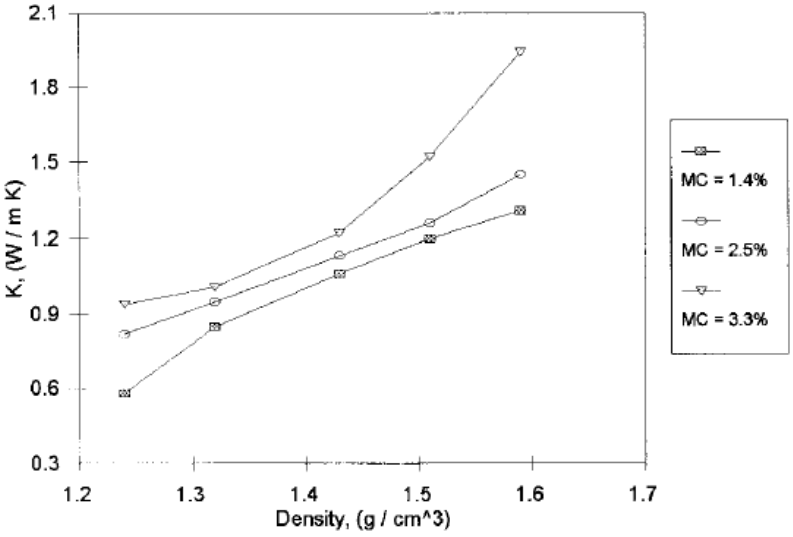

Figure 2.11. Thermal conductivity vs. density sand soil (Abu-Hamdeh and Reeder, 2000)

Sultan et al. (2002) conducted an experimental research to define the temperature influence on the pre-consolidation pressure of Boom clay and its respective effect on volumetric strain (Figure 2.12). Sultan et al. (2002) reported from different studies (i.e. Tidfors and Sällfors (1989); Boudali et al. (1994)) that for low to medium plasticity clays (ranging PI from 14 to 39), effect of temperature on the pre-consolidation pressure reduction from $0\text{-}50°C$ is approximately linear. However, they also reported that from Eriksson (1989) a significant non-linear behavior in reduction of the pre-consolidation pressure for very highly active clays (i.e. PI ranges from 60 to 66). Sultan et al. (2002) later concluded that the over-consolidation ratio (OCR) has effects on the volumetric strains for the transition from expansion to contraction. They also added that the volumetric portion of thermal plastic strain for the clay soil with normal consolidation condition is independent of applied stress.

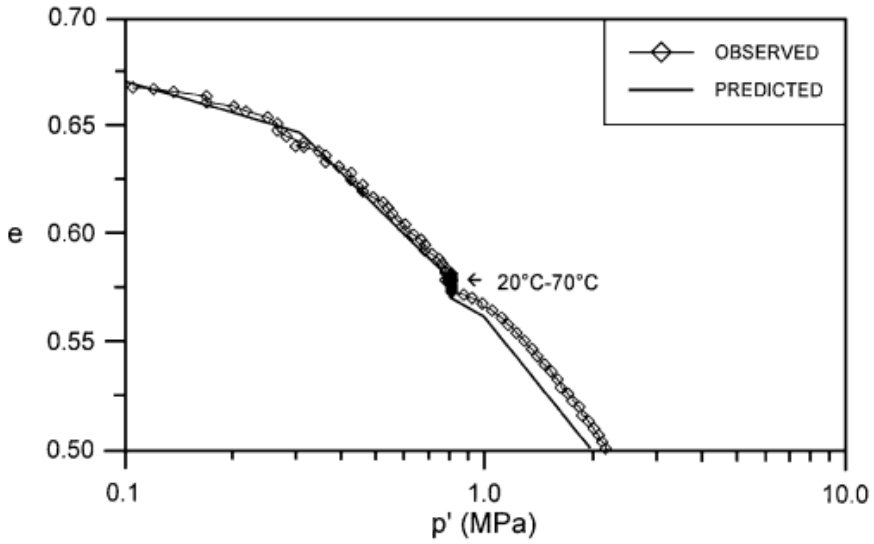

Figure 2.12. Thermal consolidation for Boom clay (Sultan et al., 2002)

Romero et al. (2005) studied the temperature variation effect on two samples of heavily over-consolidated clay through series of experimental study.

Laloui et al. (2006) conducted an in-situ testing with the following condition. The tested pile is $25.8\mathrm{m}$ deep with the diameter of $88\mathrm{cm}$. The building consists of 97 piles with the approximate depth of $25\mathrm{m}$. The soil profile from surface into ground consists of alluvial deposit (A1), alluvial deposit (A2), sandy gravelly moraine (B), bottom moraine (C), and Molasse (D), respectively. The temperature difference, which was practiced in this paper, is $21^{\circ}\mathrm{C}$ and the mechanical load up to $1300\mathrm{kN}$. They observed that at the pile toe, thermal loading effect caused much larger axial stresses than in case of mechanical loading only. They also suggested that even if the thermal loading propagates more in soil than static loading, it would still cause small strains while not altering the pore pressure and void ratio.

Hamada et al. (2006) studied the performance of energy pile foundation of an actual residential/office building for the air conditioning purpose in Sapporo, Japan. The pipe installation was described as a U-tube shaped type. The long-term analysis from heating mode measurements showed that the seasonal average temperature of HCF returning from geothermal loops were $2.4^{\circ}\mathrm{C}$ and $6.7^{\circ}\mathrm{C}$ with the COP of 3.9 for heating mode.

Pahud and Hubbuch (2007) performed in-situ experiments on the thermal performances of the energy pile system under the terminal E of the Zürich airport. Out of 400 foundation piles, 300 were incorporated with the geothermal loops. A 2-year measurement since October 2004 was mentioned that have taken place.

Khalili et al. (2010) studied the thermal expansion coefficient for a homogeneous saturated porous media. Khalili et al. (2010) reported that the coefficient of thermal expansion for a porous medium is equal to the thermal expansion coefficient of the solid particles. Additionally, they stated that the porosity, void ratio (in elastic region), and grain size distribution does not have any effect on the coefficient of thermal expansion.

Wood et al. (2010) investigated the performance of geothermal foundation for $72 m^2$ of ground floor area and piles of $10 m$ deep. Temperature variations for a period of 2007/2008 heating season were measured and compared with the naturally experienced temperature in the ground because of seasonal influence. Wood et al. (2010) found that heat exchange between the geothermal loop and ground did not affect the ground temperature at a distance of 5 m.

Brettmann and Amis (2011) presented a series of thermal conductivity tests for cases of single and pile group of three auger cast pressure grouted (ACPG) piles. They reported the pile temperatures, water temperature, and soil temperature evolution at the center of the pile groups in a sandy and clay soil profile. Brettmann and Amis (2012) showed the temperature evolution in 3 piles and well as the soil temperature change during the same operation span (Figure 2.13).

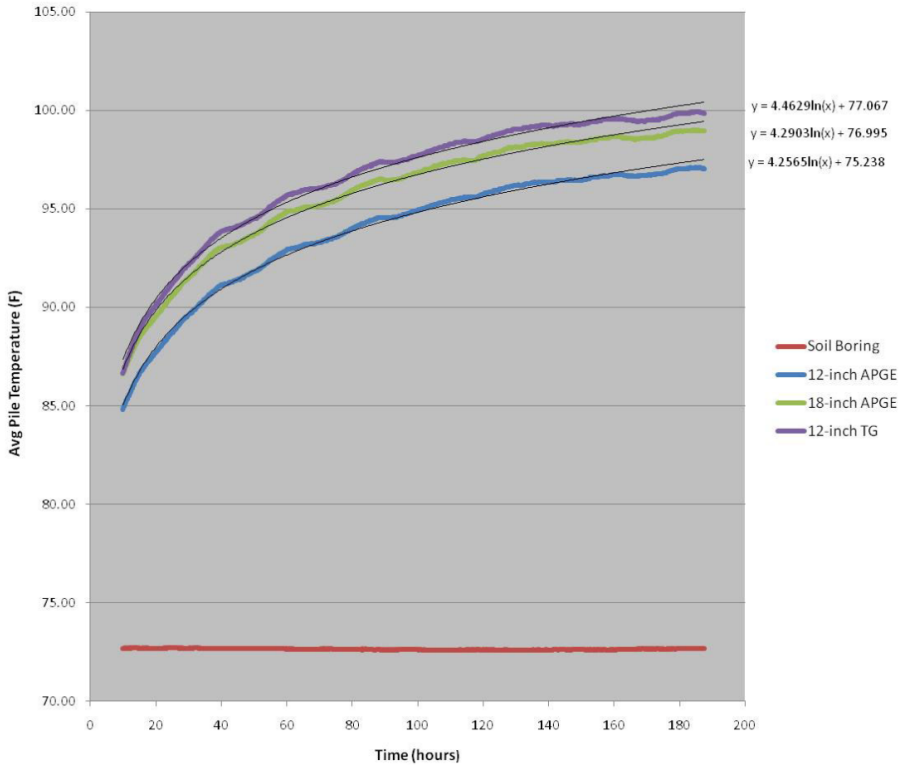

Figure 2.13. Measured pile group and soil temperature (Brettmann and Amis, 2011)

Akrouch et al. (2015) developed a new in-situ testing procedure by combining the cone penetrometer test (CPT) with thermocouples behind the cone tip. As the probe is pushed into the ground the friction between probe and soil increases the temperature in soil and the measurements are done for 30 minutes to monitor the decay of temperature in soil. The heat conduction coefficient of the soil profile can be back calculated as the CPT probe is pushed down in the ground. Akrouch et al. (2015) compared their results from TCT with the lab tests and finite element numerical simulations to validate the findings correlations with numerical model. They reported that a great agreement between TCT, lab tests, and numerical simulations were found for the 11 TCTs conducted (Figure 2.14).

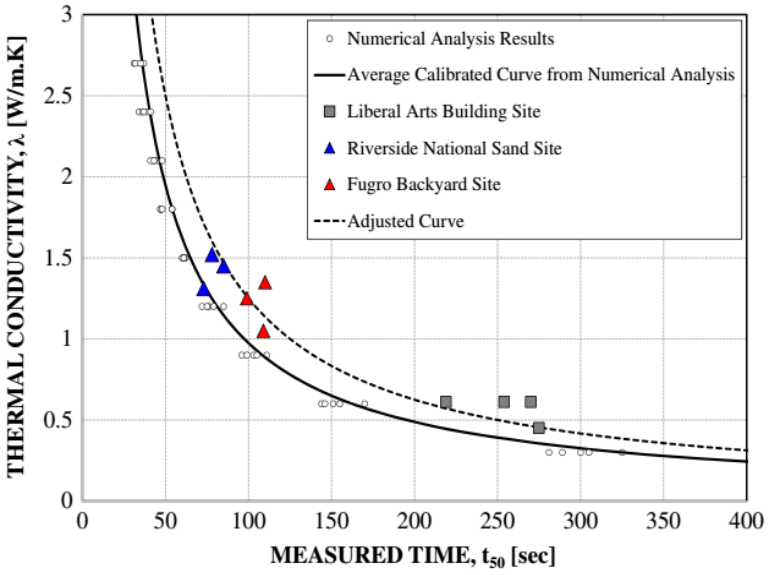

Figure 2.14. Comparison of TCT, lab test, and numerical analysis (Akrouch et al., 2015)

Sutman et al. (2015) performed a series of tests on three different energy piles installed out in Richmond, TX. The maximum and minimum applied temperatures were $45°C(113°F)$ and $8°C(47°F)$, respectively for a period of six weeks. Sutman et al. (2015) presented the

mechanical and thermal measurements. Sutman et al. (2017) performed a series of full-scale tests on three energy piles with different end-bearing conditions.

2.3 Existing Numerical Work

Baldi et al. (1988) investigated the effect of thermal loading (heating/cooling) on the volumetric deformation both mechanically and pore water pressure for various low permeability clay soils. They reported that with respect to the thermal effect on pore pressure, the thermal expansion for the pore water within clay soil matrix is significantly lower than the free water. Additionally, Baldi et al. (1988) stated that change in the over consolidation ratio can cause the clay soil to experience both compression and expansion while the thermo-mechanical loading occurs. Baldi et al. (1988) suggested the experimental equation for determining the free water thermal expansion coefficient in clay soils as a function of pore pressure and temperature $\alpha_w = f\left(T, p_w\right)$as follows

$$\alpha_w\left(T, p_w\right) = \alpha_0 + \left(\alpha_1 + \beta_1 T\right)\ln\left(mp_w\right) + \left(\alpha_2 + \beta_2 T\right)\left(\ln\left(mp_w\right)\right)^2 \tag{1}$$

The p_w is the pore water pressure. Baldi et al. (1988) reported the constants as

$$\begin{aligned} &\alpha_0 = 4.505e-4(°C^{-1}), \alpha_1 = 9.156e-5(°C^{-1}), \alpha_2 = 6.381e-6(°C^{-1}) \\ &\beta_1 = -1.2e-6(°C^{-2}), \beta_2 = -5.7662-8(°C^{-2}), m = 15000kPa \end{aligned} \tag{2}$$

However, Baldi et al. (1988) showed that the undrained thermal expansion coefficient for the normally and over-consolidated saturated clay for the typical temperature range for the energy pile varies $2\times10^{-4}\left(1/°C\right)$ to $4\times10^{-4}\left(1/°C\right)$ as shown in Figure 2.15.

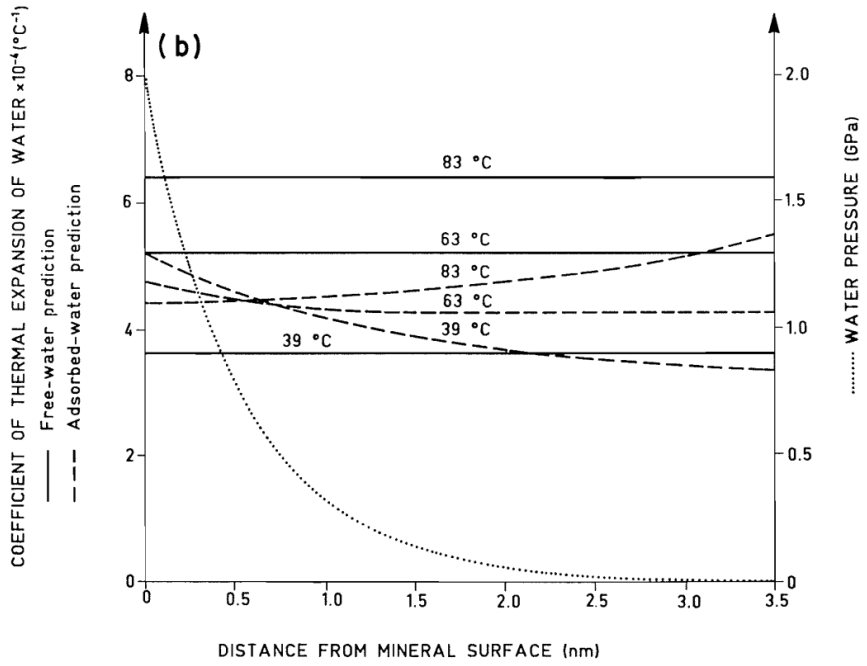

Figure 2.15. Undrained thermal expansion coefficient for Boom clay (Baldi et al., 1998)

However, Graham et al. (2001) presented a special form of the Cam-Clay model modified to consider the temperature changes for clay soil. Graham et al. (2001) model is able to predict the effect of thermal loading (i.e. both heating and cooling) on volumetric deformations, pore pressure, and strength evolution for normally and over consolidated fully saturated clay soil. Graham et al. (2001) reported that the undrained thermal expansion coefficient which couples the change in temperature to the pore pressure in solid matrix is independent of temperature and pressure magnitude, contrary to the equation 1 presented by Baldi et al. (1988). Graham et al. (2001) stated that their value of approximately $2\times10^{-4}\left(1/^{\circ}\mathrm{C}\right)$ regarding the undrained thermal expansion coefficient is in complete agreement with the reports by Agar et al. (1987).

Cui et al. (2000) stated that it is commonly accepted that the cooling cycle strains are reversible and is governed by soil structure thermal expansion and the water content level. On the other hand, during heating mode the strains are dependent on the rate of heating (Cui et al.

2000). The pre-consolidation pressure is directly affected by the temperature variations in soil medium such that when temperature increases the pre-consolidation pressure reduces creating a yielding locus relating temperature to stress variation in soil. Thermally induced plastic deformation varies with the degree of over consolidation ratios.

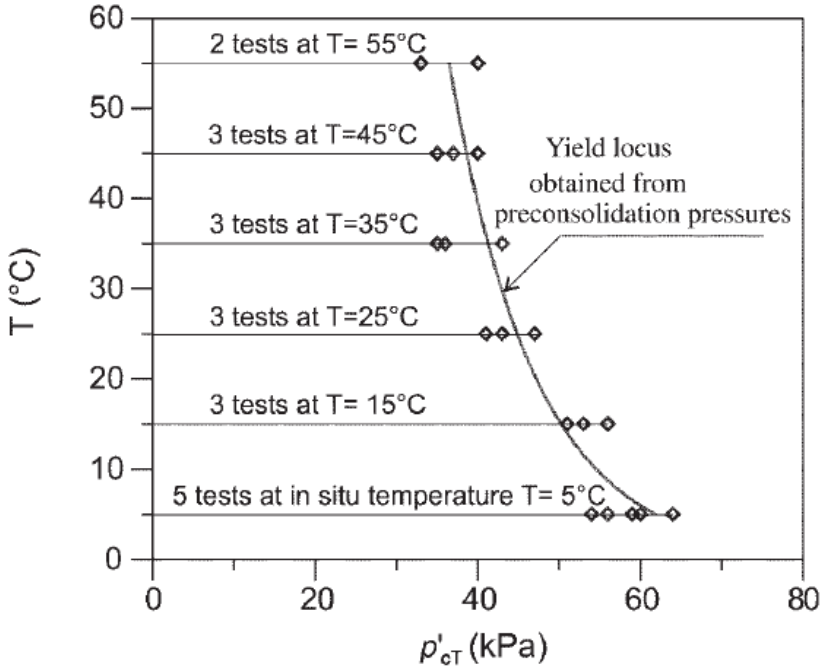

Figure 2.16. Pre-consolidation pressure vs. soil temperature (Cui et al., 2000)

Modaressi and Laloui (1997) proposed the cyclic thermo-viscoplastic model to simulate the effect of temperature on mechanical behavior and soil properties assuming no phase change. They suggested that the continuous variations of mechanical behavior of the soil with temperature decreases the shear resistance in some cases. They also observed that during thermal loading, the compression of material (hardening or expanding yield surface) increases the density and shear resistance of the material.

Rees et al. (2000) reviewed the effect of energy piles on performance and serviceability of deep foundation. The review showed that the bulk thermal conductivity is highly dependent

on moisture content and hydraulic properties of soil matrix in which are affected by thermal loading of geothermal foundation. Rees et al. (2000) also concluded that the groundwater regime fluctuations will affect the efficiency of heat transfer including precipitation, climate change, and manmade as the primary factors affecting the groundwater variation.

Laloui (2001) investigated the existing experimental efforts in literature in three ways of thermal loading, isothermal behavior, and thermo-mechanical tests. A new thermo-mechanical model is then implemented to predict the experimental results. On the experimental side, Laloui (2001) reported that the NC clay contracts upon heating and exhibits significant plastic deformation during cooling in which both are contradictory behavior to any other material. In general, for NC clay he stated that the thermal loading deformations are mostly irreversible with cyclic heating and cooling. However, for OC clay the higher the OCR number, the less compaction of soil when heated and then reversible dilation occurs (Figure 2.17).

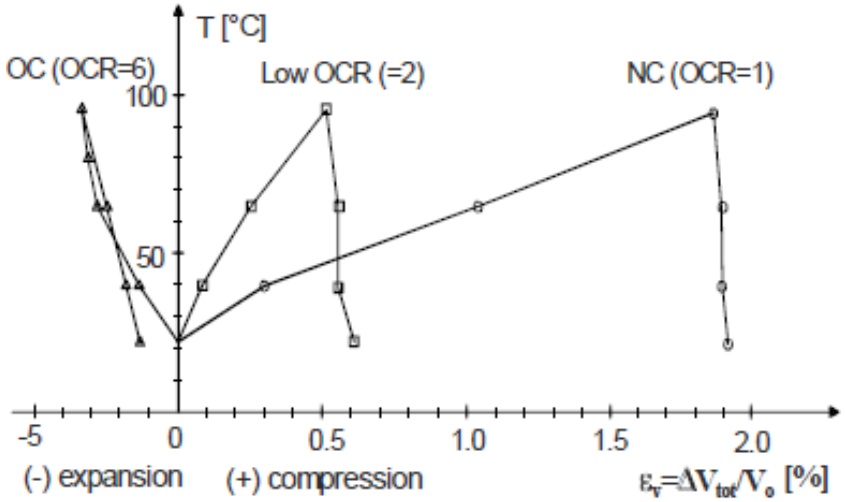

Figure 2.17. Thermal loading of Boom clay for different OCR numbers (Laloui, 2016)

Wu et al. (2003) proposed a thermos-hydro-mechanical constitutive model along with the numerical simulation with an FE code called LAGACOM for unsaturated soils. They studied the

thermal softening in particular in which decreases the magnitude of pre-consolidation stress and suction pressure for critical state for heating process. Wu et al. (2003) compared the numerical with the experimental results, concluding the fact that the constitutive model can reasonably simulate the unsaturated soil for coupling of thermo-hydro-mechanical behavior. Cekerevac and Laloui (2004) performed series of temperature controlled triaxial tests over Kaolin clay for both normally and over consolidated stress condition.

Cekerevac and Laloui (2004) presented their findings with the focus on the thermal loading effects on volumetric strain, pre-consolidation pressure, initial secant modulus, critical state line, and Terzaghi's consolidation compression coefficient $\left(C_c\right)$. They reported that the pre-consolidation pressure will drop by increasing the temperature $\left(22°\text{C} \rightarrow 90°\text{C}\right)$, as well as the secant modulus shows a slight increase within the same temperature change.

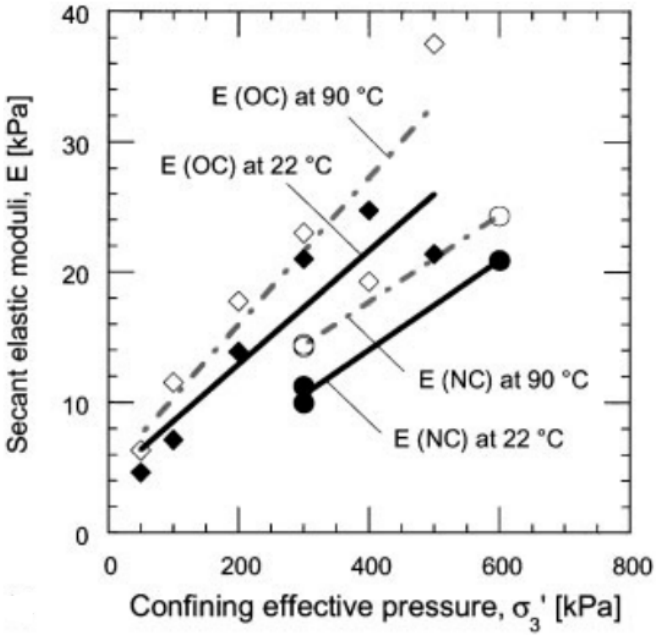

Figure 2.18. The secant modulus vs. temperature for Kaolin (Cekerevac and Laloui, 2004)

According to Mita et al. (2004) there has been various studies in order to predict the peak strength in more accurate fashion such as “cap models” by Baladi and Sandler 1980; Siriwardane and Desai 1981, or drained failure envelope prediction by Pender (1978) (Figure 2.19). Mita et al. (2004) investigated the Hvorslev-MCC model to better predict the peak strength for highly over consolidated clay soil in compression, extension, and plain strain (Figure 2.19). They reported that the model’s predictions for volumetric deformations in different shear modes show good agreement with triaxial data.

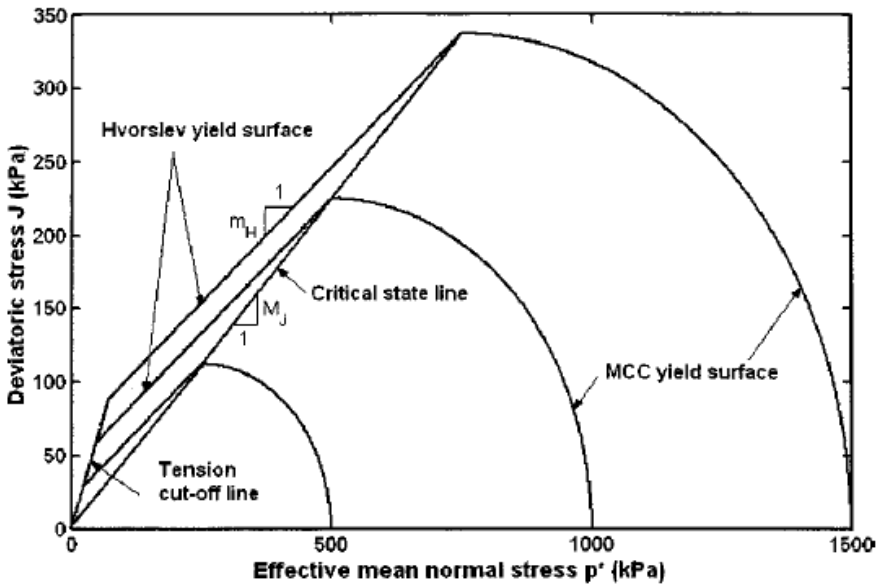

Figure 2.19. Comparison of traditional failure envelope vs. Hvorslev (Mita et al., 2004)

François and Laloui (2008) presented the ACMEG-TS, a constitutive non-isothermal model for saturated and unsaturated soil. They proposed two coupled constitutive aspects to describe the full coupling behavior under non-isothermal condition. Mechanical part is based on the bounding surface theory whereas for hydraulic part, the soil-water retention curve (SWRC) is capable of replicating hysteresis behavior due to the thermal and density variations. Gao et al. (2008) presented the performance of a GSHP system designed for a building in Shanghai, China.

They reported that the system was designed to accommodate for 30% of the cooling and heating loads. Gao et al. (2008) also performed the numerical simulation over the effects of pile type, average flow rate of circulating HCF, and various inlet temperature on the performance of the system.

According to McCartney et al. (2010), due to underestimating the heating and cooling demand for building or incorrect operation, process could cause in decrease in system efficiency in long-term. In addition, it would affect the soil heat transfer capacity by reducing it as the soil temperature increases. Abdelaziz et al. (2011) investigated the design challenges and operational strategy issues facing the geothermal foundation systems. The heat transfer performance of the energy piles were studies through numerical simulations under various operational conditions.

Gurpersaud et al. (2011) performed series of pullout tests on nails, which were installed in vertical, horizontal, and inclined at $15°$ to the vertical condition. The experimental tests were conducted focusing on the effects of matric suction on the nail pullout capacity installed in sand for both saturated and unsaturated soil condition. Gurpersaud et al. (2011) reported that the soil-water retention curve (SWRC) has considerable relationship with the nail pullout capacity.

McCartney et al. (2012) presented the design, installation, and maintenance details regarding the geothermal foundation application in North Dakota. Additionally, McCartney and Murphy (2012) investigated the performance of two full-scale energy pile systems at the new Denver Housing Authority Senior Living Facility in Denver, Colorado. Thermally induced axial strains are measured for both foundations and reported that the results agree with the expectation of having larger strains close to top of foundation. McCartney and Murphy (2012) also concluded that the thermal induced strain would be compensated by the side shear stresses.

Rouissi et al. (2012) proposed a heat transfer model for thermo-mechanically loaded drill-shaft foundations. This 2D finite difference based numerical method simulates the unsteady temperature distributions in soil and indoor/outdoor heat fluxes. Rouissi et al. (2012) reported that sensitivity analysis showed that geothermal foundation could be significantly improved by optimizing the HCF velocity, foundation depth, and materials.

Tsutumi and Tanaka (2012) studied the effect of temperature and strain rate on the viscous property, which leads to the change in secondary consolidation behavior of clayey soils. The tests were done under constant strain rate (CSR) with the temperature-controlled condition ranging from $10°C$ to $50°C$. Tsutsumi and Tanaka (2012) indicated that for the normal strain condition such as the other of $10^{-6}\left(s^{-1}\right)$ and high temperature, the samples showed dilation, which increased the hydraulic conductivity. Additionally, the yielding stress threshold decreased by increasing the temperature.

Suryatriyastuti et al. (2012) studied the thermo-mechanical behavior of an energy pile in homogeneous soil with finite difference method. Numerical results indicated that the thermally induced stress and deformation prediction by model is significantly dependent on the form of the interface between soil and pile. Akrouch et al. (2013) reviewed analytical, constitutive and numerical models available to predict the thermo-mechanical behavior of soil while using energy pile system. Finite element simulations were carried out for a square shallow box filled with dry sand coupled with geothermal loops. Finite element model predictions were focused on the impact of pile-soil de-bonding once coupled with geothermal. The more de-bonding, the less efficient the energy pile system become in transferring heat with the surrounding medium. Akrouch et al. (2013) also studied the loss of frictional capacity of the pile when de-bonding

occurs. They concluded that energy pile requires to be designed oversized at toe to compensate the possible loss of side frictional capacity.

Abdelaziz (2013) studied the challenges in designing of a deep energy foundation system. He proposed several solutions to the principle challenges toward designing an energy pile foundation with respect to the required thermal load as well as mechanical loading considerations. Di Donna and Laloui (2013) presented a constitutive model (i.e. ACMEG-T) with the capability of studying the tolerable displacement in soil-pile foundation, allowable stresses in concrete piles, and the risk level with respect to failure when it is subjected to thermo-mechanical loading. Di Donna and Laloui (2013) tested the performance of the ACMEG-T model for the NC Bangkok clay samples reported through series of temperature dependent triaxial tests presented by Abuel-Naga et al. (2006) ().

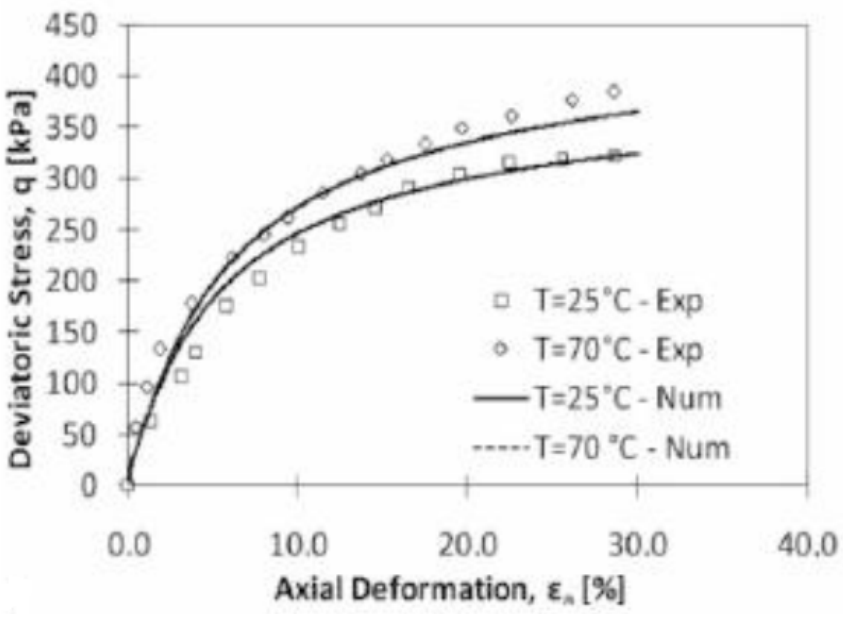

Figure 2.20. The ACMEG-T model results on Bangkok clay (Donna and Laloui, 2013)

Saggu and Chakraborty (2014) simulated the behavior of dense and loose sand-pile interactions under series of 50 cyclic thermal and constant axial loading with a nonlinear

transient numerical finite element model. Results indicated that for high and close to limit load mechanical loading, thermal loading does not affect the soil-pile interactions. Saggu and Chakraborty (2014) concluded that for the low to moderate mechanical loading condition, heating of pile, which results in expansion would create the uplift force. This uplift causes a negative shear force between pile and soil.

Salciarini et al. (2014) implemented a fully coupled three dimensional thermo-mechanical finite elements to study the soil-pile interaction for a small raft energy pile system. The axial loading distribution along the piles and thermal heat transfer efficiency variation were investigated. They concluded that the axial load changes considerably in energy pile system during the transition period of soil-pile reaching to thermal equilibrium condition and once the temperature variation reduces this axial load changes become less significant.

Salciarini et al. (2014) studied the time effect on the thermal transferability of soil and reported that significant reduction in specific heat flux to and from soil occurs for long-term application of energy pile. Mimouni and Laloui (2014) investigated the thermal loading impact on the mobilizing bearing capacity of geothermal piles using Thermo-Pile software for the Ecole Polytechnique Fe´de´rale de Lausanne (EPFL) and Lambeth College test piles. They have concluded that the mechanism resulting in geotechnical failure of pile foundation will not be mobilized by the additional thermal loading.

Additionally, Mimouni and Laloui (2014) concluded that even in the case of inducing failure capacity of the energy piles (side friction and end bearing capacity), the null point location in which the movements are zero will remain stable during thermal expansion or contraction and will provide the stability of the foundation. However, this stability relationship

between bearing capacity of the pile foundation and null point on the pile to provide stability to the structure is not thoroughly discussed.

Di Donna and Laloui (2014) applied a thermo-elastoplastic constitutive model to simulate the behavior of geothermal foundation for both cases of single and group of pile. The mechanical loading was constant and thermal loading was applied in a cyclic manner providing heating and cooling condition. They suggested that based on the results the strains induced by thermal loading is not significant, however, they needed to be considered when designing a geothermal foundation system. Di Donna and Laloui (2014) implemented a finite element numerical code to simulate the behavior of geothermal foundation for both cases of single and group of pile. The mechanical loading was constant and thermal loading was applied in a cyclic manner providing heating and cooling condition. Di Donna and Laloui (2014) applied a thermos-elastoplastic constitutive model to simulate the soil and soil-pile behaviors. They suggested that based on the results the strains induced by thermal loading is not significant, however, they needed to be considered when designing a geothermal foundation system.

Additionally, Morrone et al. (2014) suggested that based on their research outcomes in mild climate zone, the application of geothermal foundation system would increase the ground temperature up to about 10℃ over many years of operation while for the cold climate this increase is negligible.

Di Donna et al. (2015) studied the behavior of group pile under thermal loading by geothermal foundation for both conventional and extreme thermal loading condition by means of a 3-D finite element thermo-hyrdo-mechanical model. Caulk et al. (2015) presented the calibration of a 3D numerical simulation code dealing with conductive heat transfer principle from the energy pile foundation system to the soil surrounding. They also performed a

parametrization study over two influential factors including the effect of heat exchanger configuration inside the energy pile and the pile spacing. Caulk et al. (2015) reported that for a non-uniform temperature distribution, thermal axial stresses might be affected.

Yavari et al. (2016) studied the mechanical behavior of a model energy pile under thermo-mechanical loading. The axial loading was implemented in steps to monitor the resistance of the pile to mechanical loading and then while holding the axial loading constant, heating/cooling cycles were imposed. Results indicated that pile head moves upward during heating while settling downward during cooling mode. Yavari et al. (2016) reported that plastic (irreversible) deformations occurred due to thermal loading with the trend in which by increasing the mechanical loading the thermal settlement magnitude becomes larger. Another important observation by Yavari et al. (2016) confirms the findings of Akrouch et al. (2014) regarding the increase in creep rate of the clay as the pile head load approaches to the ultimate bearing capacity while remaining negligible for low applied pile head load.

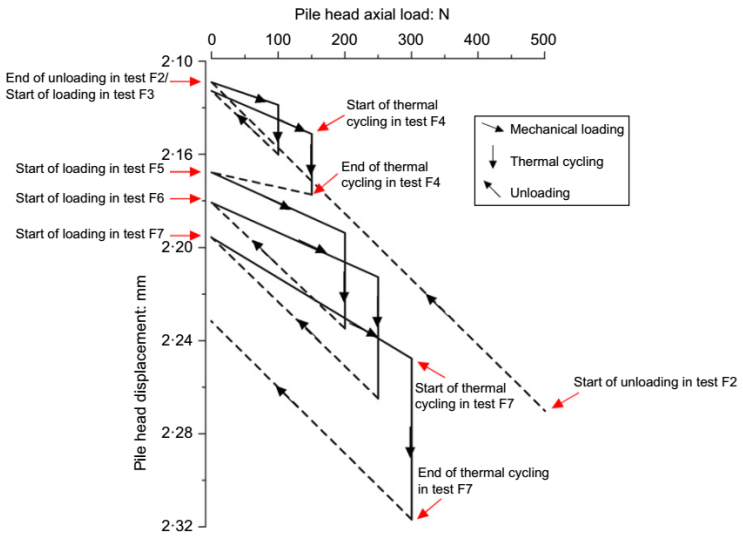

Figure 2.21. Load displacement curve under thermo-mechanical loading (Yavari et al., 2016)

McCartney and Murphy (2015) reported the axial strains for a geothermal foundation system under an 8-story building over a period of 5 years of operation. McCartney and Murphy (2015) stated that although the cyclic loading effect of thermal loading on piles by geothermal loops inside are observed to be consistent during each year, the axial strains at various depths show a diverging trend or in other words showing the down-drag issue. They also observed that the overall dominating contractile strains are lumped over the expansion and contraction of the pile specifically near the pile's toe.

Caulk et al. (2016) studied the parametrization of geothermal foundation system in Colorado Springs. They calibrated a numerical model for heat transfer conduction for a group pile. Results indicated that thermally induced stresses in piles varies over cross-sectional area of the piles with core of the pile could sustain as much as 20% greater than the reinforcing cage. Additionally, Caulk et al. (2016) recommended that the heat exchangers in the piles, should be distributed uniformly to prevent extreme thermal stress impact on piles due to uneven distribution of heat exchangers. Finally, they concluded that performance of an energy pile system depends significantly on the cross-sectional temperature distribution in pile.

Saggu and Chakraborty (2016) studied the behavior of energy pile group in sand using the state parameter-based constitutive clay and sand model (CASM) through finite element software as a custom constitutive model. Results included the analysis of displacement at the pile base and axial force distribution for different scenarios of source and receiver piles. Saggu and Chakraborty (2016) reported that during heating cycle, the amount of thermally induced displacement and axial stress than the case of mechanical loading only.

Liu et al. (2017) proposed a modified version of the pile load transfer model by Zhang and Zhang (2012) in which the matric suction was implemented in the pile-soil interface shear

strength. They further demonstrated their new adjustment to the load transfer model by focusing on the effect of infiltration on the load displacement behavior of a single pile embedded in Regina clay with expansive properties. Figure 2.23 shows the model result on the pile load displacement relationship under three separate matric suction profiles: state 1, state 2, and state 3. The state 1 represents the initial suction profile before any water infiltration; state 2 shows the transient state of infiltration; and state 3 is the steady state condition (Figure 2.22).

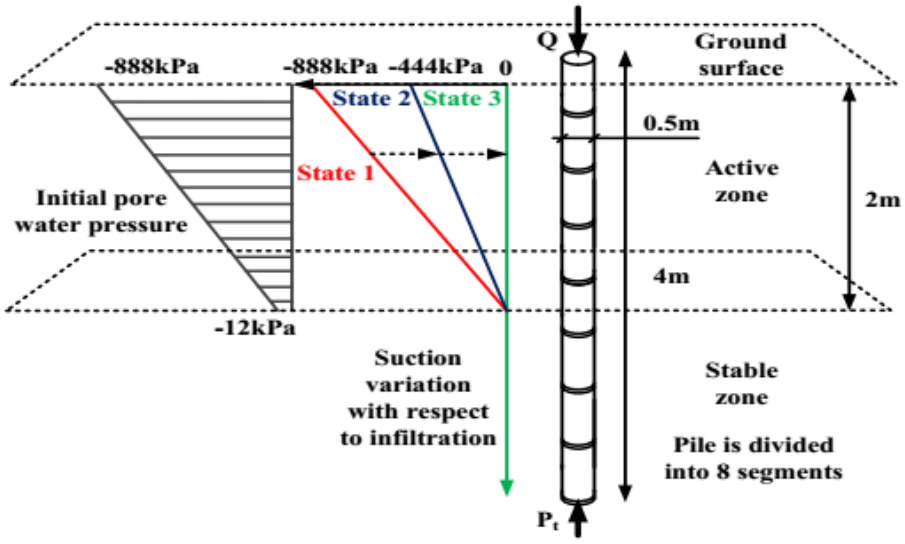

Figure 2.22. Three different matric suction profiles applied (Liu et al., 2017)

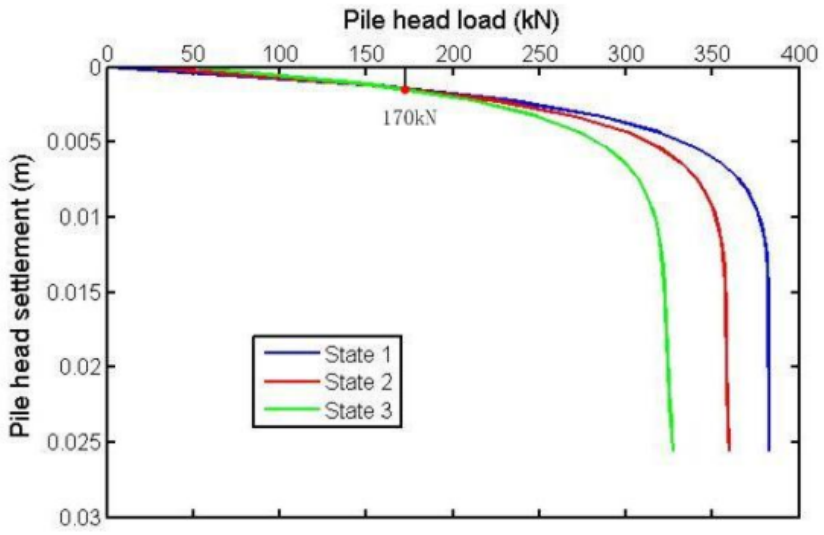

Figure 2.23. Pile load displacement result for various (Liu et al., 2017)

Deqi et al. (2017) investigated the effect of thermo-physical properties of the porous media on the heat transfer efficiency of the geothermal foundation. They concluded that the variation of the thermo-physical properties of the pile and soil leads to considerable errors in estimating the temperature difference for span of 10 years, especially when dealing with relatively small diameter piles. Sutman et al. (2017) studied the effect of pile capacity evolution for an energy pile system with the emphasis on the influence of fixed and free to move parts of the shaft.

Nguyen et al. (2017) performed a small-scale laboratory test of an energy pile in completely dry sand subjected to various fraction of its ultimate bearing capacity. Nguyen et al. (2017) stated that an asymptotic model could estimate the variation of the plastic pile head displacement against the number of thermal loading cycles. Wu et al. (2018) conducted an experimental study on the effect of five cyclic thermal loading on a floating pile system in a NC clay to monitor the temperature propagation in soil, pile displacement, and the excess pore pressure evolution.

3. LABORATORY AND FULL-SCALE WORK

3.1 Introduction

In this chapter, the details of a mini full-scale geothermal foundation system performance in the TAMU Liberal Arts and Humanities (LAAH) building deep foundation. Additionally, a unique model scale laboratory test which was conducted at TAMUS RELLIS campus is presented. This testing effort provides valuable information on the two very important soil behavior of typical clay in Texas including shrink-swell and creep.

3.2 TAMU LAAH Building: Mini Full-Scale Geothermal System

The existing system in LAAH building performs as a mini full-scale geothermal foundation setup containing 6 supply and return pipes for circulating heat carrying fluid (HCF) in which for our system is water into the pile foundation and heat pump. An 8-channel PICO Tech data logger, connecting six thermocouples, measures the water temperature. There are three Auger Cast in Place (ACIP) foundation piles with instrumentations for temperature measurements and three additional boreholes with various distances from ACIPs to monitor the heat flow in the ground. The temperatures are measured by thermistors in all three boreholes and ACIPs. They are connected to two, 16-channel data loggers from Lakewood System. This system is currently capable of functioning as heating or cooling unit for the crawlspace area in the LAAH building. However, this system is not connected to the central HVAC for the LAAH building. The plan view is shown in Figure 3.2, the soil profile in Figure 3.1, the cross section view of boreholes in soil in Figure 3.3, and the Figure 3.4 is a photo of the ground surface system setup in the crawl space area of the LAAH building.

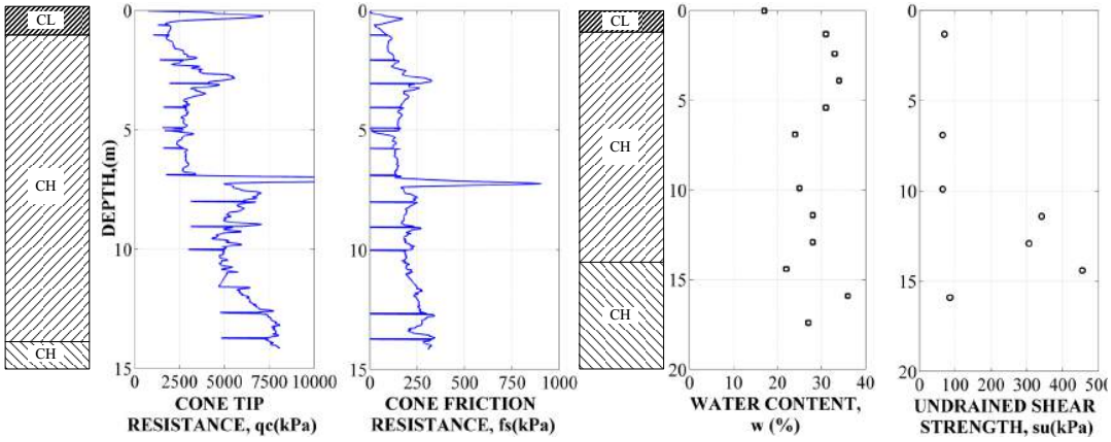

Figure 3.1. Soil profile characteristics under LAAH building (Akrocuh et al., 2015)

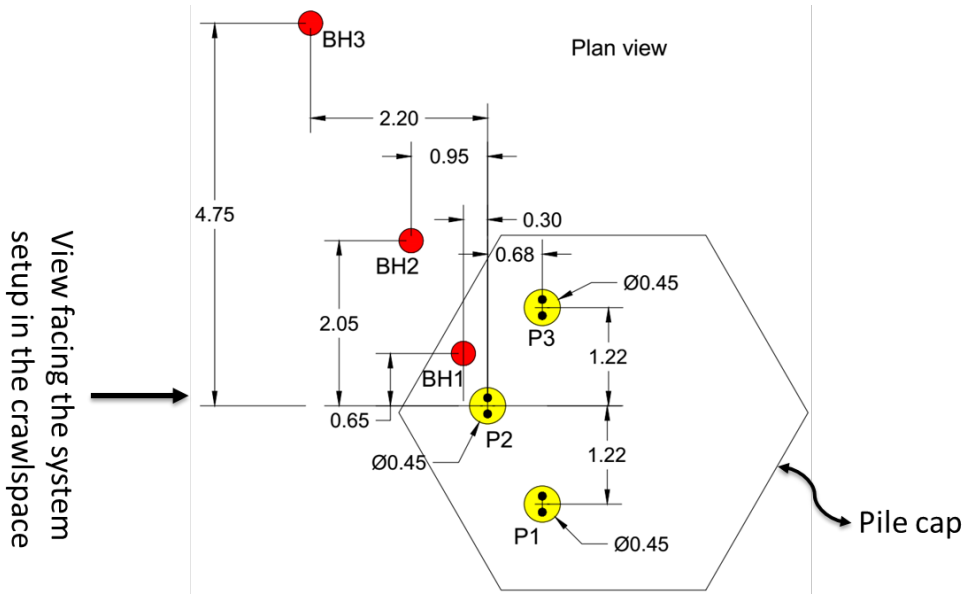

Figure 3.2. LAAH ground loops and monitoring boreholes sizes and dimensions

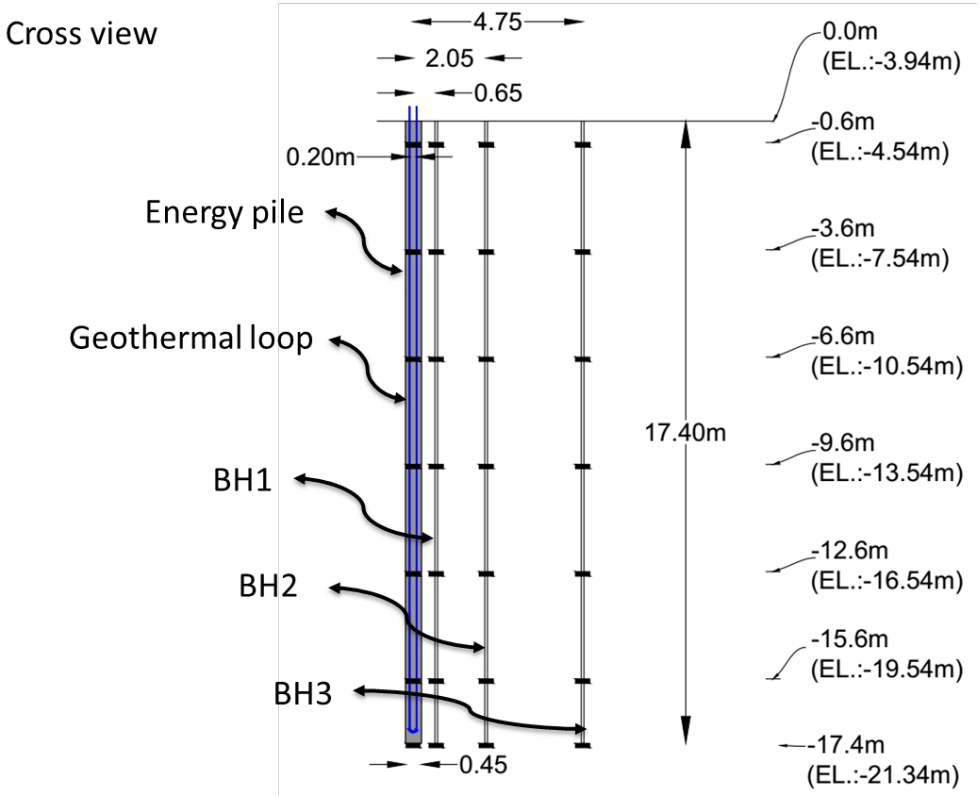

Figure 3.3. LAAH thermistor sensor positioning

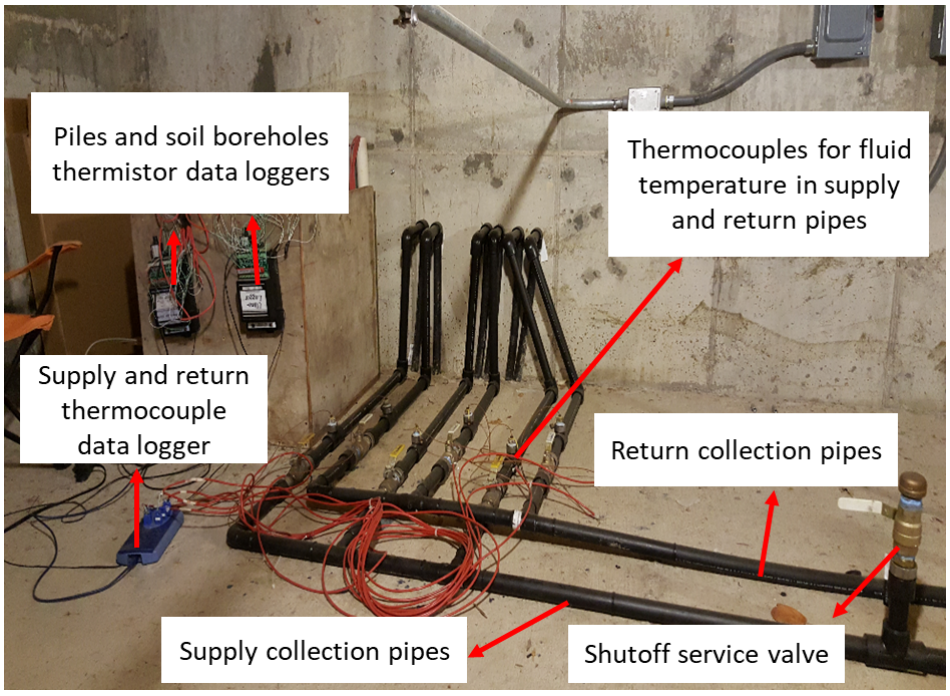

Figure 3.4. Geothermal system components installed at LAAH building.

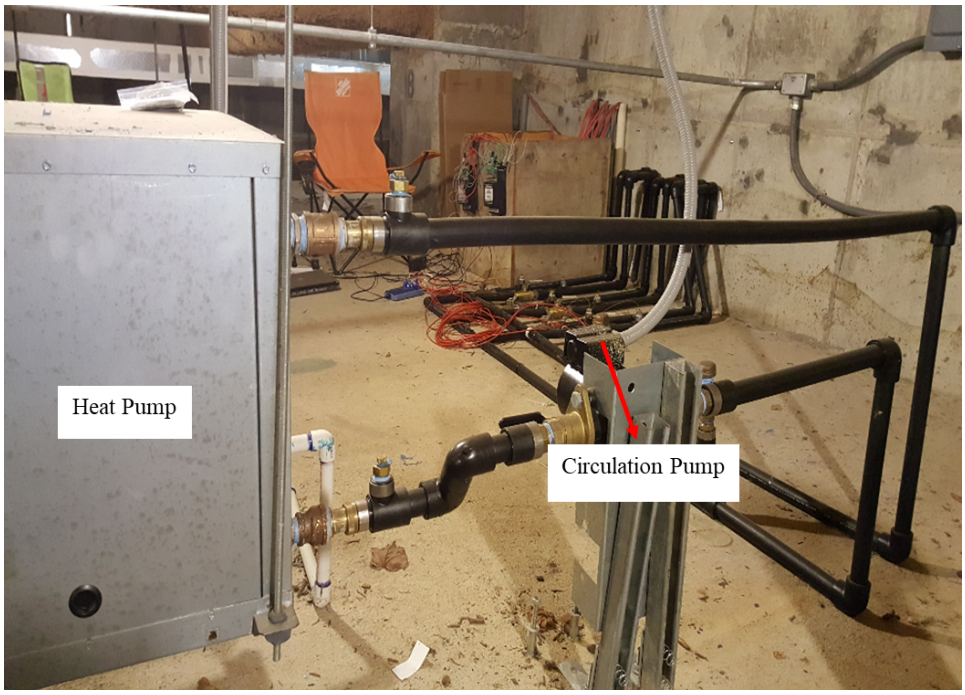

Figure 3.4. Continued

As part of this experimental program, the system was used in both heating and cooling mode for a period of over a month. The cooling mode operated from February 24, 2016 until March 4, 2016. The temperature measurements inside the piles and borehole number 2 are presented in Figure 3.6 and Figure 3.7, respectively. For the cooling mode, Figure 3.9 (a) and (b) show the increase in temperature versus time for the pile and for the soil about $2.5m$ away from the piles as a function of time. The heating mode started from January 30, 2016 until February 15, 2016 and switched off to monitor the temperature recovery until February 18, 2016 (i.e. outlined in the Figure 3.10a). The temperature measurements inside the piles and borehole number 2 are presented in Figure 3.8 and Figure 3.9a, respectively. In addition, the system thermostat was set on the auto mode and it was switched off automatically once during these 17 days of heating mode (i.e. outlined in the Figure 3.10a).

3.2.1 Cooling and Heating Mode

In the cooling mode (Figure 3.5a), the heat generated in the circulating fluid by the hot side of the coolant is transferred from plastic pipes to concrete pile and then to the surrounding soil. Figure 3.6 and Figure 3.7 show the temperature profile measured in all 3 geothermal piles and the temperature in the monitoring borehole #2, respectively. As can be seen the temperature in the pile is increasing relatively rapidly from $10°C$ to $48.9°C$ and on to an apparent asymptotic value during the 12 days of operation (Figure 3.9a). It appears that the temperature would reach an asymptotic value of about $54.4°C$. The temperature in the soil at a distance of $2.5m$ from the pile increases much more slowly as can be seen in Figure 3.9b).

In the heating mode, the cold generated in the circulating fluid by the cold side of the coolant is transferred from the plastic pipes to the concrete pile and then to the surrounding soil. Figure 3.8 shows the temperature profile measured in all 3 geothermal piles. As can be seen the temperature in the pile is increasing relatively rapidly from $24°C$ to $6°C$ and on to an apparent asymptotic value during the 17 days of operation (Figure 3.10a). It appears that over time the temperature would reach an asymptotic value of about $5°C$. However, the temperature in the soil about $2.5m$ from the pile is erratic and shows much less decrease slope (Figure 3.10b).

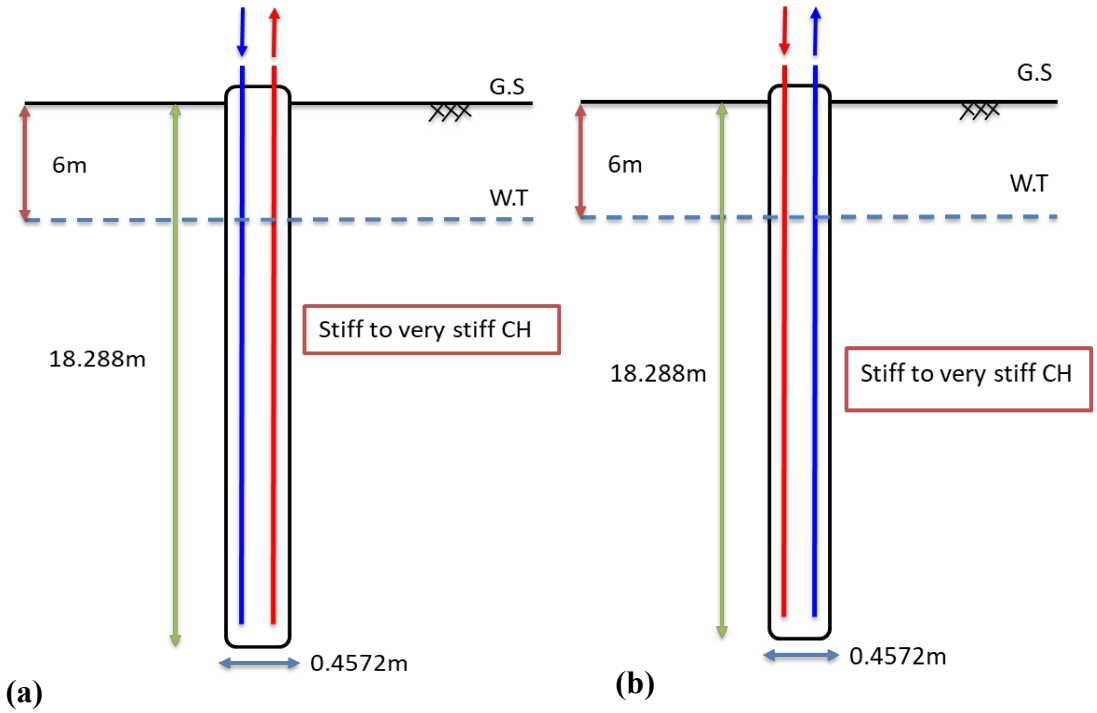

Figure 3.5. (a) Shows the LAAH energy pile schematic for building's heating mode and (b) shows the LAAH energy pile schematic for building's cooling mode

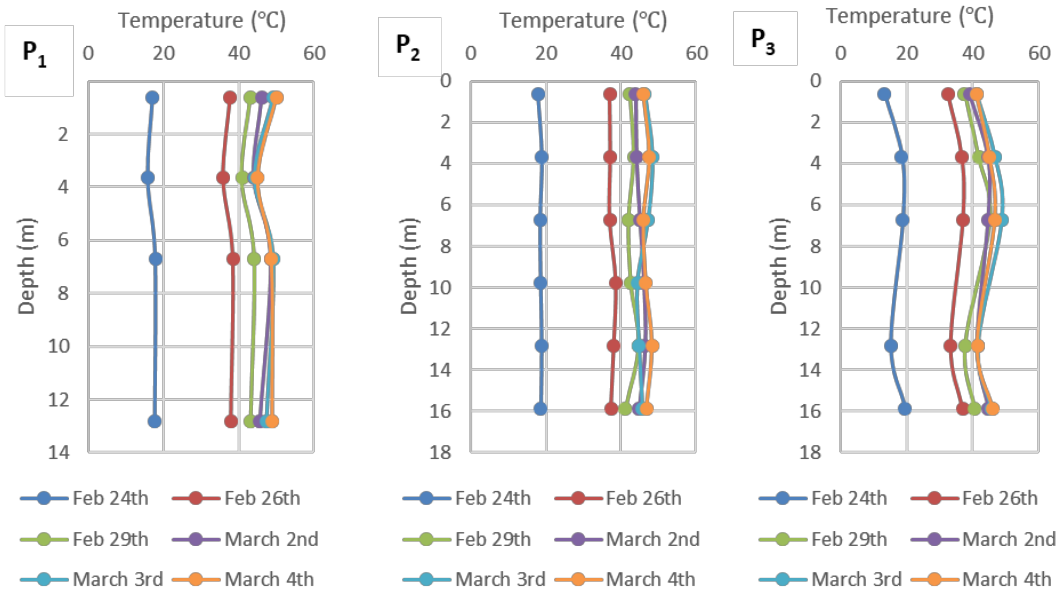

Figure 3.6. Temperature profile inside the three piles during 12 days of cooling mode.

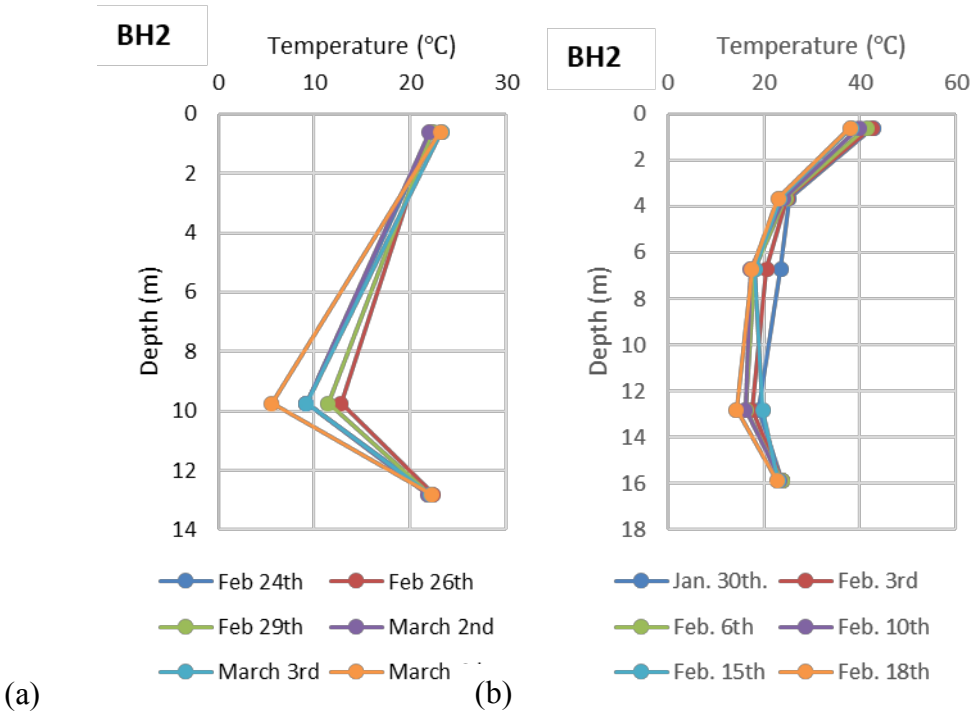

(a) (b)

Figure 3.7. (a) Temperature profile in borehole #2 during heating and (b) cooling mode

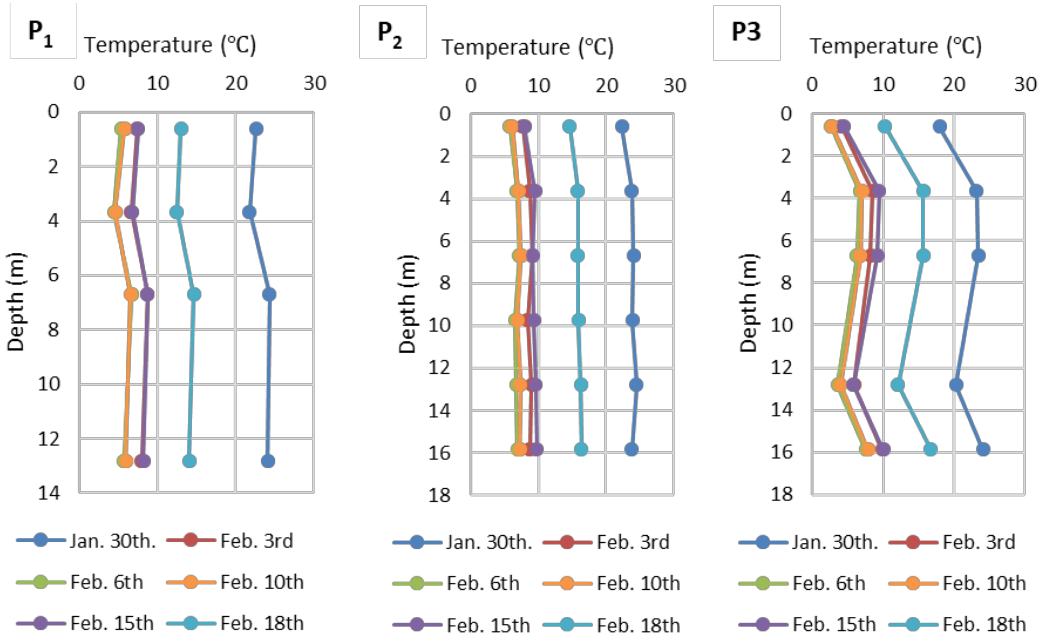

Figure 3.8. Temperature profile inside the 3 piles for 17 days heating mode

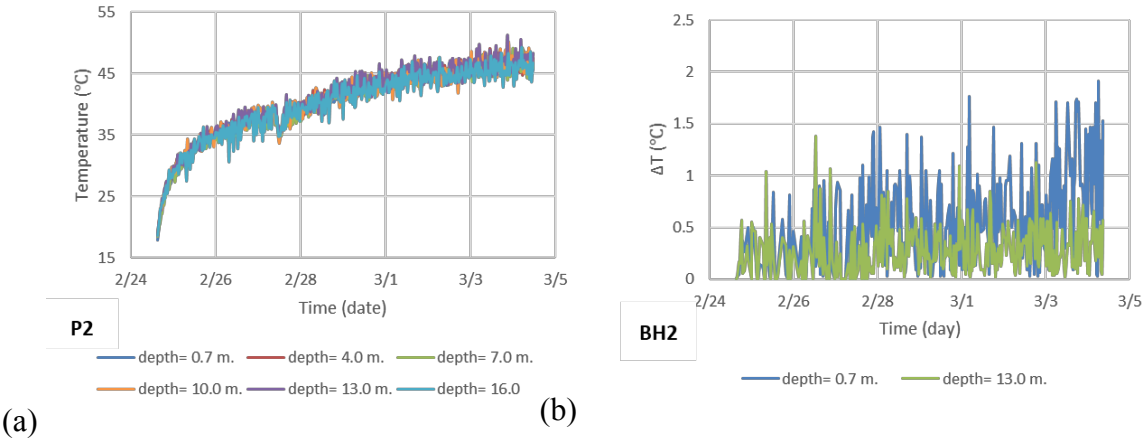

(a) (b)

Figure 3.9. (a) Pile #2 temperature variation during cooling mode and (b) borehole #2

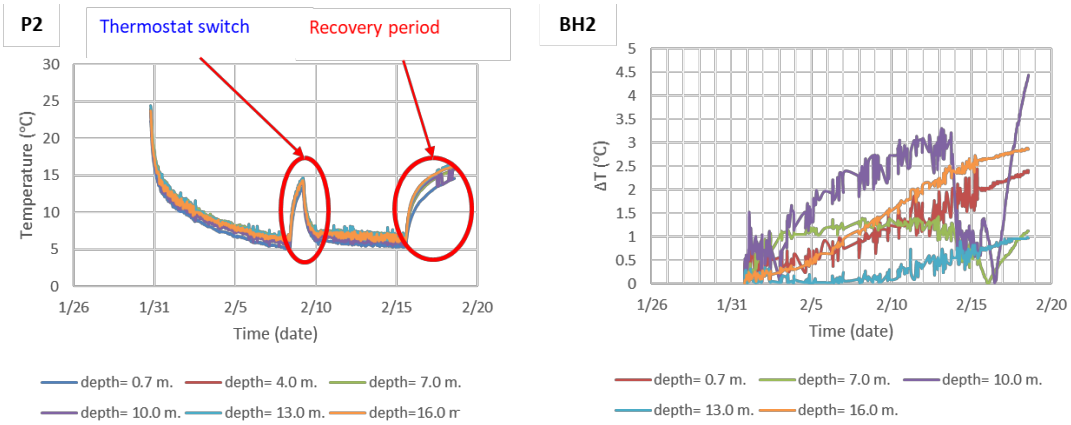

(a) (b)

Figure 3.10. (a) Daily pile #2 and (b) borehole #2 temperature during heating mode

Regarding the application of geothermal foundation systems in cooling dominated climate such as Texas, the increase in temperature in the soil mass over time during the cooling mode should be further studied to ensure that the system remains efficient for many years of operation without inducing any unseen foundation settlement.

3.3 Shrink-Swell: Temperature Controlled Condition

One of the methods used to understand the effect of temperature and in general thermal loading on clay soil was called temperature controlled free shrink test. Three different

temperature with the order of low, medium, and high were applied to the samples in temperature-controlled chambers located at McNew material lab at Texas A&M University. The free shrink-swell behavior of clay soil depends on several factors including water content variation and possibly temperature. In a geothermal foundation system due to temperature changes in soil natural condition, we may expect to observe water content fluctuations in the zones near piles and even inside soil mass for the long-term application.

Shrink-swell plot is a unique way of representation of the dependence of water content variation on volumetric strain regardless of temperature variation. This is one of the major motivations to run the temperature controlled free shrink test in which would give a better understanding of shrink-swell behavior of clay soil. However, this has to be noted that the initial expectation of this test's results would be to have the same trend on water content variation vs. volumetric strain but at possibly different rate. In other words, the shrink-swell limit plot is a unique feature for all kind of fine grain soil such as clay and the temperature effect of the rate of moving toward shrinkage or swelling will be focused on in this test (Figure 3.11a and Figure 3.11b).

(a)

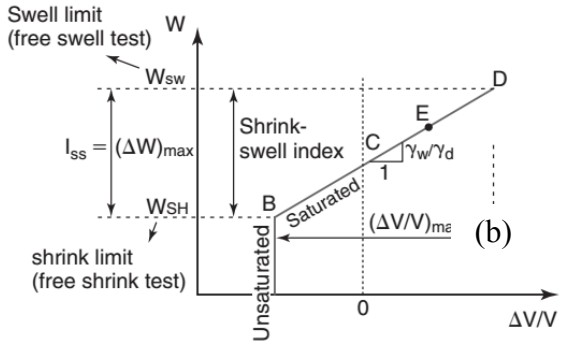

(b)

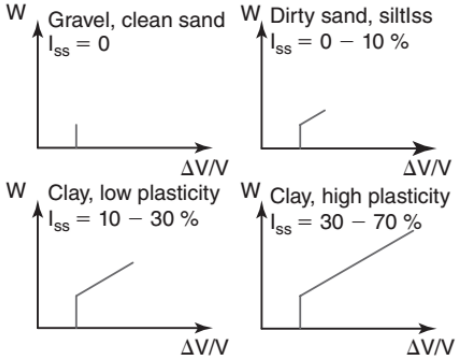

Figure 3.11. (a) Shrink-swell (Briaud, 2013); (b) different soil behavior (Briaud, 2013)

The shrink test consists of trimming a sample into a cylindrical shape, measuring dimensions (V) and weight (W) to determine the water content. The average water content can then be calculated by the following formula

$$\omega = \frac{\left(W_t - W_s\right)}{W_s} \tag{3}$$

In which, the W_s is the solid dry weight (oven and air dried), and the W_t is the sample weight at each time step. Then the volumetric strain is then written as

$$\dot{\varepsilon}_{vol.}^{mech} = \Delta V \Big/ V_0 = \frac{\left(V_t - V_0\right)}{V_0} \tag{4}$$

For the current test all these measurements were repeated for three temperatures.

3.3.1 Sample Preparation and Test Procedure

Porcelain clay is chosen to use in this test. The batch received from Austin Clay factory is in cube shape. Three samples are prepared with the dimension of $76.2\text{mm}\left(3"\right)$ and $38.1\text{mm}\left(1.5"\right)$ are shaped in cylinder. Then all the samples are placed on a light weight dish to be able to measure the sample's weight easier. At the start of each of the three different temperature, the weight and geometry will be measured. Geometry includes length (three ways) and dimeter (three ways) for each measuring time step. The time steps are based on hour intervals including: 0-0.5-1-2-3-4-6-8-16 and 24 hours. At the end of 24-hour period the water content will be measured for each sample.

Figure 3.12. Porcelain clay sample trimmed to the dimension.

3.3.2 Results

Results are presented in three plots of volumetric strain $(\varepsilon_{vol.})$vs. time in hours, water content $(\omega\%)$vs. volumetric strain, and water content $(\omega\%)$vs. time. Plots presented for the three temperatures from the low $(2.8°C)$, medium $(22.2°C)$, and high $(60°C)$.

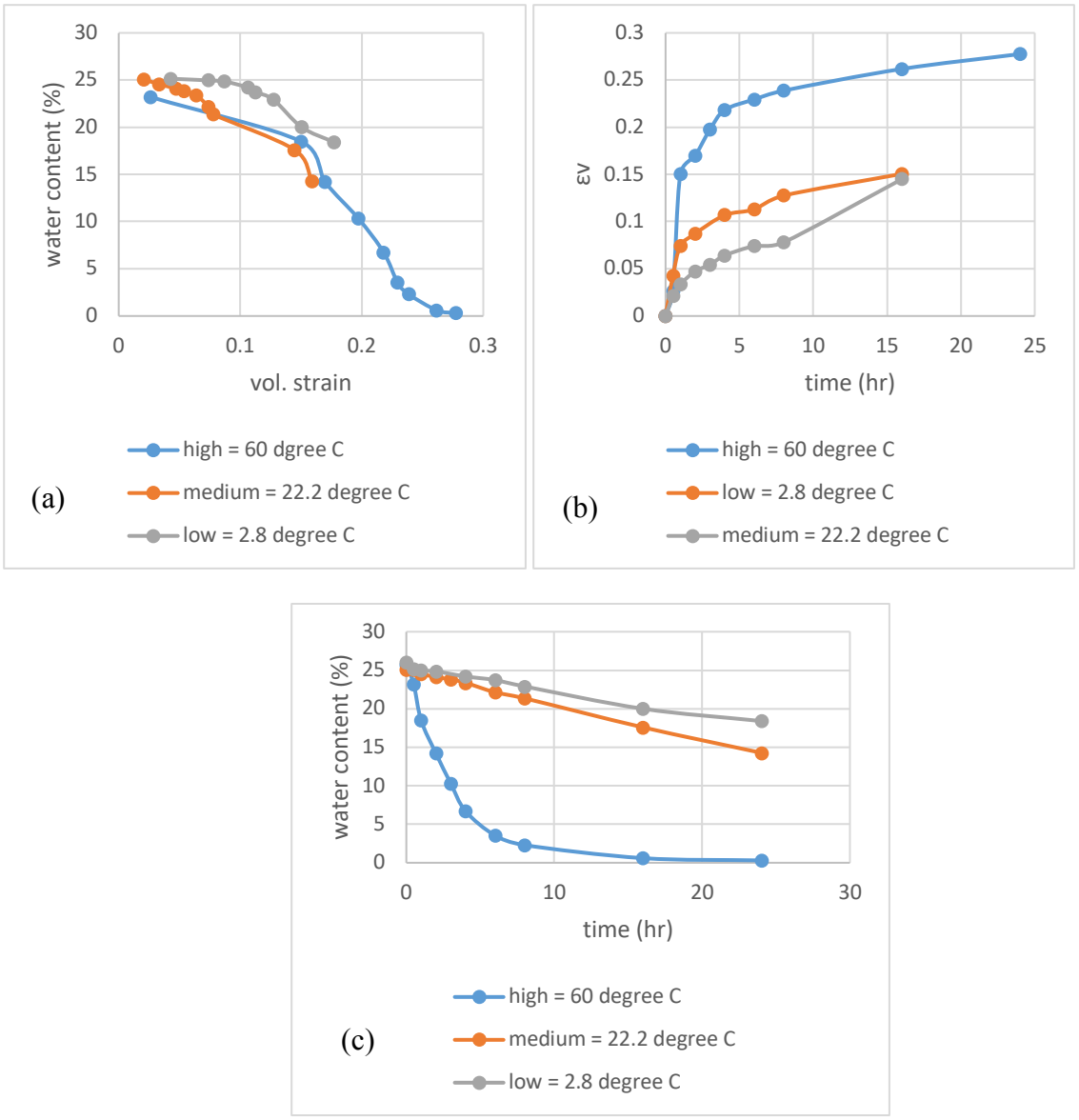

Figure 3.13. Temperature controlled free shrink test on porcelain clay, (a) water content vs. volumetric strain; (b) volumetric strain vs. time; and (c) water content vs. time.

3.3.3 Discussion of the results

These free shrink tests were conducted in a constant temperature chamber with a certain relative humidity and without the presence of any water that could enter the soil. The sample was not subjected to vertical loading or to any confinement. This preliminary lab work shows that the temperature has practically no effect on the relationship between the water content of the volumetric strain (Figure 3.13a) but does have an impact on the rate at which the water content

decreases (Figure 3.13c). These observations warrant the development of a full-scale numerical study, which would simulate the behavior of the soil mass as the temperature in the soil changes due to the use of geothermal foundation.

3.4 TAMUS RELLIS Campus: Model Scale Laboratory Test

To better understand the effect of thermal loading from the energy pile system on highly plastic clay soil, a model scale laboratory test was conducted on a remolded natural clay soil sample. The intention is to replicate the energy pile setup in scaled down level not element size. This prototype will encompass a slice of energy pile system setup for the purpose of studying the effect of the cyclic thermal loading by heating and cooling the soil on the heat/cold propagation, the shrink-swell, the short-term, and long-term pile settlement. This experiment will allow to study the effect of both heating and cooling on highly over-consolidated clay soil representing the single pile setup. The instrumentations and samplings will monitor the thermo-hydro-mechanical behavior of the system. The soil samples are taken from clay site at RELLIS (former Riverside) campus of Texas A&M University System (TAMUS).

3.4.1 Phase 1: Design and Drawings

The first step to design the experiment focused on selecting the proper sample size feasible to be made with respect to the clay soil properties in the RELLIS campus clay site. For the single pile installed in the experiment, a steel pipe with $762mm(30")$ diameter and $457.2mm(18")$ long were selected. The pile dimension within the pipe is $76.2mm(3")$ in diameter and $304.8mm(12")$ long; reinforced with a B7 rod $2.46mm(5/8")$ diameter. The thermal loops include two copper pipes with U-shape represents the supply and return part of a GSHP system.

There were two trials to take native clay soil samples out of the RELLIS campus clay site. However, both failed due to the insufficient amount of collected samples inside the pipe. After these two failures, it was decided to compact the native soil in the pipe in situ to 100%. There are four pad eye connections to bolt the bottom of the plywood to the bottom of pipe container, which are welded on the outer wall of the pipes while being positioned flushed with the bottom of pipes. The positioning of these four pad eyes are designed to be in the diagonal directions with respect to the centerline of the pipes. The pad eyes are drilled with 1 bolting hole with the diameter of $6.35mm$ and threaded all the way to provide support for 1 fully threaded steel bolt with 1 nut tightening the top contact of bolt and pad eye.

3.4.2 Phase 2: Instrumentations

Three different types of instrumentations were used for this experiment:

1. Mechanical sensors, which monitors the soil movement, will be telltale rod type. Telltale rods are designed to be placed in 2 separate locations with various depths; one with length of $0.1778m\left(7"\right)$, anchored at $0.1524m\left(6"\right)$, and the other one with length of $0.3048m\left(12"\right)$, anchored at $0.2794m\left(11"\right)$. At each telltale location, the LVDT sensors are placed on the flat top of the nails. The LVDTs will then be connected to the laptop through the data acquisition box. The nails are steel heavy duty from McMaster-Carr. One iron angle arm cross over each other to provide the support for magnetic base of the LVDTs.
2. Load cell, with the ultimate nominal capacity of $9\text{kN}\left(2000\text{lbf}\right)$ by Interface. Figure 3.14 shows the calibration setup of the load cell.

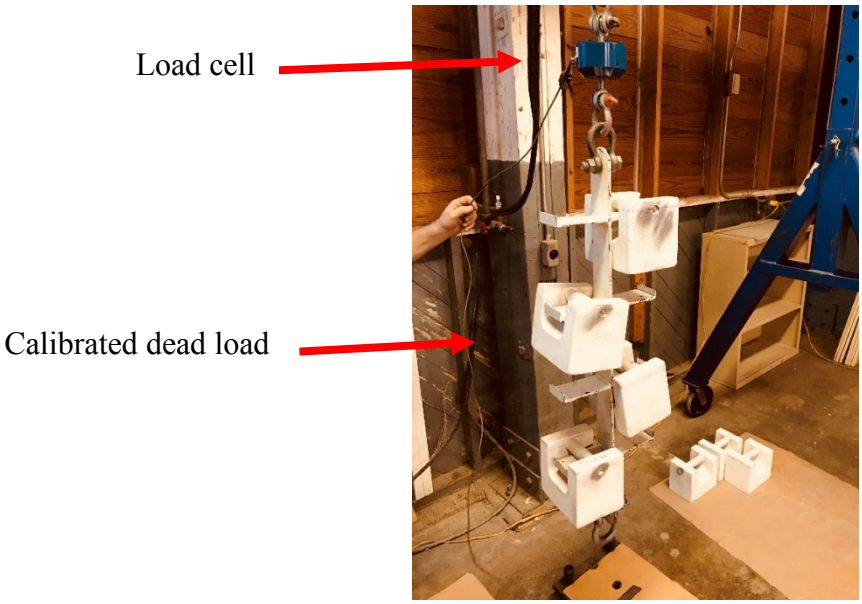

Figure 3.14. Calibration of the 9kN (2000 lbf) load cell by accurate dead weight

3. 16-channel data logger by Lakewood System is used to record the thermistor's readings. This specific data logger was also modified to synch with the load cell to record a very accurate history of load variation within the range of applied tension load for both of the testing procedures.
4. The thermal sensors monitor the development of temperature inside the energy pile and soil mass. Each thermistor string has two measuring points on them. The total number of 5 strings and 10 measuring points were embedded within the pile and soil mass. One string was installed inside the grout and attached to the copper pipe and the B7 rod in the pile with the spacing of $0.3048m\left(12"\right)$as shown in Figure 3.15 and Figure 3.16. The other four strings were installed inside the soil mass surrounding the pile. The spacing for thermistors inside the soil is $0.254m\left(10"\right)$and $0.127m\left(5"\right)$.

Figure 3.15. Installed the instrumented pile at the center of the sample.

3.4.3 Phase 3: Energy pile construction and installation of instruments

The B7 fine threaded rod will not be embedded up to the bottom of grout. Once the pile construction is done, the grout was left to dry up for 7 days. During this time, all the other instrumentations in their respective locations were installed. The telltale rods are installed by drilling a hole to their desirable depths and anchoring the nails to the bottom of the holes. Each nail is covered with Vaseline to reduce the friction between the nail's wall and the soil. The thermistor sensor's holes will be filled with very fine sand once the strings are installed and the LVDTs were then placed on the top of the two telltales.

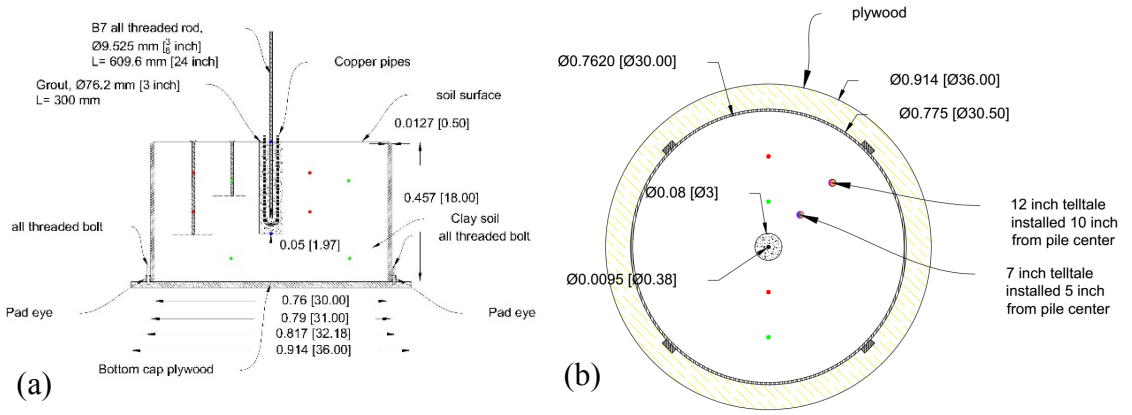

Figure 3.16. (a) Cross section view and (b) plan view for the single pile setup

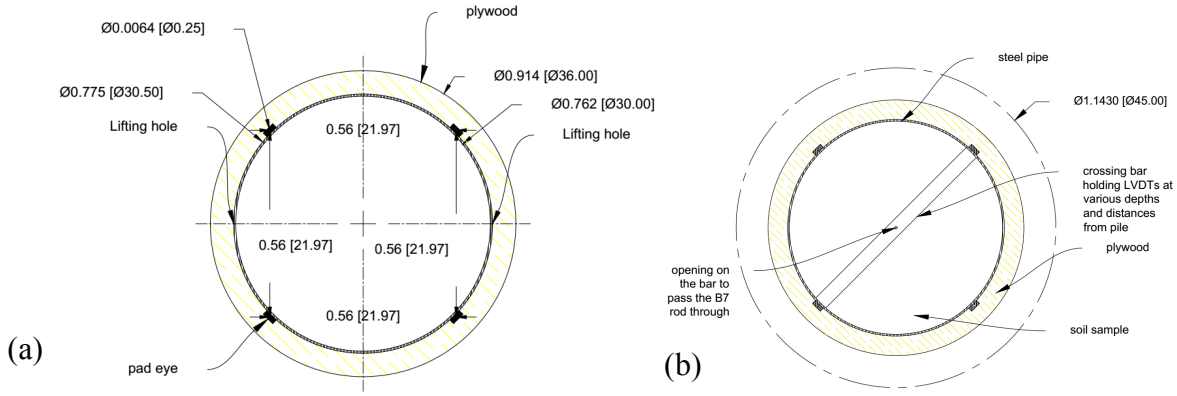

Figure 3.17. (a) Pad eyes and lifting holes positioning; (b) the beam plan view

a. All units are in meters with inches in brackets unless otherwise is mentioned.
b. Thermistors are manufactured in a string type.
c. The minimum spacing between each sensor provided by Geokon is 127mm.
d. In order to reduce costs toward the thermistors installation, the number is reduced.
e. The square plywood for both pipes will be cut in circle shape.
f. The all threaded bolts for both cases will be tied down with nuts.
g. The all threaded bolts will be screwed down only half way through the plywood.

Telltale rods @ depth = 177.8 mm

Telltale rods @ depth = 304.8 mm

Pad eyes connection. 1 bolt

Thermocouples placed at different depths

Telltale rods

Figure 3.18. Legends associated with the details of test setup for single pile case.

The test setup for the group pile case couldn't be built due to the restriction in the geometry of the pipe, piles, and the load testing mechanism.

3.4.4 Heating and Cooling System

In order to provide a reliable system to provide hot and cold water circulating within the pile's copper loop, two separate heating and cooling system were designed and built. The two systems are combined with a single five-gallon construction bucket as the fluid's reservoir. The bucket is insulated with Styrofoam to prevent the heat or cold loss. The circulating hoses are separated in two parts, one for the circulation of hot or cool water through the soil loop, and one for the circulation of water between the reservoir and cooling machine (Figure 3.19).

The reason to use copper pipes as the thermal loops inside the pile was to provide the fastest way of transferring heat or cold into the grout and the soil. The copper pipe has high thermal conductivity and is a great choice for the current application. Heat carrying fluid is distilled water. A digital temperature control box was used to measure the water temperature inside the reservoir. The control box was also used to set the target temperature for the heating cycle, in which will adjust the start and shut off time of the heater. For the cooling cycle, the thermocouple probe connected to the control box will only be used to monitor the water temperature in the reservoir, as the cooling system possess its own internal temperature sensor. The details of how each component is connected to one another are shown in Figure 3.19 and Table 3.1. The ambient temperature of the room is controlled by a single AC unit. Due to the poor insulation condition and the gaps within the doors and windows, the ambient temperature changes a lot because of the hot summer weather.

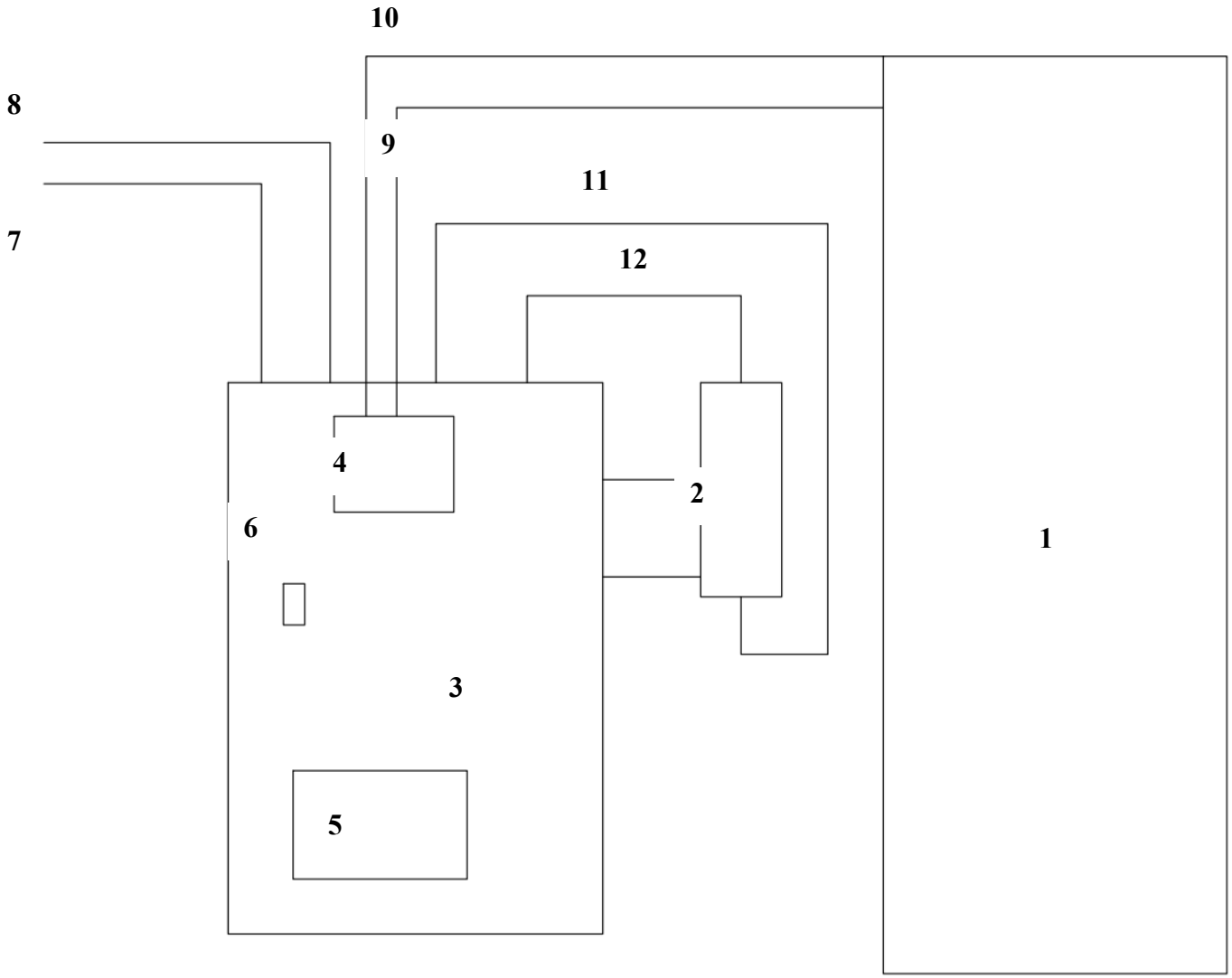

Figure 3.19. Complete schematic of heating and cooling system.

Table 3.1. Heating and cooling system components description

Part Number	Description
1	Water cooling system - a water fountain retrofitted
2	Water heater - based on a 1500 W car heater
3	Insulated water reservoir - five-gallon construction bucket
4	Cold water circulation pump for the cooling system – upper pump
5	Hot water circulation pump for the cooling system – Soil loop pump
6	Thermocouple sensor to monitor the water temperature in reservoir
7	Soil loop supply line
8	Soil loop return line
9	Cold water supply line to the cooling system
10	Cold water return line to the cooling system
11	Hot water supply line to the cooling system
12	Hot water return line to the cooling system

3.4.5 Remolded Soil Properties

The soil profile and characterization are very well defined through works done by Ballouz et al. (1991) and Briaud (2000) as it is shown in Figure 3.20.

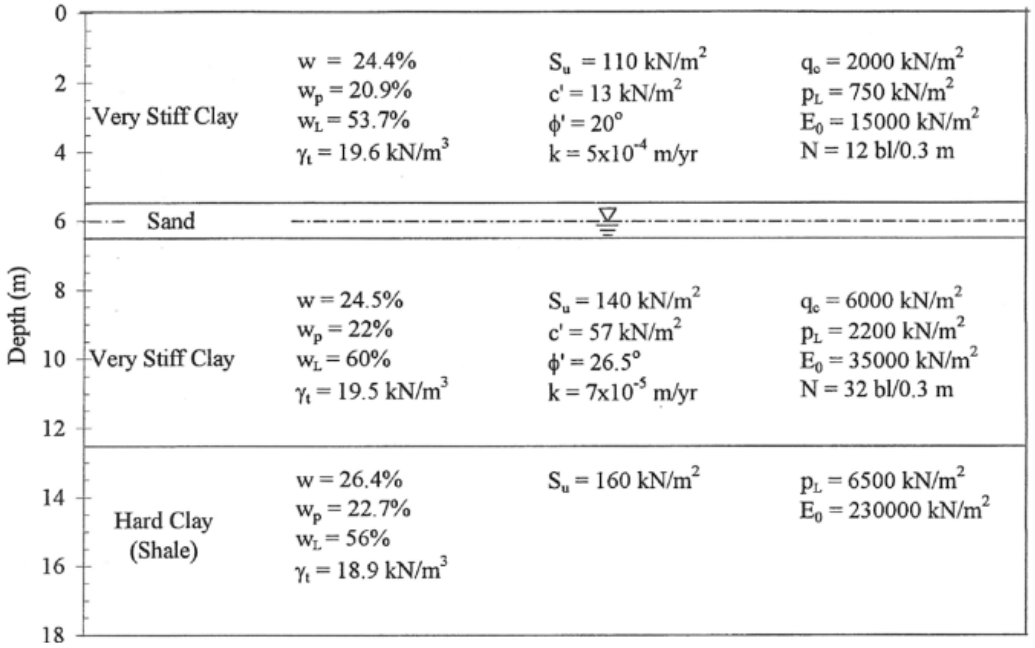

Figure 3.20. RELLIS campus clay site soil profile (Briaud, 2000)

The soil is a remolded sample built and compacted inside the pipe. The soil is taken from the excavated depth of $1.83m\left(6'\right)$, and then the compactor is used to compact the soil until there is no room inside the pipe to compact the soil. The compactor type was the vibratory plate compactor from KNT KHP with 65 HP and a flat base plate with the surface area of $610\times610mm\left(24\times24"\right)$. It can compact an area of $0.53\text{m}^2\left(5.7\text{ft}^2\right)$.

The in-situ tests performed on the sample were small shear vane, pocket penetrometer, density, and water content. The mini vane shear test showed 110kPa for the undrained shear strength and the Pocket Penetrometer Test (PPT) measured $363.89\text{kPa}\left(3.8\text{tsf}\right)$ for the unconfined compression strength. Additionally, the water content samples were taken to analyze the variation of water content, while the outside weather changes affecting the moisture level in the soil.

During the sample preparation, water content samples at each compaction layer (Table 3.6), mini vane shear, and pocket penetrometer to measure the in-situ condition of the remolded sample. The Intercomp wheel load weigher, model PT300 was used to measure the weight of the sample to calculate density of the remolded soil inside the pipe. Table 3.2 shows the calculation steps for density of the remolded sample.

Table 3.2. Density calculation details for the remolded sample.

Remolded Soil Density Calculation									
Sampling depth (in)	depth (ft.)	pipe diameter (in)	pipe length (in)	pipe diameter (ft.)	pipe length (ft.)	pipe diameter (m)	pipe length (m)	$W_{empty\ pipe + plywood}$ (lbs.)	$W_{soil + pipe + plywood}$ (lbs.)
74.5	6.21	30	18	2.5	1.5	0.762	0.4572	170	1040
W_{soil} (lbs.)	$W_{empty\ pipe + plywood}$ (kg)	$W_{soil + pipe + plywood}$ (kg)	W_{soil} (kg)	Volume (in^3)	Volume (ft^3)	Volume (m^3)	Density ($lbs./ft^3$)	Density (kg/m^3)	Density ($tones/m^3$)
870	77.11	471.73606	394.62536	12723.45	7.3631078	0.2085	118.15663	1892.68765	1.892687646

3.4.6 General Observations and Adjustments

During the testing process, several issues were noticed and adjustments were done accordingly. Initially, the angle arm setup to place the LVDT sensors for pile top and soil vertical displacement were placed directly on the concrete floor. The issue which was noticed later during the data reduction, was due to the fact that because the resolution of displacement magnitude (e.g. $0.01mm$) is very low, the concrete slab displacement interferes with the measurements of pile top displacement. The angle arm was then welded to the pipe's walls to prevent such interference with the pile top displacement recordings by the LVDT.

Although the reservoir and all of the supply-return lines are carefully insulated, due to occasional ambient temperature from AC failures, the water temperature circulated through soil supply line drops by an average value of $5°C$.

The load transferring cable is a parachute cord able to sustain up to $550lbs$ of weight. This limit brings enough strength to put on dead load up to the pile failure.

One interesting observational technique was to take water content samples from the native soil at the location of excavation at arbitrary time. It was done during the period of making the sample and after that, which gave direct information of how the water content changes once the soil is exposed to the outside temperature. By looking that the Table 3.3, it can be interpreted that for example at the depth of $1.07m(3.5')$the water content from November 20, 2017 to November 28 doesn't change. It should be noted that the surface was completely exposed to the outside temperature. Same for the depth $0.6096m(2')$ and $1.2192m(4')$, the water content stays constant for the span of one week and two days, respectively. Our explanation for this result is that because of the existence of the water table in the soil and the very high suction, the thermal

loading by energy pile will not affect the water content and consequently doesn't cause shrinkage.

Table 3.3. Water content sampling results from clay site at RELLIS campus

Action	Date	$W_{container}$ (gr)	$W_{wet\ soil + container}$ (gr)	$W_{dry\ soil + container}$ (gr)	$W_{wet\ soil}$ (gr)	$W_{dry\ soil}$ (gr)	water mass (gr)	water content (%)
CS - d=3.5ft	11.20.17	101	236.3	222.8	135.3	121.8	13.5	11.08
CS - d=2ft	11.20.17	133.4	264.2	250.1	130.8	116.7	14.1	12.08
CS - d=3.5ft	11.28.17	133.4	250.2	238.7	116.8	105.3	11.5	10.92
CS - d=2ft	11.28.17	135.3	368.2	343.8	232.9	208.5	24.4	11.70
CS - d=4ft	11.28.17	134.1	260.3	246.6	126.2	112.5	13.7	12.18
CS - d=4ft pipe sample	11.30.17	134.1	193.2	186.3	59.1	52.2	6.9	13.22
CS - d=3.5ft	12.15.17	1	35.3	29.9	34.3	28.9	5.4	18.68
CS - d=6ft	12.15.17	1	27.3	22.9	26.3	21.9	4.4	20.09
CS - d=7'3"	12.15.17	1	30.9	25.9	29.9	24.9	5	20.08

3.4.7 Testing Procedure

The model-scale laboratory test aims to study the effect of thermal loading cycle on the water content variation (i.e. shrink-swell), the ultimate pullout capacity, creep rate, and temperature propagation in soil. One of the challenges to overcome for this scale of testing setup is to find the most accurate and sustainable loading mechanism on the pile. The applied tension pullout load on the pile must encompasses the following features:

1. Stay constant for the long duration of the mechanical and thermal loading.
2. Load increment matches with the overall capacity of the single pile.

The test was performed in a controlled climate room to minimize the effect of temperature and relative humidity fluctuations on testing procedure. In order to make sure the applied tension load has the above criteria; two testing procedures were performed:

1. Displacement control (3.4.8).

2. Load control (3.4.9).

The following sections will discuss the details of the two procedures taken, along with their respective results and discussion over them.

3.4.8 Displacement Control

3.4.8.1 Testing

The displacement-controlled method was achieved with the help of a tightening nut placed on the top of the pile. Turning the nut will generate the displacement and as a result the applied tension load is achieved (Figure 3.21).

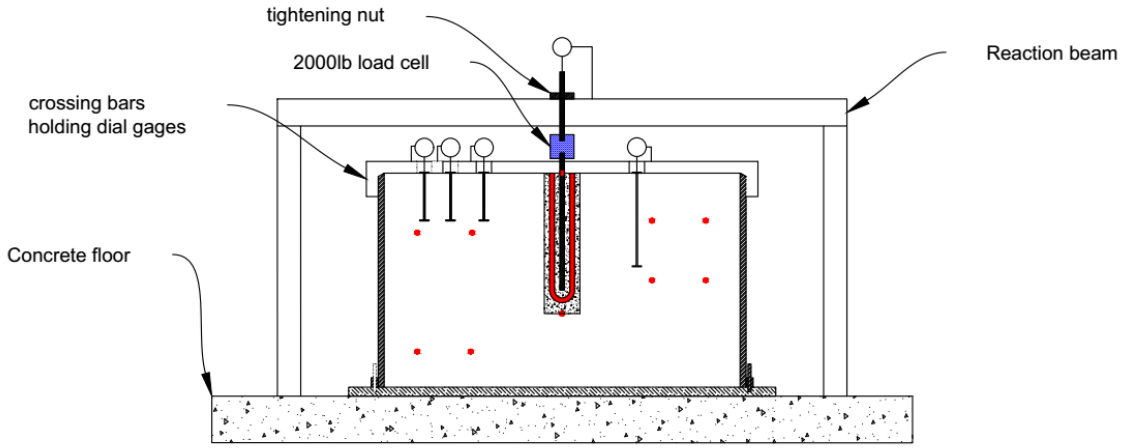

Figure 3.21. Load test setup for the displacement-controlled method for single pile case

In this method, the reduction of the load is monitored in which it represents the relaxation of stress. Results from this round of testing include load reduction evolution for both mechanical and heating cycle, log-log load vs. time, temperature variation for both pile and soil vs. time.

3.4.8.2 Results

The log-log plot of the normalized applied tension load vs. time as shown in Figure 3.23 shows the trend of load reduction during the mechanical only and thermo-mechanical loading. The mechanical loading only was started on January 30, 2018 with the maximum recorded tension load as $3.411kN\left(766.84lbf\right)$until February 11, 2018 with the minimum tension load of

$1.743kN\left(391lbf\right)$. The heating mode initiated after the induced tension load was increased to $2.21kN\left(500lbf\right)$ and was continued until February 27, 2018. The minimum monitored tension load at the end of the thermo-mechanical loading was $0.414kN\left(93.07lbf\right)$.

Since the nature of this round was inducing fixed displacement to generate the tension load, the relaxation "n" value can be calculated as the slope of the line for both of the loading parts. Figure 3.24 demonstrates the results of the calculations for the relaxation "n" value. The general equation used to calculate this parameter can be written as

$$\left(\frac{L}{L_0}\right)=\left(\frac{t}{t_0}\right)^{-n} \tag{5}$$

$$n_{relax}=-\frac{\log\left(L/L_0\right)}{\log\left(t/t_0\right)} \tag{6}$$

The L is the current applied load (i.e. depending on the type of loading), L_0 is the initial state of either applied load or state of load (i.e. depending on the type of loading), t is the current time, and t_0 is the initial time. Since for this test there are two different type of loading applied on the pile, the calculations of the relaxation "n" value is different for each part.

For the mechanical loading only the, the L and L_0 will be the loads read from the start of the test. However, for the thermo-mechanical portion, the L_0 will be the load recorded at the end of the mechanical loading only portion and the L is the current state of the monitored tension load on the pile. The t_0 for the thermo-mechanical stays the same as the initial time used in mechanical loading only. As shown in Figure 3.24 the effect of the thermal loading on relaxation "n" value.

Based on the calculation for the relaxation "n" parameter, during the mechanical loading only, the n value shows the maximum of 0.041 and the minimum value of 0.022, while with the hearing process activated, the relaxation parameter starts at 0.044 and ends at about 0.167. There is however, a sudden drop in recorded tension as shown in Figure 3.22 from February 7th, 2018 until the day of starting the heating mode on February 11th, 2018.

There was no activity regarding the testing procedure during this period of time and this anomaly might be due to either the data logger and load cell read out box connection malfunction or any outside disturbance by the passing the individuals in the lab space. Nevertheless, before starting the heating process all the parts and status of sensors, load cell, data logger, and dial gage readings were checked to make sure of no disturbance in the monitoring.

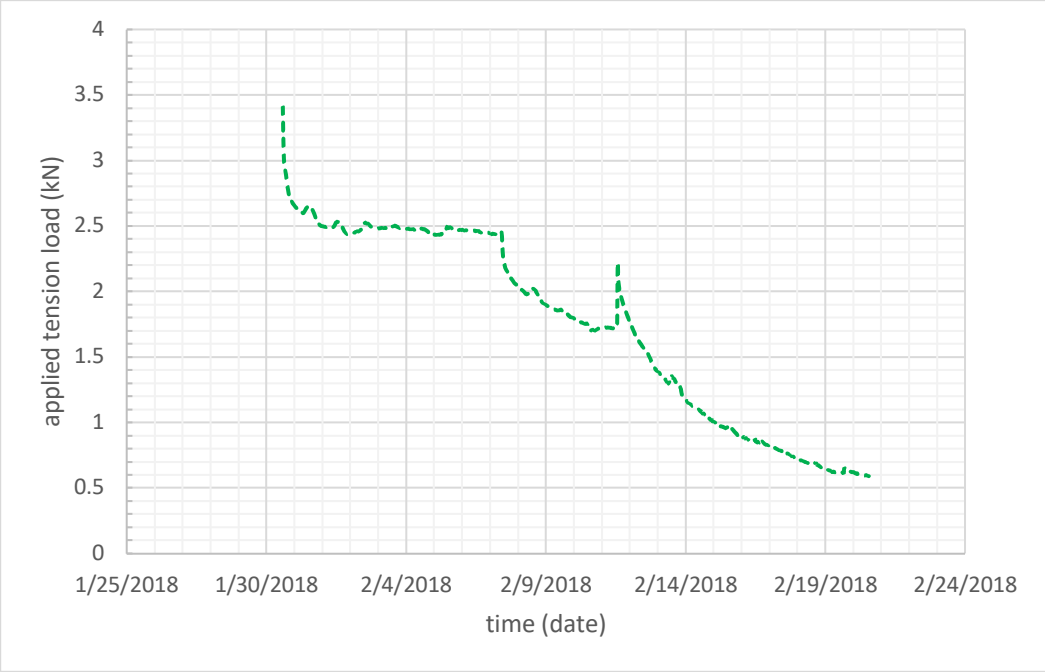

Figure 3.22. Tension load vs. time for mechanical and thermo-mechanical loading

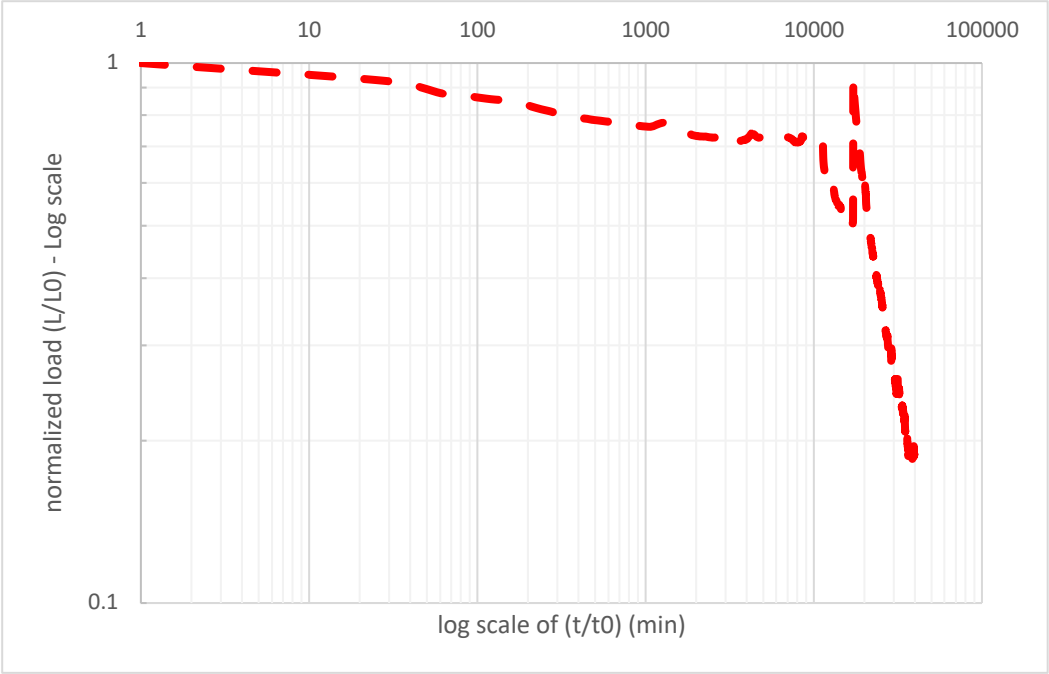

Figure 3.23. Normalized load vs. time for thermo-mechanical loading (log-log scale)

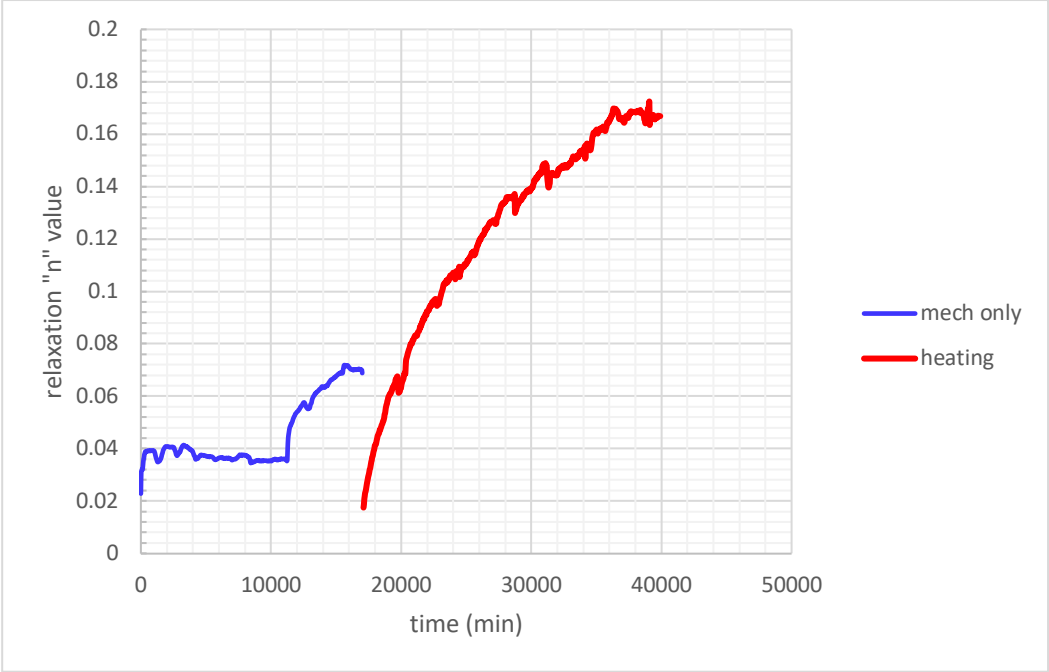

Figure 3.24. Relaxation “n” value vs. time for mechanical and heating process

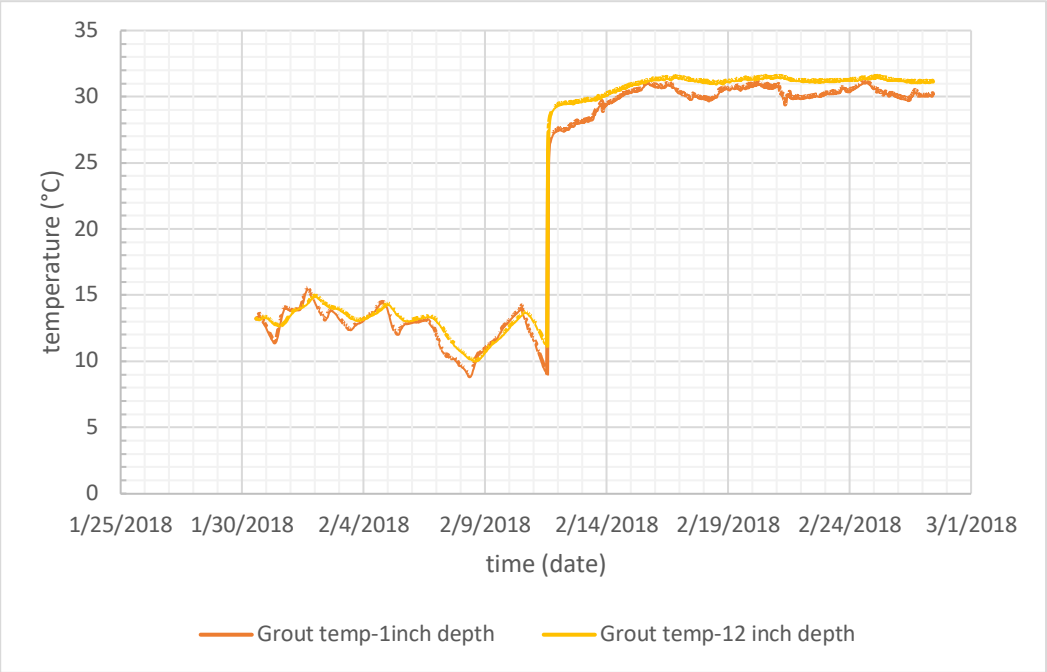

Figure 3.25. Temperature evolution vs. time in grout.

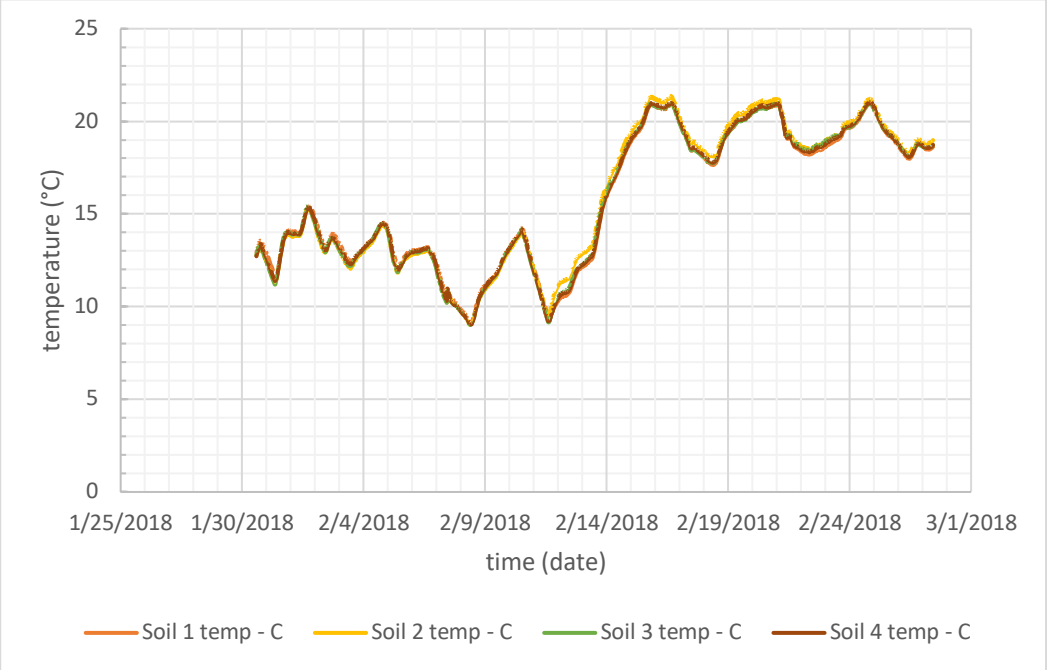

Figure 3.26. Temperature evolution vs. time in soil.

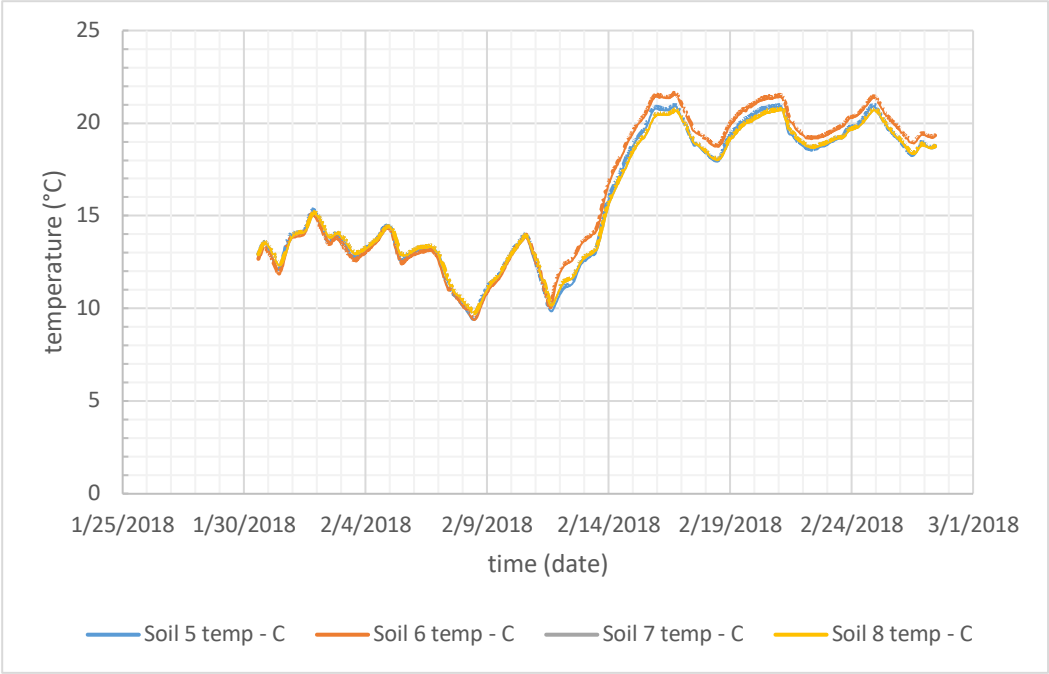

Figure 3.27. Temperature evolution vs. time in soil.

3.4.9 Load Control

In this method, the load is held constant and the displacement on the pile is monitored as a function of time (Figure 3.28). During this testing procedure, the applied load is kept constant increasing at $22.6796kg\left(50lbs\right)$increments. The load transferring mechanism is designed to double the amount of dead weight being applied on the pile top in the ideal frictional condition. However, due to the pulley's imperfection friction condition, this doubling of applied load was not observed. The pile displacement is measured by a fixed plate with two bolts on each side at a close space to the bottom of the load cell. The methodology used in this setup includes the following steps:

1. Performing incremental tension mechanical load only.
2. Heating and cooling process while holding the mechanical load.
3. Monitoring water content, temperature, soil and pile top displacement.

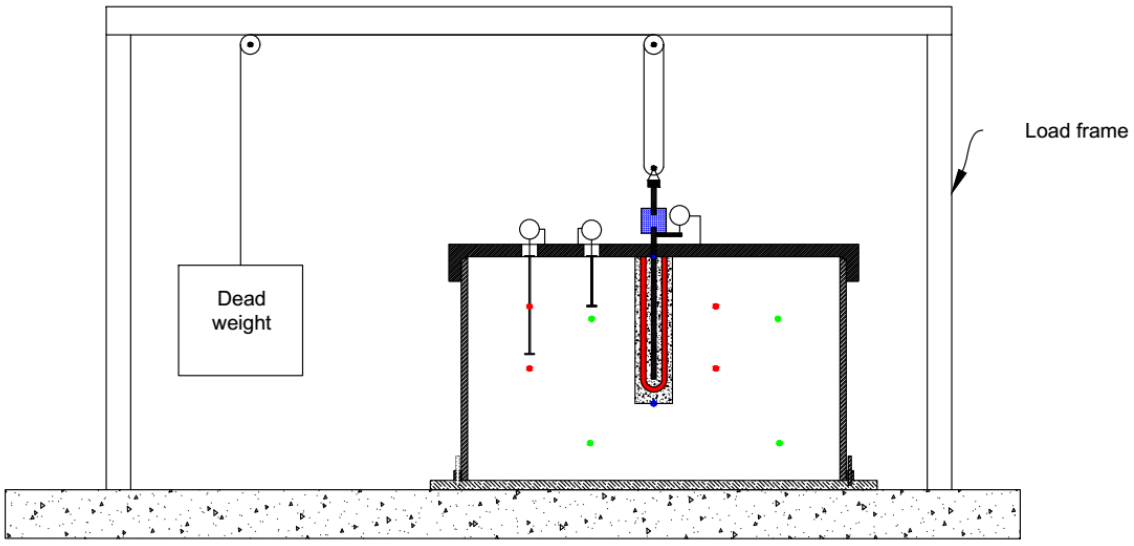

Figure 3.28. Load test setup for the load-controlled method for the single pile case.

3.4.9.1 Testing

The following timeline describes the details of each stage of the testing (Figure 3.29). At each stage, the $22.6796kg\left(50lbs\right)$increment was added on top of the existing load and the unloading or resting times was not done. Readings from LVDTs are reset at the start of each change in load and heating/cooling process. Additionally, as a general note from now on to the end of the large-scale laboratory section, the mechanical only refers to the loading condition that only mechanical load was applied, the heating refers to the condition that heating cycle applied while the mechanical load was held constant, and the cooling refers to the condition that heating cycle applied while the mechanical load was held constant. Every stage starts with one day of applying mechanical loading only, then followed by heating for one day, and finally the heating was stopped and cooling cycle starts for another day.

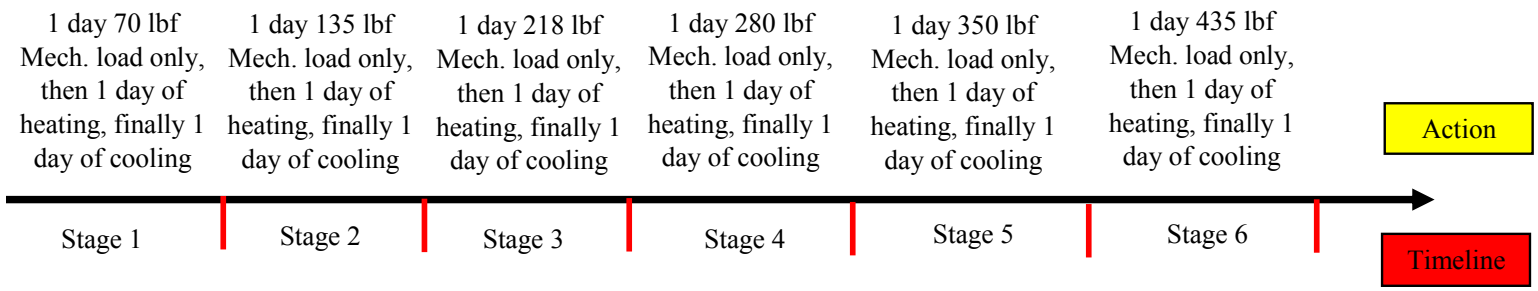

Figure 3.29. Testing timeline with the details of loading condition for each stage of the test.

Table 3.4. Round 2 of the load control testing details for every stage

Round 2			
Stage	Applied dead load (lbs.)	Applied tension load (lbf)	Applied tension load (kN)
1	50	70	0.311
2	100	135	0.6
3	150	218	0.97
4	200	280	1.245
5	250	350	1.557
6	300	435	1.935

Table 3.5. Data logger configuration of the thermistors for load control test

Thermistor string number	Data logger channel	Distance from the pile (in)	Distance from the pile (m)	Depth (in)	Depth (m)
1	3	10	0.254	0	0
	8	10	0.254	10	0.254
2	4	5	0.127	0	0
	9	5	0.127	10	0.254
3	1	5	0.127	0	0
	6	5	0.127	5	0.127
4	2	10	0.254	0	0
	7	10	0.254	5	0.127
5	5	-	-	0	0
	10	-	-	12	0.3048

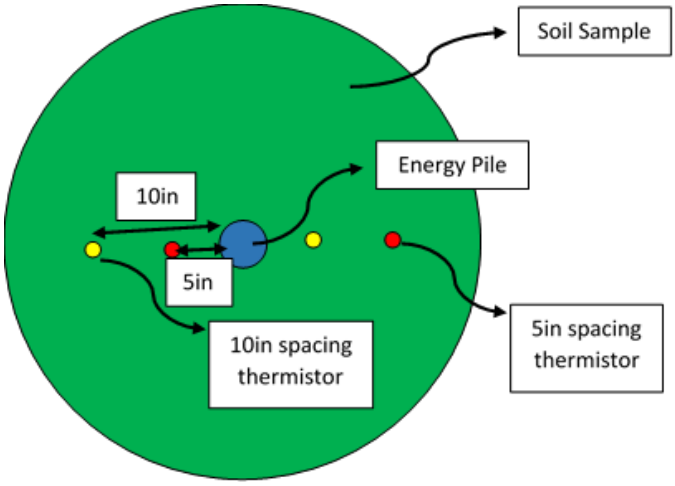

Figure 3.30. Graphical schematic of the thermistor's setup inside the soil

The load control testing in what we called round 1 started with the following execution plans. At each load step, the mechanical load is initially held for one-week period, then the heating starts while maintaining the mechanical load constant for another one week, and finally the heating is switched to the cooling cycle again while having the mechanical load constant for one week.

Continuous measurements of the pile top displacements, the soil vertical displacement at two depths of $0.1778m(7")$ and $0.3048m(12")$, and the temperature evolution in soil and grout were made. The measurement interval was set to be every 30 minutes.

During the round 1 testing, after three load steps it was noted that the reading of the pile top displacement vs. time doesn't represent the actual displacement of the pile top. On the contrary, the readings indicated that instead of having instant large displacement at the time of applying the load and then creep movement as time goes on, there was continuous displacement recorded on any step of the loading condition. After reviewing all the reduced data for the pile

top displacement as well as the calculated creep "n" values, it was found that the angle arm which is anchored into the concrete floor doesn't behave as a stiff and stable settlement beam for the magnetic base of the LVDT on the pile top. Since the range of displacement recorded are so small, the explanation for such anomaly is that the concrete slab deformation was also factored in the recordings of the sensor.

This issue was then solved by welding the two sides of the angle arm to the pipe, which will provide the solid and stiff platform for the magnetic base of the LVDTs. The round 1 went up to $68.0389kg\left(150lbs\right)$dead weight and it stopped to make the proper adjustments to the instrumentation system. Once these corrections were made, the so-called round 2 started from the $22.6796kg\left(50lbs\right)$load with the same load increasing strategy as the round 1. However, for this round the mechanical load will only be applied for one day, then heating process starts for another one day while the load is constant, and finally the cooling for one day with the constant load applied on top. After the initial data reduction for the round 2 testing, the issue of slab deformation effect on pile top displacement is resolved.

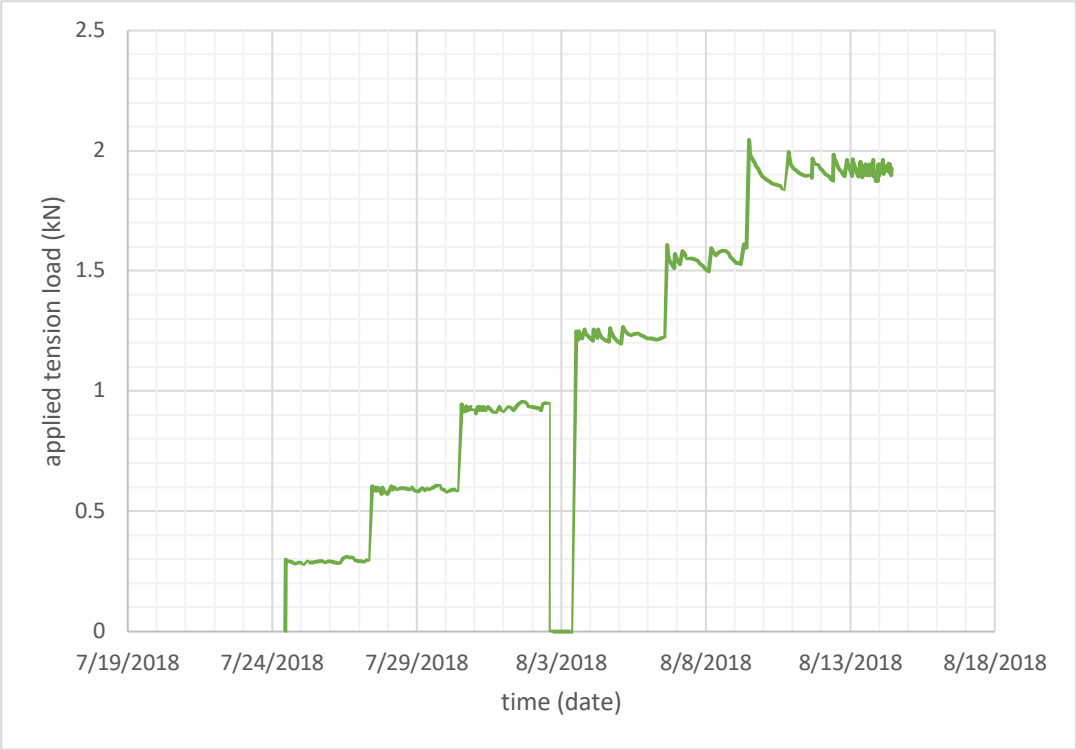

Figure 3.31. Applied tension load (kN) vs. time for round 2 of testing

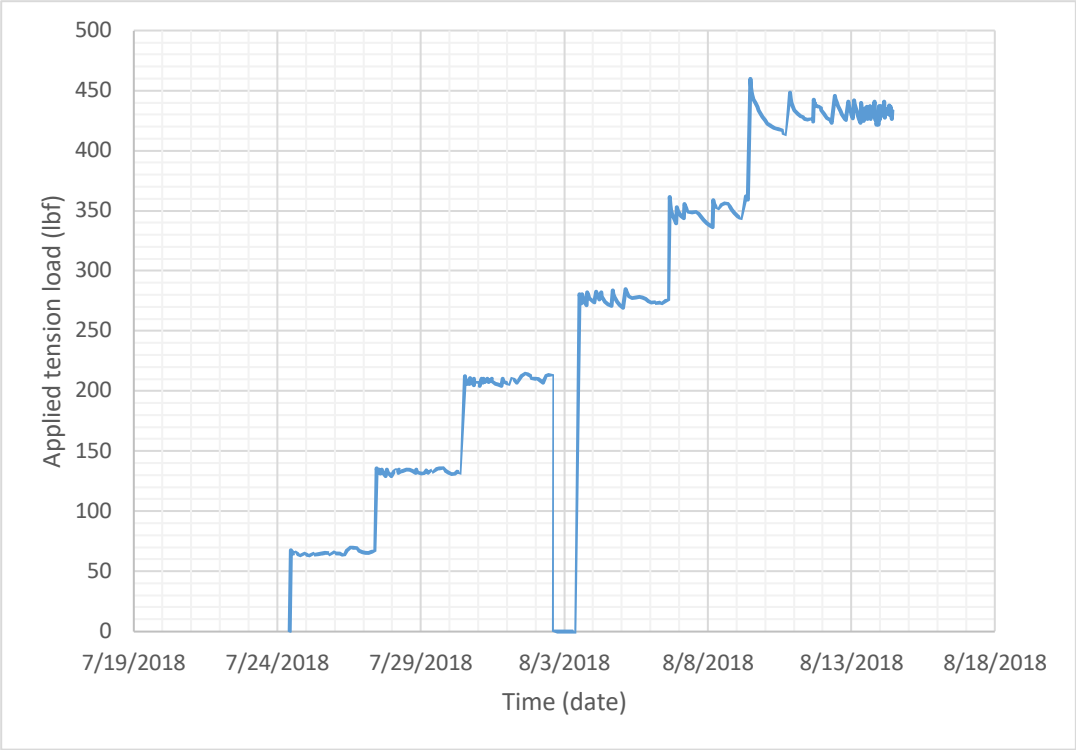

Figure 3.32. Applied tension load (lbf) vs. time for round 2 of testing

3.4.9.2 Shrink-Swell with Heating-Cooling Cycle

One of the first concerns regarding the application of geothermal foundation in a high plastic clay, is the shrink-swell issue especially when the soil goes under additional cyclic thermal loading. The literature and background understanding of shrink-swell consideration under mechanical loading only condition is very well documented. However, the cyclic thermal loading could pose unseen impacts on the shrink-swell behavior of high plastic clay. During the test in the first round, since the duration of heating and cooling cyclic was seven days, the water content measurements were done at the start and end of each process. By tracking the water content variation in the soil, the shrink-swell occurrence could be identified. The location of sampling was chosen in a way to avoid the impact of ambient temperature in the room.

Since the entire test in the round 2 started from the beginning, none of the displacement recordings are valid to use. However, during the round 1 at the end of each heating period, water content of the soil in the pipe was measured at a point $0.127m(5")$ from the pile center and at the $0.2159m(8.5")$ depth. The water content measurements are used to discuss the possibility of the energy pile application on shrinkage of high plastic clay soil. Table 3.6 shows the evolution of the water content throughout each loading condition over time.

As it can be seen the water content doesn't get affected significantly by the cyclic thermal loading, therefore the soil shrink-swell problem will not be influenced. This is a very important findings within the framework of the application of geothermal foundation system in high plastic clay.

Table 3.6. Water content measurements over time for shrink-swell analysis

Action	Date	$W_{container}$ (gr)	$W_{wet\ soil\ +\ container}$ (gr)	$W_{dry\ soil\ +\ container}$ (gr)	$W_{wet\ soil}$ (gr)	$W_{dry\ soil}$ (gr)	water mass (gr)	water content (%)
Sample preparation	04/16/18	1.5	120.3	101.4	118.8	99.9	18.9	18.91
	04/16/18	2.5	116.5	98.7	114	96.2	17.8	18.50
	04/19/18	134.7	308.6	281.2	173.9	146.5	27.4	18.70
Heating	05/15/18	134	183.1	176.2	49.1	42.2	6.9	16.35
Heating	05/15/18	135.2	224	210.2	88.8	75	13.8	18.4
Heating	06/25/18	134.6	159.8	155.7	25.2	21.1	4.1	19.43
Cooling	07/03/18	134.6	158.7	154.9	24.1	20.3	3.8	18.72

3.4.9.3 Heat Propagation

The thermistor sensors are installed in a radial setup with two distances from the pile on both sides $0.127m(5")$ and $0.254m(10")$ (Figure 3.30). According to Table 3.5, there are two spacing between each measuring points at the $0.127m(5")$ and $0.254m(10")$. Figure 3.33 shows the temperature evolution over time for each heating and cooling cycle at the surface and bottom

of the pile. Figure 3.34 and Figure 3.35 both show the temperature variation inside the soil at depth of $0.127m(5")$ and $0.254m(10")$.

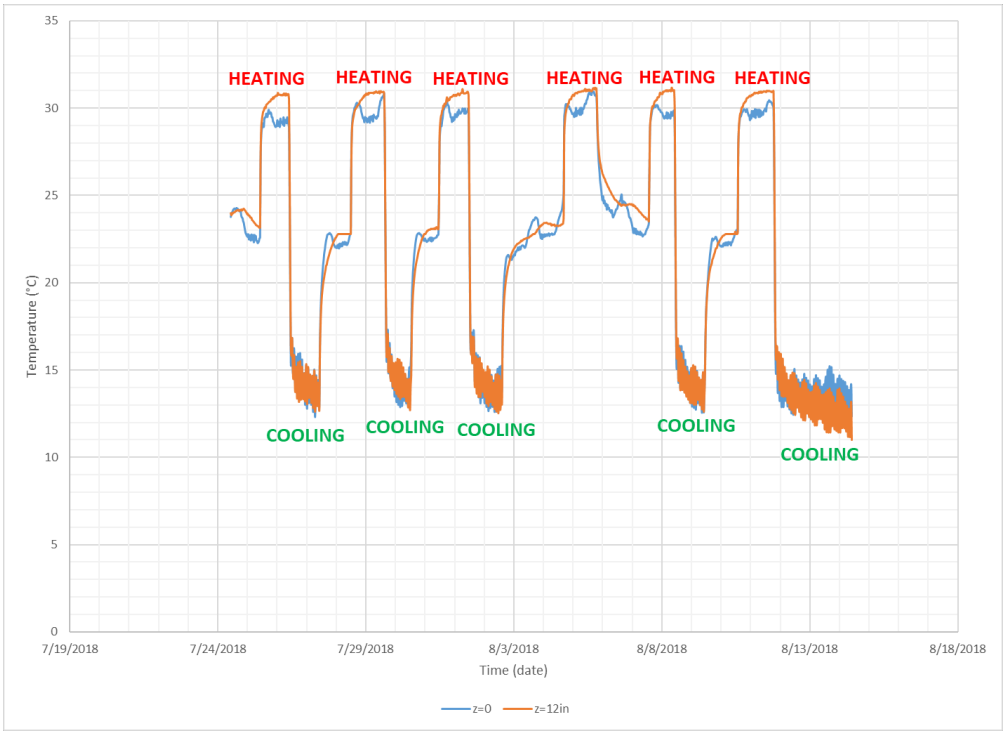

Figure 3.33. Temperature evolution inside the energy pile under cyclic thermal loading

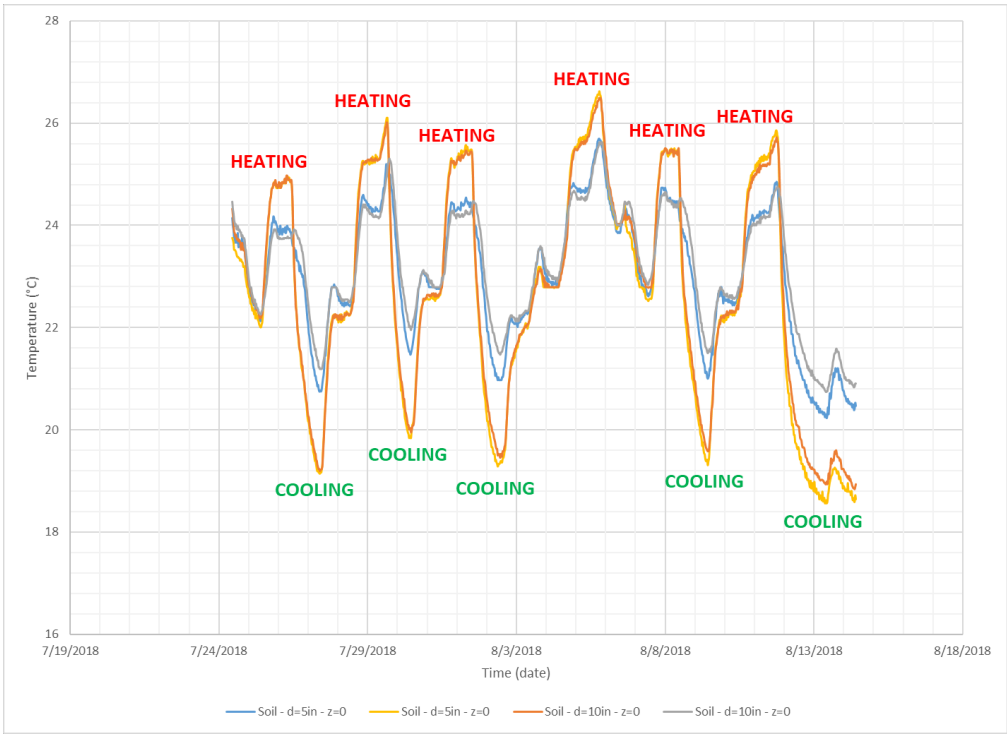

Figure 3.34. Temperature evolution inside the soil

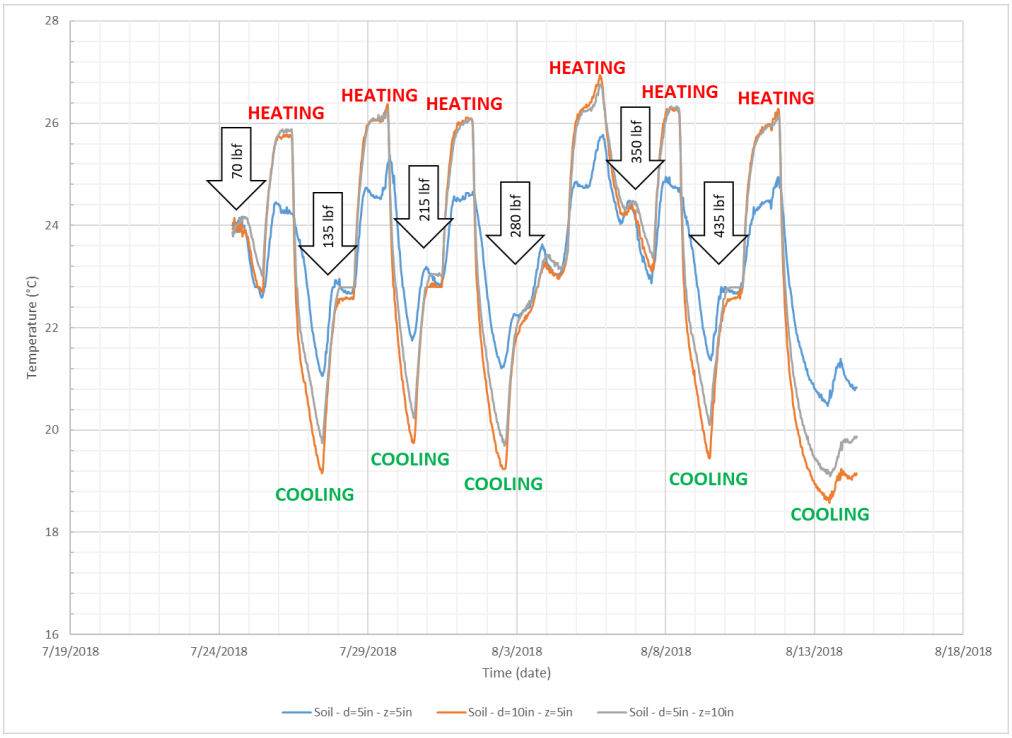

Figure 3.35. Temperature evolution inside the soil (continued)

3.4.9.4 Creep "n" Value

One of the critical focus of the round 2 testing was to investigate the influence of the thermal cyclic loading on the creep "n" value of the clay soil. Traditionally, the creep analysis will be done by holding the applied load (either in tension or compression) on top of the pile, while recording the induced displacement for a short period of time (e.g. few hours). However, in order to properly track the impact of the thermal cyclic loading on the pile, the extent of the applied load (i.e. mechanical or thermal) should be long enough to let the thermal load propagates in the soil. As stated in section 3.4.9.1, the duration of mechanical loading only, heating, and cooling was set to be one day for round 2 of the testing. The creep "n" value was calculated based on the following equation

$$n = \frac{\log\left(S/S_0\right)}{\log\left(t/t_0\right)} \tag{7}$$

The S_0 is the initial pile top displacement reading after 30 minutes of applying the load during the mechanical only condition; the S is the pile top displacement at any time during either mechanical only, heating, or cooling condition; the t_0 was set to stay constant for all of the stages in round 2 equal to 30 minutes; and the t is the time since the start of each stage. Figure 3.36 to Figure 3.41 demonstrates the pile top displacement vs. time for each stage up to the pile failure. Also, based on the formulation demonstrated above for the calculation of the creep "n" value, Figure 3.43 to Figure 3.47 shows the creep "n" value back calculated at each stage under various loading condition.

In the Figure 3.39 and Figure 3.46 which demonstrate both of the pile top displacement vs. time and the calculated creep "n" value at stage 4, the cooling cycle didn't happen due to a mechanical issue with the cooling system's internal tubes. For this reason, there is no record of cooling cycle for the stage 4 of the load control test.

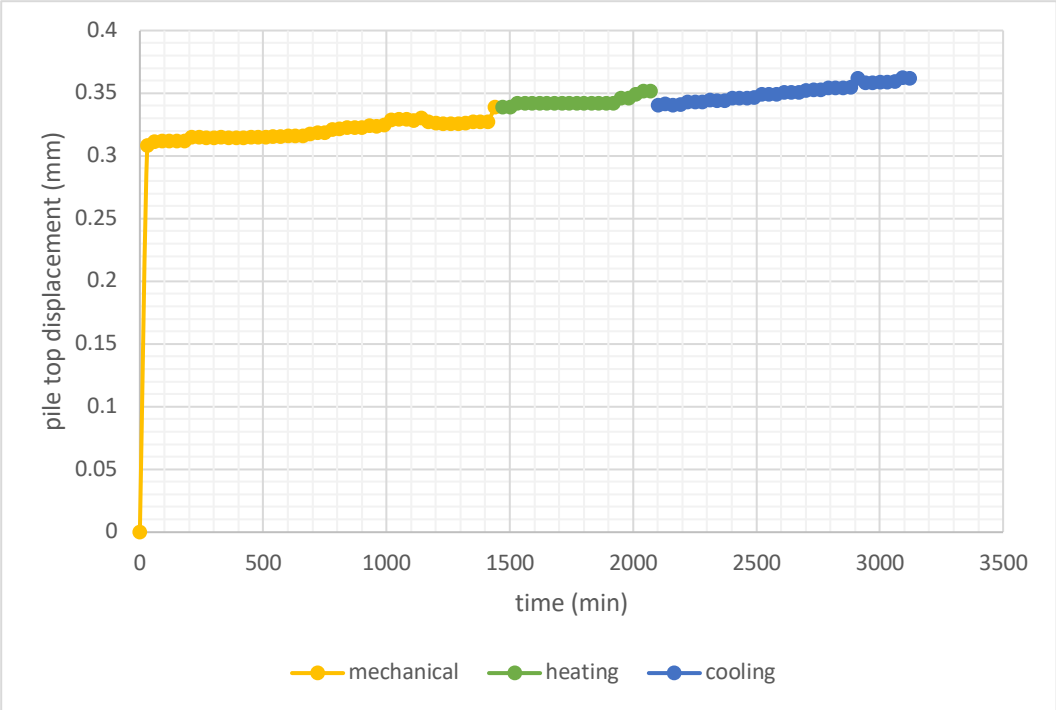

Figure 3.36. Pile top displacement vs. time for stage 1 load under various condition

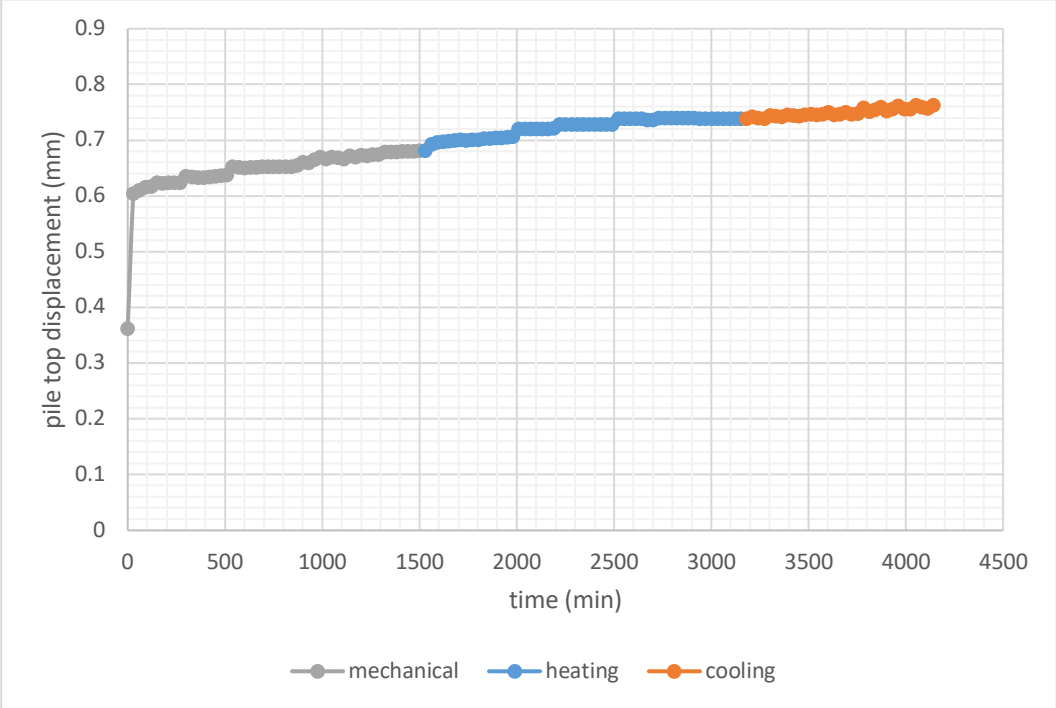

Figure 3.37. Pile top displacement vs. time for stage 2 load under various condition

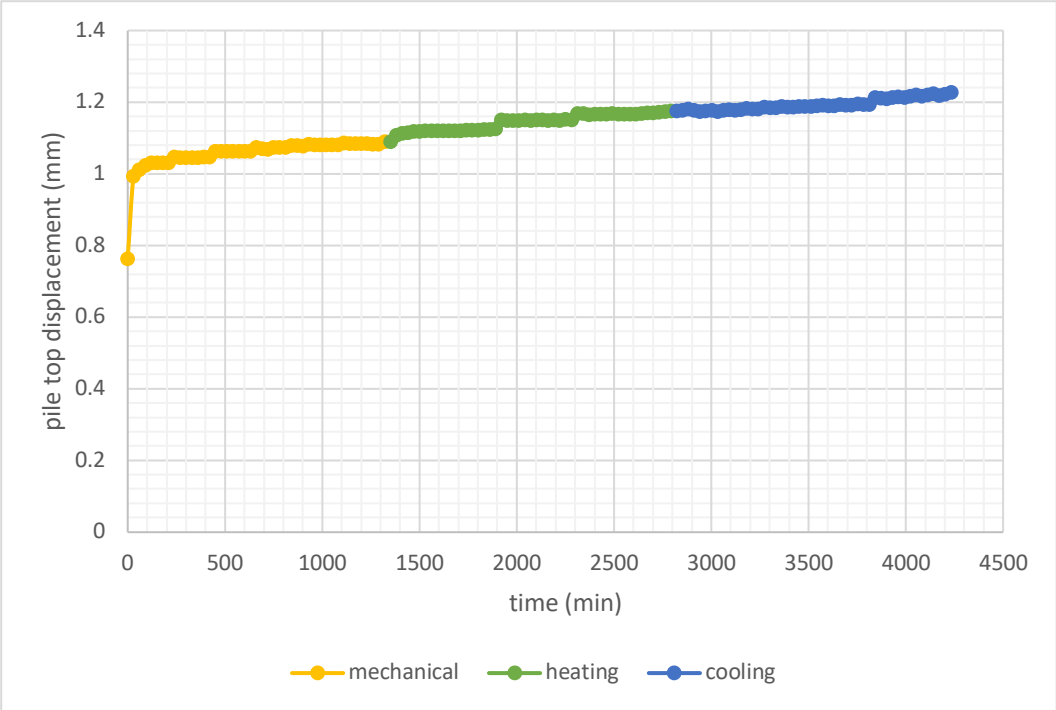

Figure 3.38. Pile top displacement vs. time for stage 3 load under various condition

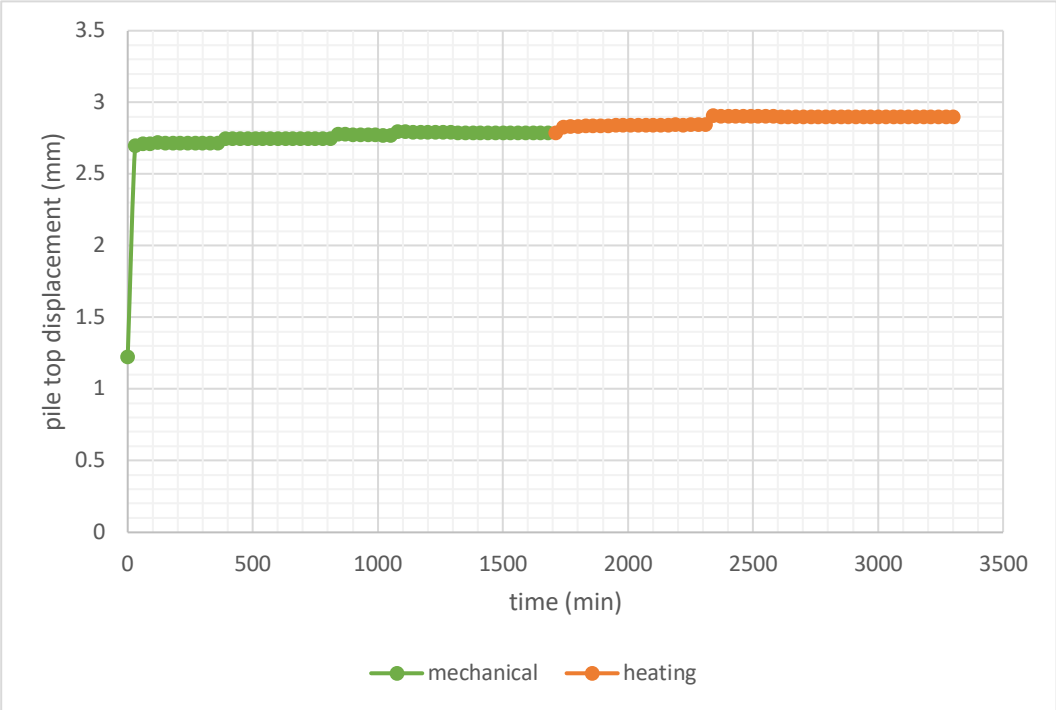

Figure 3.39. Pile top displacement vs. time for stage 4 load under various condition

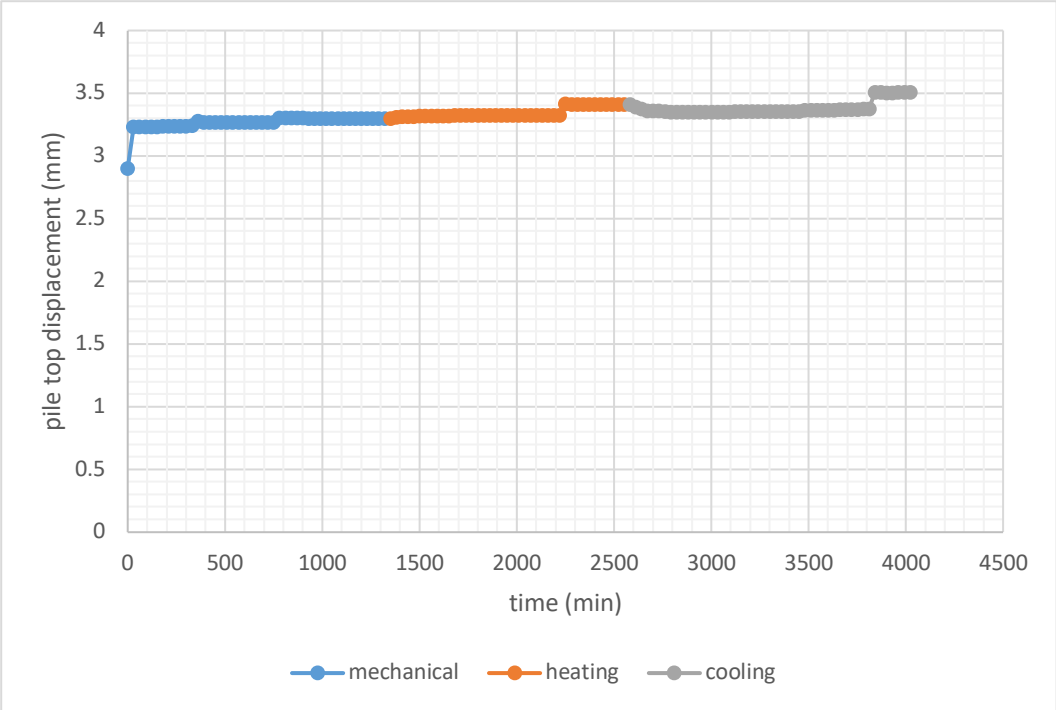

Figure 3.40. Pile top displacement vs. time for stage 5 load under various condition

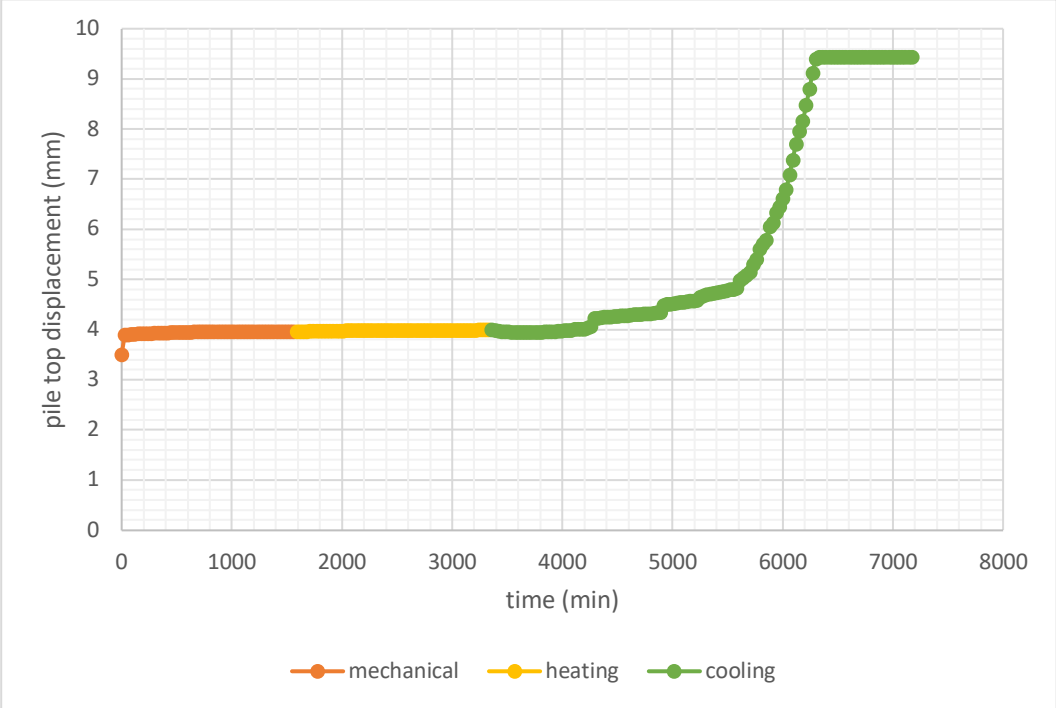

Figure 3.41. Pile top displacement vs. time for stage 6 load under various condition

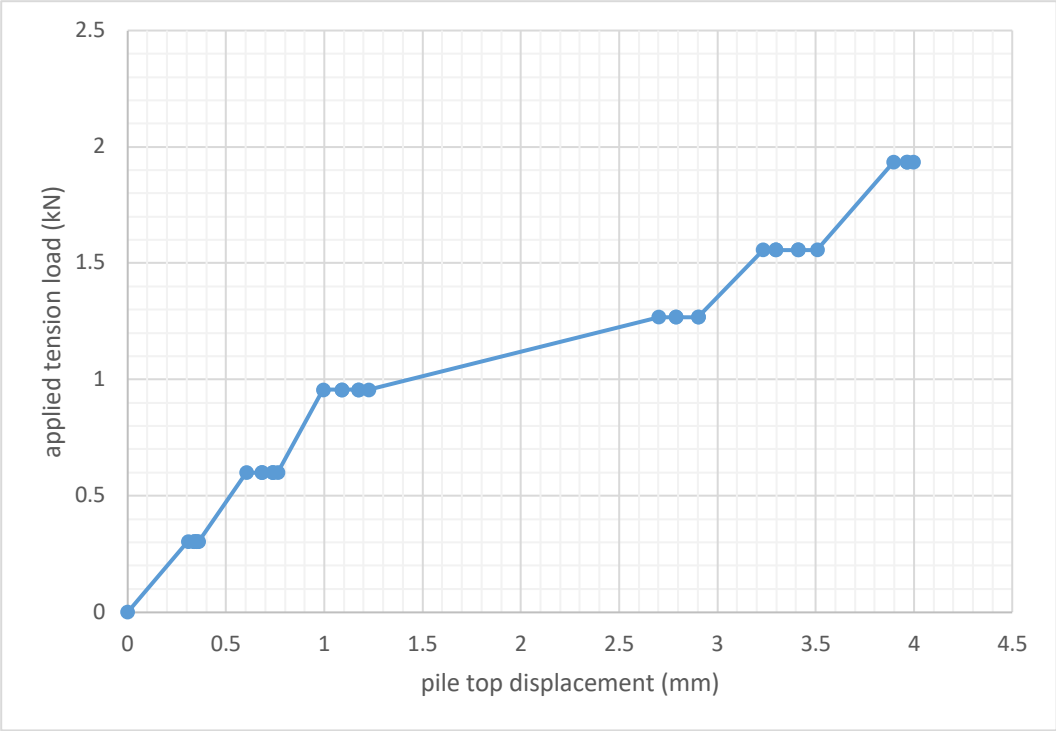

Figure 3.42. Load vs. displacement for the round 2 of the load control test

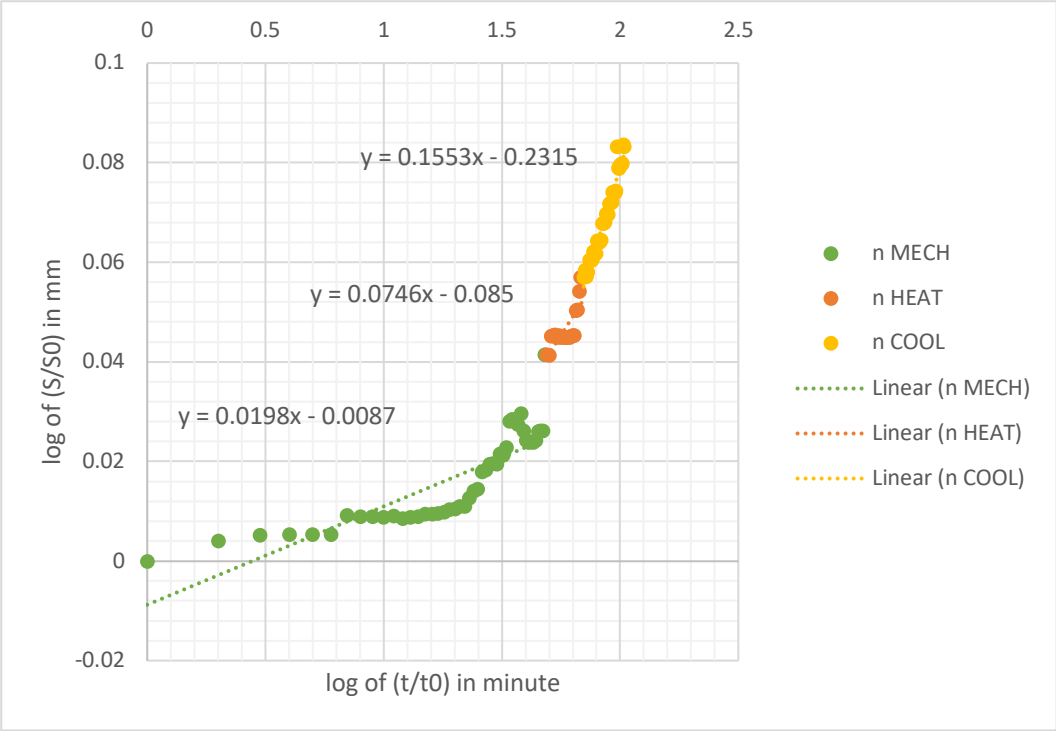

Figure 3.43. Creep "n" value variation under various loading condition at stage 1

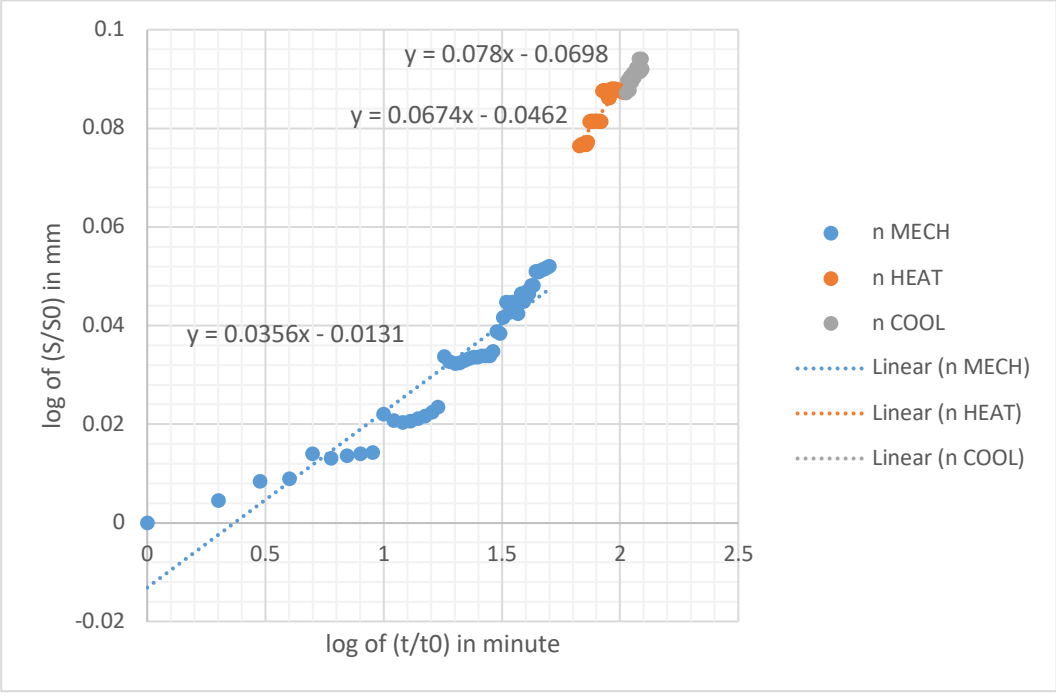

Figure 3.44. Creep "n" value variation under various loading condition at stage 2

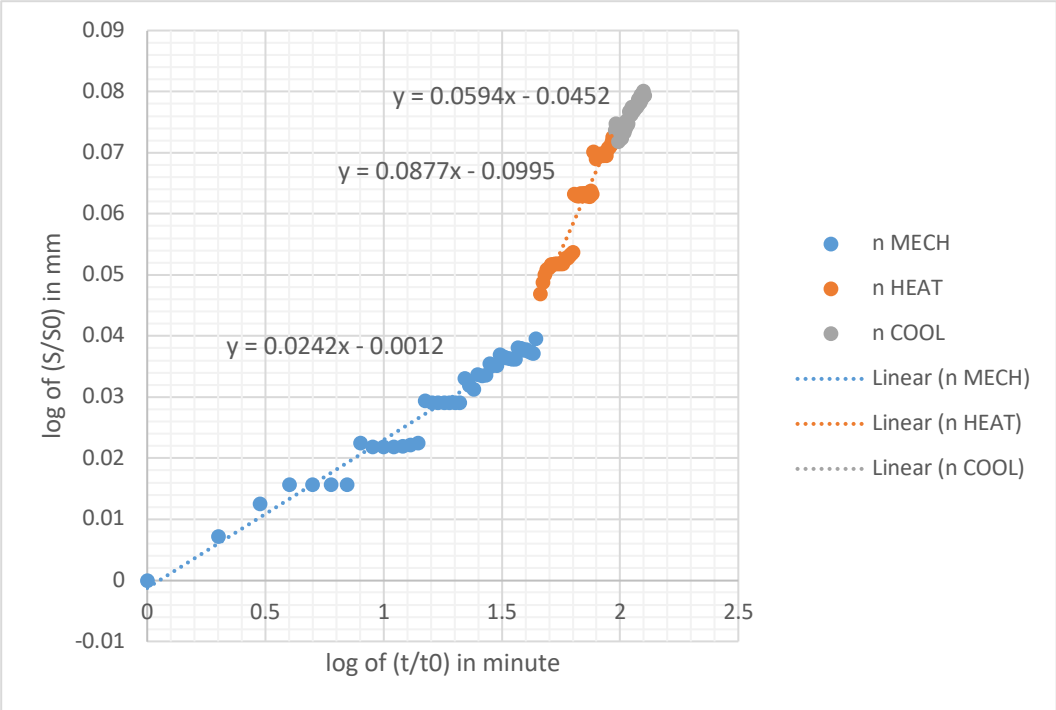

Figure 3.45. Creep "n" value variation under various loading condition at stage 3

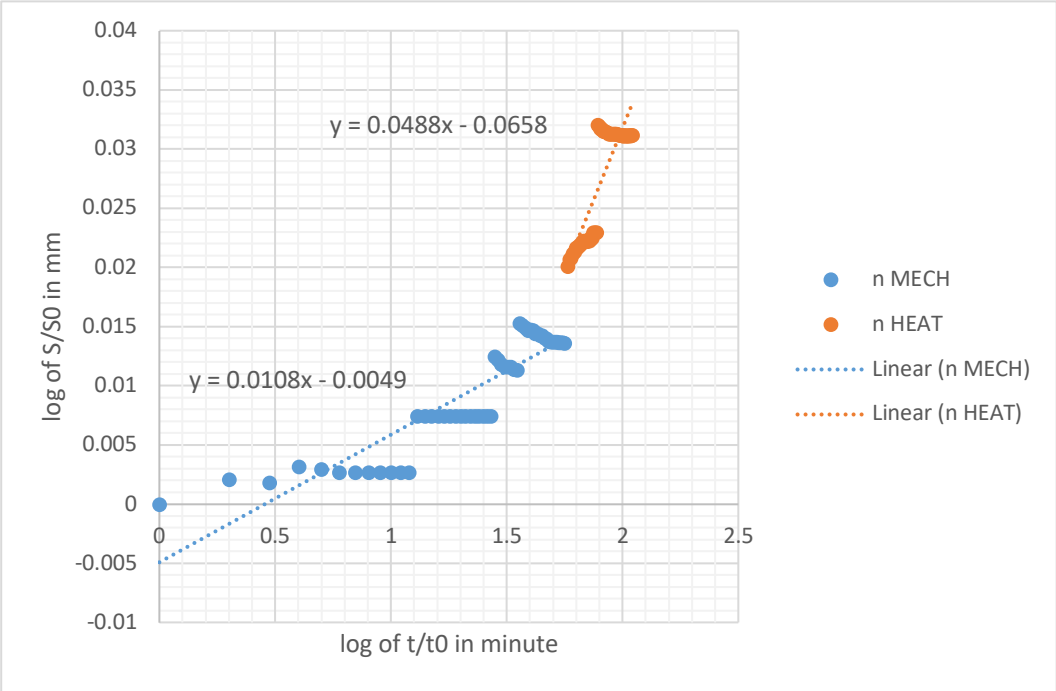

Figure 3.46. Creep "n" value variation under various loading condition at stage 4

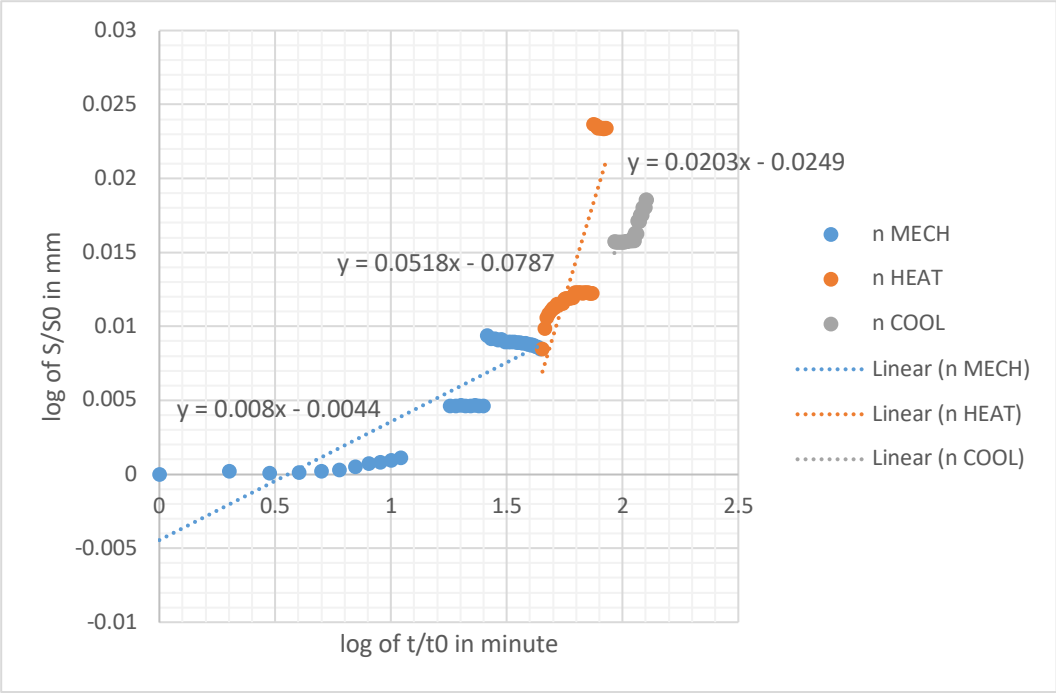

Figure 3.47. Creep "n" value variation under various loading condition at stage 5

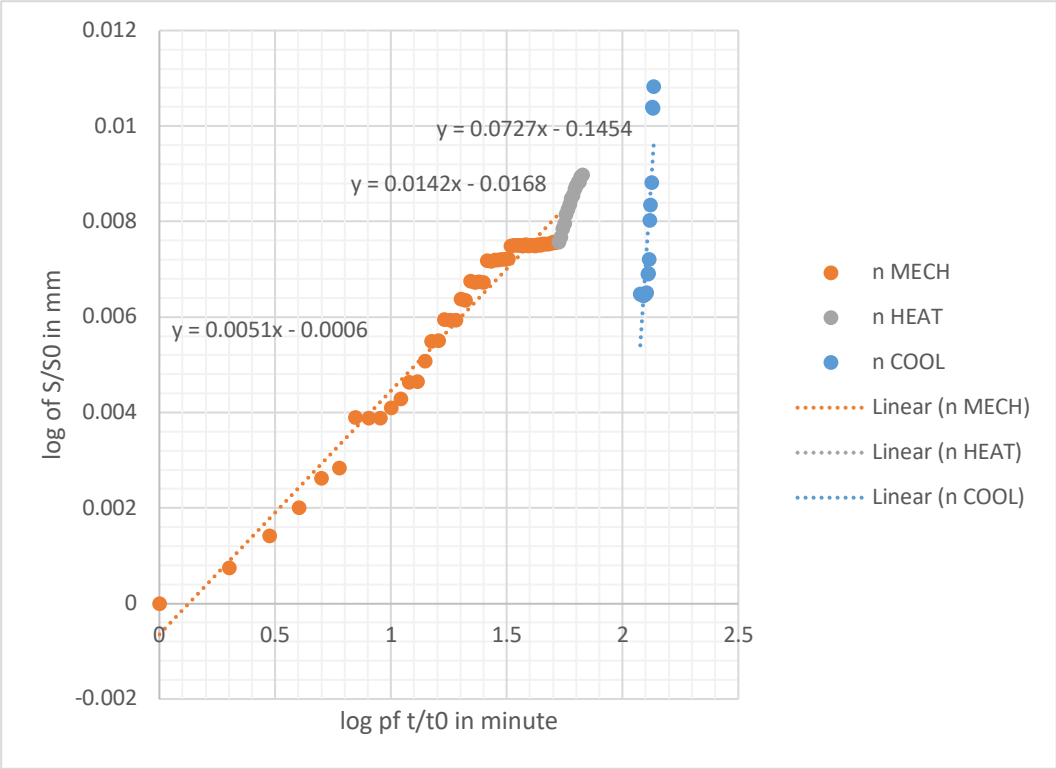

Figure 3.48. Creep "n" value variation under various loading condition at stage 6

Table 3.7 shows the summary of the calculated creep "n" value according to the formulation presented earlier in the beginning of this section.

Table 3.7. Creep "n" value summary for each stage of load control test

Creep "n" value calculation			
Load (lbf)	Mech. Only	Heating	Cooling
70	0.0185	0.0746	0.224
135	0.0356	0.0674	0.078
218	0.0242	0.0877	0.0594
280	0.0108	0.0488	system malfunction
350	0.008	0.0518	0.0203
435	0.0051	0.0142	0.0727

3.5 General Conclusions

On the issue of shrink-swell, the most possible process to have an impact on the increase of shrinkage of clay soil was the heating cycle. According to the findings presented in Table 3.6, it was found that the heating cycle doesn't change the water content of the clay soil. As it was expected, the cooling cycle doesn't show any impact on the water content of the soil matrix and didn't cause any movement due to the shrink-swell issue.

Another important observation was the pattern of heat propagation within the soil matrix under heating and cooling cycle. The soil is a remolded native highly over consolidated clay soil in which will form even slightly more compacted once the compaction of 100%. The soil exhibited a behavior of an isotropic conduction heat propagation model for both of the heating and cooling cycle. A comparison between Figure 3.33, Figure 3.34, and Figure 3.35 shows that the heat transfer model for grout is very much similar to the pattern followed in the soil measurements at various depths and distances from the pile. Similarity between the temperature variation measurements along the pile and the soil shows that the isotropic conduction model for heat transfer analysis can be applied to study the larger full-scale cases in the numerical simulation work. Another interesting observation made based on the temperature variation in the pile and soil, showed that the radius of temperature propagation in the soil is related to the thermal conductivity coefficient rather than the size of the energy pile.

The time dependent movement or "creep" is impacted by the cyclic thermal loading from heating and cooling cycle. The creep "n" value increased by heating process, showed that by increasing the soil's temperature the matrix structure might be softened and therefore the creep process accelerates. Nevertheless, during the cooling cycle the effect on the creep behavior won't be as significant as the heating process. Theoretically, under an isothermal condition the creep

value for a clay soil should not change with the change in the applied load. However, in the energy pile application when the soil goes under cyclic thermal loading, the creep value could be affected.

By comparing the creep "n" value for each mechanical loading only steps in Table 3.7, the effect of cooling from the end of previous step can be seen. The round 2 of load control test was the continuation from round 1, where the pile was loaded up to $150lbf$ in tension. The first three steps of loading in round 2 was basically moving along the reloading path. This might also explain why in the load vs. displacement plot (Figure 3.42) there is a significantly large displacement occurring in the $200lbf$ load. This load is the one right after the final applied tension load in round 1. At the final step, the "creep" failure occurred during the cooling cycle. The failure load was predicted to occur at around $500lbf$ as applied tension load. According to Figure 3.32, during the stage 6, the applied tension load reading from the load cell was about $430lbf$. The ratio between applied tension load over ultimate capacity at this step is 86%. Although, the applied tension load was not at the maximum mechanical load capacity of the pile, the cyclic thermal loading seems to have affected the overall capacity.

Another observation was made during the cooling process starting right at the end of heating. Since there is a transition period from the hot fluid to cool one, there was some indication of contraction of pile components specifically the rod within the measurement of the pile top displacement. In the creep "n" value calculations, we didn't consider those measurement points to avoid interference with the actual pile top movement due to creep movement.

Additionally, in the displacement-controlled testing method, the evolution of the relaxation "n" value was tracked under thermo-mechanical loading. Only heating process was available at the time of displacement control testing. According to Figure 3.24, the relaxation

value increases significantly during heating process compared to mechanical loading only condition. If the relaxation “n” value and creep “n” value of these two testing procedures are compared, it can be noted that the effect of thermal loading on the relaxation value is more than the creep movement.

4. NUMERICAL SIMULATION WORK

4.1 Introduction

So far, we introduced the geothermal foundation system application as an efficient and energy saving way for cooling and heating of any size buildings. According to McCartney et al. (2010), Laloui et al. (2006) and Amis et al. (2009), the thermo-mechanical loading on a foundation creates a unique stress condition and respective displacement as shown in Figure 4.1a and Figure 4.1b.

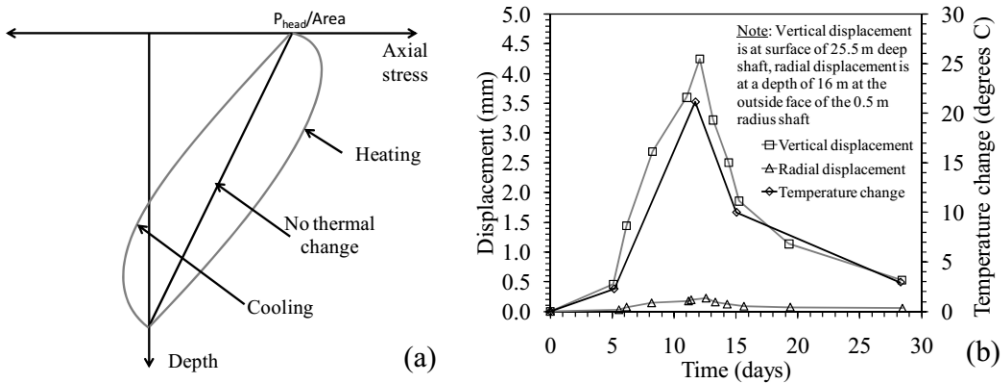

Figure 4.1. (a) Axial stress variations for mechanical and thermo-mechanical loading (McCartney et al. 2010); (b) foundation displacements vs. time (Laloui et al. 2006).

The cooling operation of ground loops inside the piles induces the contraction in pile creating a tensile force. According to Amis et al. (2009) this tensile force could become a dominating stress in case of strong cooling operation. Continuing this contraction would cause the decrease in lateral stresses and side friction with soil. For the case of heating operation, the expansion of the pile creates increasing stress on soil and soil-pile interaction. However, when having both of cooling and heating operation by geothermal foundation system the cyclic thermal loading could result in decrease in side friction (McCartney et al. 2010).

The additional thermal loading imposed on both pile and soil in local and global system engages the soil solid matrix, pore water pressure, structural integrity of the foundation

embedded in soil, and the building built on top. The thermal loading effect on the fully saturated soil matrix accounts for solid medium, pore pressure, and solid-pore pressure coupled together to induce changes on effective stress. The pile foundations are connected to the soil domain via links which represents the normal and shear interaction between the pile and soil. For the pile and building structure behavior, it will only be the rigid link between the elements and the building's dead weight is assumed for the applied working load on the pile foundation. The axial load distribution, vertical displacement profile, pore pressure evolution, and thermal efficiency analysis will be presented in the following sections.

4.2 FLAC3D: Introduction and Background

Numerical simulation tools including finite difference (FDM) and finite element (FEM) have been widely in use for practical and research purposes to enhance and give more details of soil behavior as well as its interaction with structures. Both of the above methods have the capability of delivering detailed and accurate analysis of soil behavior by using proper and realistic constitutive models for elastic and plastic behavior, boundary conditions, and loading patterns. Selecting a proper numerical modeling code or software can be extremely challenging depending on the complexity of the purpose of use. For the current research study, FLAC3D 6.0[1] by Itasca Consulting Group Incorporation was chosen.

The FLAC3D 6.0 is an explicit finite difference numerical simulation program capable of modeling numerically the mechanical behavior of a continuous three-dimensional medium marching toward equilibrium or steady state plastic deformation. Mechanical behavior of

[1] Fast Lagrangian Analysis of Continua in three dimensions, developed at Itasca Consulting Group Incorporation. Under Itasca Educational Partnership (IEP) program.

materials is modeled by general equation of motion in which is the definition of strain, equation(8), and the use of constitutive equations defining the idealized material.

$$\rho \frac{d\dot{u}_i}{dt} = \frac{\partial \sigma_{ij}}{\partial x_j} + \rho g_i \qquad (8)$$

The resultant of these two will create a set of partial differential equations in which relates the mechanical (stress, σ_{ij}) to kinematic (strain rate or velocity, $\frac{d\dot{u}_i}{dt}$) and will be solved for any particular problem. An important aspect of the model is the inclusion of the equations of motion, although FLAC3D 6.0 is primarily concerned with the state of stress and deformation of the medium near the state of equilibrium. In the following sections the discussion will be provided over the differences and principles of FLAC3D 6.0 for analysis of the full-scale energy foundation in highly plastic shrink-swell clay soil. Regarding the sign convention in FLAC3D 6.0, the tension and extension are positive.

4.2.1 Explicit vs. implicit

There are two school of thoughts; explicit which is the dynamic finite difference formulation, whereas the implicit which is the finite element discretization of the domain. In the explicit or FDM, we have grid points instead of nodes and zones instead of elements as in FEM. The calculation cycle starts by freezing the displacement and force in nodes and calculating the velocity according to the equation of motion or so-called equilibrium equation.

The calculated velocity is implemented into the constitutive equation (i.e. provided by the constitutive model selected) through Gauss's theorem, converted to strain rates, and new stresses for the zones are calculated. Then the zonal stresses are converted to nodal forces and put back into equation (8) to calculate new displacement and velocities.

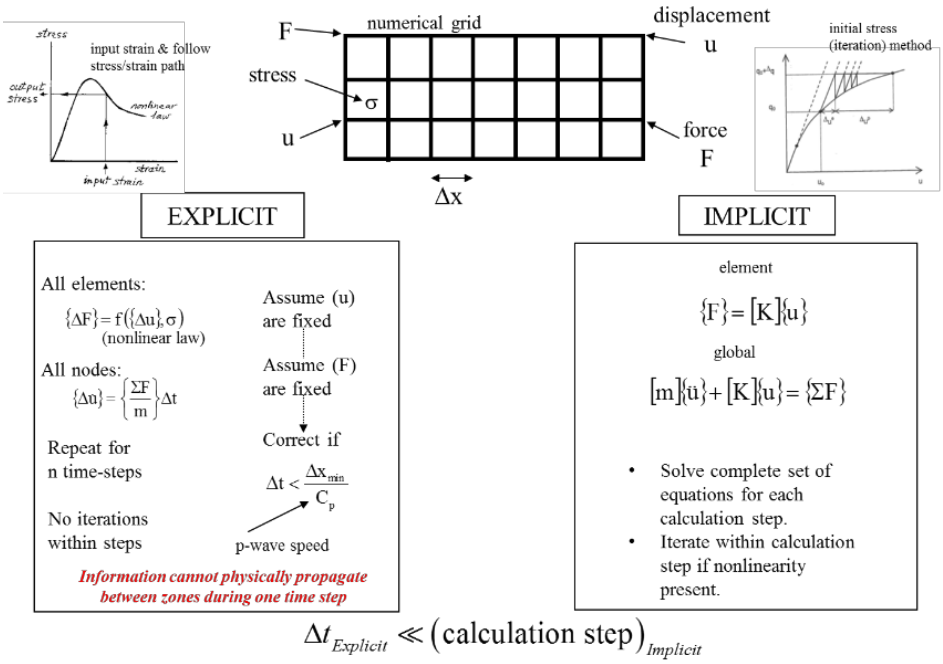

Figure 4.2. Explicit vs. implicit comparison flowchart.

The explicit (FDM, dynamic, time-marching) has several advantages over implicit (FEM, static) discretization method including:

1. Non-linear laws can be easily followed by model since displacements are frozen inside the constitutive model at each time step.
2. Physical instability natures will not affect the numerical stability.
3. Very efficient in large strain and large-scale problem with respect to computing time.

4.2.2 FLAC3D Numerical Formulation

In FLAC3D 6.0, the numerical discretization of the governing equation is structured according to the following steps:

1. Finite difference approach with 1st order derivatives over space and time and the linear variation of variables over the finite space and time step in the domain;

2. The discrete model approach will have all the interactive and applied forces lumped into three dimensional nodes discretized the soil domain; and
3. The dynamic solution is used to provide equilibrium for both static and quasi-static condition of the problem.

4.2.3 Zonal Damping

Since FLAC3D 6.0 solves the equation of motion, it will require to provide means of damping the osculation in each cycle to reach static or quasi-static (non-inertial) solutions. In the problems which don't deal with viscosity, the "local non-viscous damping" is implemented by default. However, for problems with significant uniform motion during the path to steady-state solution state, the so called "combined damping" is used. These include bearing capacity of an axially loaded pile or creep analysis. Combined damping will be more efficient for the pile foundation problem in reducing kinetic energy.

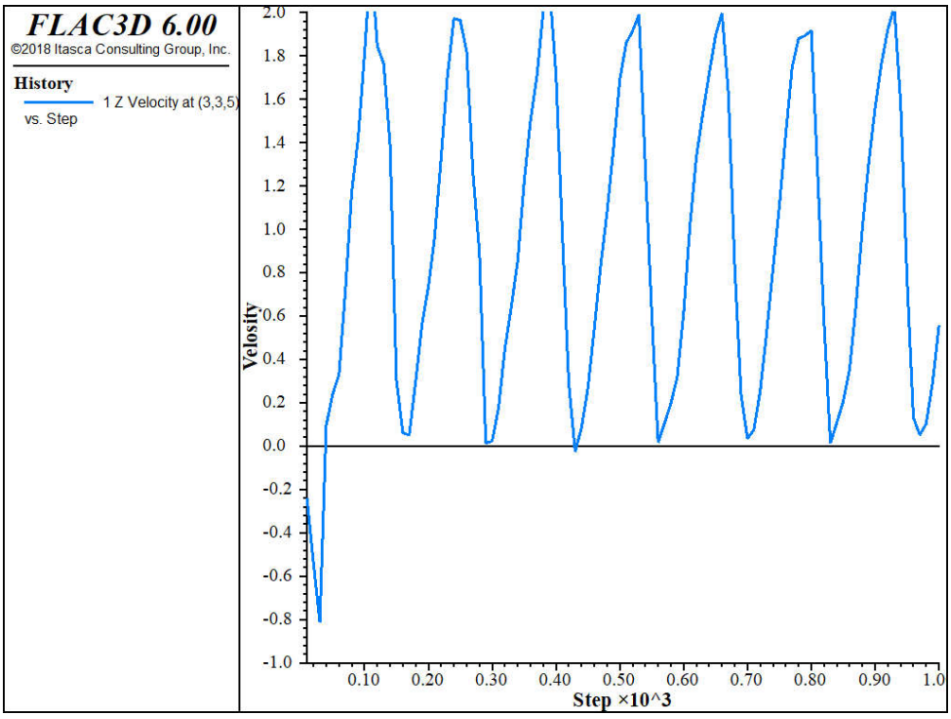

Figure 4.3. Local damping for velocity (FLAC3D documentation, 2018)

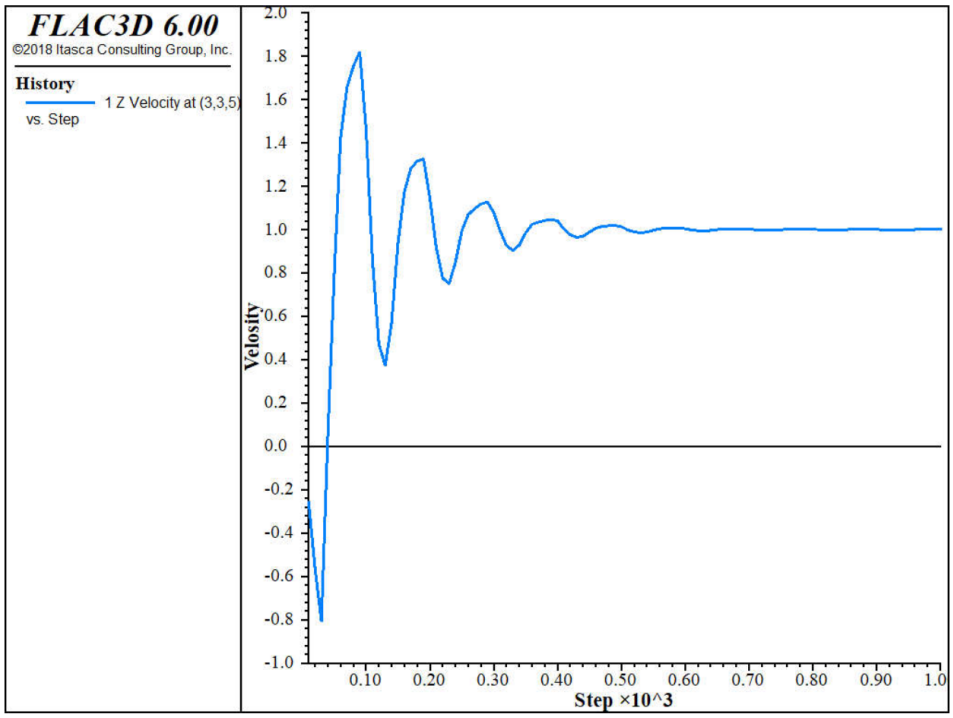

Figure 4.4. Combined damping for velocity (FLAC3D documentation, 2018)

4.2.4 Structural Element (SEL)

The essential goal of the current research effort is to carefully study and analyze the pile-soil interaction under the thermo-mechanical loading from the building and geothermal system operation. Within FLAC3D the structural element option can provide various range of soil-structure interactions. The implementation procedure of the structural elements will be the same explicit, Lagrangian method to solve the full dynamic equation of motion for both static and dynamic problems. In this study, the beam, pile, and shell elements are used to simulate the full-scale interaction of pile-soil-building under thermo-mechanical loading from the application of geothermal foundation.

Some general considerations regarding application of structural elements to study the full-scale behavior of a geothermal foundation system include:

1. Dimensionality of the element: There is no heat transfer mechanism defined for any of the beam, pile, and shell elements since they are only one dimensional or two-dimensional elements with no actual volume.
2. Slab attachment condition: this is found to be a significant of importance when it comes its interaction with the soil underneath.
3. Building elements only represent the dead weight analysis with rigid links between all the elements of the building and slab.

In the following section, details of the logics and constitutive equations for each of the structural elements used in this study are discussed.

4.2.4.1 Beam Structural Element

The beam element is a finite element two-nodded straight line, with six degrees of freedom at each node. This element constitutes a linear elastic material with no failure limit which is a proper assumption for the current study. Any beam can consist of several beam elements to form the full geometry of the beam. Each beam element, has two nodes with its local coordinate system which encompasses the properties of that element. Since the main focus here is not the exact simulation of the building, a general beam frame is set to properly simulate the actual building behavior.

4.2.4.2 Pile Structural Element

The pile element is a finite element two-nodded, straight line with coupling springs in both axial and shear direction. These spring connections allow the element to interact with its surrounding grid zones in both longitudinal and shear direction. Similar to the beam element, the pile element consists of two nodes at the both end of the line. The element has its own local

coordinate system to with respect to the local numbering of the two nodes forming that element (Figure 4.5).

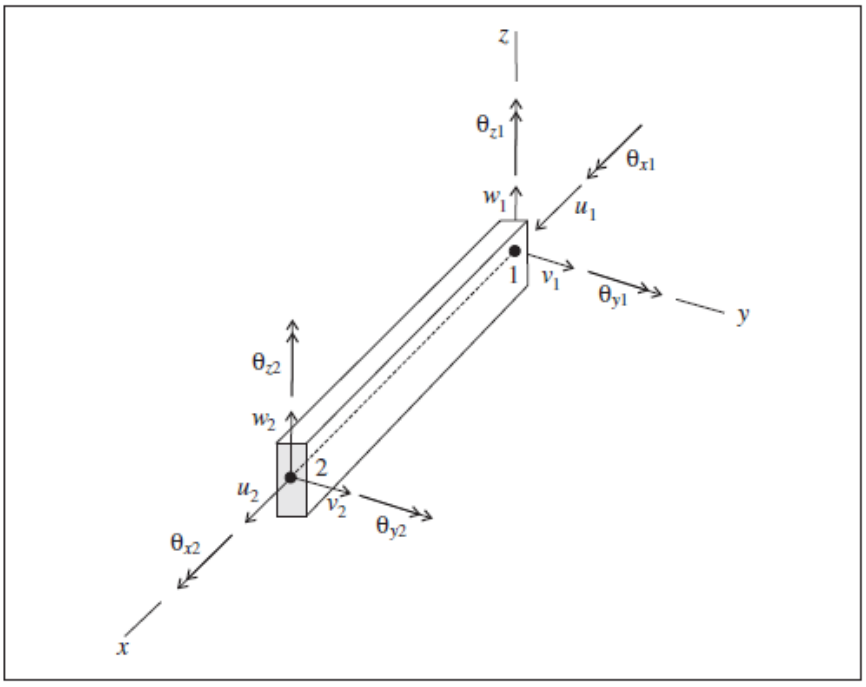

Figure 4.5. FLAC3D pile SEL coordinate system (FLAC3D documentation, 2018)

The orientation of the local coordinate system is so that the x axis along the line that goes from point 1 to 2 for every single pile SEL component. The local y and z direction is then perpendicular to the x axis. This local coordinate system orientation is set after the very first cycle. The pile SEL interacts with the grid through shear and normal coupling springs, which are defined at each SEL node. Then through proper link type based on the expected behavior of the pile, the shear and normal coupling springs communicate forces and movements between the SEL node and the connected grid point.

The shear behavior of the coupling spring is cohesive and frictional. The simplified demonstration of a single reinforced auger cast-in place pile is shown in Figure 4.6. The main

pile SEL properties to define shear behavior is spring stiffness, (k_s) cohesion strength in unit of force per unit length, (c_s) friction angle, (ϕ_s) and the exposed perimeter (p).

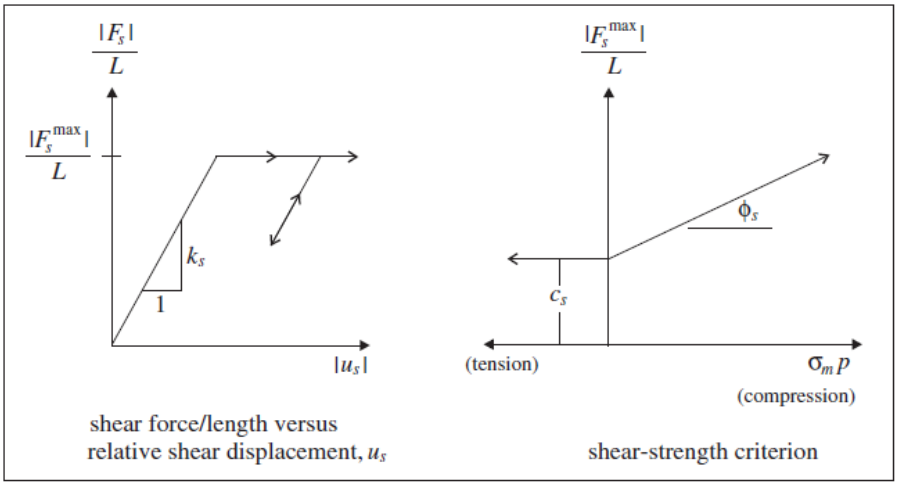

Figure 4.6. Pile SEL shear coupling spring demonstration (FLAC3D documentation, 2018)

The normal coupling springs can represent the confinement of the pile by the surrounding soil mass due to the frictional and cohesive. In nature this confinement (i.e. normal to the pile local axial orientation) is also frictional and cohesive. The combination of normal coupling spring parameters including spring stiffness, (k_n) cohesion strength in unit of force per unit length, (c_n) friction angle, (ϕ_n) and the exposed perimeter (p) with the effective confining stress, (σ'_m), which can replicate the mechanical behavior of the pile in normal direction. The properties assigned for the normal coupling spring is averaged at each pile SEL node.

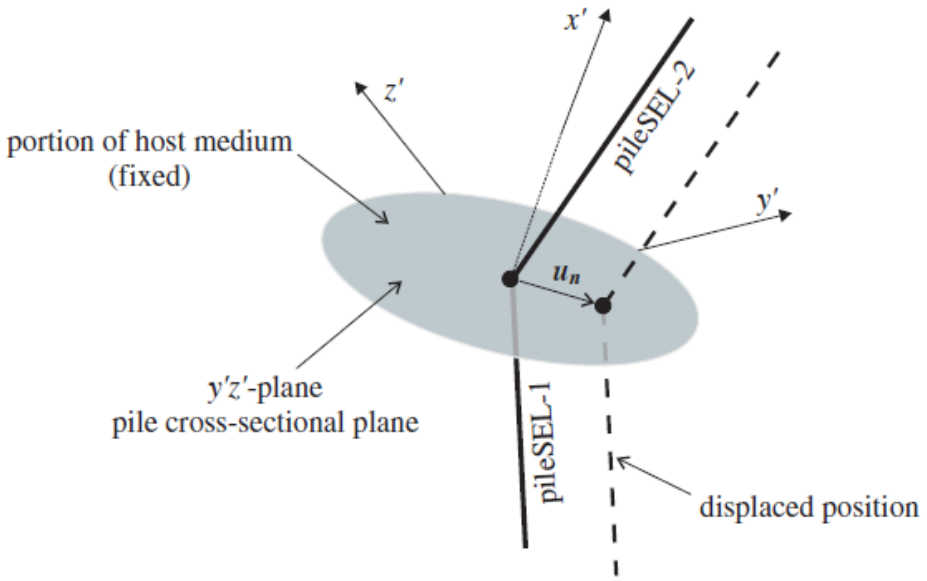

Figure 4.7. Normal coupling spring (FLAC3D documentation, 2018)

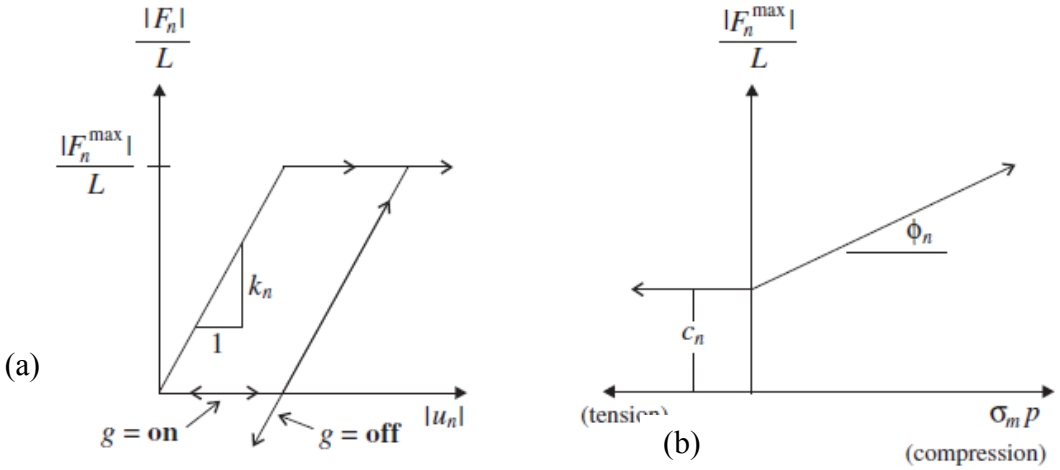

Figure 4.8. (a) Pile SEL normal force per unit length vs. relative normal displacement, and (b) normal coupling spring strength criterion (FLAC3D documentation, 2018)

4.2.4.3 Shell Structural Element

The shell element is a three nodded flat finite element with the structural responses based on membrane loading only, bending only, or both (Figure 4.9). The shell element is either

isotropic or orthotropic, linearly elastic with no failure limit. This structural element is commonly thin comparing to its span. The bending stresses in shell element correspond to the ones causing bending and transverse shear forces. The membrane stresses on the other hand are the ones that occurs in a plane-stress problem, producing mid-surface tangent forces. Each shell-type element like other ones has its own local coordinate system.

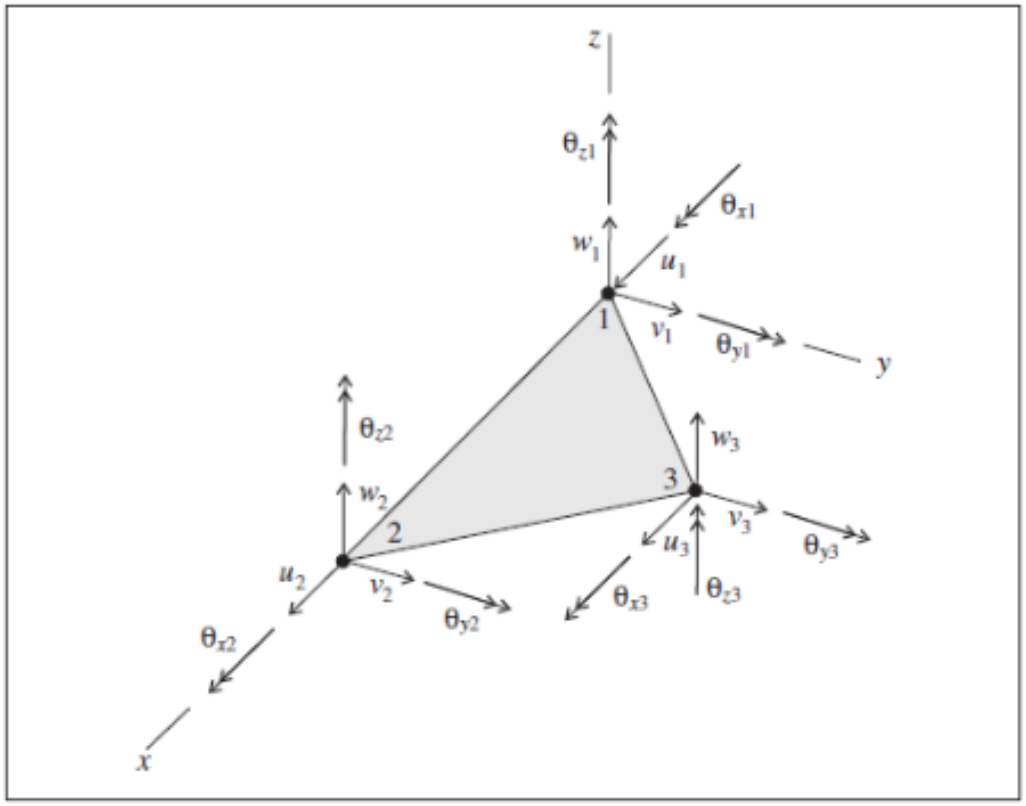

Figure 4.9. FLAC3D shell structural element details with the local coordinate system

The shell SEL properties are dependent on the type of the element chosen. The intention of using shell SEL in this research effort is to replicate the concrete slab attached to the pile group top and building's columns. Such slab can be assumed to be isotropic, linear elastic with no failure for the working load condition considered. For an isotropic material, the properties required for the SEL are density (ρ), thickness (t), Young's modulus (E), and Poisson's ration

(ν). Additionally, there are several different types of shell SEL available in FLAC3D library as a three nodded flat finite element. For the concrete slab, the 15 degrees of freedom shell SEL (DKT-CST) is the appropriate one to choose. For more details please refer to FLAC3D v.6.0 documentation by Itasca Consulting Group (2018).

4.2.5 Structural Element Links

In general, any structural elements used in FLAC3D can interact with another structural element or grid point in the zones through the appropriate links. The links will provide the means of defining the existing condition between the soil-structure systems. There are two types of links need to be defined to properly simulate the interaction between the various structural elements and also soil's zones. The link in FLAC3D represents the three attachment conditions:

1. Free: this condition makes the corresponding structural element node to be completely free (no contact) with either the other structural element or soil zones. The movement of the nodes with such an attachment condition will be completely independent of the either surrounding target nodes or grid points.
2. Rigid: on the contrary to the free condition, the rigid attachment will be slaved to the velocity of the target nodes or grid points (Figure 4.10).
3. Deformable: very similar to the rigid condition, except for the fact that the connection between the target node or zone and the node will be springs instead of roller ones (Figure 4.11).

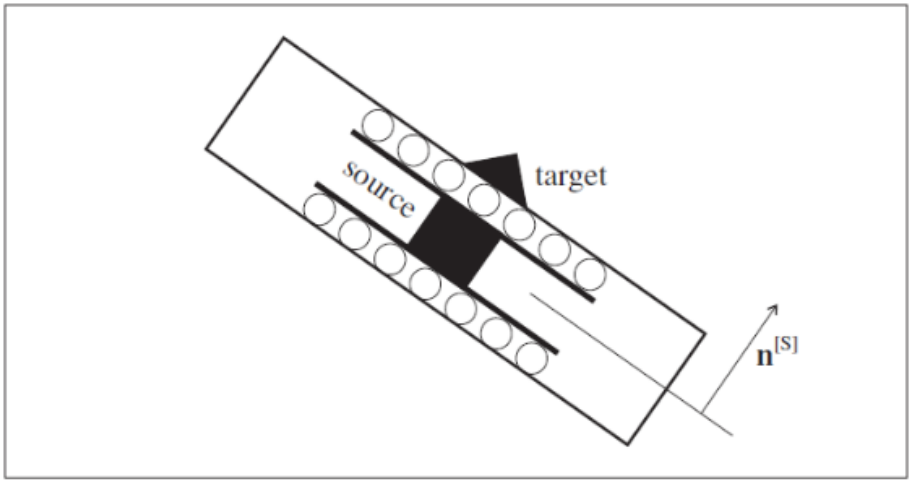

Figure 4.10. Rigid link (FLAC3D documentation, 2018)

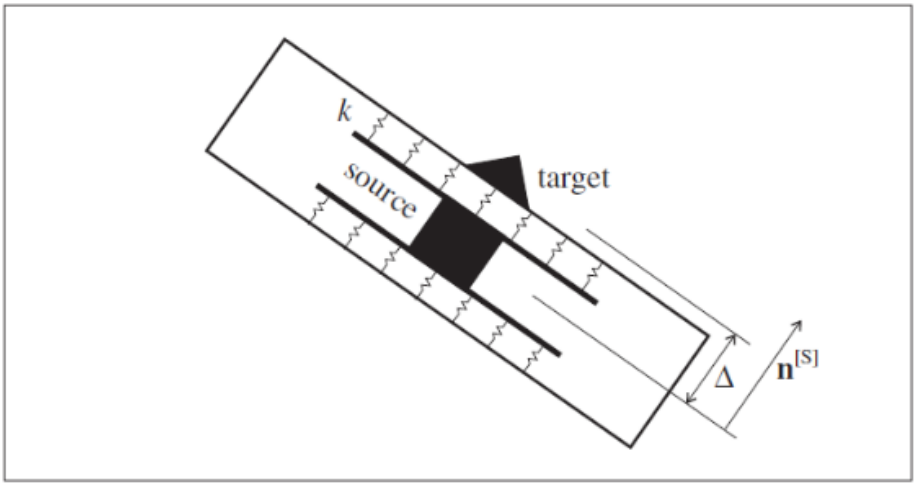

Figure 4.11. Deformable link (FLAC3D documentation, 2018)

Each structural element in FLAC3D poses a default setup of the attachment condition for each of their nodal degree of freedom. For the current study, in all of the different section of the work, the pile element for the pile foundation, the beam for the building structure, and the shell for the concrete foundation slab. The link condition varies with respect to the actual attachment

of each of the model components. The beam elements representing the building frame are all rigidly connected.

The pile elements representing the pile foundation must interact with surrounding soil grid points, slab foundation, and building frame on top. Therefore, the nodes along the pile length will have the attachment condition of "SY: shear yield", "PY: pile yield", and "PYDP: pile yield dependent. The SY condition will demonstrate the frictional and the PY - PYDP link shows the confinement along the pile length. In order to simulate the end bearing behavior of the pile, the bottom node link will be replaced by the "NY: normal yield" spring connection, in which defines the elastic perfectly plastic behavior in both compression and tension.

The shell element nodes depending on their contact condition with the soil, will be "NC: no contact" and "FC: full contact". In the NC condition, the nodes on the shell elements have no link with only the soil grid points, whereas, in the FC condition, the opposite condition exists. The shell nodes in contact with the beam and pile nodes will be rigidly connected. The effects of the NC and FC attachment conditions will be discussed in details in section 4.10.

4.2.6 Thermal Coupling in Structural Element

With the heat conduction in the grid points or the temperature re-initialization in the structural element nodes, the linear thermal expansion occurs in the structural element nodes. Although the linear thermal expansion in considered, there is no heat conduction occurring in a structural element. The grid points are assumed to instantaneously communicate the temperature with the structural element and causes only axial direction of expansion or contraction in the element. Lateral expansion or any other coupling doesn't take place. The incremental axial force generated by the thermal coupling in the structural element is then formulated as

$$\Delta F = EA\alpha\Delta T \tag{9}$$

Where E is the Young's modulus of the element, A is the cross-sectional area, α is the linear thermal expansion coefficient, and ΔT is the temperature change. This temperature change in the structural element node is taken from the average nodal temperature magnitudes of the host zone.

4.3 Numerical Simulation Methodology

In this section, the details, steps, and mechanism used to build, analyze, making design recommendations, and drawing conclusions from the numerical simulation's work. First, the constitutive model along with its coupling structures to the thermal and hydraulic module is explained. Then, the initial model to calibrate the mechanical model with the coupled hydraulic and mechanical approach. After the initial model discussion, the sensitivity analysis to generate appropriate script structure in FLAC3D to perform the fully thermo-hydro-mechanical coupling simulation for design recommendation and case history section. The design recommendation section is discussed in details after sensitivity analysis section. Finally, the case history of the Liberal Arts and Humanities building on the Texas A&M University main campus will be presented and analyzed.

4.4 Constitutive Mechanical Model

There are several models to simulate the behavior of any soil structure under different loading conditions. There are 17 constitutive models in FLAC3D: 3 elastic and 14 elastic-plastic. The main focus of this research effort is on the high plasticity clay soil and the selection of the constitutive model should be in such a way that it incorporates the properties suitable to simulate such non-linear soil behavior.

In order to count for the stress-strain modeling of a highly plastic and over consolidated clay soil, there has to be a constitutive model with the capability of capturing the proper shearing

and volumetric behavior under thermo-mechanical loading with the presence of pore pressure in the porous medium. One of the most widely constitutive models used in industry is the Plastic-Hardening model based on the work presented by Schanz et al. (1999).

Schanz et al. (1999) presented a new constitutive framework based on the classical plasticity theory. The modulus in this model is stress dependent for virgin loading and unload-reloading stress path. The plasticity for this model is taken care by introducing the multi surface yield criterion for volumetric and shear hardening mode. For the cap volumetric and the shear hardening portion of the plastic deformation calculation, an associated and a non-associated flow rule is assumed, respectively.

The principle of utilizing a double stiffness and hyperbolic stress-strain relationship developed by Duncan and Chang (1970) had a significant flaw. The inability of the model to distinguish between the loading conditions of the soil, whether it is loading or unloading, was not accepted by the users. Schanz et al. (1999) further modified the model by Duncan and Chang (1970) to account for plastic strains based on the plasticity theory not elasticity (i.e. Mohr-Coulomb elastic perfectly-plastic model), soil dilatancy and its corrections, and implementing two new yield criterions. This constitutive model has been incorporated within FLAC3D 6.0. In summary, the main features of the plastic-hardening model are:

1. Hyperbolic stress-strain relationship;
2. Shear hardening when friction is mobilized;
3. Volumetric hardening when subjected to virgin compression loading;
4. Stiffness for loading and unload-reload condition based on stress level;
5. Pre-consolidation stress hysteresis;
6. Mohr-Coulomb failure criterion.

The sign convention for the principle stresses is positive for tension and negative for compression mode, with all referring to the effective stress. Also, the principle stress order is $\sigma_3 \geq \sigma_2 \geq \sigma_1$, while the σ_1 is the maximum principle stress (i.e. most compressive).

As mentioned above, the PH model utilizes hypo-elasticity analogy to describe the elastic behavior of a soil medium,

$$\begin{aligned} \Delta p &= -K \Delta e_v^e \\ \Delta s_{i,j} &= 2G e_{i,j} \end{aligned} \tag{10}$$

where p is the mean pressure defined as $p = 1/3\left(-\sigma_{ii}\right)$, $e_v^e = \varepsilon_{ii}^e$ is the volumetric elastic strain, $s_{i,j} = \sigma_{ij} + p\delta_{ij}$ is the deviator stress tensor, and $e_{ij} = \varepsilon_{ij} - \left(e_v^e / 3\right)\delta_{ij}$ is the deviator elastic strain tensor. The bulk modulus, K and shear modulus, G are defined based on the unload-reload Young's modulus, E_{ur} as follows

$$\begin{aligned} E &= \frac{E_{ur}}{3(1-2\upsilon)} \\ G &= \frac{E_{ur}}{2(1+\upsilon)} \end{aligned} \tag{11}$$

One of the key distinctions of PH model with other Mohr-Coulomb failure-based models is its stress level dependency of the Young's modulus according to the multiplier defined as

$$\begin{cases} E_{ur} = E_{ur}^{ref} Z^m \\ Z = \left(\frac{c.cot\phi - \sigma_3}{c.cot\phi + P_{ref}}\right) \end{cases} \tag{12}$$

Additionally, the PH model incorporates another type of modulus called E_{50}, which is the slope of the initial stiffness at the 50% strain from the hyperbolic stress-strain curve

$$E_{50} = E_{50}^{ref} Z^m \tag{13}$$

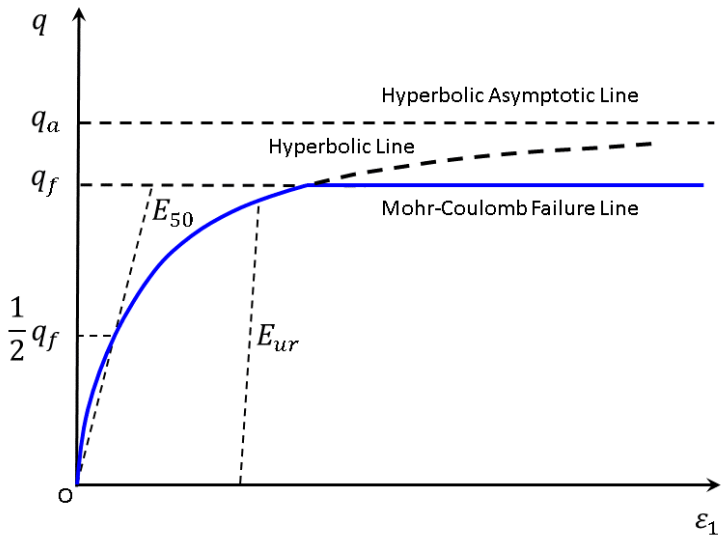

Figure 4.12. PH model hyperbolic stress-strain curve (FLAC3D documentation, 2018)

The effect of pre-consolidation pressure is counted toward the volumetric yield parameter calculation. The initial hardening parameter, $p_{c,ini}$ in which is determined by the pre-consolidation pressure can be estimated in the model as

$$p_{c,ini} = OCR.\sqrt{\frac{\tilde{q}_{ini}^2}{\alpha^2} + p_{ini}^2} \tag{14}$$

The OCR is the over-consolidated ratio, $\tilde{q}_{ini}$ is the initial shear stress, p_{ini} is the volumetric stress, and the α is a material constant parameter calculated either internally or taken as an input. Another volumetric hardening material parameter is needed to get track the evolution of the hardening parameter. The H_c same as the α considered to be either internally calculated or taken as an input by user

$$\begin{aligned} \Delta p_c &= H_c.Z^m \Delta\gamma_v \\ \Delta\gamma_v &= -\Delta\varepsilon_v^p = -\left(\Delta\varepsilon_1^p + \Delta\varepsilon_2^p + \Delta\varepsilon_3^p\right) \end{aligned} \tag{15}$$

4.5 Mechanical Model Implementation

In order to properly setup the mechanical model for the mechanical and thermo-hydro-mechanical simulation procedure, there are several steps need to be taken to accommodate such a complex behavior. The Mohr-Coulomb model is used to generate the initial stress field for the model domain with nonrealistic (very high) strength parameter. The reason to use nonrealistic parameters is to prevent any plastic deformations during the stress initialization step. Once the model reaches equilibrium, the realistic values for Mohr-Coulomb parameters are implemented and the new stress field is brought to equilibrium.

In order to maintain the model setup consistent with the ultimate goal of the research which is a fully thermo-hydro-mechanical scheme, the stress initialization stage is set to be de-coupled to avoid the unnecessary lengthy simulation time and the unforeseen issues with the model status. Such de-coupling is done for the thermal and hydraulic module with respect to the mechanical model during the stress initialization field. One of the observations made was effect of pore pressure not being numerically stabilized before the moving on to the next step. This is particularly noticeable when the mechanical load on the foundation starts, nonrealistic settlements are observed. The nature of the numerical instability comes from the fact that the entire numerical simulation work in this research effort is based on the effective stress calculations, which is directly affected by the pore pressure effect on total stress status.

Once the desirable equilibrium along with the stress status is reached, the constitutive model is changed from Mohr-Coulomb to Plastic-Hardening. The PH model main input parameters critical to the model's stability and initialization can be calculated by the results from seismic CPT. Mayne (2007) presented the relationships and correlations for the broad range of soil type's various parameters. For the current research effort, since there is an extensive study

background available in literature, the seismic CPT reported by Briaud (2000) is used. Therefore, the following material parameter calculations are taken from Mayne (2007) NCHRP report on the reduction of the data from any type of CPT test.

The starting parameter for PH model is to get the initial modulus value $G_{\max}$ from the shear wave velocity V_s. The shear wave velocity for the clay soil type considered in this research can be estimated from the following equation

$$V_s\left(m/s\right) = 1.75.[q_t^{0.627}] \tag{16}$$

Where the $q_t(kPa)$ is the tip resistant value for an arbitrary depth. Then the slope of the initial modulus can be calculated as

$$G_{\max} = \rho_t V_s^2 \tag{17}$$

In which the $\rho_t\left(tones/m^3\right)$ is the soil's total (saturated) density. The unload-reload modulus and the initial slope line both in kPa are then calculated as

$$E_{ur} = \frac{2G_{\max}(1+\upsilon)}{3}; E_{50} = \frac{E_{ur}}{3} \tag{18}$$

The rest of the required input parameters for PH model are taken from the previous step by the Mohr-Coulomb model.

The mechanical boundary conditions are set to be roller on the outer far reach of the domain such that fixity along the x and y direction and free to move in z direction. The bottom of the domain is fixed in all three directions. One important note is that because of different mesh and zone setup used in this research, in some cases the mechanical boundary conditions will be different. Examples of these conditions are the half-symmetry and the pile's concrete zones.

Additionally, there are two numerical modeling schemes available in FLAC3D: wet and dry method. In the "wet" scheme, all the soil strength parameters and failure envelope are defined based on the "effective stress" condition (i.e. $c', \phi', \sigma'_{i,j}, pp$). In this scheme, the pore pressure is assigned to each zone and the calculations will be based on the effective stress change of the soil. On the contrary, in the "dry" scheme, the total stress calculation is performed and there is zero effect of water in the porous medium considered.

4.6 Fluid Module Implementation

As previously mentioned, the effective stress modeling work in FLAC3D should be controlled such that not it only couples correctly with the mechanical and thermal model, but also represents the correct drainage behavior associated with the clay soil under study. There are several fluid models available in FLAC3D based on the soil type, groundwater flow condition, soil's permeability in three dimensions, and type of application of the fluid module (e.g. consolidation, well, etc.).

It is also important to note that the current version of FLAC3D does not accommodate for unsaturated soil condition (i.e. negative pore pressure). In order to properly adjust the numerical script structure for the soil zones that are above the water table, several sensitivity analyses were conducted to optimize and form the most accurate and logical scheme for de-coupled and coupled analysis. The initialization of the pore pressure is set to be dependent on the depth of water table, while defining the fluid module boundary conditions such that the effective stress calculation doesn't get affected in a negative way.

The highly plastic, over-consolidated clay under study suits the isotropic fluid model greatly. The isotropic model will take as an input for domain configured for all the three

processes of mechanical, fluid, and thermal, the permeability coefficient, porosity, and undrained thermal expansion coefficient.

The isotropic permeability coefficient in FLAC3D by definition relates the coefficient of pressure term in Darcy's law and hydraulic conductivity

$$k = \frac{k_h}{\rho_f g} \tag{19}$$

The ρ_f is the mass density of the material. The next two important fluid module characterization of a transient fluid flow through porous media in FLAC3D are L_c, the characteristic length, and c, the fluid diffusivity

$$L_c = \frac{\text{volume of flow domain}}{\text{surface area of flow domain}}$$

$$c = \frac{k}{\frac{1}{M} + \frac{\alpha^2}{\alpha_1}}; \alpha_1 = K + \left(4/3\right)G$$

For any coupled or de-coupled simulation of hydraulic module in FLAC3D, the mass density can be defined in three different ways: dry density of the material, ρ_d the saturated density, ρ_s and the fluid density ρ_f. When modeling with the fluid module being activated (i.e. wet approach), the dry density must be used. Then FLAC3D internally will calculate the saturated mass density based on the degree of saturation in each zone and the defined porosity. On the contrary, if the calculation is carried out without the activation of the fluid module, then the saturated density, $\rho_s = \rho_d + ns\rho_f$ must be used.

As mentioned before, the current version of FLAC3D doesn't support unsaturated soil. This means that if at any zone, the degree of saturation falls below 1, then the pore pressure will set to zero for that zone. Additionally, the effect of imperfection in water such as dissolved and

trapped air can be considered through the fluid bulk modulus and tension limit while keeping the saturation at 1.

Now that the principle framework of the fluid module implementation mechanism has been drawn, the governing equation and transport laws is discussed. The isotropic conduction fluid module coupled with thermal and mechanical module in FLAC3D is defined as follows

$$\frac{1}{M}\frac{\partial p}{\partial t}+\frac{n}{s}\frac{\partial s}{\partial t}=\frac{1}{s}\frac{\partial \xi}{\partial t}-\alpha\frac{\partial \varepsilon}{\partial t}+\beta\frac{\partial T}{\partial t} \tag{20}$$

The M is the Biot's modulus $\left[N/m^2\right]$, n is the porosity, s degree of saturation, p is the pore pressure, the ξ is the fluid volume change per unit volume of porous material, α is the Biot's coefficient, β is the undrained thermal expansion coefficient, and ε is the mechanical volumetric strain.

The Biot's coefficient determines the ratio of the volume of the fluid leaves (or enter) the material zone over the volume change of the same element when the pore pressure changes. This coefficient varies from $\frac{3n}{2+n}$ to 1 with the n as the soil's porosity. The general formulation for Biot's coefficient can be written as

$$\alpha=1-\frac{K}{K_s} \tag{21}$$

The K is the drained bulk modulus of the soil medium and the K_s is the soil grain modulus value. Based on the definition for the Biot's coefficient, the Biot's modulus can be formulated as follows

$$M=\frac{K_u-K}{\alpha^2} \tag{22}$$

The $K_u = K + \alpha^2 M$ is the undrained bulk modulus of the soil material. According to the definition in FLAC3D, for an ideal porous media, the Biot's modulus can be related to the fluid bulk modulus, K_f as

$$M = \frac{K_f}{n + (\alpha - n)(1 - n).\frac{K_f}{K}} \tag{23}$$

For a typical highly plastic, over-consolidated clay soil, the assumption of incompressible grain (i.e. $\alpha = 1$) is valid. Therefore, the Biot's modulus is rewritten as

$$M = \frac{K_f}{n} \tag{24}$$

For an incompressible grain, the fluid diffusivity can be re-written as

$$c = \frac{k}{\frac{n}{K_f} + \frac{1}{\alpha_1}} \tag{25}$$

4.7 Thermal Module Implementation

Any soil medium is a three-phase zone including solid, liquid and gas. For most of the geotechnical project application including geothermal foundation, water as the liquid phase has a transition between solid, which is ice to liquid, and liquid to gas which is vapor due to temperature variations under certain pressure.

For soil the temperature-oriented problems, the thermal properties in general for a conduction model is the thermal conductivity $\lambda\left(W/m°C\right)$, the specific heat $c_v\left(J/kg°C\right)$, and thermal expansion coefficient $\alpha\left(1/°C\right)$. The high thermal conductivity means that the heat transfers fast in material; the higher specific heat indicates that it will take large amount of heat to raise the temperature of material, and the high value of diffusivity will have the temperature to

rise in material rapidly. These thermal characteristics depend on temperature, pressure, moisture content, and density.

Table 4.1. Thermal properties of the earth materials (after Briaud, 2013)

Material	Density $\rho\left(kg/m^3\right)$	Specific Heat $c_v\left(J/kg°C\right)$	Thermal Conductivity $\lambda\left(W/m°C\right)$
Air	1 to 1.4	1000 to 1050	0.02 to 0.03
Water	960 to 1000	4190 to 4220	0.5 to 0.8
Clay (unfrozen)	1400 to 1800	750 to 920	0.8 to 2.8
Clay (frozen)	1400 to 1800	650 to 800	1.0 to 3.6
Sand (unfrozen)	1500 to 2200	630 to 1460	2.3 to 3.8
Sand (frozen)	1500 to 2200	500 to 1200	2.9 to 4.7

Heat transfer in soil includes different processes: conduction, convection, radiation, vaporization, condensation, and Freezing-thawing.

The most applicable process in a full-scale geothermal foundation projects for clay soil is the conduction and convection. The conduction is a process in which without moving masses to transport the heat through homogeneous or heterogeneous mediums. The convection on the other hand will transport the heat by moving masses as the carrier of the energy (i.e. heat in the case of geothermal foundation). When the porous medium has a very low permeability coefficient and therefore the groundwater flow velocity is very low, the convection process will be minimal effect comparing to the conduction. In this research effort, the focus will be on the highly over-consolidated and highly plastic clay soils, which will constitute the use of the conduction model to represent the heat transfer.

For the type of clay soil under study, the thermal isotropic conduction model is selected from the FLAC3D thermal library. According to the conduction definition, the energy transported from one region to another region without having the solid/fluid phase transported. The fully coupling between three in order to properly study the conduction model, the energy balance equation which consists of

$$-q_{i,i} + q_v = \frac{\partial \xi}{\partial t} \tag{26}$$

Where the $q_{i,i}$ is the thermal heat flux (W/m^2), q_v is the heat source/sink (W/m^3), and the $\frac{\partial \xi}{\partial t}$ represents the amount of heat stored per unit volume (J/m^3). Generally, the temperature change in a porous media comes from either the storage term in the equation 3 or the thermal volumetric strain ε_{th}, and for that we can write the temperature change over time as

$$\frac{\partial T}{\partial t} = M_{th}\left(\frac{\partial \xi}{\partial t} - \beta_{th}\frac{\partial \varepsilon_{th}}{\partial t}\right) \tag{27}$$

The M_{th} and β_{th} are dependent on the type of the material. The effect of β_{th} in change of temperature reflects on the fact that the thermal volumetric strain causes temperature change, in which it can be neglected. In FLAC3D, the fully coupled process of thermo-hydro-mechanical formulation utilizes the same assumption and the equation 4 can be rewritten as

$$\frac{\partial \xi}{\partial t} = \rho C_v \frac{\partial T}{\partial t} \tag{28}$$

The ρ and C_v are the porous media density (t/m^3 = 10^{-3} kg/m^3) and specific heat at constant volume (J/kg℃), respectively. Finally, substituting equation 3 into 6, the energy balance equation can be formed as

$$-q_{i,i} + q_v = \rho C_v \frac{\partial T}{\partial t} \tag{29}$$

It is worth noting that the specific heat at constant volume is practically the same as the one in the constant pressure for almost all types of soil media. Another term in the energy balance equation for a thermal conduction model is the transport law, and follows the Fourier's law. For a homogeneous, isotropic, and stationary porous media, the heat flux transport term can be expressed as

$$q_i = -k[\![T_{,i}]\!] \tag{30}$$

The $k_{[\![}$ is the heat conductivity matrix and for the isotropic heat conduction case, which is a valid assumption for the clay soil under study, it will form as follows

$$\mathbf{k} = k.\begin{bmatrix} 1 & 0 & 0 \\ 0 & 1 & 0 \\ 0 & 0 & 1 \end{bmatrix} \tag{31}$$

4.8 Thermal-Hydraulic-Mechanical Coupling in FLAC3D

The coupling is the combination of at least two mechanisms, which interacts between each other. In the current study, the goal of modeling would be to couple the three process of heat transfer through pores and solid skeleton, pore fluid, and mechanical loading for a saturated highly nonlinear elastoplastic clay soil.

In FLAC3D, the thermal module can be fully coupled with the mechanical and fluid module. For the case of thermal-mechanical coupling, all the calculation features in the thermal module such as transient and steady-state heat transfer and implicit-explicit solution algorithm. The coupling logic for thermal-mechanical interaction is to track the effect of temperature variation on the volumetric change of a soil zone according to the following equation

$$\Delta\varepsilon_{ij} = \alpha_t \Delta T \delta_{ij} \tag{32}$$

Where α_t is the linear volumetric thermal expansion coefficient. During a thermal-mechanical coupling with a conduction heat transfer model, there are two important observations must be made. The first one is the difference between the physical definitions for time scales in thermal and mechanical modules. Since the time scale in both of these processes directly controls the required time for the propagation of information from one node to the next, there is a correlation between the two time scales. Generally, the so-called time scale for a mechanical process calculation in FLAC3D is defined as

$$\Delta t_{mech} = \sqrt{\frac{\rho}{K + \left(4/3\right)G}} L_c \tag{33}$$

Where the L_c is the thermal module characteristic length of the domain

$$L_c = \frac{\text{volume of solid}}{\text{surface area exchanging heat}} \tag{34}$$

Now, this mechanical nonphysical time scale parameter can be related to the time scale of thermal module as

$$\frac{\Delta t_{ther}}{\Delta t_{mech}} = \sqrt{\frac{K + \left(4/3\right)G}{\rho}} \frac{L_c}{\kappa} \tag{35}$$

Where the κ is the thermal diffusivity defined as

$$\kappa = \frac{k}{\rho C_v} \tag{36}$$

Where k is the thermal conductivity of the material. Generally, $\frac{\Delta t_{ther}}{\Delta t_{mech}}$ for typical soils is of the order $10^5 L_c$ which means even with the very small value of the L_c, still this ratio remains

high. Consequently, it can be concluded that in practical application of thermal-mechanical coupling, the mechanical effects occur almost instantaneously comparing to thermal ones.

The second concern is directed toward the coupling of the thermal and mechanical process, in which this only represents "one-way" coupling. In other words, the temperature change induces thermal mechanical strains that influences the stress tensors; whereas the mechanical changes will not cause any disturbance in the thermal calculation.

For an elastic material which the transient is not of significance, the thermal-mechanical calculation can be de-coupled and run in succession. Therefore, the thermal calculation is performed first to the desired thermal time and the mechanical process is executed to the equilibrium condition. However, for a highly nonlinear, plastic material such as an over-consolidated clay the communication of information between thermal and mechanical module must be at a very closer time interval. This provides the necessary condition of mechanical quasi-static status for each thermal step.

The coupling of hydraulic module particularly the undrained and drained behavior simulation coupled with the mechanical and thermal module is explained in the section 4.8.1.

Since existence of the water inside the porous zones changes the behavior of soil structure under an arbitrary loading, undrained and drained condition should be studied separately (section 4.8.1). The mean of coupling the thermal module to the hydraulic is through the coefficient called undrained thermal expansion. This coefficient corresponds to the pore pressure variation divided by $3\alpha M$ per unit change in temperature in undrained condition (no deformation). For an ideal porous material, the undrained thermal expansion coefficient can be calculated based on the β_g for grain and β_f for fluid as

$$\beta = 3\left[\beta_g\left(\alpha - n\right) + \beta_f n\right] \tag{37}$$

According to various sources including Graham et al. (2001), Agar et al. (1987), and Baldi et al. (1988), the undrained thermal expansion coefficient for a normally or over consolidated clay is about $2\times10^{-4}\left(1/^{\circ}C\right)$.

4.8.1 Undrained and Drained Condition

In general context of the soil mechanic terminology, the undrained loading condition for any soil medium relates to the effect of the rise in pore pressure magnitude when the soil is loaded, and its impacts on effective stress state of the soil. For the soils with very low permeability such as the highly over consolidated clays, when subjected to an external load, the water cannot escape and will take the applied load almost instantly. By increase in pore pressure, the effective stress reduces. Then pore pressure induced by loading starts to dissipate and consequently the effective stress changes. This process is called consolidation.

The consolidation due to the mechanical loading only has two parts: primary and secondary. During the primary consolidation, the excess pore pressure induced by external loading dissipates, while the effective stress changes and deformation occurs. Once all the excess pore pressure is dissipated, the secondary consolidation part starts, in which the time dependency deformation or "creep" occurs without changes to the effective stress condition of the soil. It has to be noted that the secondary consolidation behavior commonly occurs in fine grain soil such as clay.

Since the thermal loading for either heating or cooling process affects the pore pressure inside the porous material, controlling the pore pressure variations under thermal and mechanical coupling is the critical part of the hydraulic module coupling. With this in mind, all of the thermo-mechanical loading parts presented in this research effort is divided into two part of the undrained and drained behavior.

Only for the mechanical model calibration in section 4.8, which discusses the PH model calibration, the undrained and drained behavior is modeled in a de-coupled approach for mechanical and hydraulic module was pursued. For all other thermo-hydro-mechanical coupled models, the undrained part consists of the fully coupled thermal and mechanical module with having the actual time dependency of the calculation for the process.

This coupling was done through the so called “master-slave” code structure developed for FLAC3D. The master-slave logic in FLAC3D allows the tedious task of coupling of any two processes with a better control over the numerical simulation stability and results. For the current research study, it was decided to structure the numerical code such that the thermal and mechanical module is first coupled through master-slave logic (i.e. undrained mode), then both are de-coupled from hydraulic module (i.e. drained mode), and finally the mechanical module will individually correct any disturbance in the stress field after the drained calculation. For the undrained calculation, the thermal module is set to be the “master” over the mechanical as the “slave”.

This analogy was selected due to the fact that the mechanical module in FLAC3D doesn’t include a realistic time stepping definition, and the thermal with the realistic time stepping concept will convey the undrained simulation within the defined timeline. Based on the “master-slave” logic, the “slave” module should reach a “quasi-static” condition before the “master” module proceeds to the next step. This concept plays an extremely important role in the convergence and control of the model stability especially for the hydraulic module drainage calculation. The undrained part of the model uses the “master-slave” logic with the thermal “master” module stepping in time to perform heat conduction calculations, while the mechanical “slave” module is brought to a quasi-static equilibrium before going to the next “master” step.

The quasi-static criteria for mechanical module are set to be satisfied when the unbalanced force ratio reaches to 10^{-5}, whereas the thermal module will continue the undrained calculations until the defined simulation time is reached. One of the critical parameters in setting up an appropriate "master-slave" coupling is to define enough numbers of mechanical (i.e. slave module) steps to reach quasi-static equilibrium, before advancing to the next thermal (i.e. master module) step. This very much important issue has been addressed in section 4.10. The defined code structure for this coupling is set to ensure satisfaction of both of the thermal and mechanical module criteria.

For the undrained thermo-mechanical coupled calculations, there are two very important parameters to define in FLAC3D including the fluid bulk modulus and fluid tension limit. The fluid bulk modulus affects the pore pressure in the porous media when the mechanical and thermal load is being applied to the medium. When the fluid bulk modulus is zero, any disturbance in the stress field will not transferred to the fluid in the porous media. However, if this value is set for a fluid such as water (i.e. $2\times10^5\,kPa$ due to the imperfections in water like dissolved air and bubbles), then any disturbance in the stress status of the domain will also be transferred to the existing pore pressure, affecting the effective stress calculations. The fluid tension limit in FLAC3D controls the desaturation of the porous material for fine grain soils such as clay.

Before the desaturation starts, the FLAC3D is able to track the negative pore pressure build up. It is crucial to notice that this so called "negative pore pressure" is not the same as "tension" from capillary pressure (a.k.a. suction), electrical, or chemical forces. The negative pore pressure by this definition will simply relate to the pressure increase from the soil medium expansion.

Once the undrained calculation is finished, the drained calculation process (i.e. the hydraulic module being active only) starts and de-coupled from the thermal and mechanical module. The fluid bulk modulus and tension limit have to be redefined properly to control the numerical stability and correct drainage calculation. The general numerical coding details and logics are discussed in the section 4.10.

4.9 Mechanical Model Calibration

This section represents the pilot study performed to identify and calibrate the mechanical constitutive model best suited for a typical highly over-consolidated high plastic clay. The work in this section includes the simulation of a typical load test performed by Briaud (1999) in clay site at TAMUS RELLIS (old Riverside) campus.

4.9.1 In Situ Test and Numerical Model Detail

According to Briaud (1999), there are a total of four drill shafts with various geometry. Shaft number seven was selected with $0.92m$ in diameter and $10m$ length. Several field tests have been reported including full scale CPT in clay site (Figure 4.13). The load test includes static compression load up to $3000kN$ and running creep test afterward.

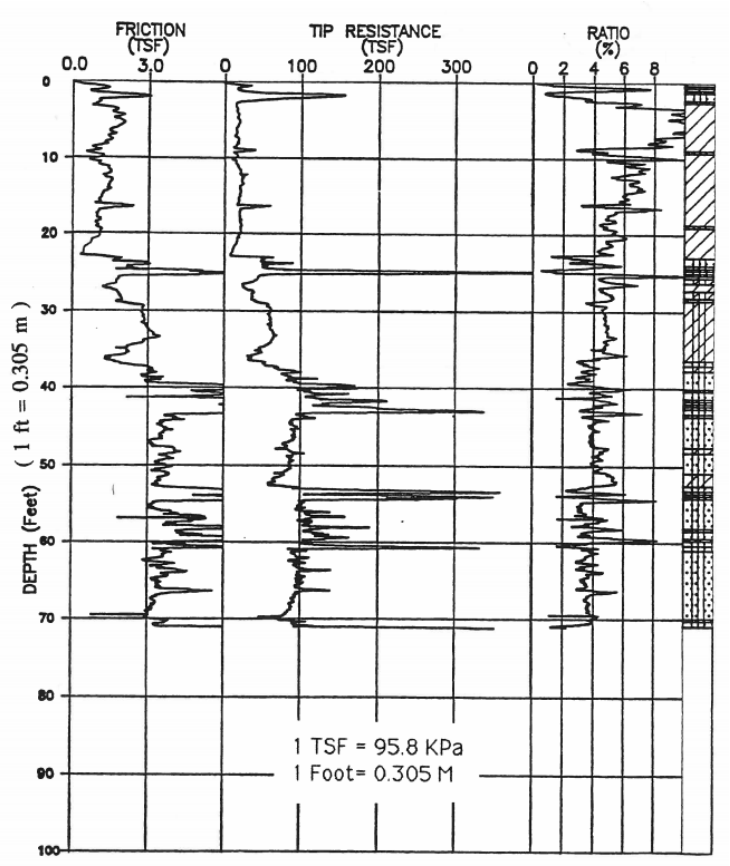

Figure 4.13. CPT result in clay site at TAMUS RELLIS campus (Briaud, 1999)

The numerical model setup is a quarter symmetry representation of the actual test on the shaft number seven. The pile is modeled with solid zones by elastic model from FLAC3D library. Mechanical boundary condition is the roller on far sides and non-elastic zones for soil. Also, the concrete zones are fixed in the (x, y)directions. The bottom of the mesh is fixed in all three directions. As far as the fluid boundary condition, all the far sides are fixed for pore pressure, which means there is no flow in and out of the domain. Table 4.2 shows the properties used for the concrete elastic model. Figure 4.14 shows the model setup details for the load test calibration.

Table 4.2. Elastic model properties for concrete zones

$\rho\left(tones/m^3\right)$	$K\left(kPa\right)$	$G\left(kPa\right)$	ν
2.5	1.39×10^7	1.04×10^7	0.2

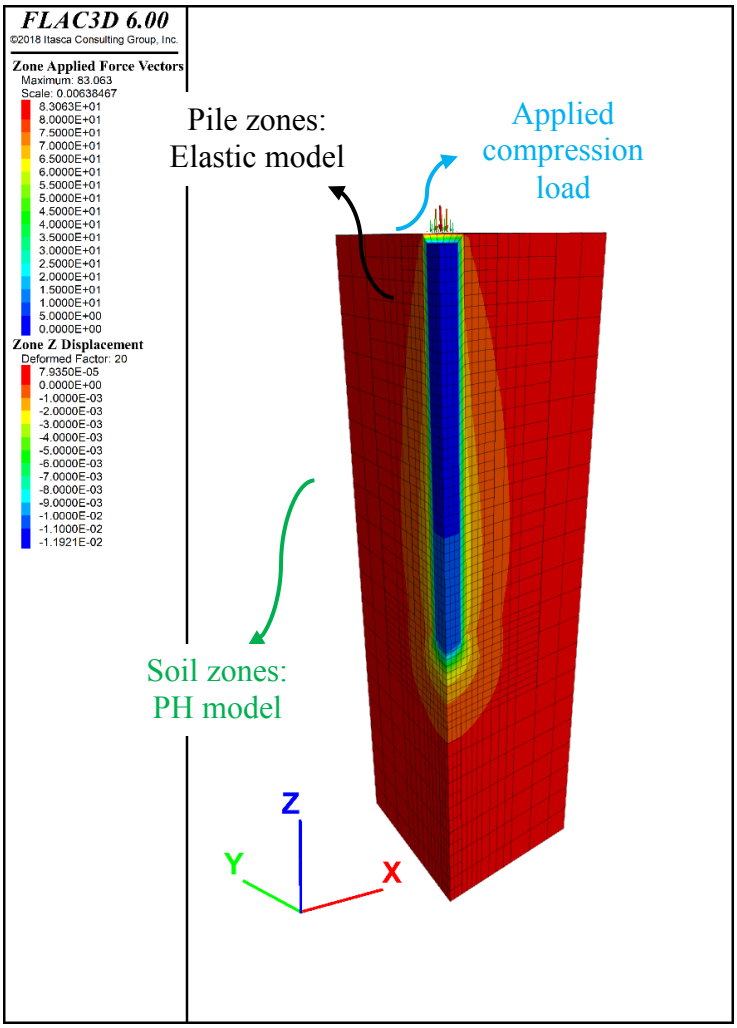

Figure 4.14. Quarter symmetry Numerical model for the mechanical model calibration

The fluid model for concrete zones are set to null or in other words no fluid calculations are done. Since the pore pressure variation within the concrete zones has very minor impact on the results, the fluid model is selected to be null from FLAC3D library.

The constitutive model sequence was Mohr-Coulomb for the stress field initialization along with the fluid module (i.e. wet approach) being de-coupled. Then the mechanical model was switched to the PH before starting the loading stage. Instead of using structural pile element from FLAC3D structural element list, actual concrete zones with “elastic” model properties were implemented from FLAC3D mechanical model library while the fluid calculation deactivated for the pile zones. The logic behind this goes to the fact the effect of pore pressure or any fluid flow calculation has negligible effect on the soil behavior and ultimately the pile top displacement.

4.9.2 Results

The main result for the PH model calibration is the load vs. displacement. The load vs. displacement comparison between the PH model and load test results are presented in Figure 4.15. There is a good agreement between the numerical and experimental results. The final calibrated soil strength parameters are summarized in Table 4.3. The calibrated parameters correspond very well with the already stablished values for such clay soil under study.

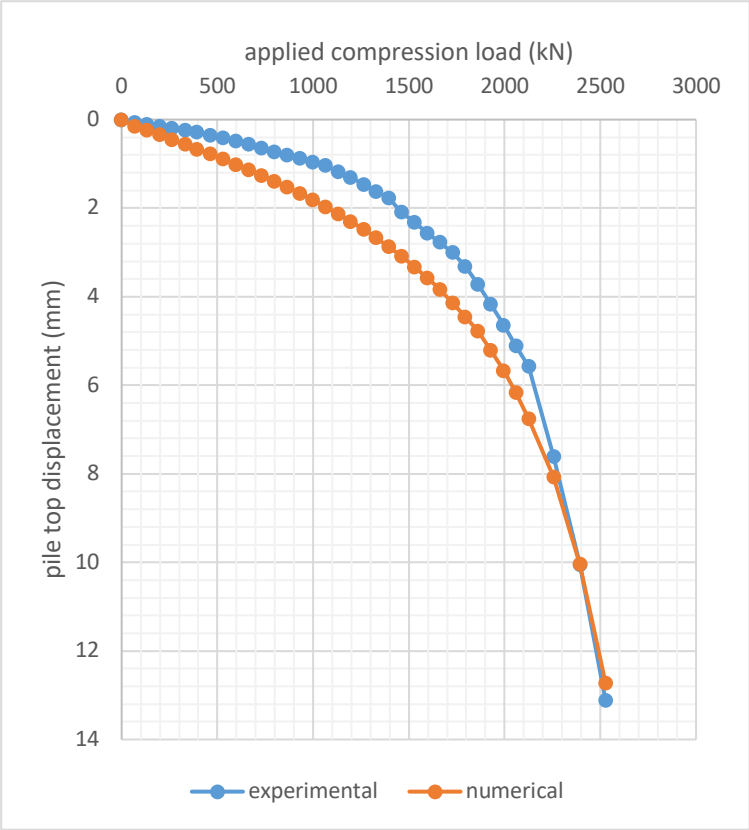

Figure 4.15. Comparison of load vs. displacement

Additionally, some general observations were made during this step. First, the approach to setup a fluid-mechanical calculation in FLAC3D was defined through performing the mechanical and fluid calculation in succession (i.e. de-coupled) to avoid unnecessary long simulation time. Second, sine the wet approach is used the two hydraulic model parameters fluid bulk modulus and tension limit has to be properly defined during each calculation step to produce accurate results. Third, the mechanical calculation step was designated to be like the undrained condition with having the fluid bulk modulus equal to realistic value of $2\times10^5\left(kPa\right)$ and zero for tension limit. Fourth, the hydraulic part represents the drained condition. In other words, low value for bulk modulus $11000\left(kPa\right)$to prevent extra pore pressure generation and

very high negative value $-1\times10^{-15}\left(kPa\right)$ during the drained calculation. This cycle was repeated for each load increments. Since FLAC3D solves a dynamic equation, the loading has to be incremental to prevent sudden disturbance in the model which could result in inaccurate results and very long convergence time.

Table 4.3. Calibrated PH model parameters

$c'\left(kPa\right)$	$\phi'\left(^\circ\right)$	$V_s\left(m/s\right)$	$q_{tip}\left(kPa\right)$	$E_{50}\left(kPa\right)$	$E_{ur}\left(kPa\right)$	$k_h\left(m/s\right)$
4	28	205.363	5500	23684.8	71054.4	10^{-8}

4.10 Sensitivity Analysis

4.10.1 Scope of Work

Once the mechanical model calibration was finished, the next step was to develop a numerical model for the tedious task of three-way coupling between thermal, fluid, and mechanical process. In order to better understand, correct, and optimize the numerical model for more complex and full-scale analysis of a thermo-active pile foundation, a simple case of single pile using pile structural element feature in FLAC3D under various conditions for soil temperature profile, mesh size, slab, water table, pile tip link type, and permeability. The simplified case allowed us to thoroughly study the effect of each parameter on the energy pile interaction with soil. Additionally, the sensitivity analysis results lead to setting up the most optimized and accurate numerical code structure for further complex cases in the design recommendation section (4.12) and the case history part (4.13). The numerical model was set to simulate two years of operation of a single energy pile with 6 months of cooling mode (i.e. heating the soil), followed by 3 months of heating mode (i.e. cooling the soil). There is no gap between each thermal cycle.

The pile geometry is constant throughout all of the sensitivity analysis cases with $0.5m$ in diameter and $20m$ in length. Since the 1D pile structural element was used, there is no heat transfer process considered within the pile and the transition period of concrete heat/cold propagation is neglected. With respect to the water table condition, two positions were studied, including water table at the ground surface and water table at $6m$ which is a reasonable estimation of water table in College Station area. Since FLAC3D doesn't account for unsaturated soil, the latter case of water table at 6m was treated with a special scheme including proper fluid boundary condition consistent with the theoretical background of the model (more details in section 4.10.2.2).

Another influential factor on the convergence and stability of the fluid module, identified as the coefficient of permeability. This coefficient eventually controls the time step size and the use of implicit or explicit solution scheme. As previously mentioned in section 4.6, the characteristic time (t_c) which controls the time step size can be written as

$$t_c = \frac{L_c^2}{c} \tag{38}$$

According to this equation, the characteristic time parameter for a uniform soil domain is only affected by the permeability coefficient and eventually the coefficient of mobility. This triggered the interest in studying the effect of different permeability coefficient on the stability and results of the numerical model fluid calculations. The permeability coefficients were chosen as $10^{-5}\left(m/s\right), 10^{-8}\left(m/s\right), 10^{-9}\left(m/s\right)$. The permeability analysis helped to understand its effect on the hydraulic process numerical stability, drainage behavior, and mechanical model unbalanced force ratio.

The condition with and without presence of a structural slab (i.e. represented by shell structural element) was studied with full and no contact to the soil. The full and no contact condition was also further studied in the design recommendation section (4.12) and the case history (4.13). The effect of mechanical and thermal boundary conditions on the pile behavior was done through different mesh sizes. Although pile behavior in clay soil is mostly dominated by friction, the tip point contribution to pile capacity was also studied by changing the link properties between the bottom node and adjacent soil grid point. Table 4.4 summarizes the list of cases for sensitivity analysis study.

Table 4.4. Sensitivity analysis case description

Case number	Description
1	Constant soil temperature profile, Water table at the ground surface, No tension link at pile tip, permeability = $10^{-8}\left(m/s\right)$, No Slab, mesh 5mx5m
2	Constant soil temperature profile, Water table at the ground surface, with tension link at pile tip, permeability = $10^{-8}\left(m/s\right)$, No Slab, mesh 5mx5m
3	Constant soil temperature profile, Water table at 6m, No tension link at pile tip, permeability = $10^{-8}\left(m/s\right)$, No Slab, mesh 5mx5m
4	Soil temperature profile, Water table at the 6m, with tension link at pile tip, permeability = $10^{-8}\left(m/s\right)$, No Slab, mesh 5mx5m
5	Soil temperature profile, Water table at the ground surface, No tension link at pile tip, permeability = $10^{-8}\left(m/s\right)$, Slab with No contact link with soil, mesh 5mx5m
6	Soil temperature profile, Water table at the ground surface, No tension link at pile tip, permeability = $10^{-8}\left(m/s\right)$, Slab with Full contact link with soil, mesh 5mx5m
7	Soil temperature profile, Water table at the 6m, permeability = $10^{-5}\left(m/s\right)$, mesh 5mx5m
8	Soil temperature profile, Water table at the 6m, permeability = $10^{-8}\left(m/s\right)$, mesh 5mx5m
9	Soil temperature profile, Water table at the 6m, permeability = $10^{-9}\left(m/s\right)$, mesh 5mx5m
10	Soil temperature profile, Water table at the 6m, permeability = $10^{-8}\left(m/s\right)$, mesh 2mx2m
11	Soil temperature profile, Water table at the ground surface, permeability = $10^{-8}\left(m/s\right)$, mesh 2mx2m

Figure 4.16 to Figure 4.21 show the numerical model setup detail for the cases from 1 to 6. In each of the figures, there are two separate contour plots for the model geometry including "zone averaged" soil temperature values (i.e. left-hand side contour plot) and z-direction soil

displacement (i.e. right-hand side contour plot). The pile structural element is presented in mapped position on the plot. On a general note, from this part to the end of the dissertation, all the compression load sign is positive and the tension load sign is negative.

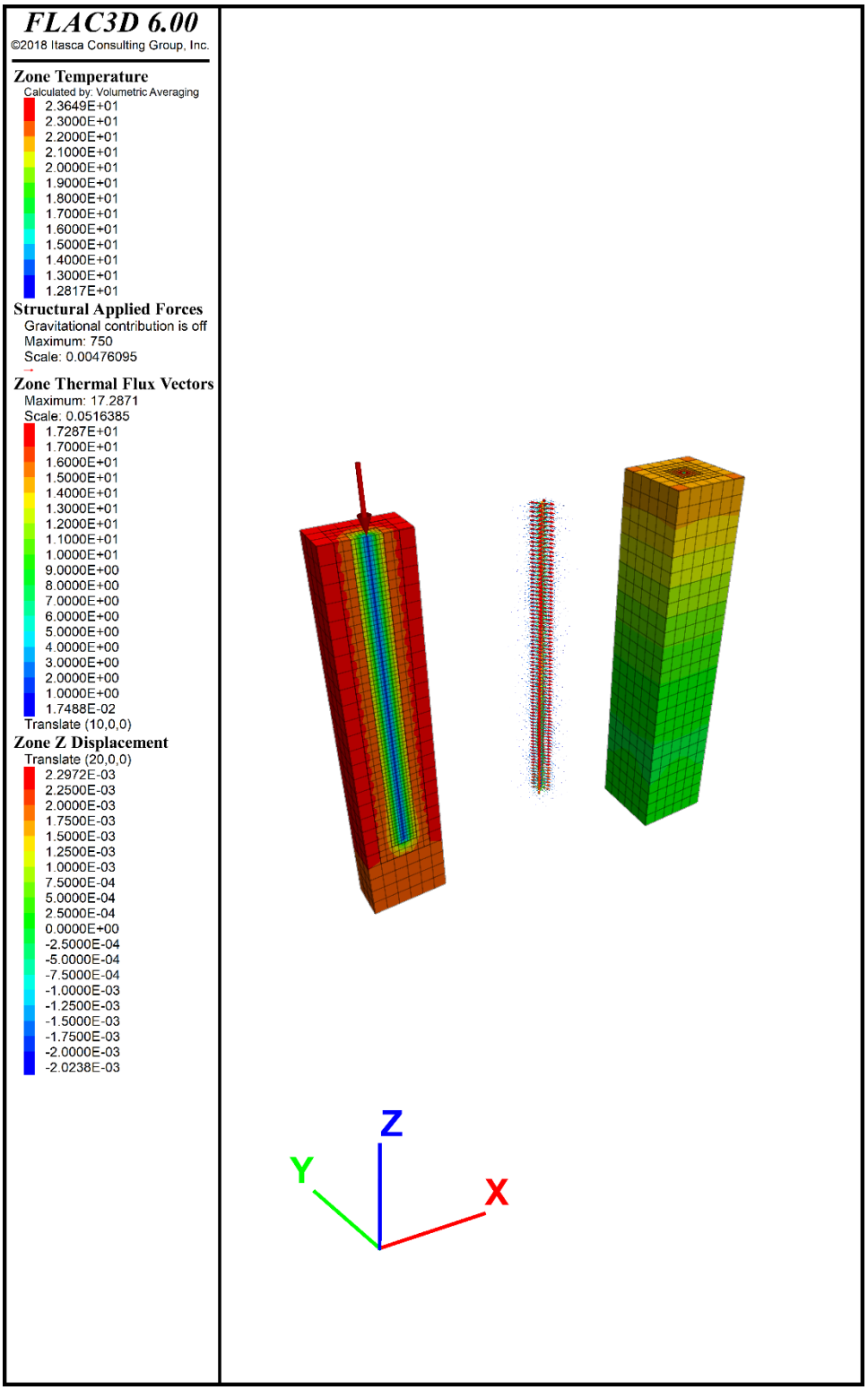

Figure 4.16. Numerical model setup for case number 1

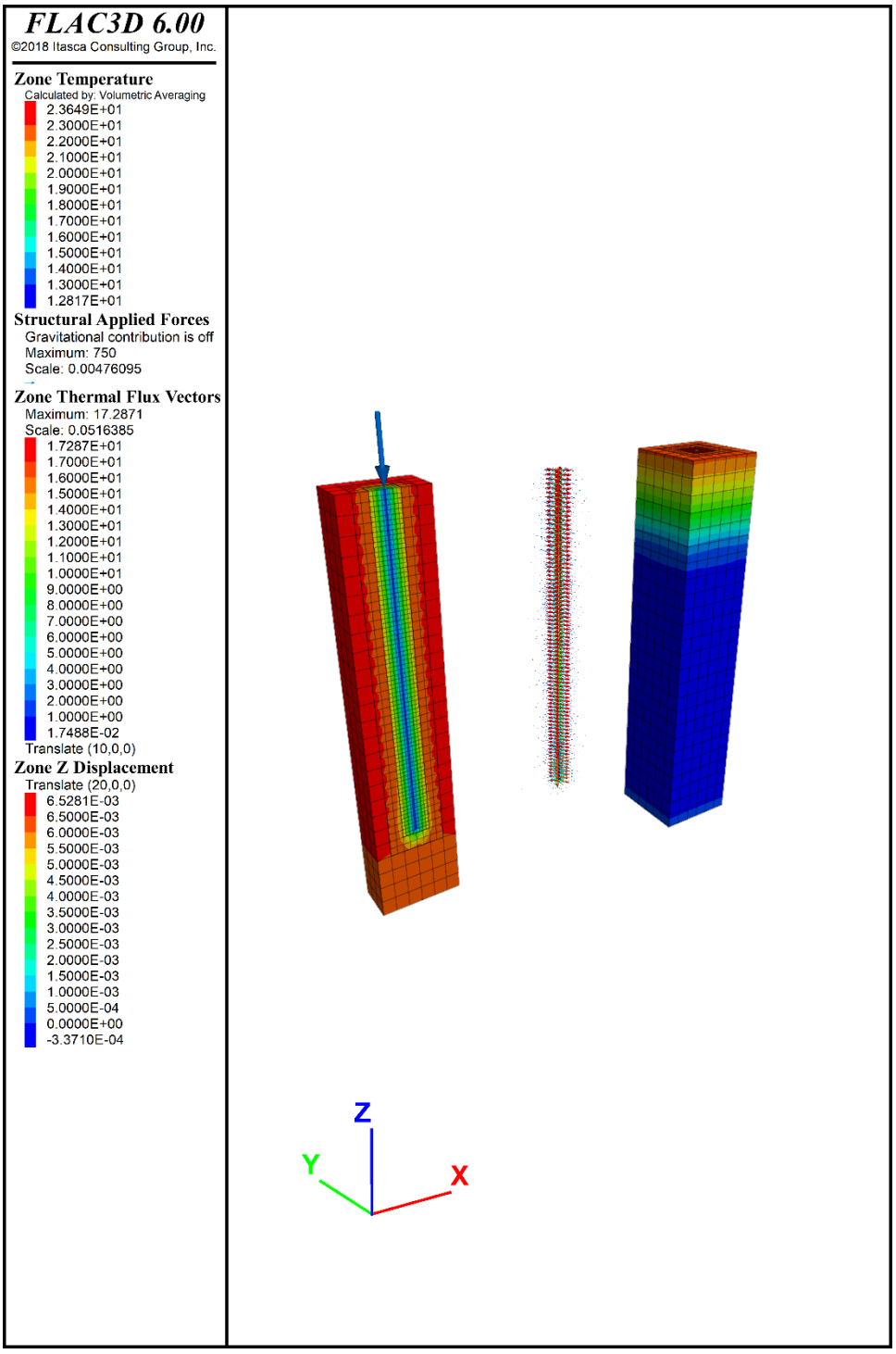

Figure 4.17. Numerical model setup for case number 2

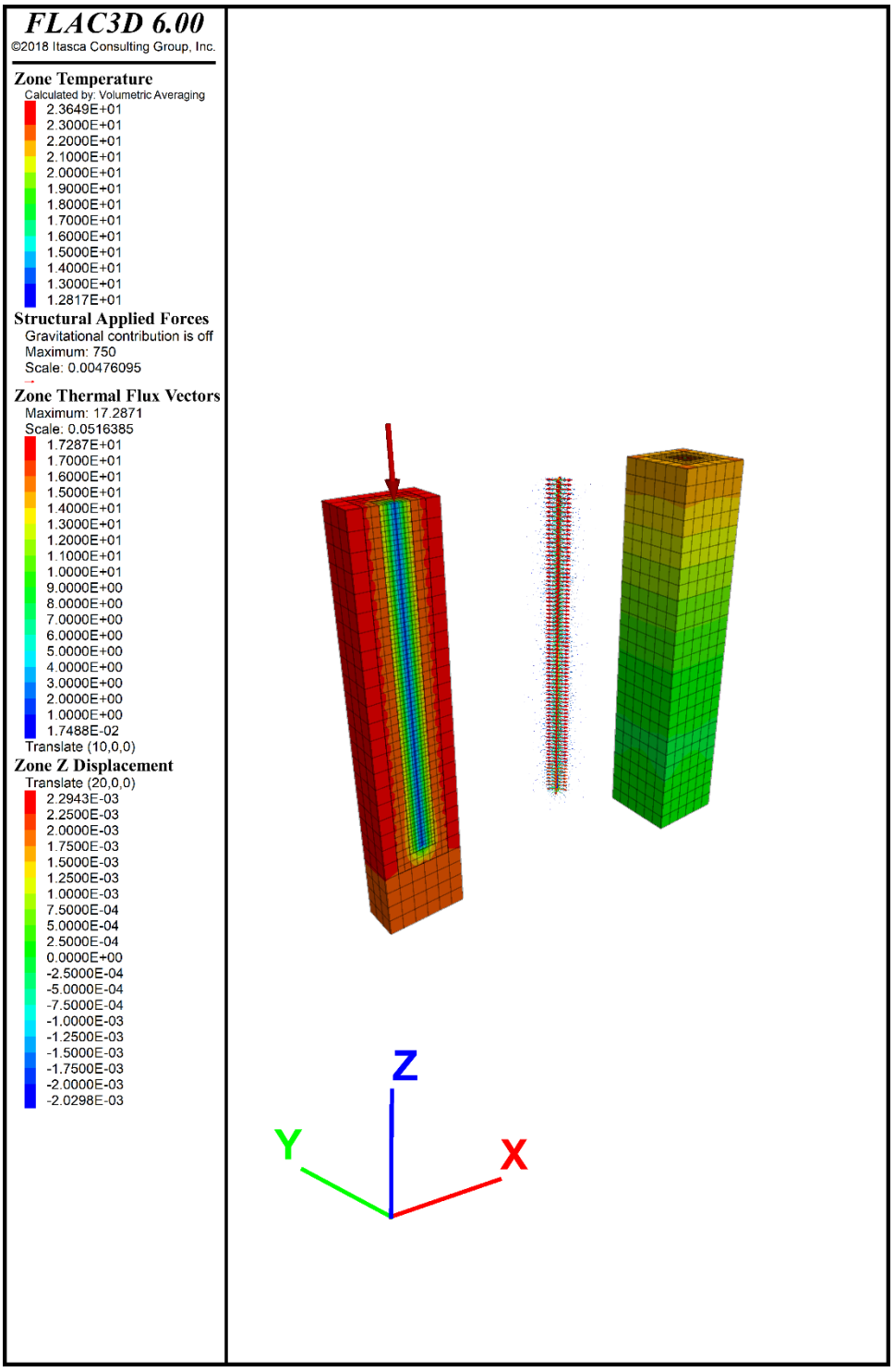

Figure 4.18. Numerical model setup for case number 3

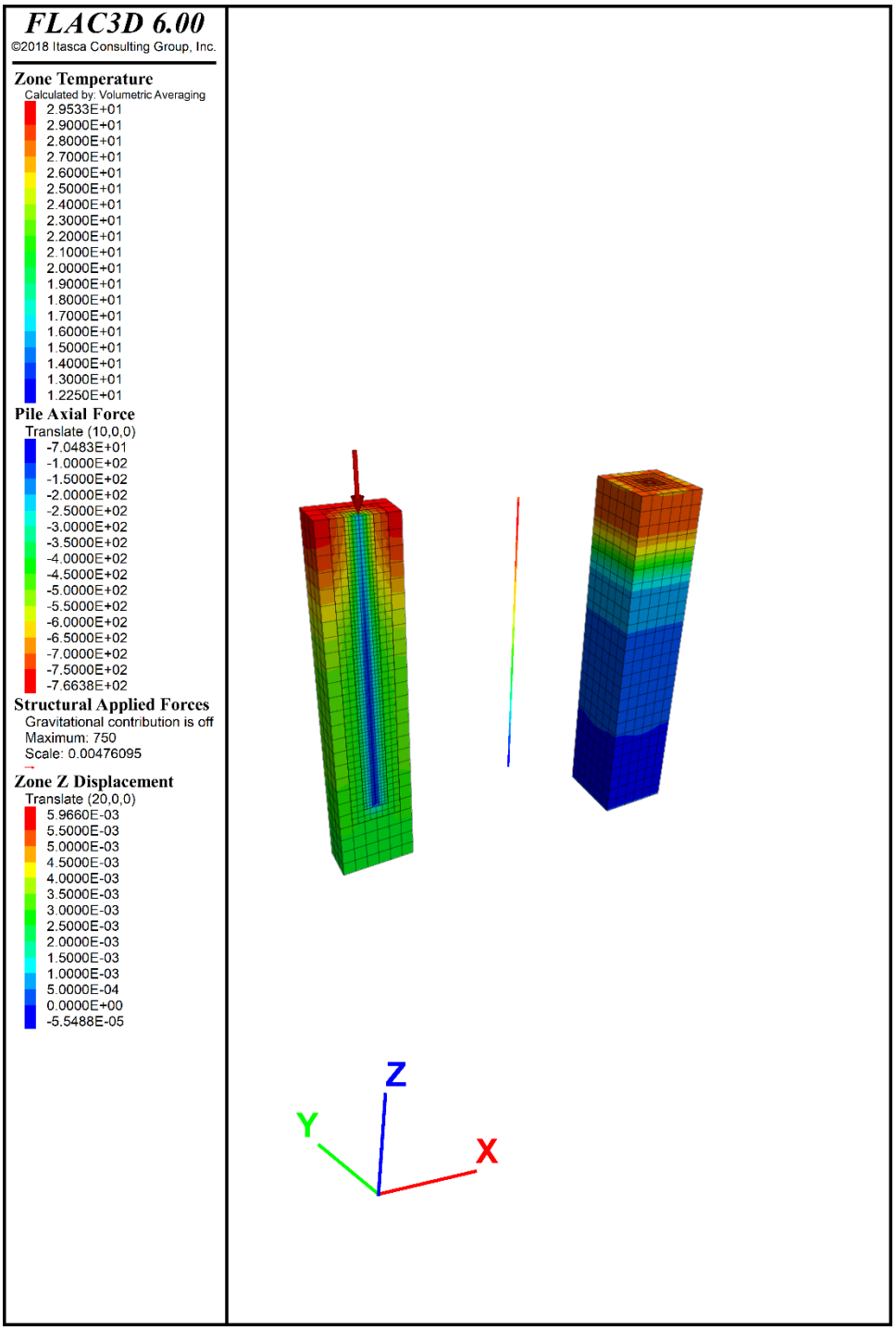

Figure 4.19. Numerical model setup for case number 4

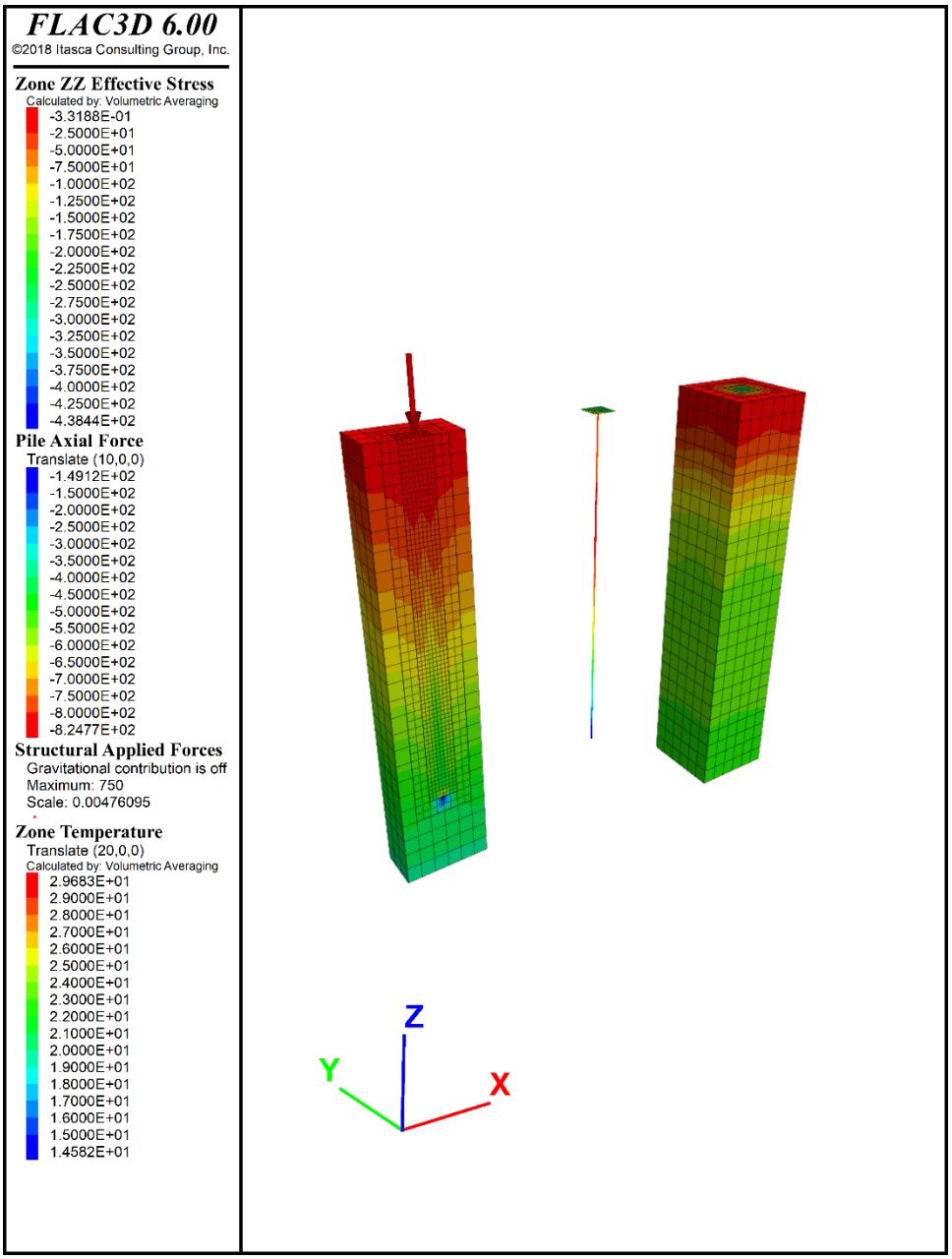

Figure 4.20. Numerical model setup for case number 5

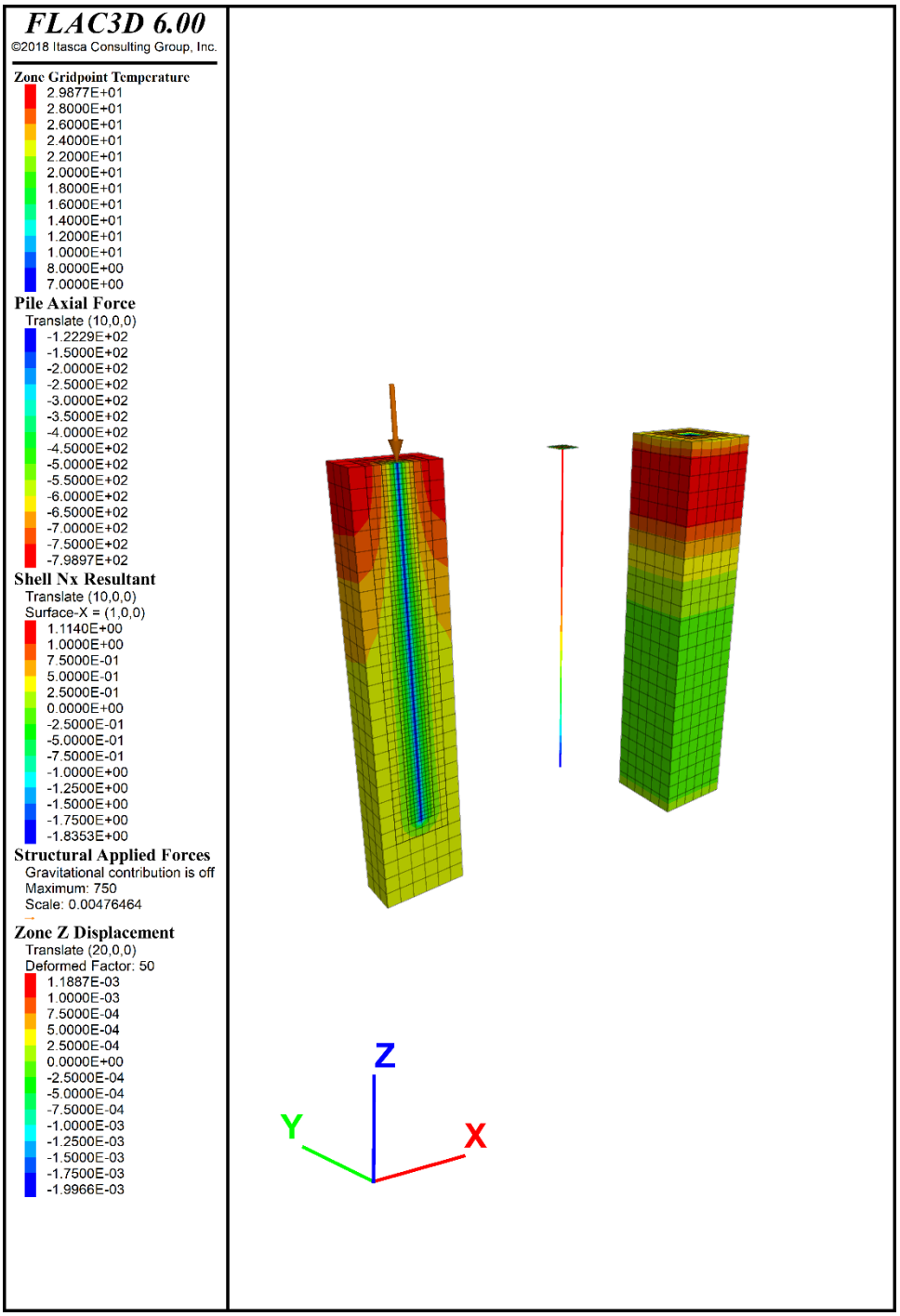

Figure 4.21. Numerical model setup for case number 6

4.10.2 Results and Discussion

In this part, the results of pile load distribution, pile nodal and soil z-direction displacement for different cases are presented for all the cases mentioned in Table 4.4. On a general note, the negative z-direction displacement shows the movement in downward direction and the positive displacement shows the upward direction. Also, all the negative loads are tension are positive ones denotes to the compression. In the plot's legend where it says "Soilc" it refers to the soil grid points at the pile SEL location.

4.10.2.1 Initial Soil Temperature Profile: Constant vs. Variable

The temperature gradient between the nodes of the pile SEL node and soil grid points was studied. Two scenarios for constant and varying temperature profile were considered. The initial profiles for both cases are based on the local reports and available literatures for the over consolidated clay soil (e.g. Akrouch et al., 2014). For the constant temperature condition, the entire numerical domain is set at $22°C$ (Figure 4.22a), while the varying profile the temperature is set to $35°C$ at the surface and down to $22°C$ at the water table. The gradient of $0.3\left(°C/m\right)$ is considered. All the zones below water table has initial temperature of $22°C$ (Figure 4.22b). From Figure 4.26 and Figure 4.30, the pile load distribution for the cases of constant and varying soil temperature profile, respectively, is very similar in trend and behavior. Additionally, the Figure 4.27 and Figure 4.31 of pile and soil vertical displacement indicates a very similar behavior for the two cases. These observations indicate that the initial soil temperature profile will not significantly change the pile-soil behavior in during cyclic thermal loading.

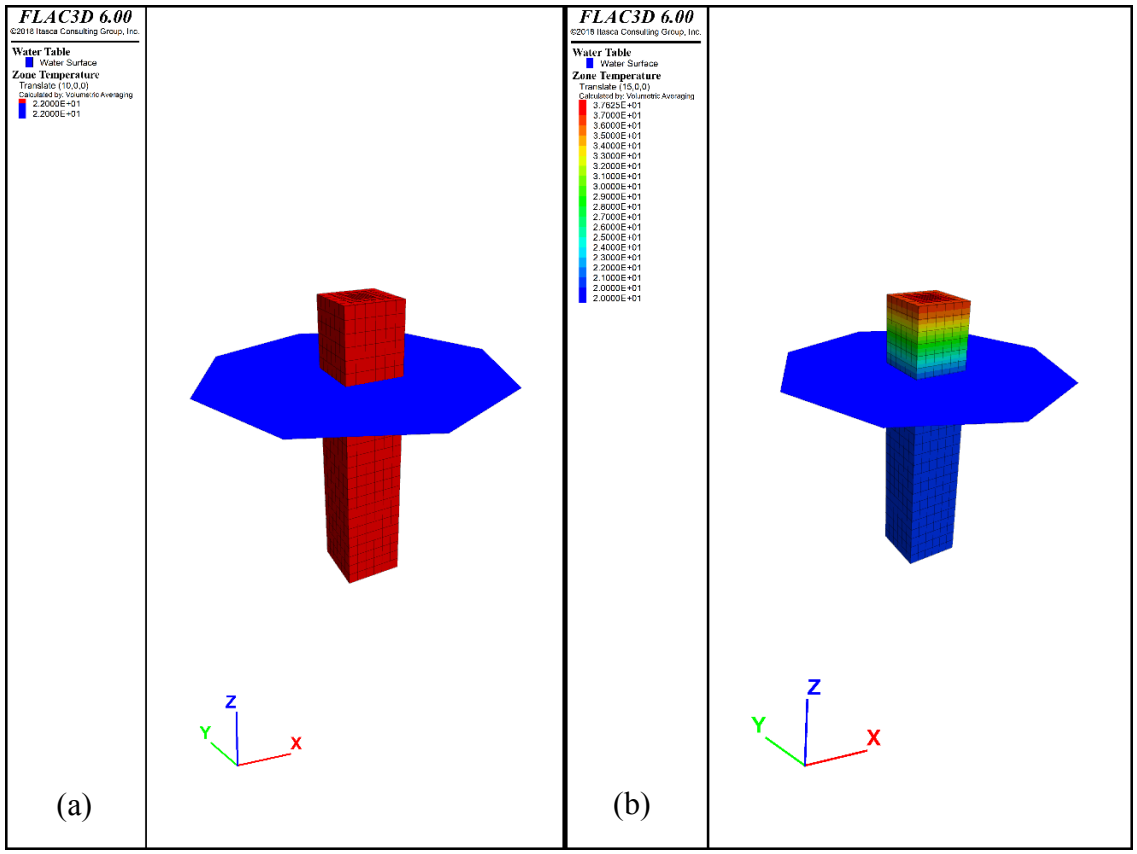

Figure 4.22. Model setup for constant temperature (a) and the varying profile (b)

4.10.2.2 Groundwater Table Location effect

As it is demonstrated in the Figure 4.24 and Figure 4.28, the pile load distribution under the influence of water table location is very much insignificant. As previously mentioned in the scope of work section, the soil zones which are placed above the groundwater table location were assigned a special case of fluid boundary condition. Through various studies and analysis based on the theoretical background of the available fluid modules in FLAC3D, it was decided to assign the "fix" pore pressure (a.k.a. permeable) condition to all the grid points above the groundwater table.

This will fix the pore pressure to prevent de-saturation of the zones and instability in the model. Also, during the undrained "thermal-mechanical" calculation, there was enough "slave"

mechanical step assigned comparing to the thermal "master" module, to make sure the pore pressure builds up as a result of the thermal loading maintains a reasonable trend. This analogy has been further demonstrated by the mean of pore pressure history plot from FLAC3D in Figure 4.39 and Figure 4.40. Part of the challenge was to define the correct fluid boundary condition for all of the presented coupled cases. Adjusting the values properly for fluid bulk modulus and tension limit as the two dominating parameters in undrained-drained calculations in the "wet" scheme solved the issues such as having zero pore pressure zones or de-saturation.

For the case of water table at the ground surface (Figure 4.23a), there is no need of assigning such fluid boundary condition since the hydrostatic pore pressure distribution directs to the fully saturated condition. However, the Figure 4.23b shows the pore pressure distribution for case of water table at 6m. The special fluid boundary condition used in this condition can be seen by fixing the pore pressure to zero for all the grid points located above the water table position. This case is also the indication of a fully saturation soil domain, but just from the numerical point of view, it is treated to compensate the limitation of FLAC3D in modeling unsaturated soil.

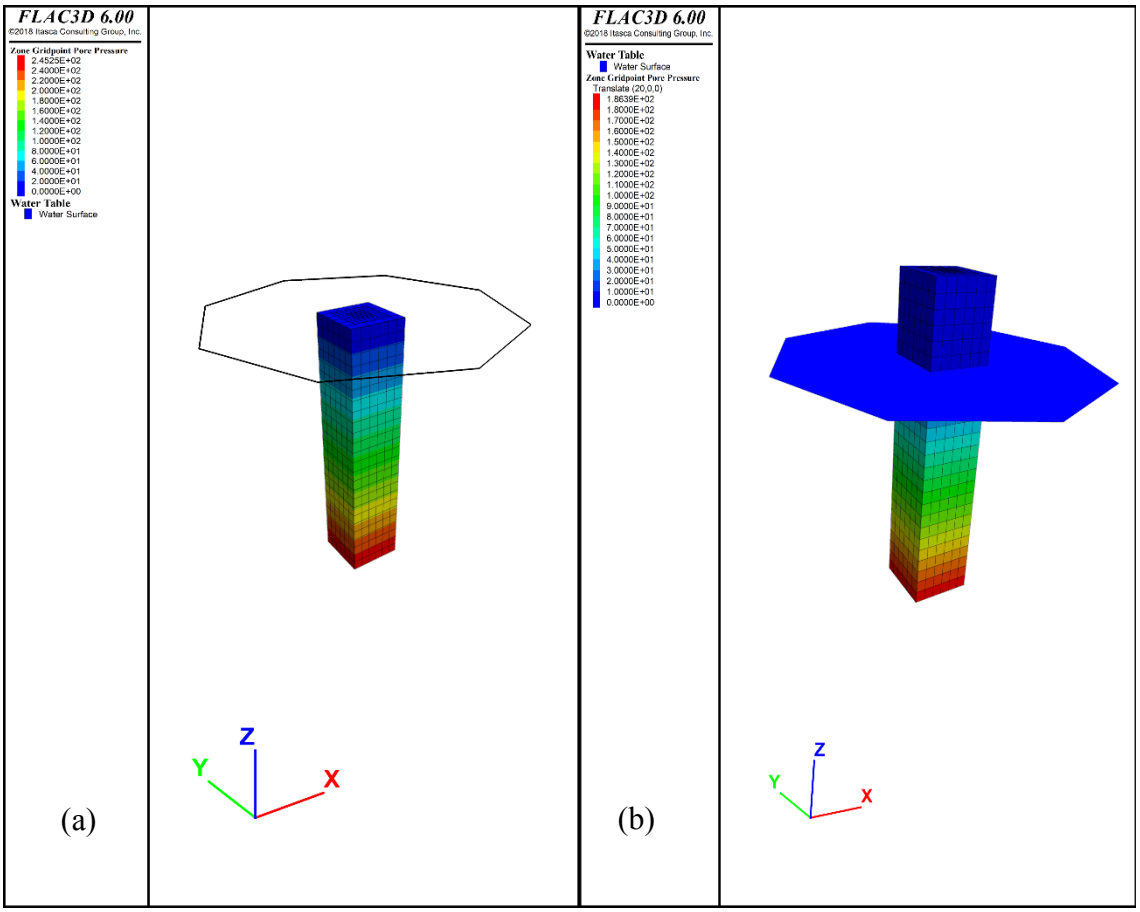

Figure 4.23. (a) Initial pore pressure for water table at the ground surface; (b) Initial pore pressure for water table at 6m

4.10.2.3 Coefficient of Permeability

As discussed in the scope of work section, the coefficient of permeability influence was studied on the coupling process. According to Figure 4.36, Figure 4.37, and Figure 4.38, the evolution of pore pressure during the undrained and drained condition can vary considerably for different coefficient of permeability. For the case number 7 (Figure 4.36), which has the highest coefficient of permeability of the cases, the convergence never been reached and the continuous cycle of sudden generation and dissipation of pore pressure occurred.

On the contrary, for the case number 8 (Figure 4.37) and number 9 (Figure 4.38), the lower coefficient of permeability resulted in a more interesting pore pressure history plot. When

coupled with the thermal module during the undrained mode, the Figure 4.37 shows a slight decrease in the generated pore pressure before the undrained calculation time scale is finished. However, such a slight decrease is not observed in the Figure 4.38 during the undrained calculations.

By tracking the evolution of pore pressure calculation based on varying the coefficient of permeability, the change in drainage behavior and its influence on the soil effective stress can be properly monitored when coupled with thermal module.

4.10.2.4 Single Pile Behavior

The pile SEL link along the axial direction replicates two mechanical behavior: frictional and confinement. These two behaviors are defined by coupling springs in "shear" and "normal" direction. Additionally, in order to properly define the pile's tip interaction with the soil, there is a special link connection available between the pile SEL's node and the adjacent zone's grid point called "Normal Yield (NY)" spring. The NY link connection is simply a definition of spring with properties including area, spring stiffness, yield-compression limit, and yield-tension limit. The yield-compression limit represents the pile's bearing capacity at the defined depth in which for this type of over consolidated clay it is set to 1100kN. The yield-tension limit will be set to zero all the time as the soil can't take tension.

The effect of the bottom link on the pile load distribution profile has been further studied for the cases of having non-zero and zero tension limit. The reason for such comparison was to track the effect of thermal expansion or contraction of the pile SEL in the load distribution profile. According to Figure 4.28 and Figure 4.30, the load distribution differs slightly at the depth from $16.0m$ to $19.5m$ along the pile. The bottom link with a non-zero yield-tension limit

affects the tension load evolution within that depth range during the cyclic heating and cooling process.

The pile load distribution, z-displacement profile for both pile and soil, and the slab effect is presented in this section's results. Figure 4.24 and Figure 4.25 shows the pile axial load distribution and soil-pile z-displacement for case number 1. The case number 1 is a simple demonstration of the single energy pile when subjected to a point load at the pile top node. Figure 4.24 indicates that load stays constant during various loading condition at the pile top. No tension at the pile SEL bottom link corrects the unrealistic tension axial load at the pile tip. Comparing Figure 4.24 and Figure 4.26 gives information on how the bottom link could affect the axial load distribution in pile while undergoing cyclic thermal loading. The influence on the trend of distribution is very minimal, however, during the heating process in first year in the case 2, it allowed to have more reduction in the compressive axial load in the pile than in case 1.

Soil and pile z-displacement profile presented in Figure 4.25 and Figure 4.27 differs in the heating process during first year of in the simulation. For the case of having none zero tension at the bottom pile SEL link (Figure 4.27), the soil and pile movement during heating process in the first year is more than the same situation in the case of zero tension at the bottom pile SEL link (Figure 4.25).

Figure 4.28 and Figure 4.30 shows the axial load distribution for the case of water table not at the ground surface (3 and 4) with the tension and no tension link at the pile bottom node. The trend is very much similar to the ones presented in cases 1 and 2. There is a slight difference between case 4 and 2 (Figure 4.30 and Figure 4.26). The effect of water table location causes the generation of small tension axial load from $16\mathrm{m}$ to $19\mathrm{m}$ and then reverses to compression at the bottom.

The effect of structural slab for a single pile is with full and no contact attachment condition. According to Figure 4.32 and Figure 4.34, the case of no and full contact of slab is presented. The no contact condition keeps the applied compression load at the pile top constant during expansion and contraction caused by cyclic heating and cooling process. This observation confirms the existence of gap between load bearing soil surface and structural slab. On the contrary, when the slab is in full contact, the axial load distribution is affected by the movement of both pile-slab and soil during cyclic thermal loading. That's the reason in Figure 4.34, it shows the axial load at top doesn't stay constant.

Since the heating process starts first, expansion in three components of the system including soil, pile, and slab induces tension load countering the compression from the building load. Then during the cooling process right after the end of heating, the contraction of all the above components induces the compression force countering the tension loads specifically in the pile.

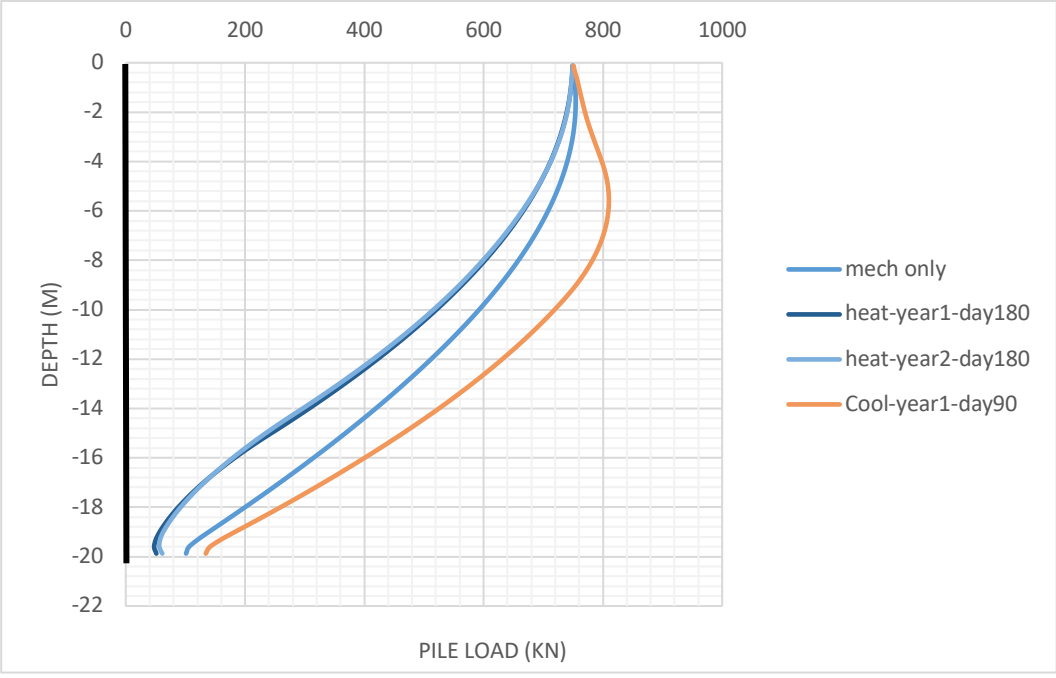

Figure 4.24. Pile load distribution for case number 1

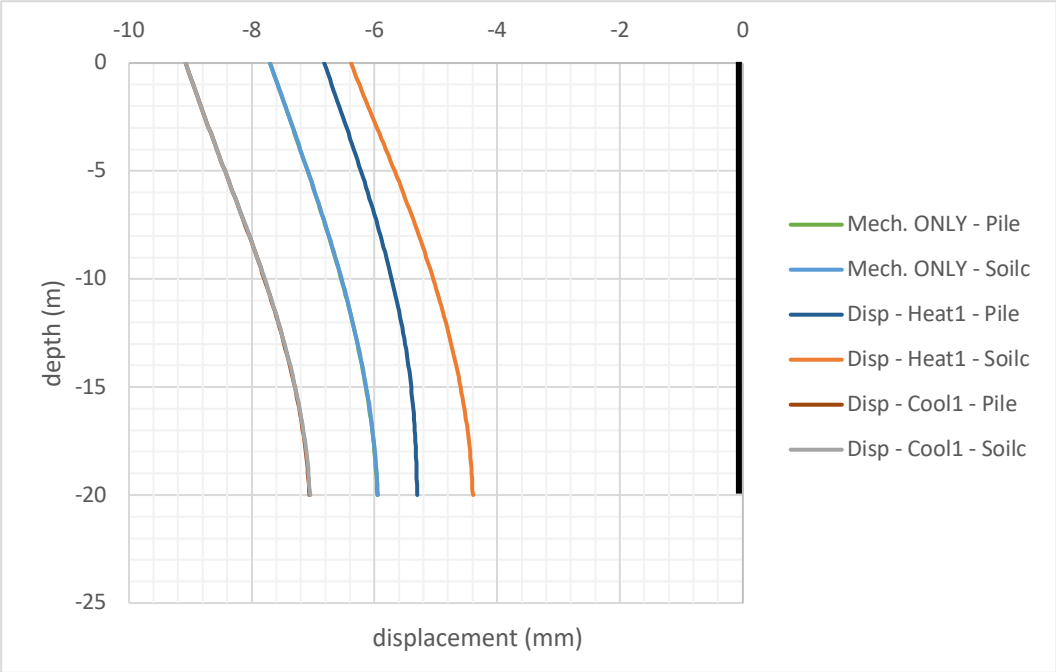

Figure 4.25. Soil and pile vertical displacement profile for case number 1

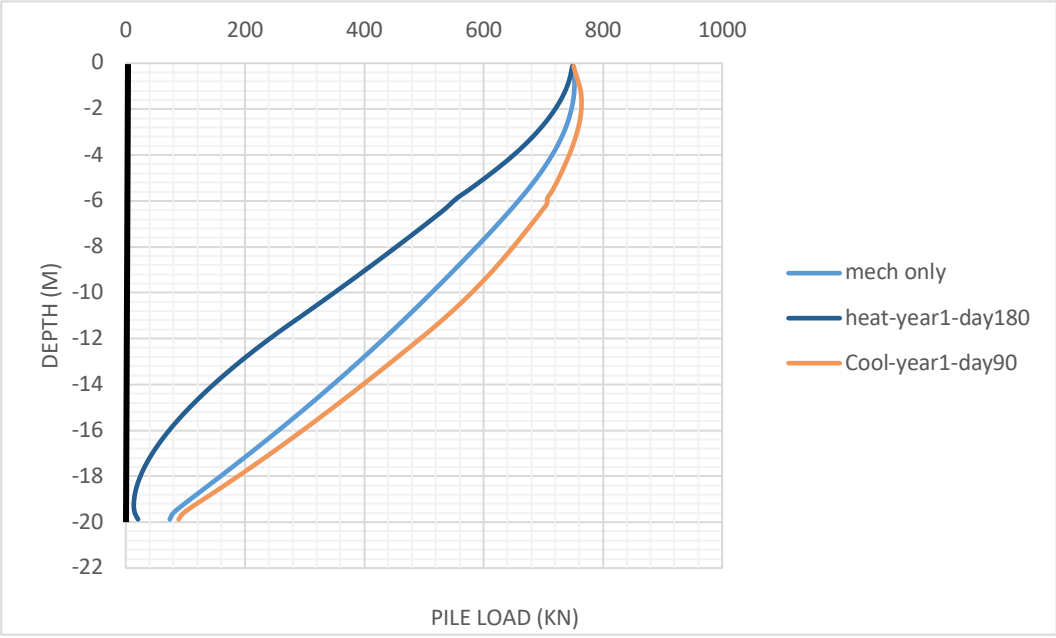

Figure 4.26. Pile load distribution for case number 2

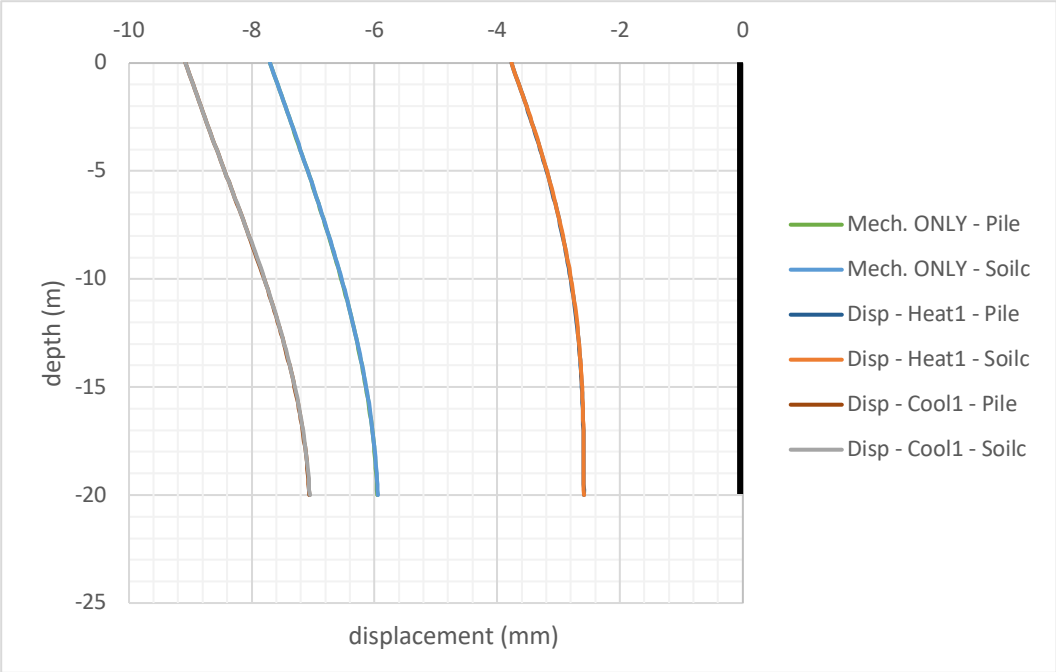

Figure 4.27. Soil and pile vertical displacement profile for case number 2

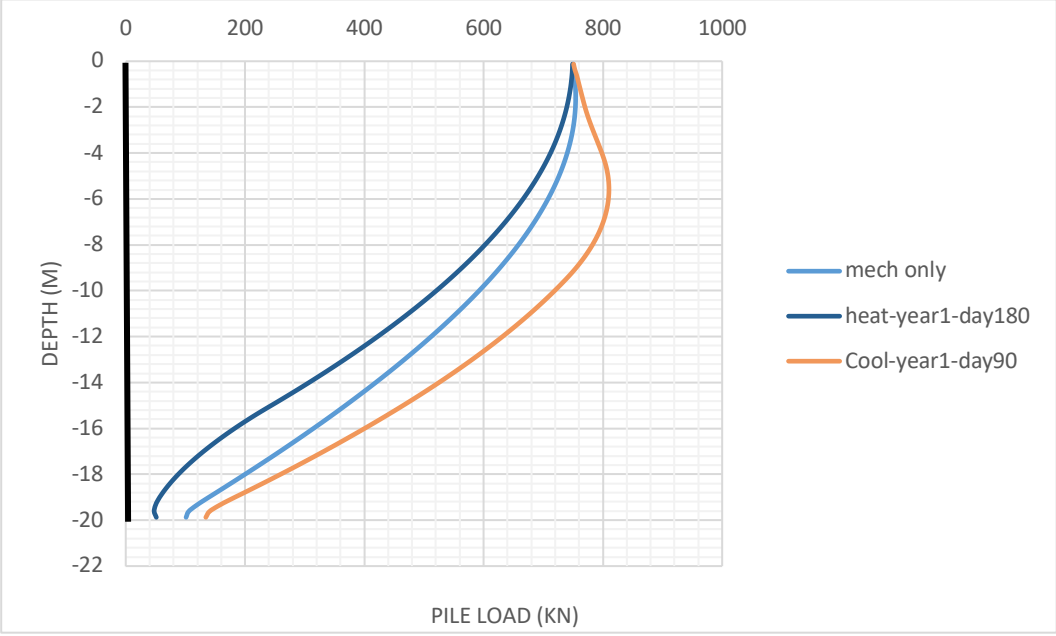

Figure 4.28. Pile load distribution for case number 3

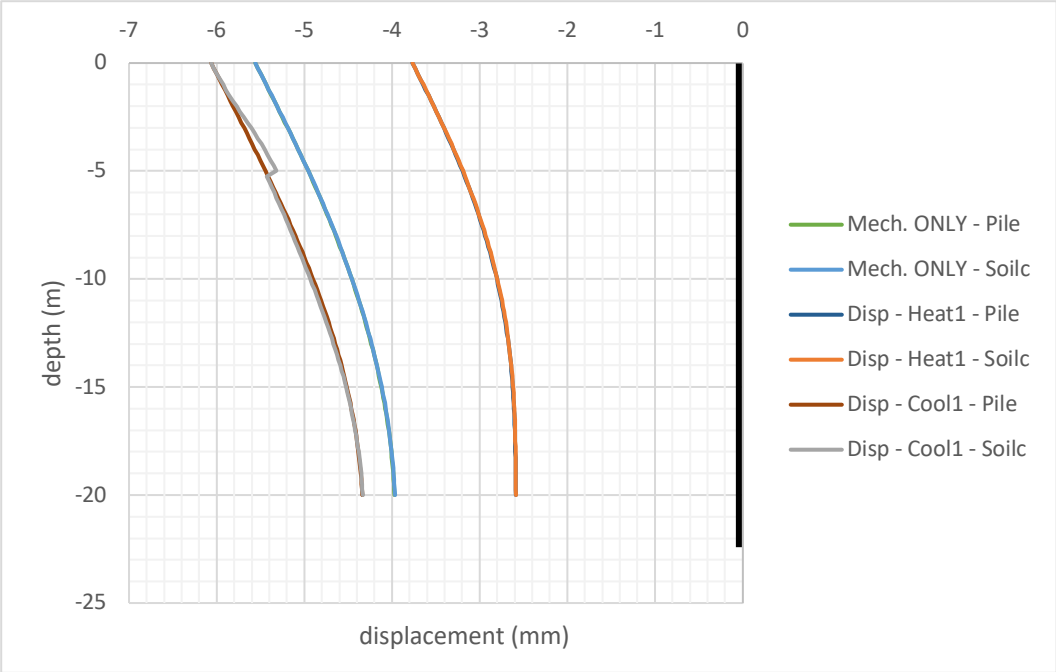

Figure 4.29. Soil and pile vertical displacement profile for case number 3

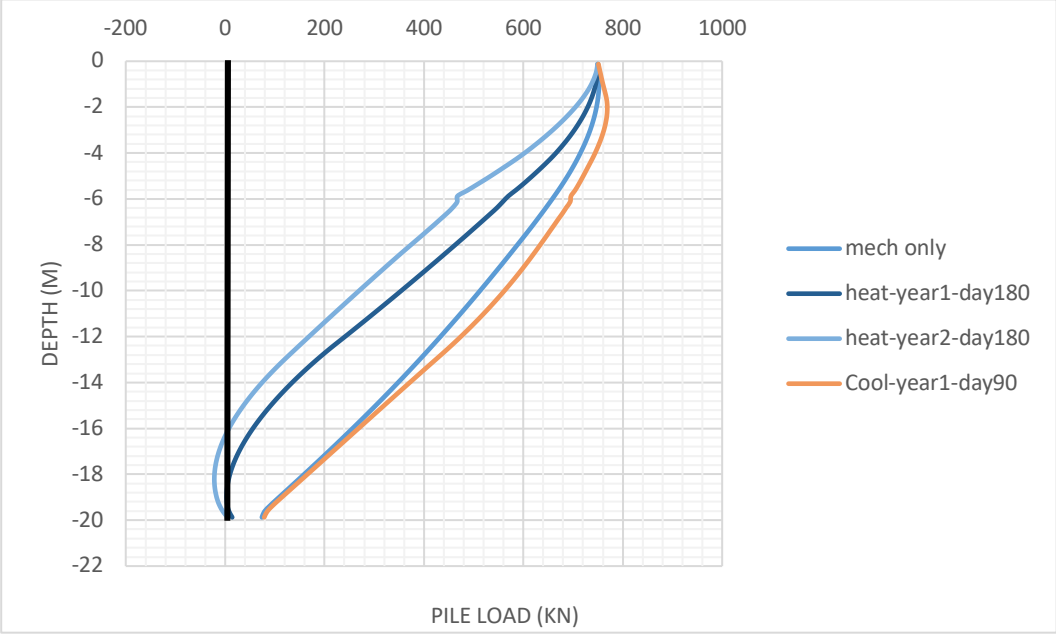

Figure 4.30. Pile load distribution for case number 4

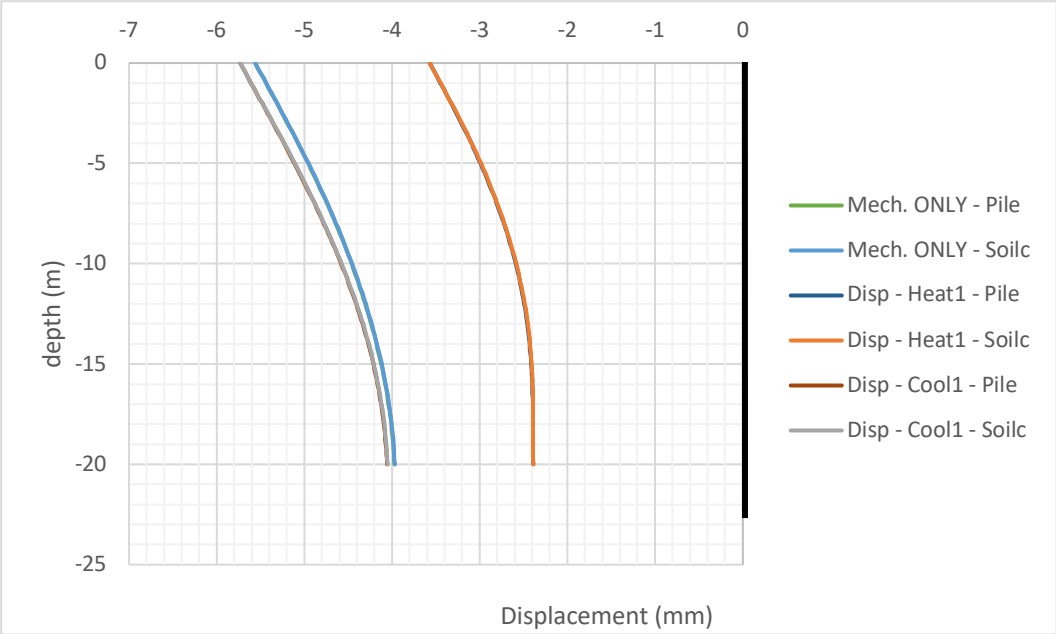

Figure 4.31. Soil and pile vertical displacement profile for case number 4

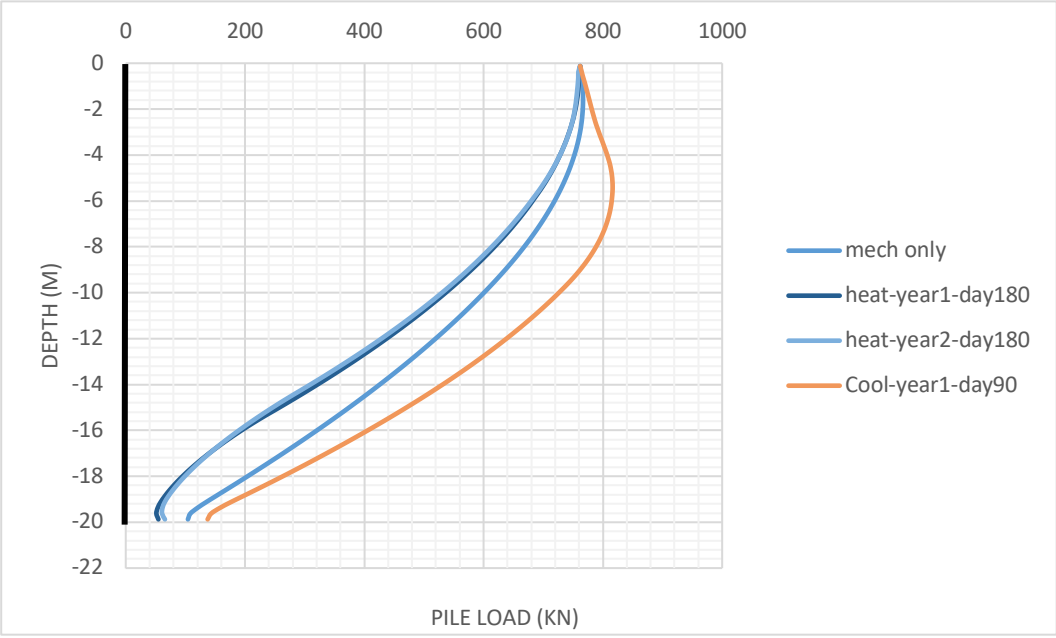

Figure 4.32. Pile load distribution for case number 5

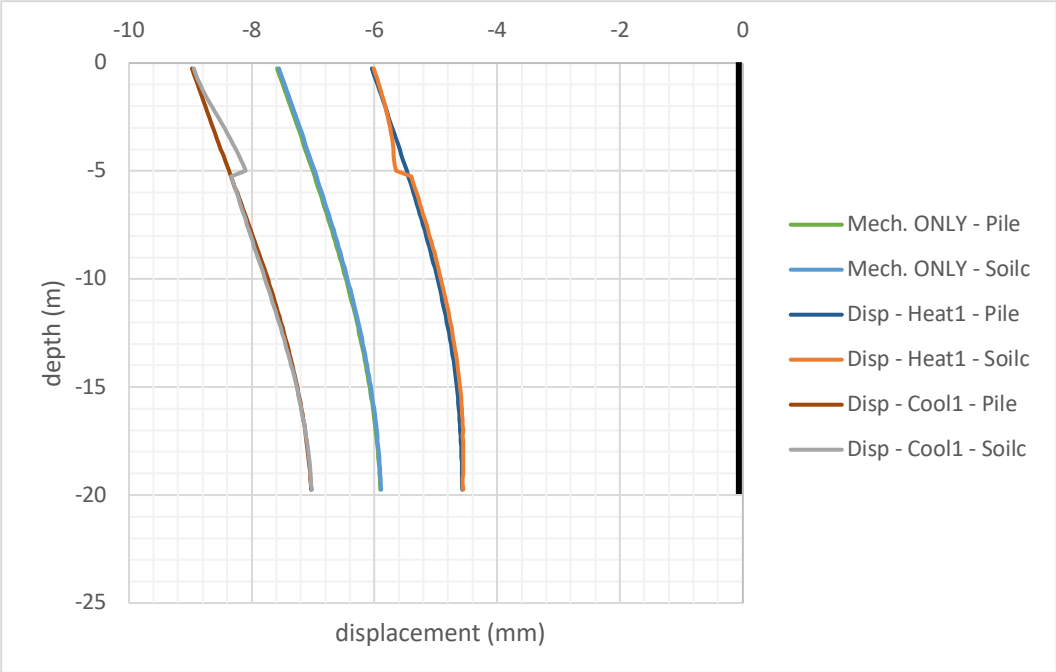

Figure 4.33. Soil and pile vertical displacement profile for case number 5

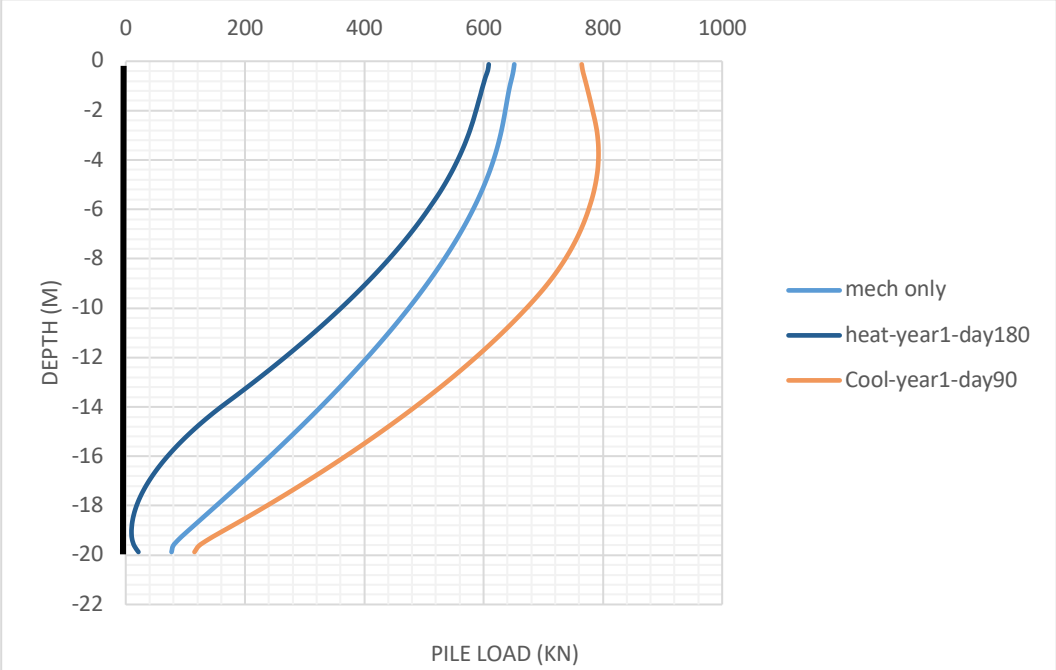

Figure 4.34. Pile load distribution for case number 6

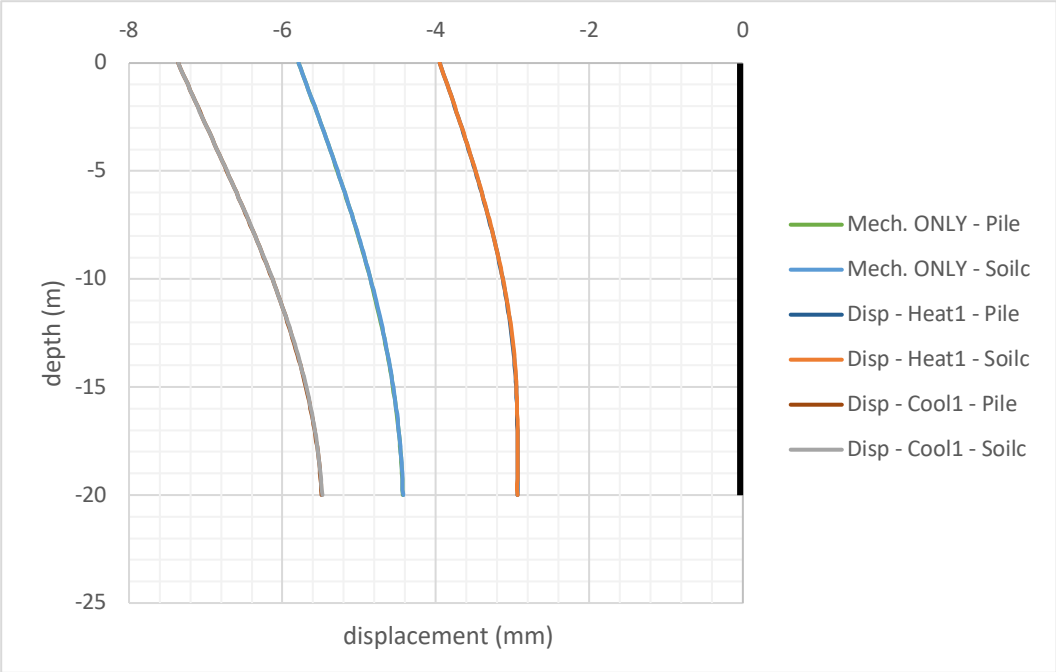

Figure 4.35. Soil and pile vertical displacement profile for case number 6

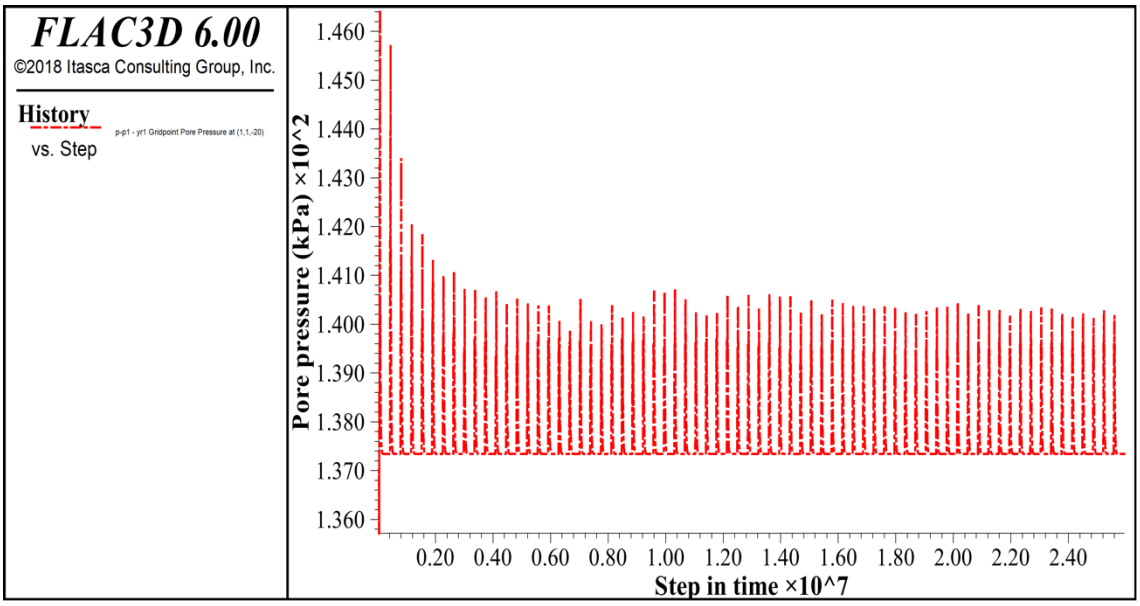

Figure 4.36. Pore pressure history plot for the case number 7

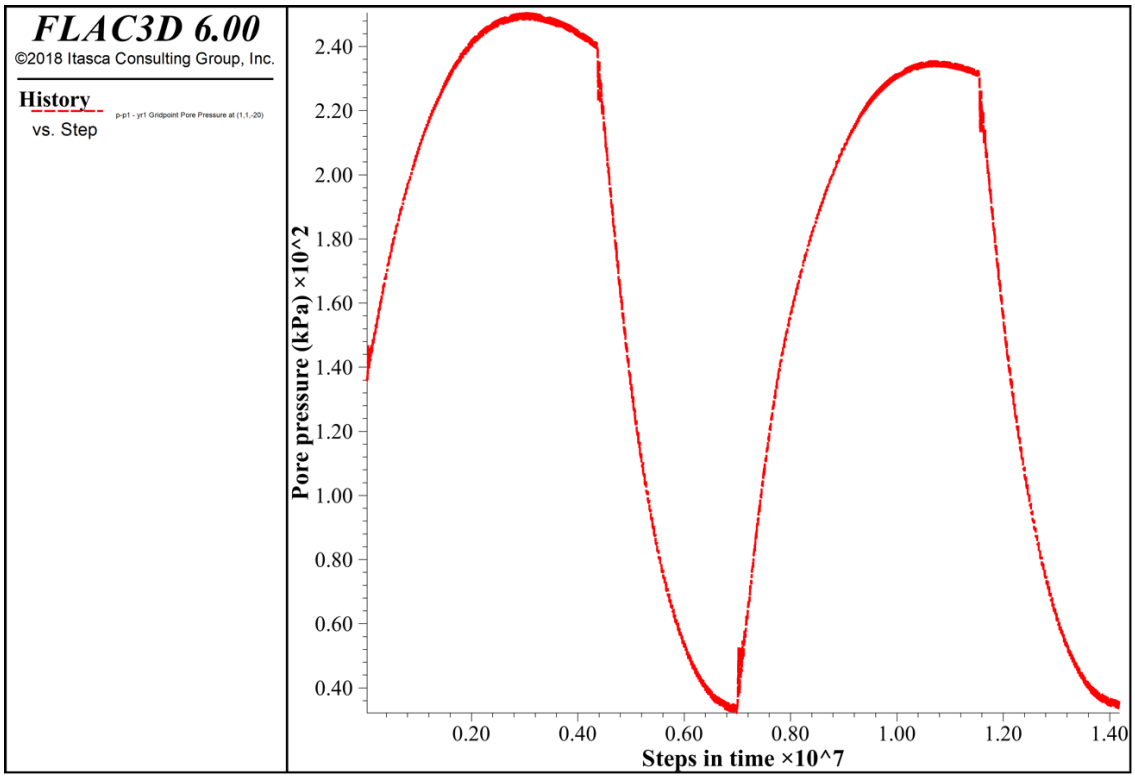

Figure 4.37. Pore pressure history plot for the case number 8

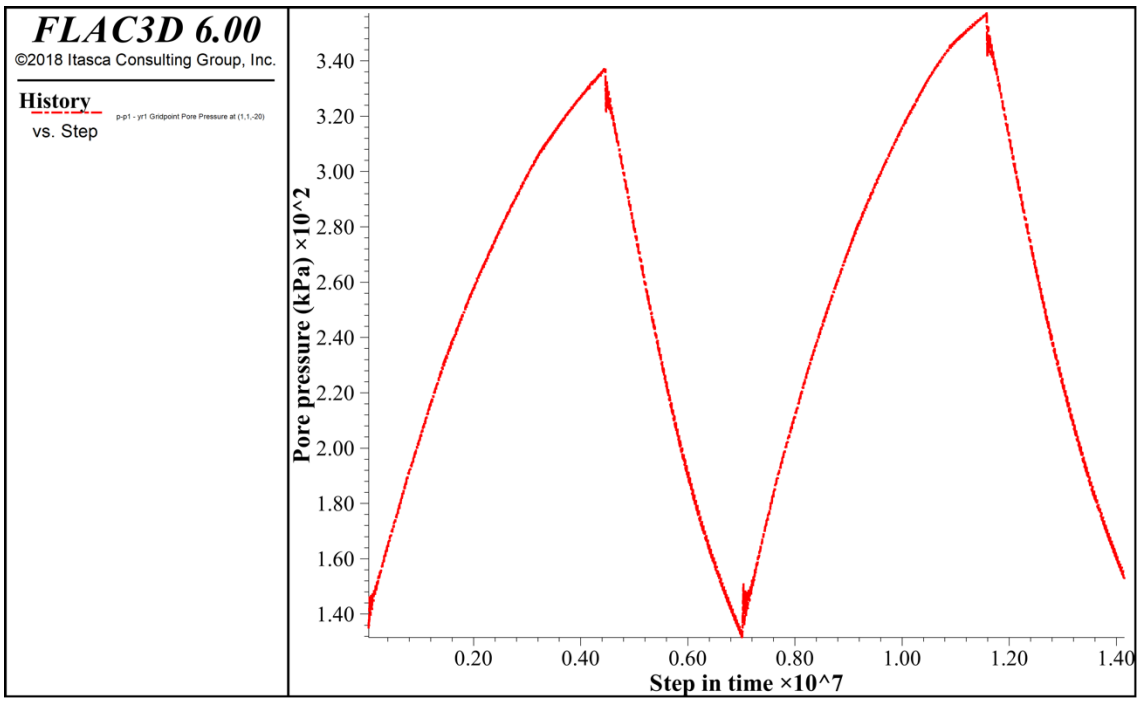

Figure 4.38. Pore pressure history plot for the case number 9

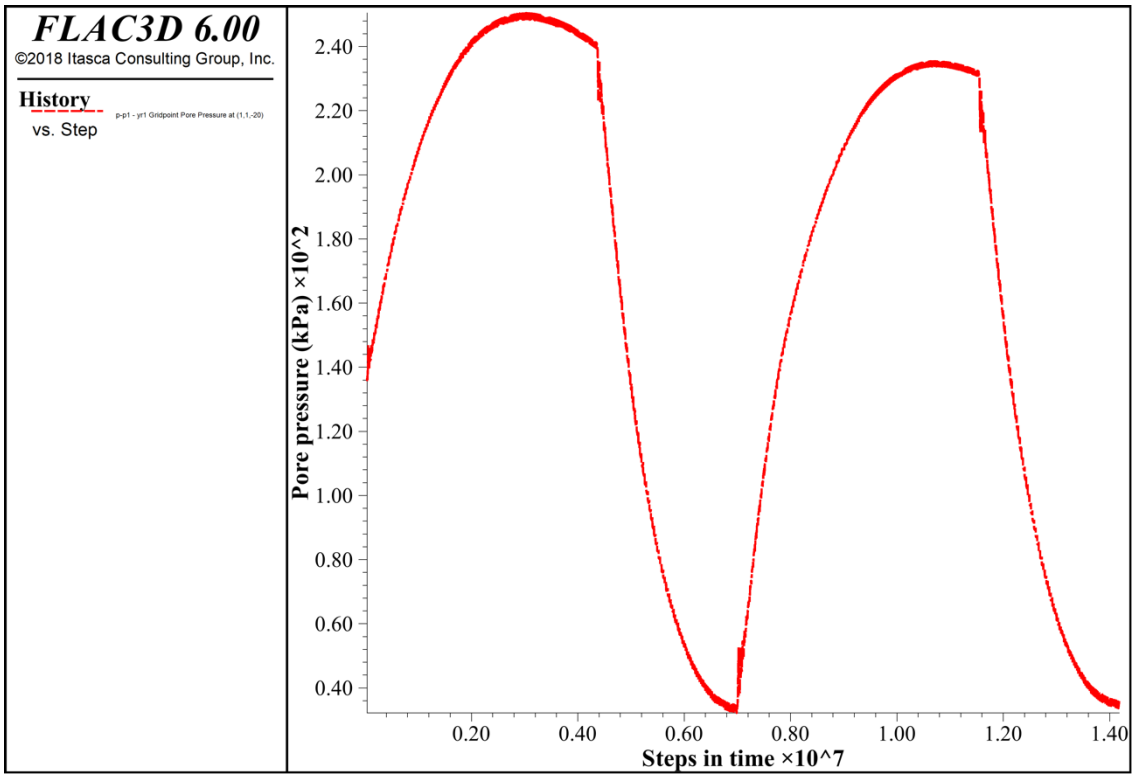

Figure 4.39. Pore pressure history plot for the case number 10

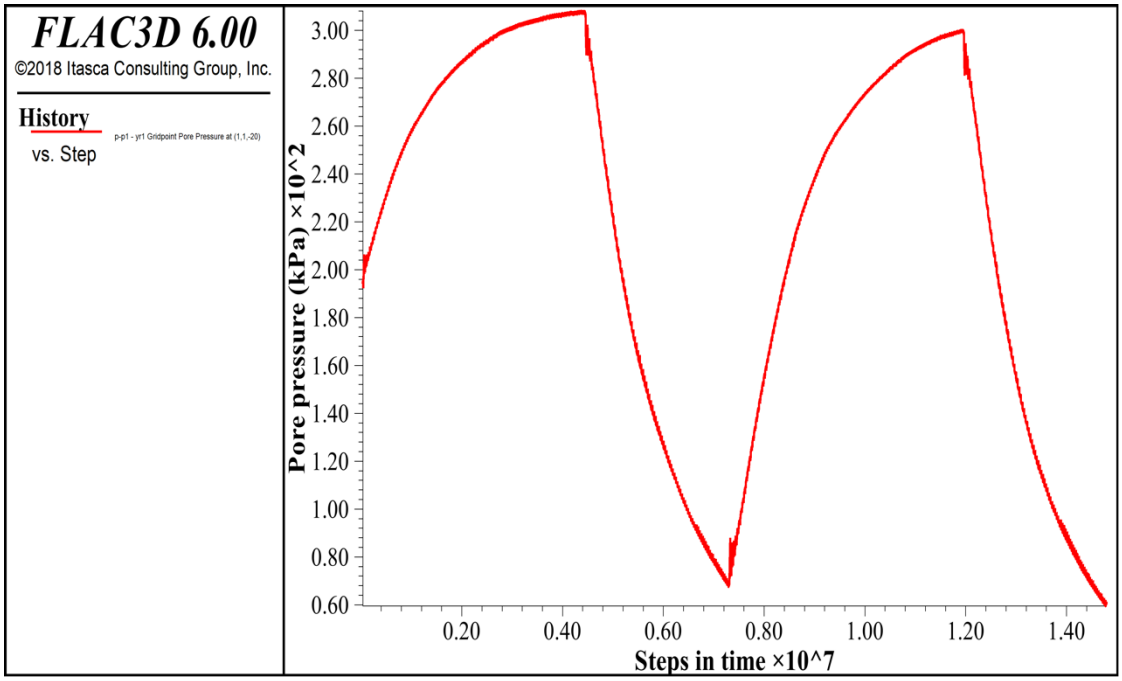

Figure 4.40. Pore pressure history plot for the case number 11

4.11 Thermo-Mechanical Model Calibration

4.11.1 In Situ Test Setup

In this section, the full-scale pullout test reported by Akrouch et al. (2014) is used to carried out the next step of model calibration; this time under the full coupling condition of all the three processes: thermal, hydraulic, and mechanical. The details of the in-situ test can be found in Akrouch et al. (2014). In summary, two energy piles were installed in clay site at TAMUS RELLIS campus. The piles dimensions were $0.18m$ in diameter and $5.5m$ long with a single steel rebar #8 as the reinforcement. The yield strength of the reinforcement was $517MPa$.

Each energy pile included one U-shape PEX pipe representing the geothermal system loop with $19mm$ inner diameter and $23mm$ outer diameter. A concrete slab with the dimension of $9m \times 6m \times 0.3m$ was constructed to serve as the platform for the load test. Thermal sensors, mechanical strain gauges, and dial gauges were used to monitor the thermo-mechanical response of the pile. Figure 4.41 (a) and Figure 4.41 (b) shows the details of the test setup.

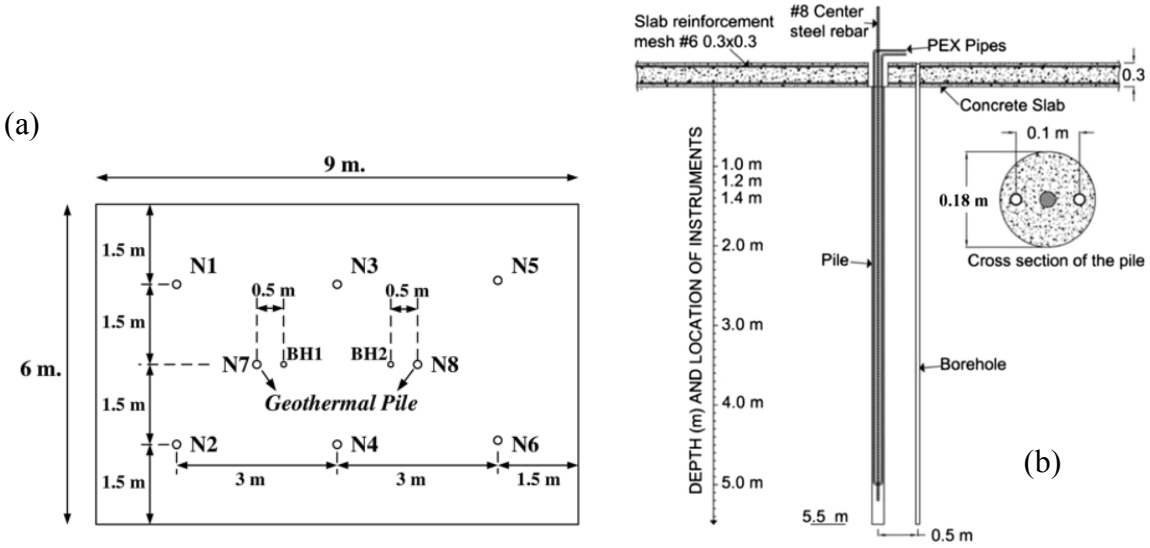

Figure 4.41. (a) Energy pile setup; (b) cross view for the pile N7 (Akrouch et al., 2014)

4.11.2 Model Details and Results

The model setup for such a straight forward looking in situ test was significantly complicated. In order to simulate the test as closely as possible to the actual condition, several different mechanisms were utilized in FLAC3D. Soil behavior were modeled by the calibrated mechanical PH model as discussed in 4.9 (Table 4.5). The thermal model and the optimized coupling codes from the section 4.10 was used (Table 4.5).

For the grout part, elastic model from FLAC3D library is used with the reinforced concrete properties (Table 4.6). The rebar #8 was simulated with beam structural element from FLAC3D with the properties demonstrated in (Table 4.7). The thermal model for soil zones was set to the isotropic conduction from FLAC3D thermal model library.

Since the concrete is represented by actual three-dimension computational zones, the thermal conduction model same as for the soil zones is used but with the concrete thermal properties (Table 4.6). The simulation time for thermal heating mode was set to 5 hours. The model's geometry extent is $1.5m \times 1.5m \times 10m$in the (x,y,z) direction, respectively. Roller mechanical boundary conditions were used at the far sides of the model, fixed in all directions at the bottom, adiabatic on the far sides and bottom, and no flow on the far sides and bottom.

Table 4.5. Thermal-mechanical properties used for soil zones.

$\rho\left(tones/m^3\right)$	1.544
$c'(kPa)$	28
$\phi'(^\circ)$	4
$V_s\left(m/s\right)$	232.486
$q_{tip}(kPa)$	5500 @ $z = 5m$
$E_{50}(kPa)$	31135
$E_{ur}(kPa)$	93405.1
$k_h\left(m/s\right)$	10^{-8}
$\lambda\left(W/^\circ C\right)$	0.53
$C_v\left(J/kg^\circ C\right)$	2800
$\alpha\left(1/^\circ C\right)$	3.3×10^{-5}

Table 4.6. Grout's thermal-mechanical properties

$\rho\left(tones/m^3\right)$	$K(kPa)$	$G(kPa)$	ν	$\lambda\left(W/^\circ C\right)$	$C_v\left(J/kg^\circ C\right)$	$\alpha\left(1/^\circ C\right)$
1.875	1.39×10^7	1.04×10^7	0.3	2.0	3300	3×10^{-7}

Table 4.7. Nail's thermal-mechanical properties for the beam structural element

$E(kPa)$	ν	$\alpha\left(1/^\circ C\right)$	$\rho\left(tones/m^3\right)$
2.04×10^8	0.3	3×10^{-7}	8.11

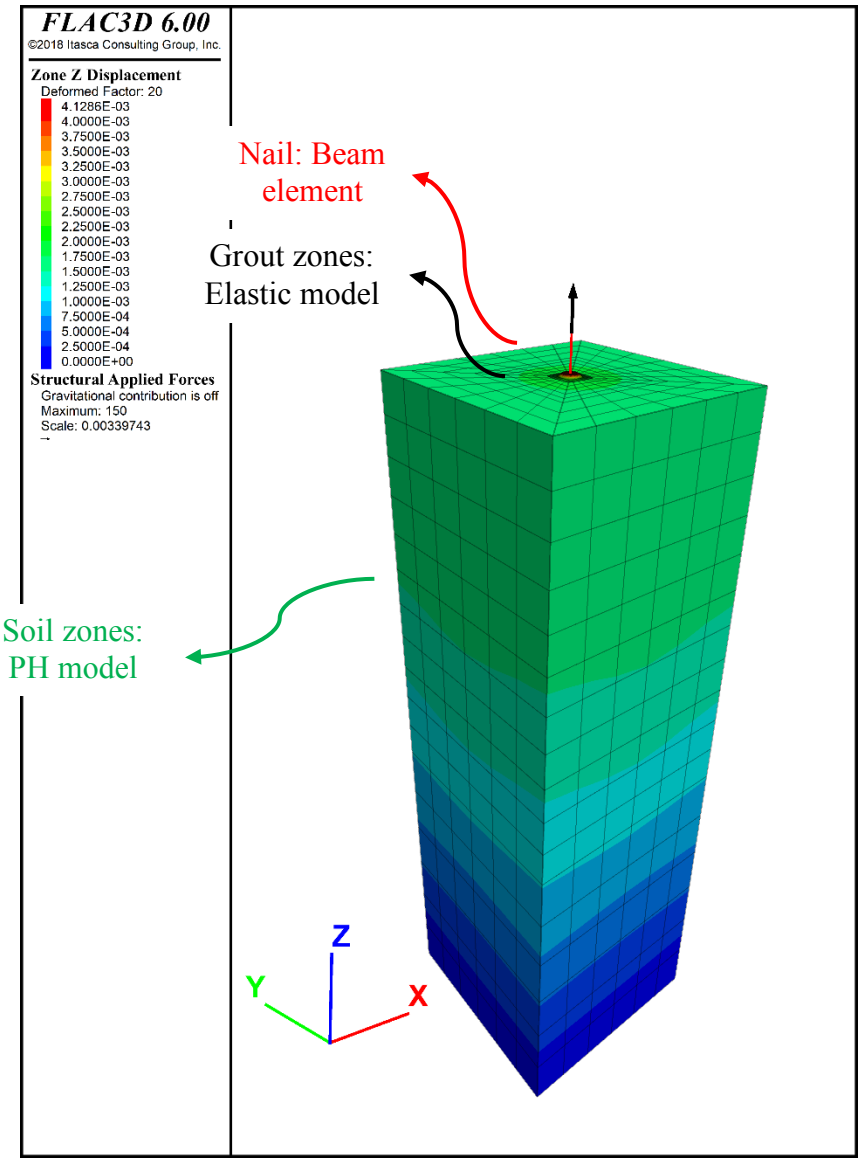

Figure 4.42. Model setup for thermal-mechanical calibration work

Since the mechanical model in FLAC3D doesn't have a realistic time stepping definition, the mechanical loading only comparison of the work against measurements from the test was done through the final readings at the end of each applied tension load. However, the thermal module incorporates the actual time stepping feature, comparison of the pile top displacement vs. time for the applied tension load of $150kN$ was completely presented.

Three plots are presented to carry out comparison between the numerical simulation and in situ test results: load displacement curve (Figure 4.43), pile top displacement (Figure 4.44), and soil temperature profile (Figure 4.45). Comparison of the results in Figure 4.43 and Figure 4.44 solidify the scheme used in the PH model to properly simulate the soil's mechanical response during the mechanical loading only and then the heating cycle. The thermal conduction model was also calibrated according to the results presented in Figure 4.45 having a reasonable agreement between numerical and measured temperature in soil profile.

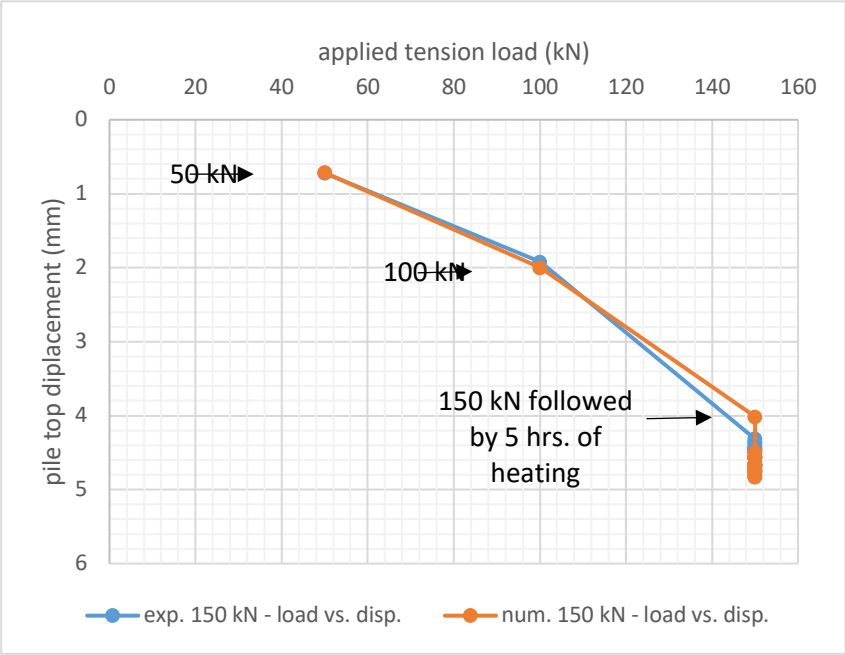

Figure 4.43. Load vs. displacement comparison for the applied tension load of 150 kN

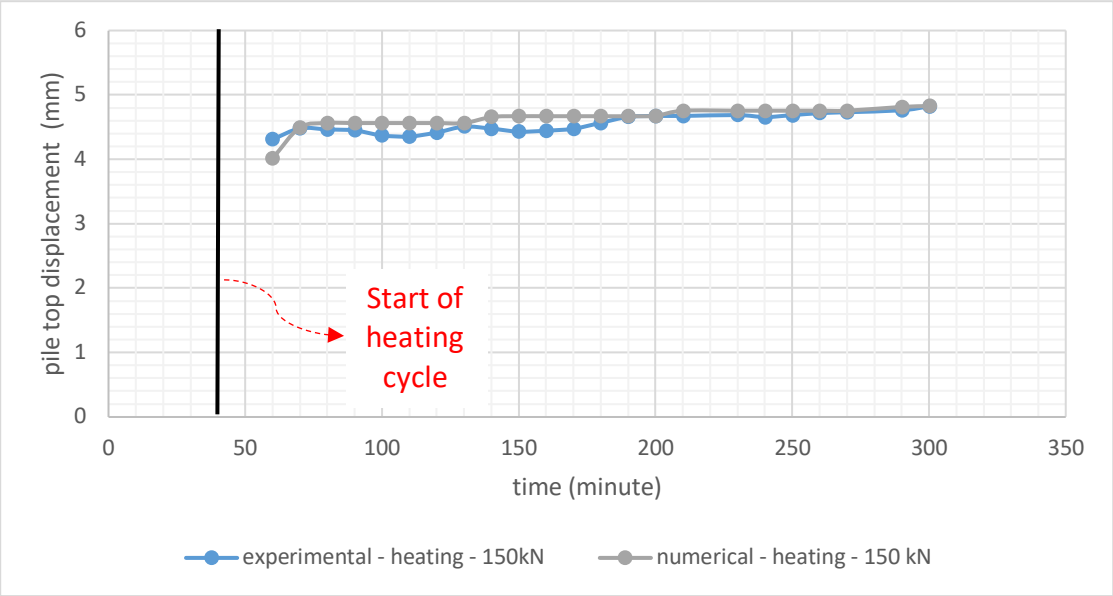

Figure 4.44. Pile top displacement vs. time during the heating process.

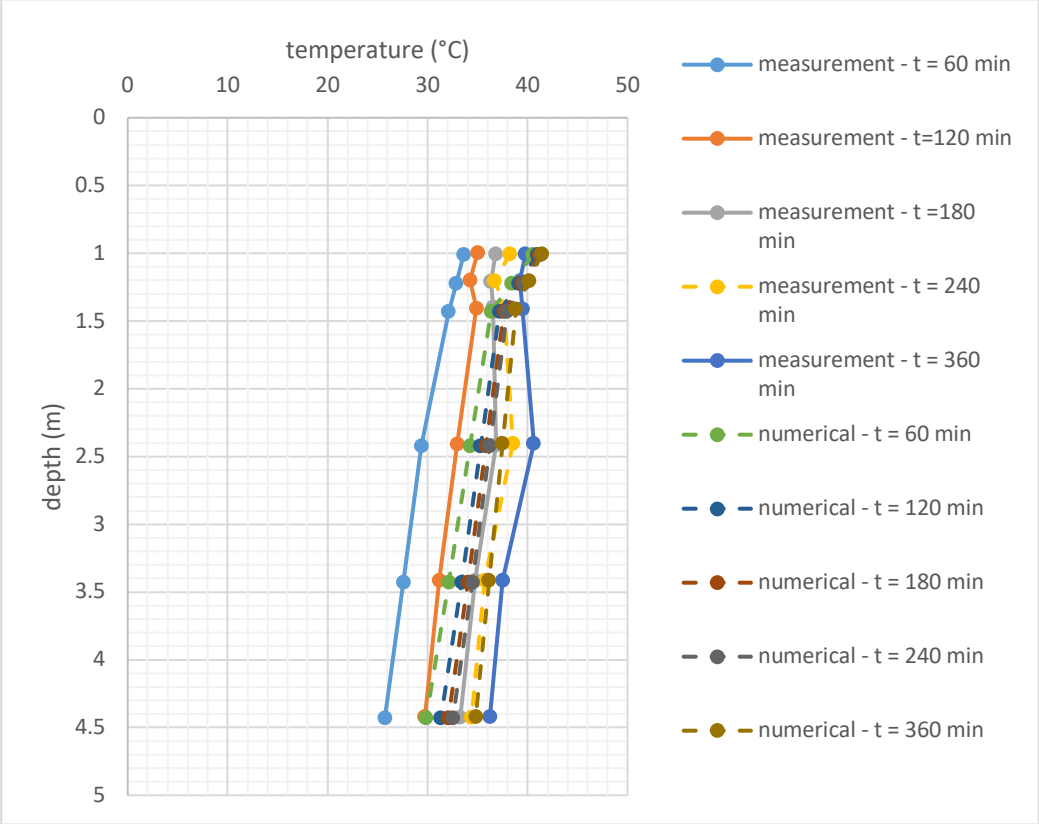

Figure 4.45. Numerical and experimental results over soil temperature profile

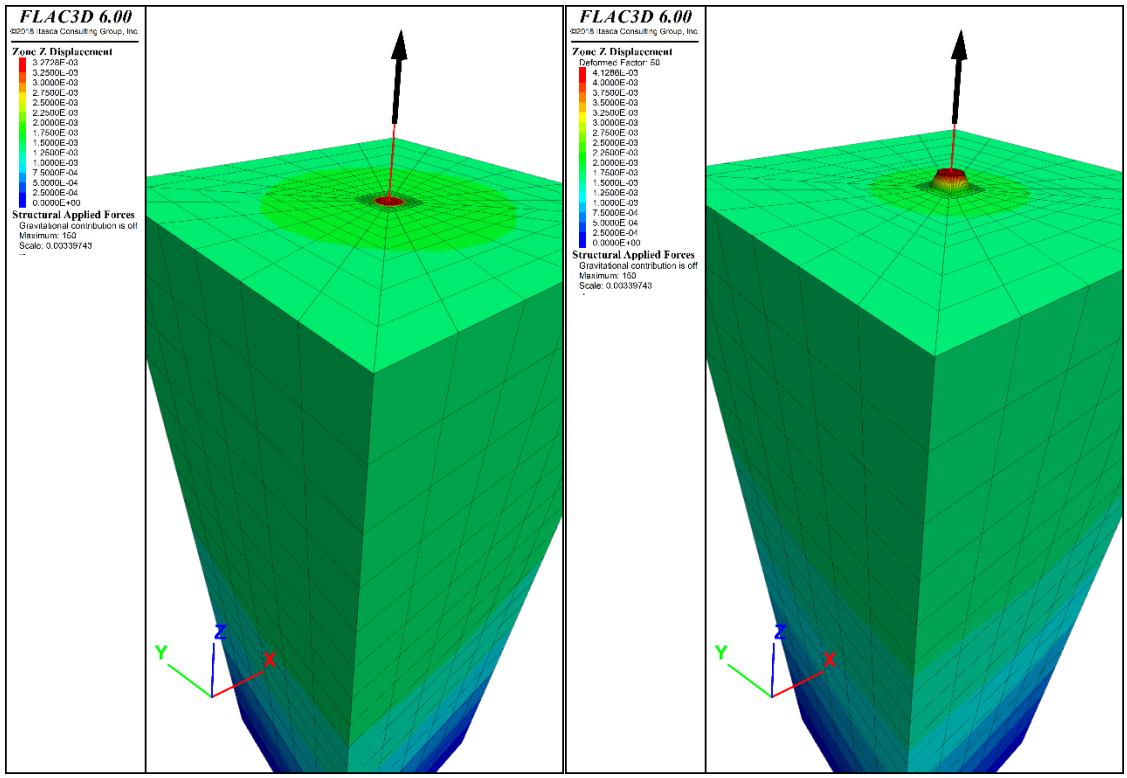

Figure 4.46. (a) Soil-grout z-direction displacement 150 kN and (b) Soil-grout z-direction displacement after 5hr heating cycle

Now that the thermal-mechanical coupling scheme is calibrated against the in-situ testing, the numerical model setup can be used to further study the more complicated cases of design recommendation (4.12) and case history analysis (4.13).

4.12 Design Recommendation Study

4.12.1 Introduction

This section covers the efforts on developing methodologies as design recommendations for engineers who deal with the full-scale application of thermo- active pile foundation. The design recommendation study aims to provide applicable and realistic solutions to the critical challenges in the way of incorporating the geothermal foundation system in a full-scale building. At the end of this section, two main questions will be answered in the form of design recommendations:

1. What is the evolution of thermal efficiency?
2. What is the thermal loading effect on soil-pile foundation interaction?

A hypothetical foundation footprint with the dimension of $30m \times 30m$ was considered to represent the full-scale application of the geothermal foundation system. The foundation vertical extent differs with respect to the length of the pile. The pile length includes $20m, 40m,$ and $60m$ with the mesh vertical extent to $40m, 60m,$ and $80m$, respectively. The pile spacing includes $2m, 3m, 6\,\mathrm{m},$ and $10m$. The piles are structural element type similar to those in the sensitivity analysis section (4.10).

The numerical model is set to simulate two years of a full-scale geothermal foundation operation, with 6 months of cooling mode (i.e. heating the soil), followed by 3 months of heating mode (i.e. cooling the soil). The soil's heating temperature is set at a constant temperature profile of $35°C$ along the pile length and the cooling is set at a constant temperature profile of $7°C$ along the pile.

The mechanical load is set to simulate an actual five story building with only the dead weight and gravitational force of the building element such as beams and columns considered to

be applied on the foundation. Due to the very large size of the mesh, mesh discretization for the foundation footprint was chosen to be $1m \times 1m \times 1m$ in the (x, y, z) direction. The pile SEL was divided into 20 components, having one element every 1m. Also, some limited sensitivity analysis based on changing the soil's thermal properties was carried out. Figure 4.47 to Figure 4.52 show the numerical model setup details for the cases presented in Table 4.9. The presented cases in Figure 4.47 to Figure 4.52 considered to be the major ones in which the entire logic of design recommendation study was based on in this research effort.

Table 4.8. Soil mechanical and thermal properties (excluding cases 3 and 4)

$\rho\left(tones/m^3\right)$	1.544
$c'(kPa)$	28
$\phi'(^\circ)$	4
$V_s\left(m/s\right)$	232.5
$k_h\left(m/s\right)$	10^{-8}
$\lambda\left(W/^\circ C\right)$	0.53
$C_v\left(J/kg^\circ C\right)$	2800
$\alpha\left(1/^\circ C\right)$	3.3×10^{-5}
β	2×10^{-4}

Table 4.9. Design recommendation case description

Case number	Description
1	$P_L = 20m,\ P_s = 2m$, Full contact slab
2	$P_L = 20m,\ P_s = 2m$, No contact slab
3	$P_L = 20m,\ P_s = 2m$, Full contact slab, $\lambda = 2.0\left(W/m°C\right)$
4	$P_L = 20m,\ P_s = 2m$, Full contact slab, $\alpha = 3.3\times10^{-6}\left(1/°C\right)$
5	$P_L = 20m,\ P_s = 3m$, Full contact slab
6	$P_L = 40m,\ P_s = 3m$, Full contact slab
7	$P_L = 60m,\ P_s = 3m$, Full contact slab
8	$P_L = 20m,\ P_s = 6m$, Full contact slab
9	$P_L = 20m,\ P_s = 6m$, No slab, Pile and building only
10	$P_L = 20m,\ P_s = 6m$, Shallow foundation mat (no pile)
11	$P_L = 40m,\ P_s = 6m$, Full contact slab
12	$P_L = 60m,\ P_s = 6m$, Full contact slab
13	$P_L = 20m,\ P_s = 10m$, Full contact slab
14	Soil free expansion, No SEL, Water table at 6m

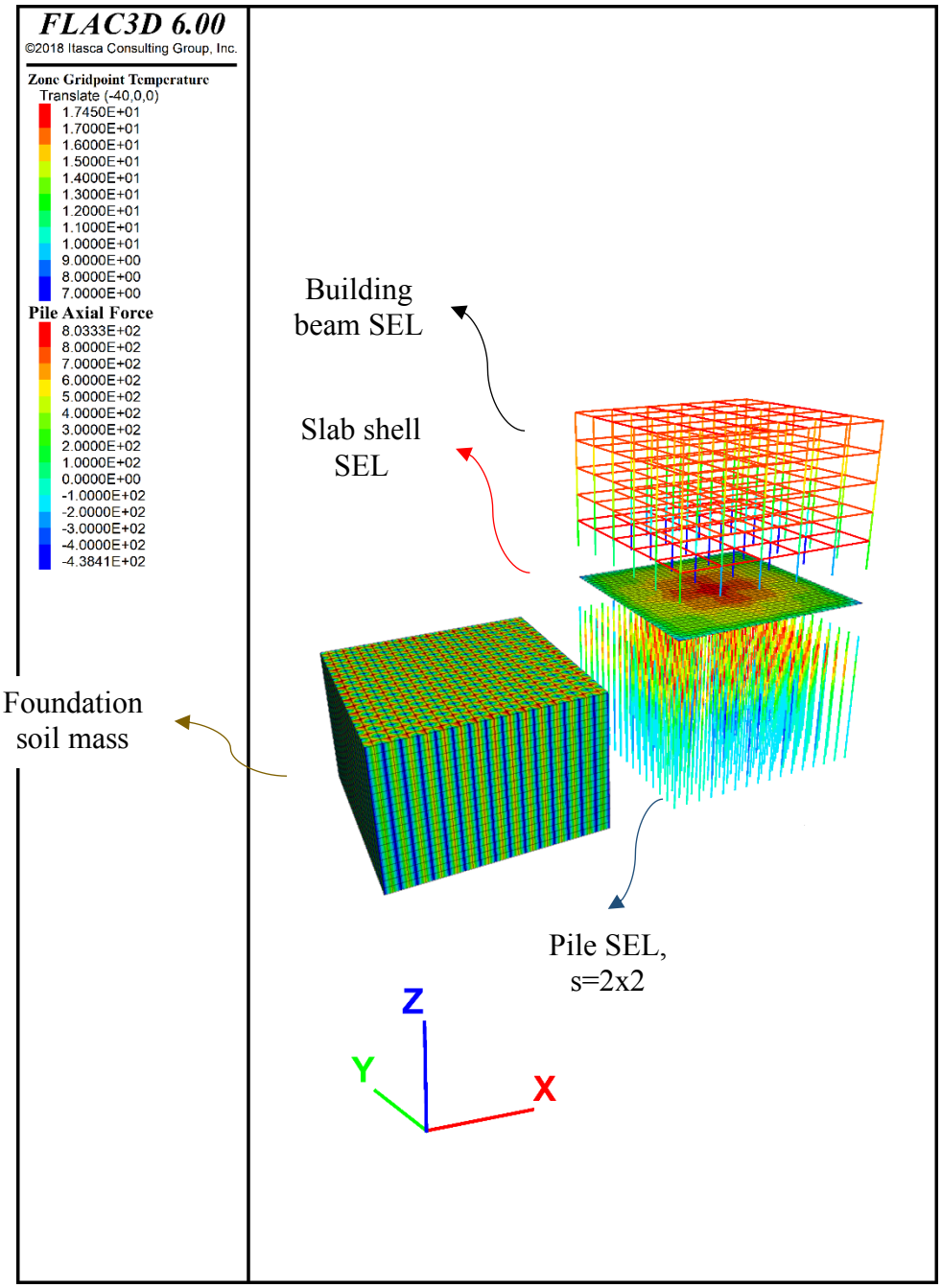

Figure 4.47. Numerical model setup detail for case number 1

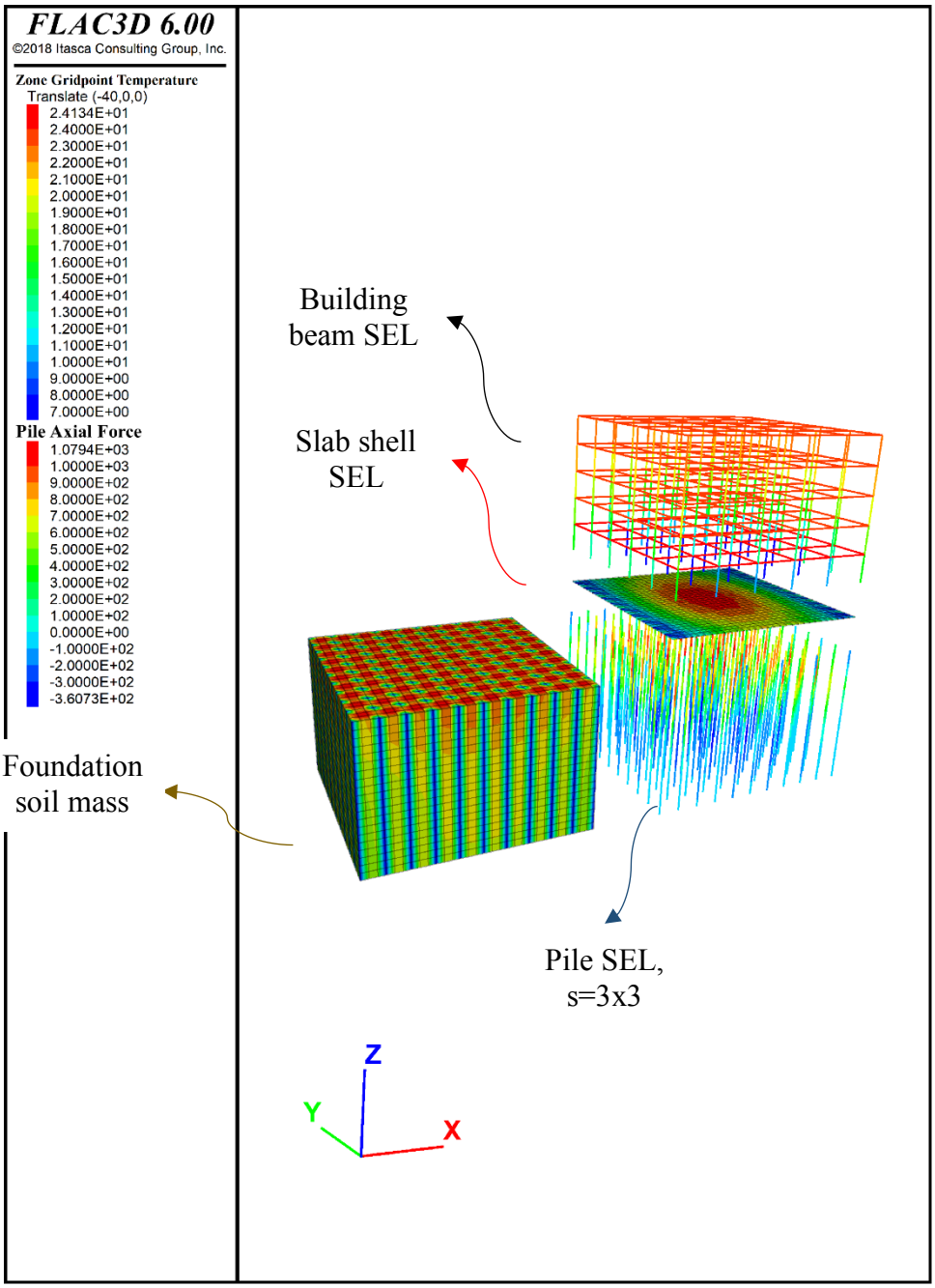

Figure 4.48. Numerical model setup detail for case number 5

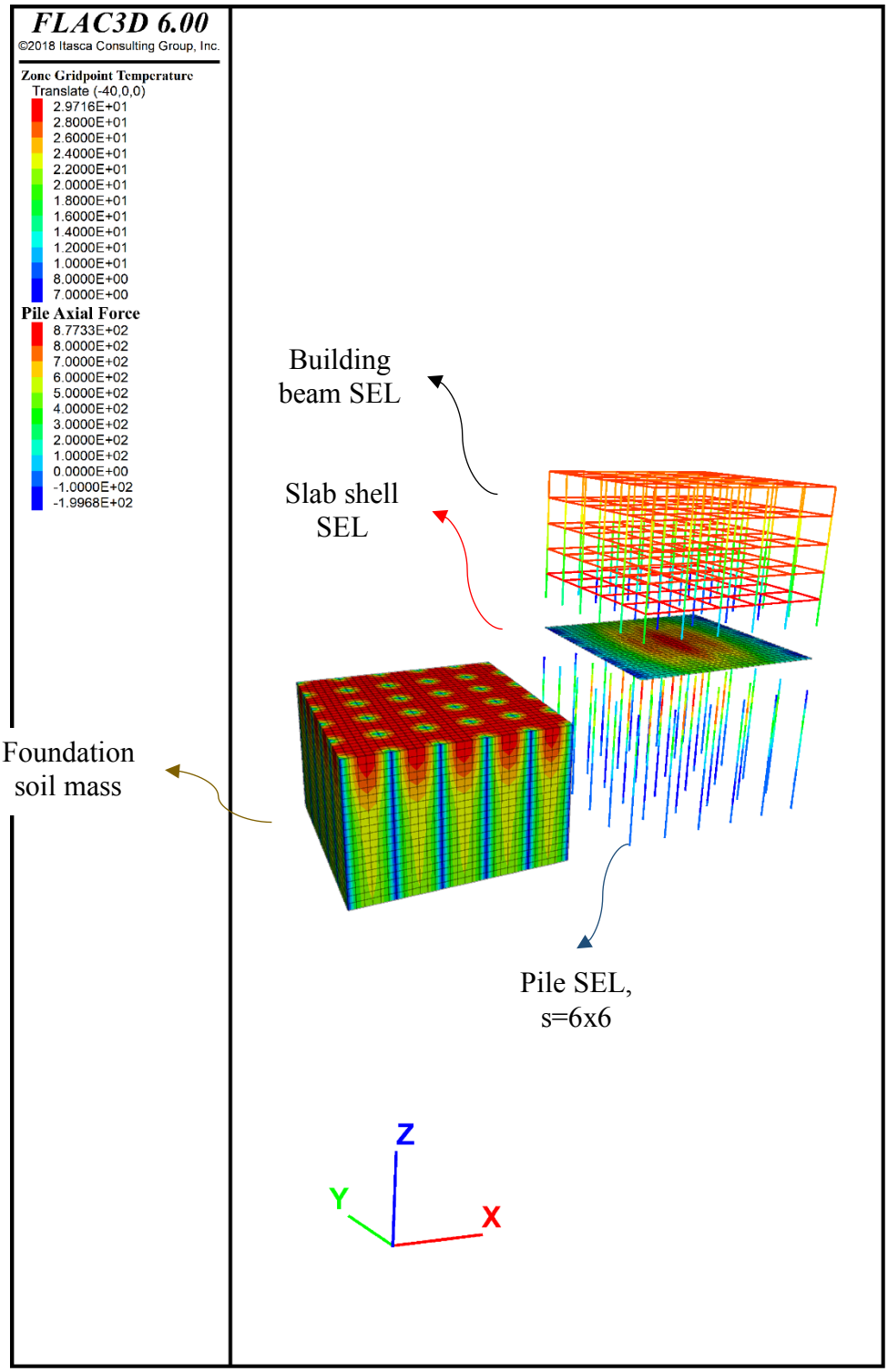

Figure 4.49. Numerical model setup detail for case number 8

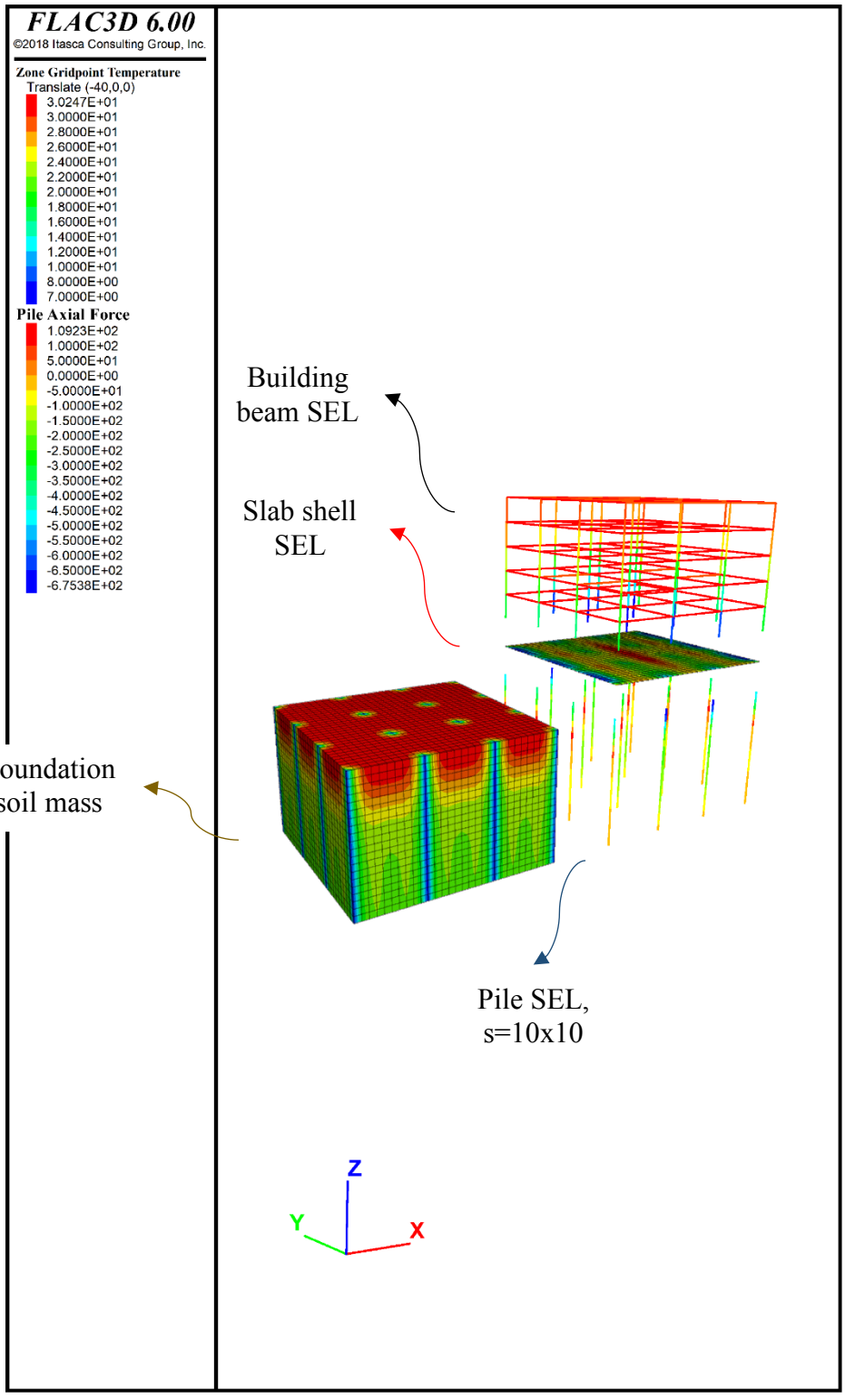

Figure 4.50. Numerical model setup detail for case number 13

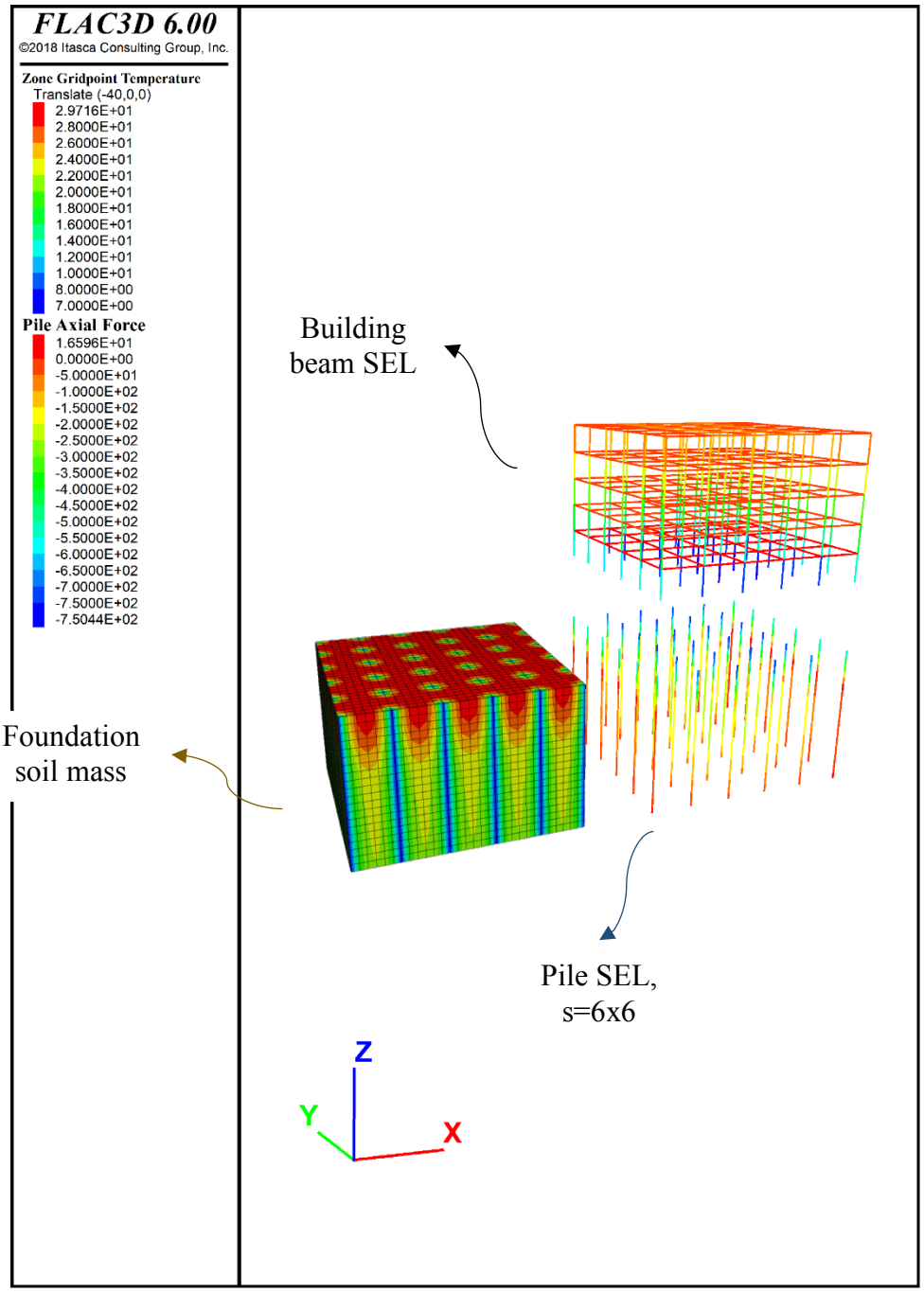

Figure 4.51. Numerical model setup detail for case number 9

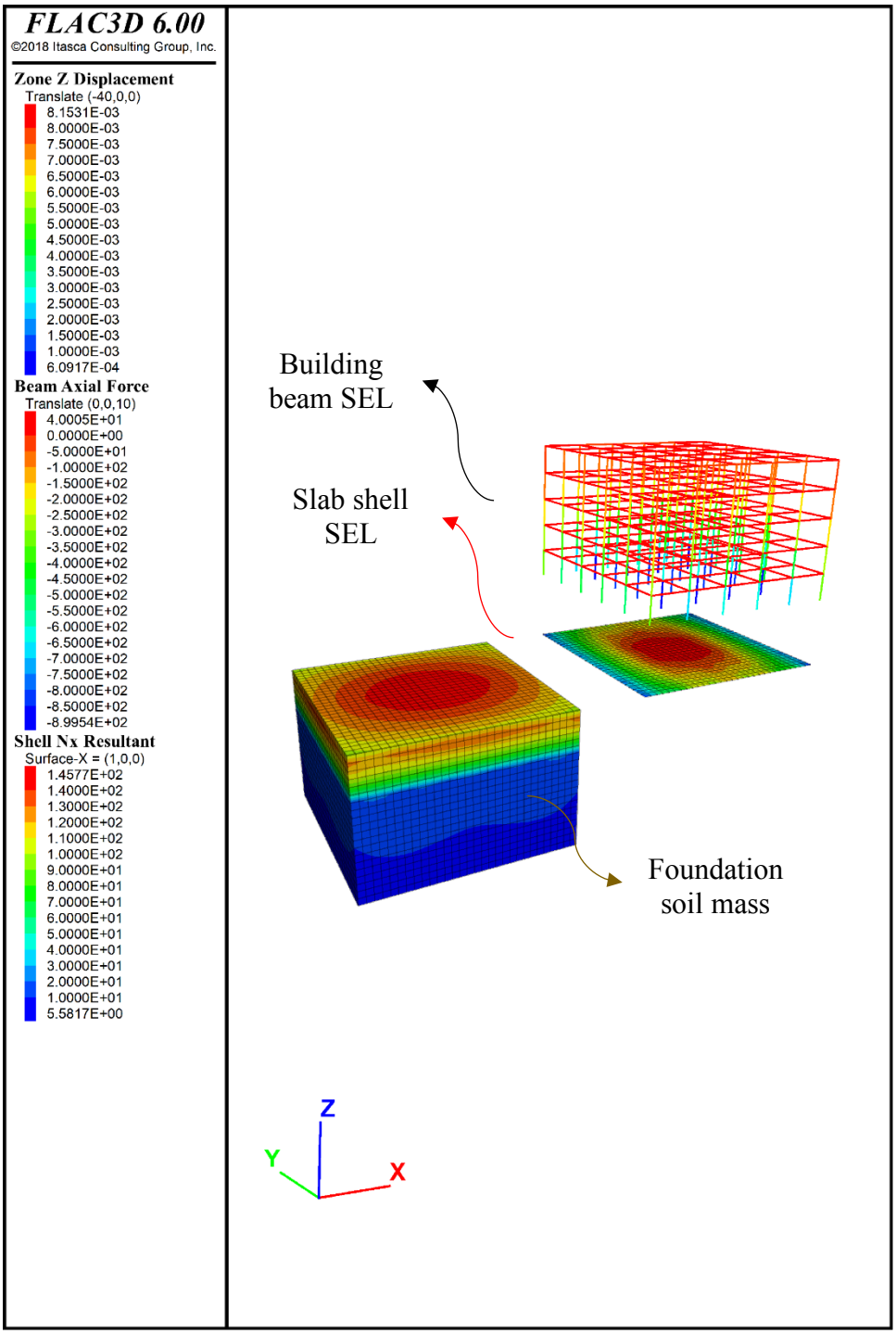

Figure 4.52. Numerical model setup detail for case number 10

4.12.2 Methodology

Since the pile SEL doesn't have a realistic volume in the numerical model, the heat transfer through the pile is not considered. Therefore, the transition step of the heat propagation from the geothermal loops through the concrete in the pile is neglected. According to the LAAH building results, there is a transition period of about 4 days from the start of the system to the asymptotic value of pile temperature. In this research effort, the thermal loading from heating or cooling cycle is implemented in the model based on this analogy and the use of the "clear" spacing instead of the "center-to-center" spacing. From the geotechnical engineering application point of view, the thermal impact on the soil-foundation behavior matters when the soil is actually starts to feel the temperature change. The terms pile "clear" spacing and pile spacing will be used interchangeably in this section.

The grid points associated with the soil zones attached to any of the pile SEL nodes, is considered to be the source of heat injecting or cooling. The geothermal foundation system is assumed to be fully functional at each energy pile location. In other words, there is no uneven distribution of heat or cold flux or mass being present inside the soil under the foundation.

One important aspect of this current recommendation study is that ALL of the proposed charts and conclusions are based on a "two-year" operational cycle of the full-scale geothermal foundation system. As mentioned before, the goal of this study was to provide preliminary answers to thermal efficiency (i.e. soil thermal pollution) and foundation behavior with respect to any possible variations within the soil properties and pile foundation design configuration. Of course, increasing the numbers of cyclic thermal loading will provide more information, however, the goal in this research was to provide some preliminary design understandings and guidelines toward the full-scale application of geothermal foundation system.

In the effort of proposing design recommendation, the focus was always on to provide sets of guidelines for engineers to follow without the need of using a complicated numerical simulation tool such as FLAC3D. This will enable a simple and practical understanding of the challenges and solutions when a geothermal foundation is used in full scale under a building foundation.

4.12.3 Results and Recommendations

The result section is divided into two parts: thermal efficiency and foundation behavior.

4.12.3.1 Thermal Efficiency

For the thermal efficiency analysis, in order to propose a practical methodology for design purposes, the entire soil mass interacting with the pile foundation will be used to get an average of all the temperature values in the grid points. Then simply by tracking the variation of this average soil temperature under the building, the thermal efficiency of the system with a specific pile configuration can be defined.

As can be seen in Figure 4.53, for the hypothetical cases with different pile spacing and length configuration, the average temperature in soil is directly affected by the foundation setup. Starting with the cases of pile "clear" spacing, the Figure 4.53 shows that by increasing the "clear" spacing, the average temperature soil increase for the cooling mode slows down as expected.

During the cooling mode, the number of days it takes to increase the average soil temperature from $23.5°C$ to $33°C$ is 180 days for "clear" spacing of 2m. With respect to the heating source temperature of only $35°C$, there will be a temperature gradient of $\Delta T = 2°C$ left in the foundation soil for additional heat exchange between the energy pile group and the soil. During the cooling mode, for "clear" spacing of $3m$, this increase is from $23.5°C$ to $29.5°C$ in

180 days with the residual temperature gradient of $\Delta T = 5.5°C$. For the "clear" spacing of $6m$, the average increase of temperature is from $23.5°C$ to $24.7°C$ in 180 days with the residual temperature gradient of $\Delta T = 10.3°C$.

Finally, for the "clear" spacing of $10m$, the average increase of temperature is from $23°C$ to $23.5°C$ in 180 days with the residual temperature gradient of $\Delta T = 11.5°C$. According to these observations, the pile "clear" spacing plays a significant role on the thermal efficiency of a full-scale geothermal foundation system. In all cases of pile spacing variation, the following cooling process and second year operation follows the same trend for both heating and cooling.

The thermal efficiency defined and proposed for both of heating and cooling cycle in this research effort is based on the ratio defined as

$$\delta_{th}^{H,C} = 1 - \left(\frac{\Delta T_{\mathrm{H,C}}}{\Delta T_{\max}} \right) \tag{39}$$

In which $\delta_{th}^{H,C}$ is the thermal efficiency for heating or cooling cycle, $\Delta T_{\mathrm{H,C}}$ is the temperature difference generated during each cycle, and $\Delta T_{\max}$ is the maximum available temperature gradient between the pile and soil at the start of each cycle. This analogy is being presented by Figure 4.54 in which the thermal efficiency vs. pile "clear" spacing is plotted. Figure 4.54 proposes a practical guideline toward designing an efficient system with respect to pile "clear" spacing of the foundation. Based on the findings for far, it can be stated that the pile spacing controls the thermal pollution of the ground rather of the amount of thermal load production.

It has to be noted that these results are based on "two-years" cyclic operation of the geothermal foundation system with assumption of no maintenance, resting period, or any stoppage.

At first this plot might convey the message that the larger spacing would be an ideal design recommendation, however, one has to note that the amount of thermal load that each energy pile can produce is limited to the size and particularly the length of the pile. As general rule of thumb, an energy pile with length of $30\text{m}(100\text{ft})$ can produce about one ton of thermal load. For example, in the cases of having various pile length with fixed spacing, Figure 4.53 shows the same amount of temperature increase in soil for all the three pile length conditions.

The analysis chart for average increase in soil temperature is based on the soil thermal properties for a typical fully saturated over consolidated clay. In the case number 3, the thermal conductivity was changed to an extreme value. This allowed to observe the effect of thermal conductivity of soil in full scale application. As it was expected, the high thermal conductivity value resulted in a very quick increase in average soil temperature and loss of thermal efficiency for both cooling and heating mode.

It is also worth noting that the current operation strategy being used applies to cooling dominated climate such as Texas area. The proposed thermal efficiency chart is derived based on the assumption of having geothermal foundation working as full air conditioning and heating system. Obviously, when the system is not being used in full capacity condition, the average temperature in foundation could vary differently. Nevertheless, the average variation should follow as it is presented in Figure 4.53. Additionally, when the soil's thermal properties are different than those used in this study (Table 4.8) or groundwater flow condition, the average foundation temperature could be different than presented in Figure 4.53. This proposed guideline on thermal efficiency is based on the properties of a fully saturated heavily over consolidated clay.

As mentioned above, Figure 4.54 shows the effect of pile spacing on the thermal efficiency of the system. The overall thermal efficiency for both cooling and heating mode stays close for both of the two years operation. For the close pile "clear" spacing (i.e. $s \le 2\text{m}$), the efficiency for cooling mode (i.e. heating the soil) is around 20%, while the heating mode (i.e. cooling the soil) is about 38%. For the close pile "clear" spacing (i.e. $2\text{m} \le s \le 3\text{m}$), the efficiency for cooling mode (i.e. heating the soil) is around 52%, while the heating mode (i.e. cooling the soil) is about 72%.

For the close pile "clear" spacing (i.e. $6\text{m} \le s \le 10\text{m}$), the efficiency for cooling mode (i.e. heating the soil) is around 88%, while the heating mode (i.e. cooling the soil) is about 94%. For the close pile "clear" spacing (i.e. $s \ge 10\text{m}$), the efficiency for both cooling (i.e. heating the soil) and heating mode (i.e. cooling the soil) is about 97%. Also, for the spacing range of $s \ge 6\text{m}$, thermal efficiency of the system tends to be consistent in the upper 90%.

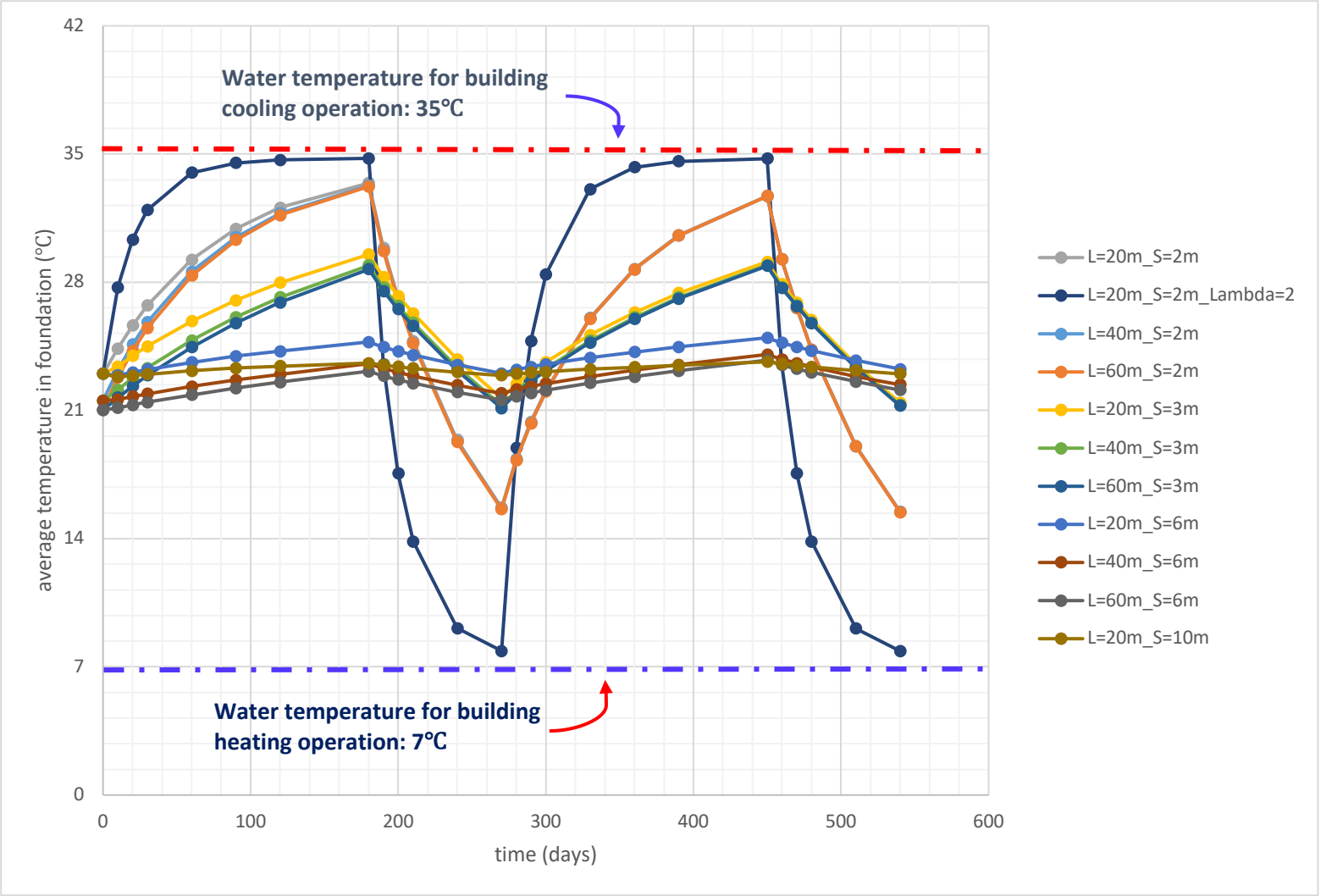

Figure 4.53. Proposed average foundation soil temperature increase

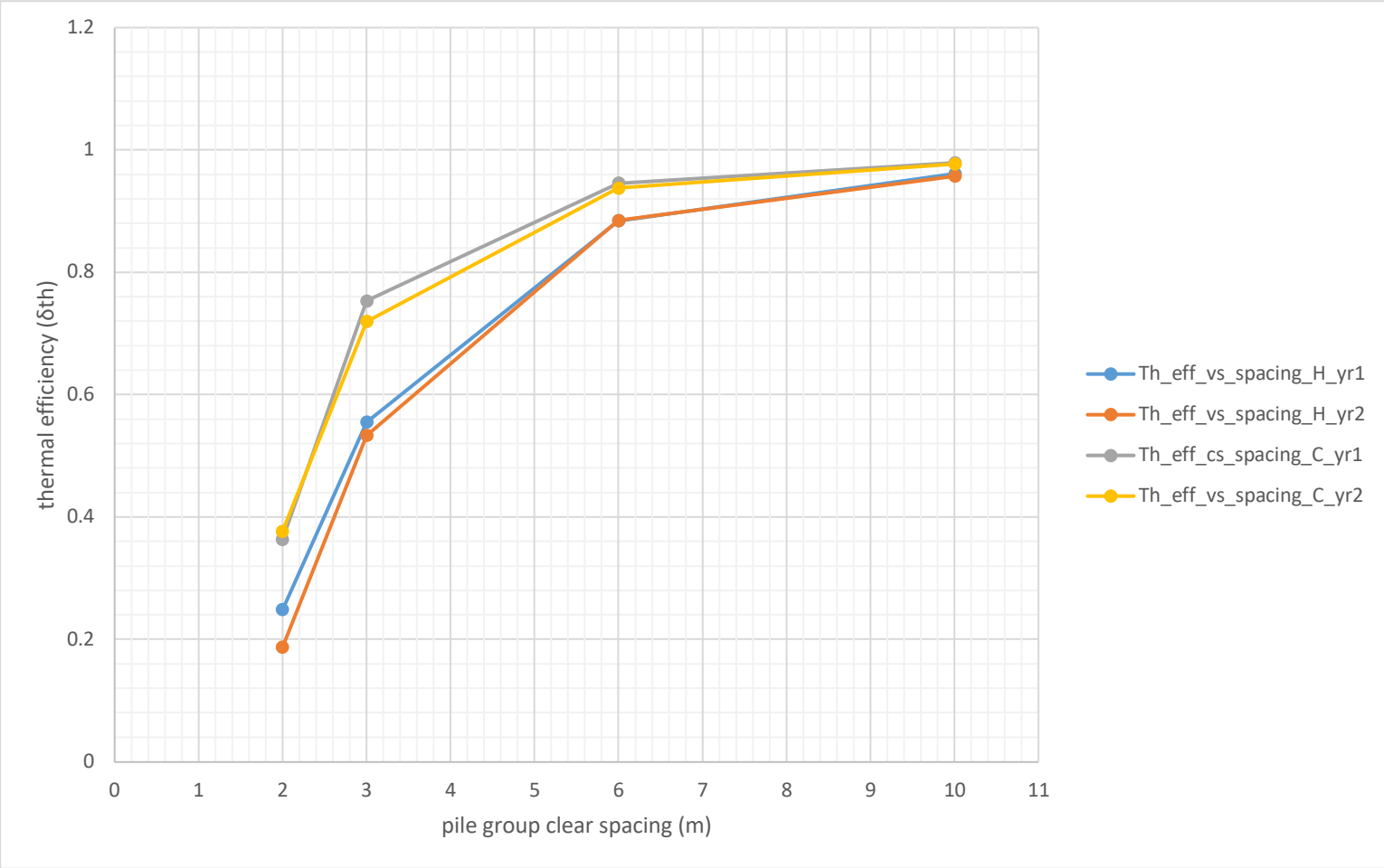

Figure 4.54. Proposed thermal efficiency analysis chart for various pile "clear" spacing

4.12.3.2 Foundation Behavior

The foundation behavior is another important design consideration for a full-scale energy pile system. In the design recommendation study, several thermo-mechanical issues were addressed:

- ✓ Pile group behavior under full scale thermo-mechanical loading condition.
- ✓ Structural slab effect on the pile group behavior.
- ✓ Attachment condition of the structural slab to the soil underneath.
- ✓ Soil z-displacement profile at pile's and further away location.
- ✓ Soil's thermal expansion coefficient effect for thermal strain calculation.
- ✓ Non-structural geothermal wells under a shallow foundation.

The first proposed comparison analysis is focused on the attachment condition of the structural slab connecting the building the pile head. In general picture, the FLAC3D thermal logic for the soil is simply the volumetric expansion or contraction in three dimensions. For the pile SEL, since there is no realistic volume to any pile SEL, it can occur only in the axial direction (i.e. one dimension). The shell SEL thermal strains will be dominated by the movement of the soil and pile SEL. There are two conditions assumed to exist between the structural slab and soil grid points:

1. Full contact: which means that the slab nodes will be in full contact (i.e. rigidly connected) to the soil grid points underneath. The full contact condition indicates that during the cyclic heating (i.e. volumetric expansion) and cooling of the soil (i.e. volumetric contraction), the slab (which also expands or contracts in plane direction) moves with the soil, while rigidly attached to it.

2. No contact: refers to the condition that there is a gap between the foundation structural slab and underlying soil mass. The mechanical movement of the soil and its volumetric expansion or contraction will be independent of the slab movement.

These two conditions are quantified through the pile load distribution, z-displacement profile for the pile nodes and soil grid points. Figure 4.55 and Figure 4.57 show the pile load distribution for the full contact and no contact condition of the slab, respectively. During the mechanical loading only, both cases show similar trend and behavior with all the loads being in the compression side as expected.

Figure 4.55 indicates that for the first year of cooling mode, the compression load in pile from the ground surface to the depth of about $5\mathrm{m}$ starts to reduce and goes toward tension mode. This is due to the fact that since the slab is in full contact with the soil and the pile top, volumetric expansion of the soil and vertical expansion of the pile SEL starts to pull on the pile top. This pulling induces tension load countering the compressive load from the building. Then from the depth of $5\mathrm{m}$ to $10\mathrm{m}$, the compression load increases due to the mobilization of friction between the pile and the soil. From $10\mathrm{m}$ to the bottom of the pile at $20\mathrm{m}$, the load in the pile follows the same reduction behavior as in the mechanical loading only condition.

Figure 4.57 also shows the same behavior for the upper $10\mathrm{m}$ length of the pile in the no contact condition. However, unlike the full contact condition where the pile load at the top changes toward tension, in the no contact condition the pile load the top stays almost the same during the heating process. One observation can be made on the fact that for both of the slab attachment condition, the thermal loading only affected up to half-length of the pile and the rest follows the mechanical loading constitutive behavior. Additionally, by looking at the Figure

4.56, the down drag occurred from the depth of $5m$ to $8.5m$. This means the soil moves relatively more in downward direction than the pile within the same depth range.

For the full contact condition, during the soil cooling in the first year, the compression loads increase in the pile due to the contraction in the soil and pile elements. Since the cooling cycle starts right after the heating, the tension loads in the pile are already countered with the compressive ones. From the ground surface to $7.5m$, the load is mostly shifted to the compression side. From the $7.5m$ to $10m$, the compressive load increases more than the values in the mechanical loading only process. From $10m$ to the bottom of the pile at $20m$, the load in the pile follows the same reduction behavior as in the mechanical loading only. The down drag issue is also observed within the same depth range as in the heating process in the first year. As demonstrated in Figure 4.56, the soil moves relatively more in downward direction than the pile.

Once the heating cycle starts in the second year, the load in pile moves toward tension in an extreme trend. Part of this erratic behavior comes from the fact that since the heating starts right after cooling process. During the cooling process, a significant temperature gradient is generated in comparison to heating process. Once the heating starts, there is more thermal influence available because of the high thermal gradient. From the ground surface to $5m$, it follows the same trend as in the previous hearing year. However, the pile load reversal from $5m$ to $10m$ follows a very steep gradient. In order to better understand this behavior, Figure 4.56 pictures a better view of the pile-soil interaction at that depth range. The pile nodes are moving less than the soil grid points with the maximum value of $6mm$ at $7m$ depth.

This unusual behavior from pile and soil can be explained due to a superposition of slab and pile behavior when it is loaded thermo-mechanically. There are two separate cases, number 9

and 10, which deals with the details of slab only and pile only as a foundation, respectively. Results presented in Figure 4.62 and Figure 4.64 shows the details of this superposition.

Figure 4.62 shows the pile load distribution in the case of no slab and pile SELs as the foundation directly and rigidly connected to the building. The mechanical loading only shows behavior as expected, which is reduction in load within depth. During the heating in first year, the pile axial load reduces in compression value due to the fact that the pile group start to expand in vertical direction. From the ground surface to 8.5m, the change in pile axial load is steeper than the rest of the pile length. From 8.5m to the bottom of pile, the reduction in load occurs in the same trend as in the mechanical loading only.

Figure 4.63 presents the pile and soil z-displacement profile for case 9. The mechanical comparison of the pile and soil z-displacement is consistent with the theoretical basis. During the first-year heating, soil tends to expand more at the surface up to 8.5m. For the cooling process, there is negligible amount of down drag occurring at 7m. Two null points on the pile can be spotted where the pile and the soil displacement are equal. Figure 4.64 shows the soil z-displacement at the same location of soil grid points in case 9. By putting Figure 4.63 over Figure 4.64, the superposition of slab and pile behavior when subjected to cyclic thermo-mechanical load can be observed.

Figure 4.60 and Figure 4.61 both demonstrate the details of larger pile spacing influence on the behavior of the pile group. The mechanical, all compressive axial load in the pile shifts toward all tension for the first-year heating process from ground surface to 7.5m. Also, for the second-year heating, this tension propagates even more in the axial direction of the pile up to 13.5m. Cooling cycle in both years just reduces some of the tension load along the pile.

The effect of thermal expansion coefficient for soil zones is studied. The two cases of 1 and 4 can be compared for the effect of the soil's thermal expansion coefficient on foundation behavior. Figure 4.55 and Figure 4.58 shows the pile axial load distribution for cases of 1 and 4, respectively. Comparison between the Figure 4.55 and Figure 4.58 shows there is not a significant influence on the pile axial load distribution when the thermal expansion coefficient changes.

According to the design recommendation results, the followings can be concluded:

1. In the case of using energy pile in full scale, the structural slab must be elevated from the native load bearing soil. The contact between soil and slab induces considerable tension forces in the pile, which should be considered in the structural design.
2. The heating in second year which follows a long cooling process, changes the pile load, vertical displacement, and the soil movement drastically.
3. The cyclic heating and cooling causes down drag issue depending on the attachment condition of the slab and pile spacing.
4. Switching between heating and cooling cycle might lead to cracks in the pile foundation due to the fact that the tension and compressive load changes considerably at the pile-slab connection.
5. It can be recommended to allow some resting time between the two processes to avoid sudden thermal shocks to the foundation structure. This will also help in the less steep axial load variation within the pile and less settlement in the soil.

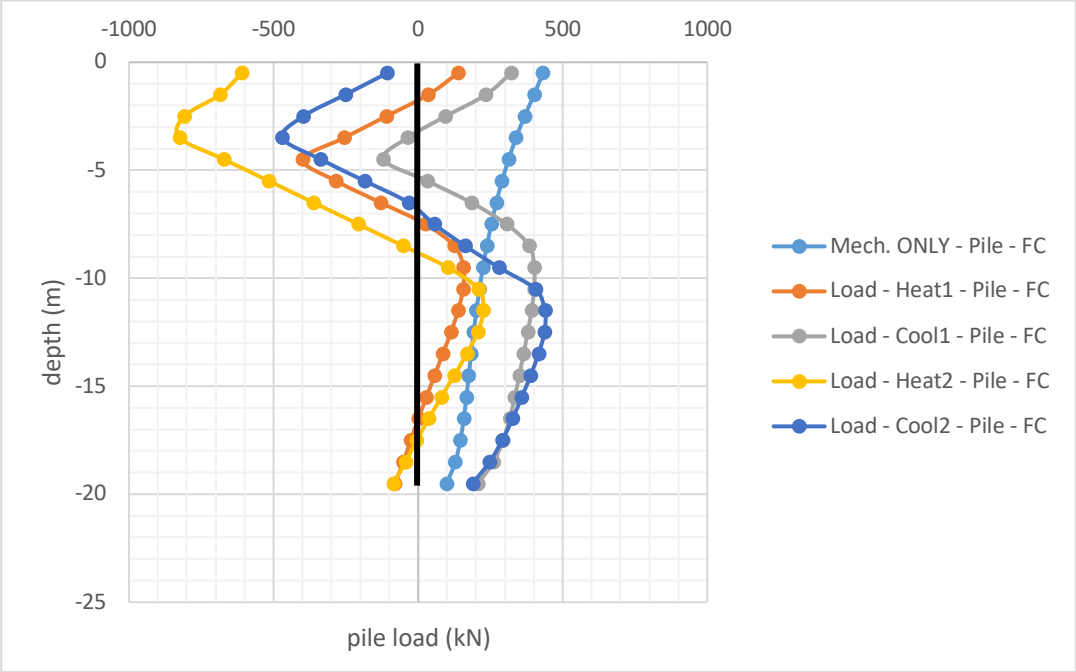

Figure 4.55. Pile load distribution for case number 1

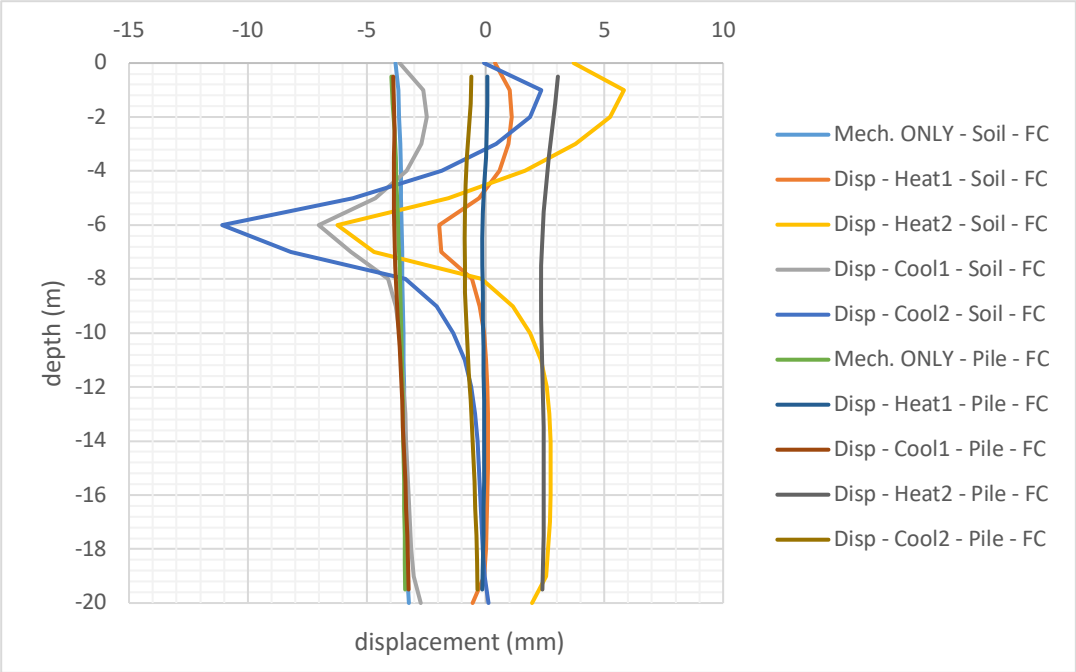

Figure 4.56. Pile and soil z-displacement for case number 1

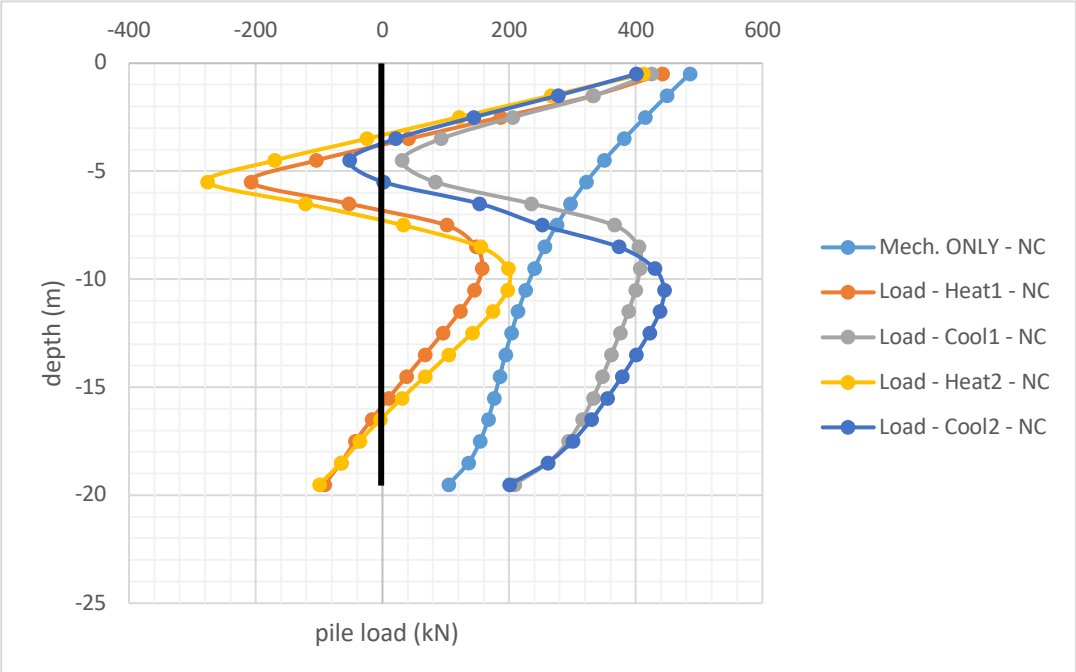

Figure 4.57. Pile load distribution for case number 2

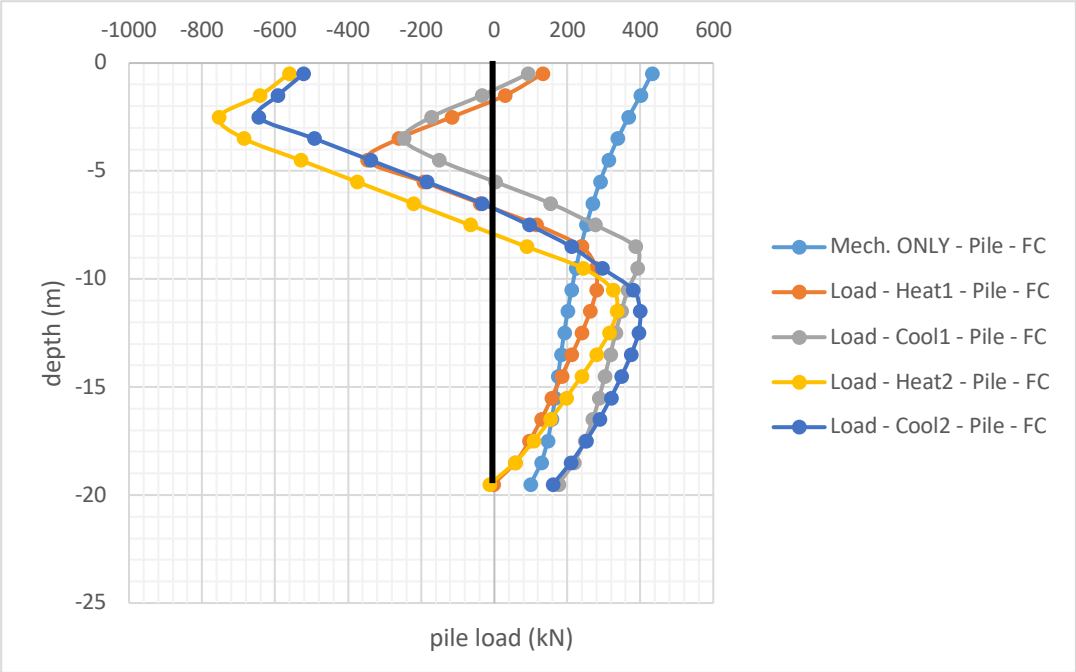

Figure 4.58. Pile load distribution for case number 4

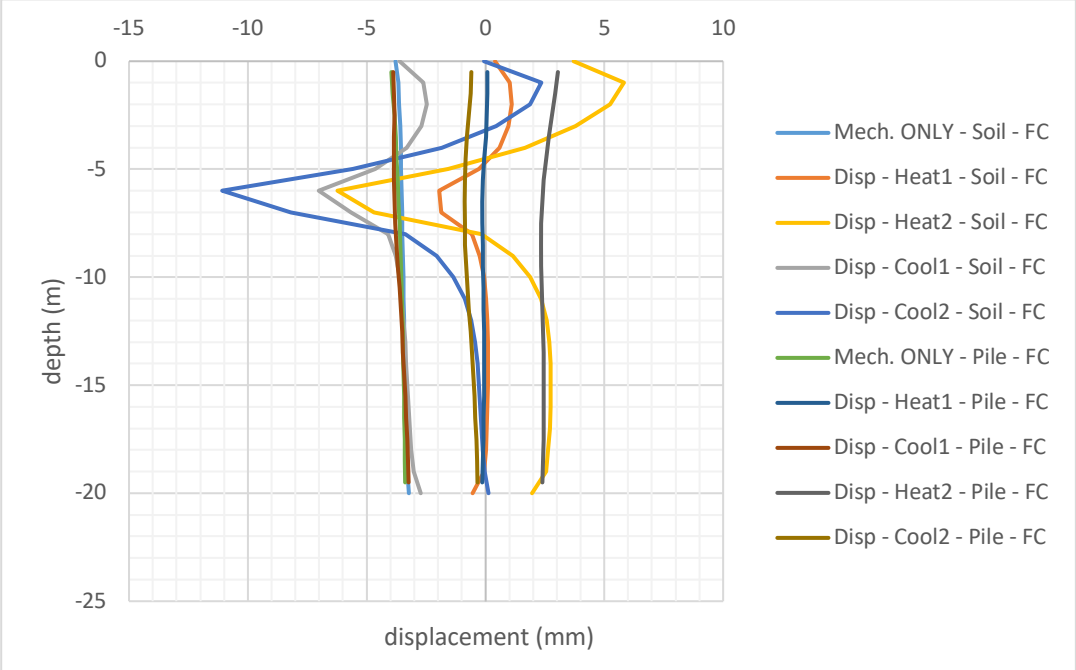

Figure 4.59. Pile and soil z-displacement for case number 4

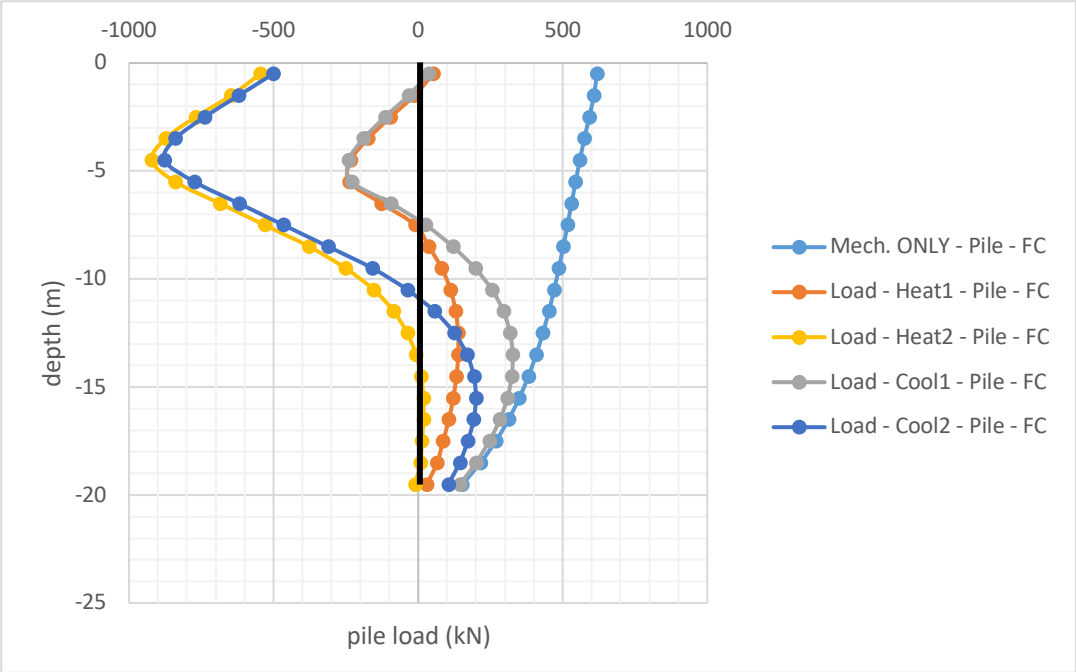

Figure 4.60. Pile load distribution for case number 8

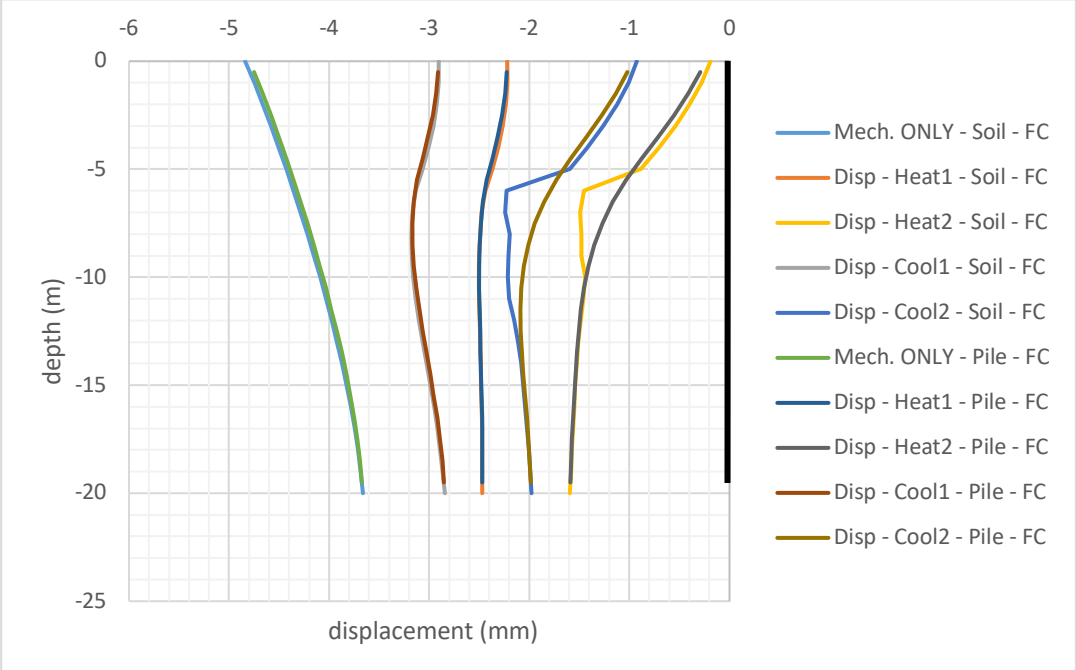

Figure 4.61. Pile and midway soil z-displacement for case number 8

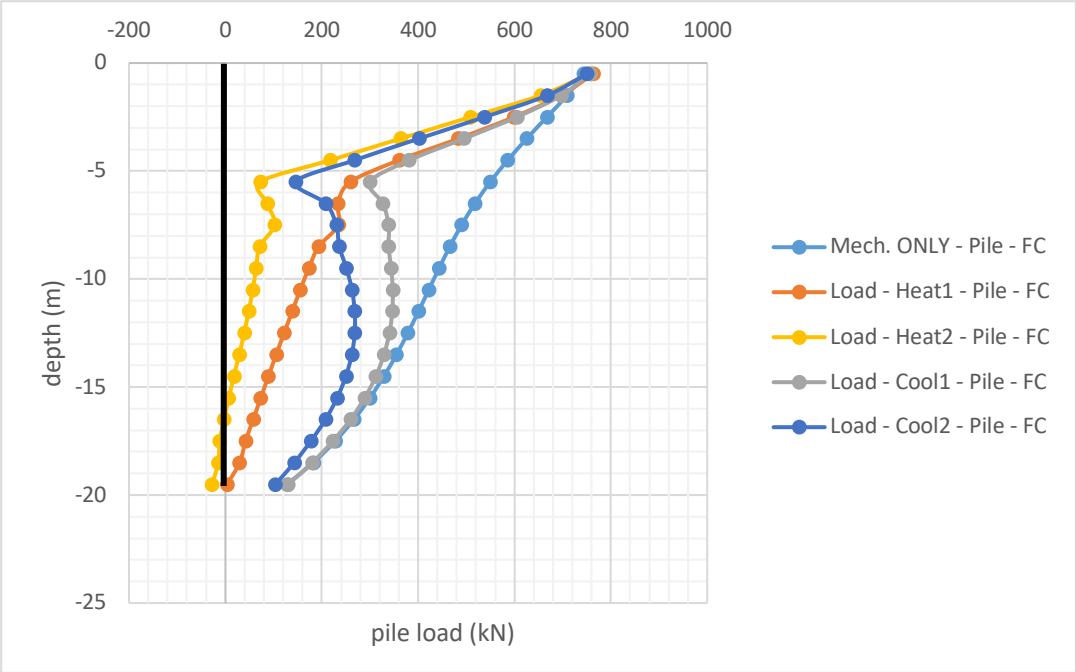

Figure 4.62. Pile load distribution for case number 9

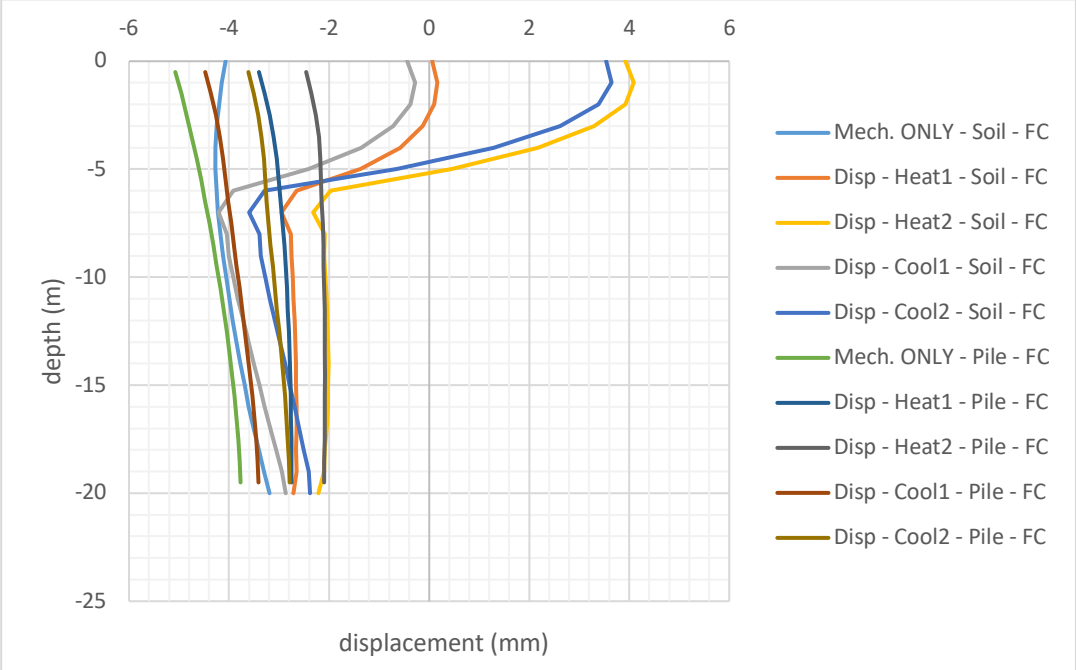

Figure 4.63. Pile and midway soil z-displacement for case number 9

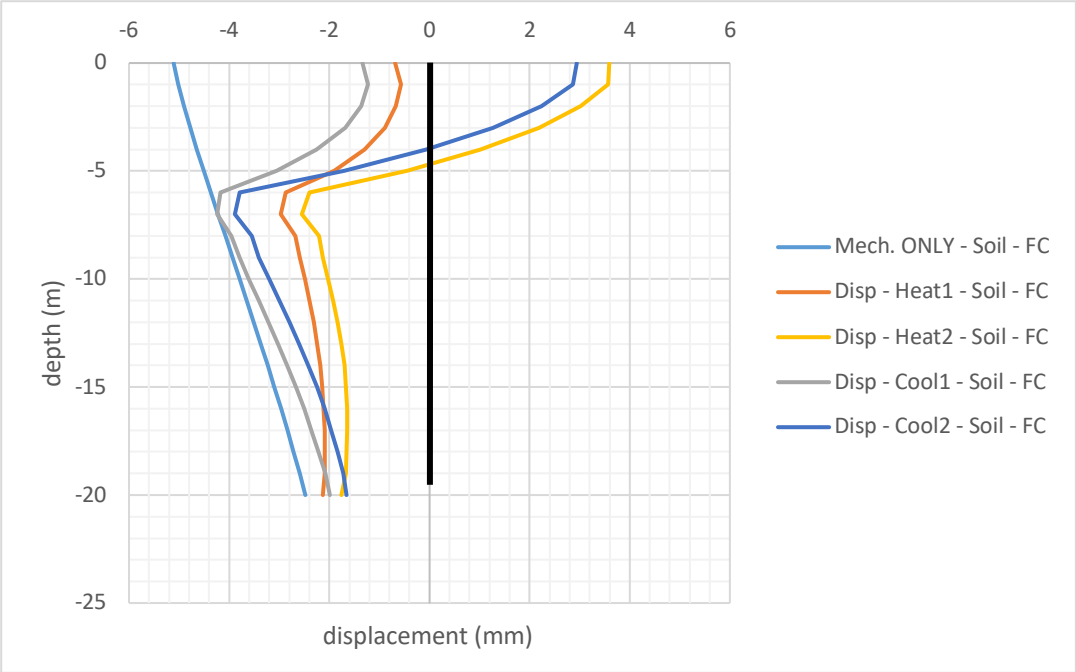

Figure 4.64. Pile and midway soil z-displacement for case number 10

4.13 Case History: TAMU Liberal Arts and Humanities Building

4.13.1 Introduction

Based on the findings in the design recommendation section (4.12), a case history of LAAH building is modeled and analyzed to check the validity of the proposed findings. The numerical model is constructed based on the actual building foundation footprint, pile geometry, building geometry, and geothermal temperature profile. Instead of using small pile in different pile group setup, an equivalent single pile geometry was used. There are two major reason to take this approach:

1. The spacing between the piles in pile group was small and fell in the range of being inefficient to study the interaction between these smaller diameter piles. It is assumed that each pile group behaves as a single drill shaft.

2. To avoid unnecessary complications to define various pile cap and use a single slab connecting the building and pile top.

The equivalent pile diameter used for the case of LAAH building is 1.2m with the length of 20m. The structural slab thickness is $0.6096\text{m}(2\text{ft})$. According to the geotechnical design report, there is a $0.0762\text{m}(3")$ gap between the ground surface and bottom of structural pile cap. However, for comparison reasons the full contact condition was also simulated for the LAAH building case history. Soil thermal and mechanical properties are the same as shown in Table 4.8. The reason to pick the same values was due to the fact that according to the geotechnical design report, the boring logs indicated the same soil type (i.e. highly over consolidated and high plastic clay) as the one used in all of the previous cases.

The numerical model is set to simulate two years of a full-scale geothermal foundation operation, with 6 months of cooling mode (i.e. heating the soil), followed by 3 months of heating mode (i.e. cooling the soil). The soil's heating temperature is set at a constant temperature profile of $51°C$ along the pile length and the cooling is set at a constant temperature profile of $7°C$ along the pile. Table 4.10 shows the summary of studied cases for the full-scale analysis of LAAH building.

Table 4.10. LAAH building cases description

Case number	Description
1	$P_L = 20m$, $P_s =$ varies, No contact slab, without the bottom tension link
2	$P_L = 20m$, $P_s =$ varies, No contact slab, with the bottom tension link
3	$P_L = 20m$, $P_s =$ varies, Full contact slab, with the bottom tension link
4	$P_L = 20m$, $P_s =$ varies, Full contact slab, with coupling cohesion strength (CCS) link corrected, without the bottom tension link

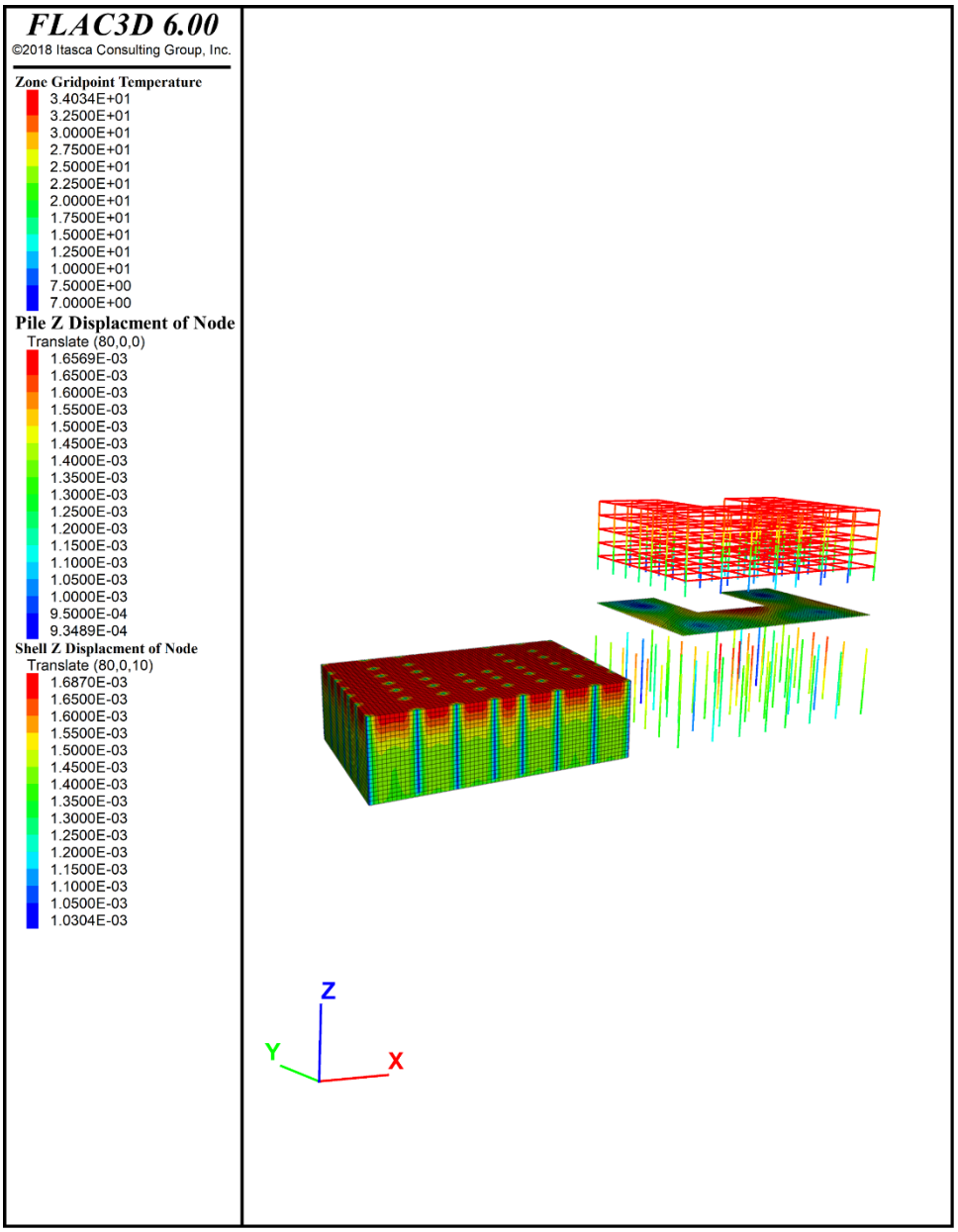

Figure 4.65. Numerical model setup for LAAH building case number 1

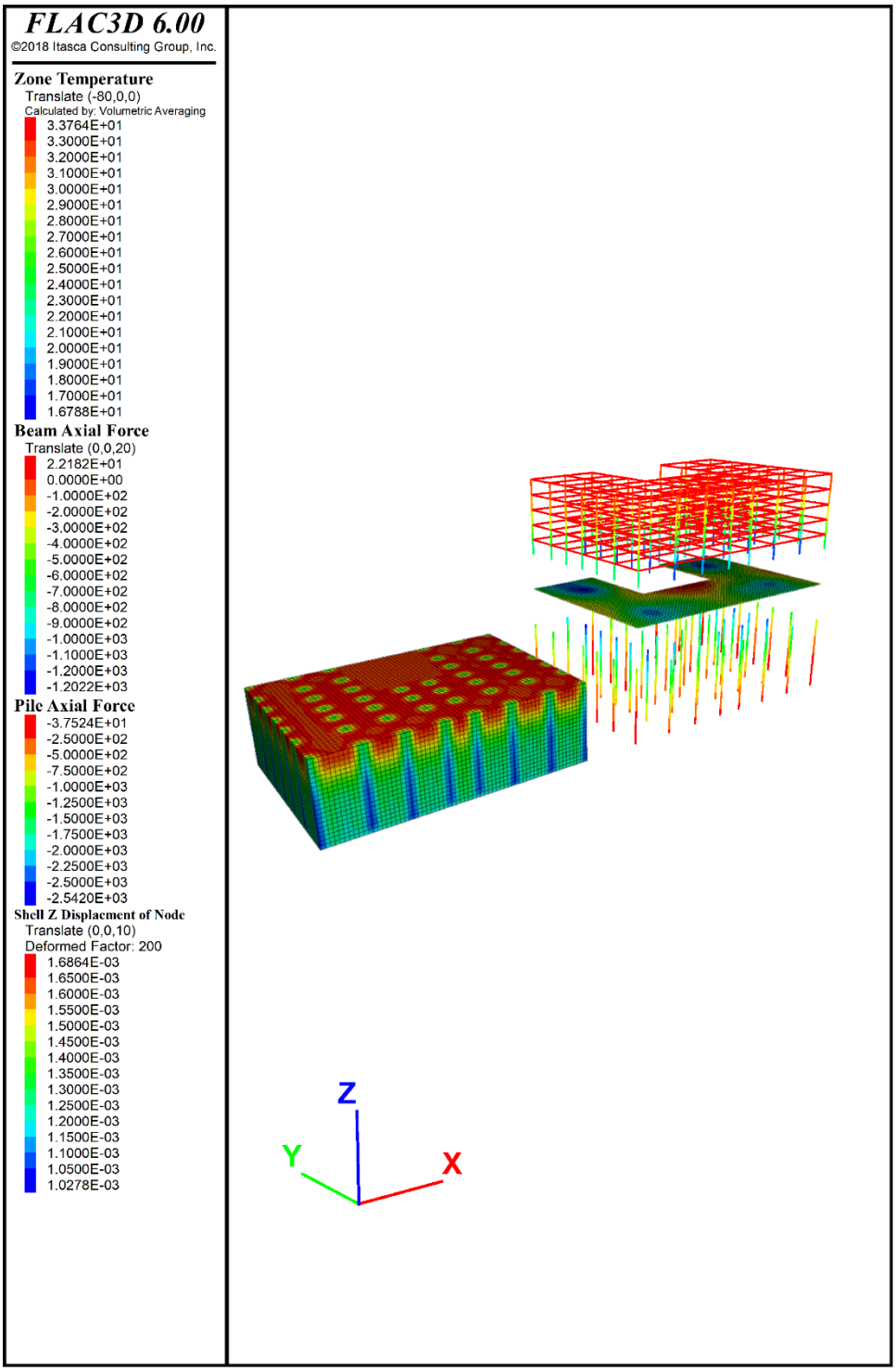

Figure 4.66. Numerical model setup for LAAH building case number 2

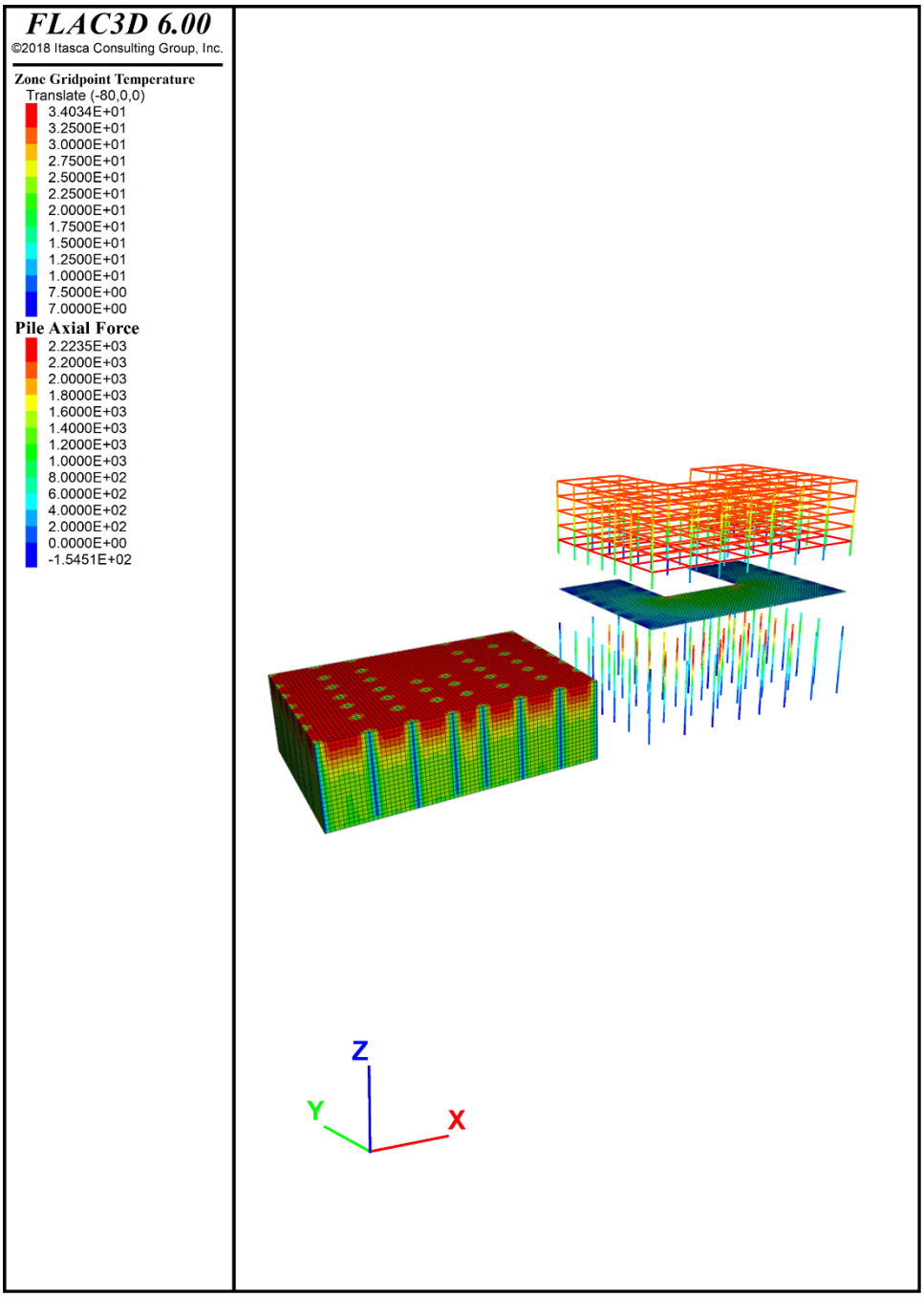

Figure 4.67. Numerical model setup for LAAH building case number 3

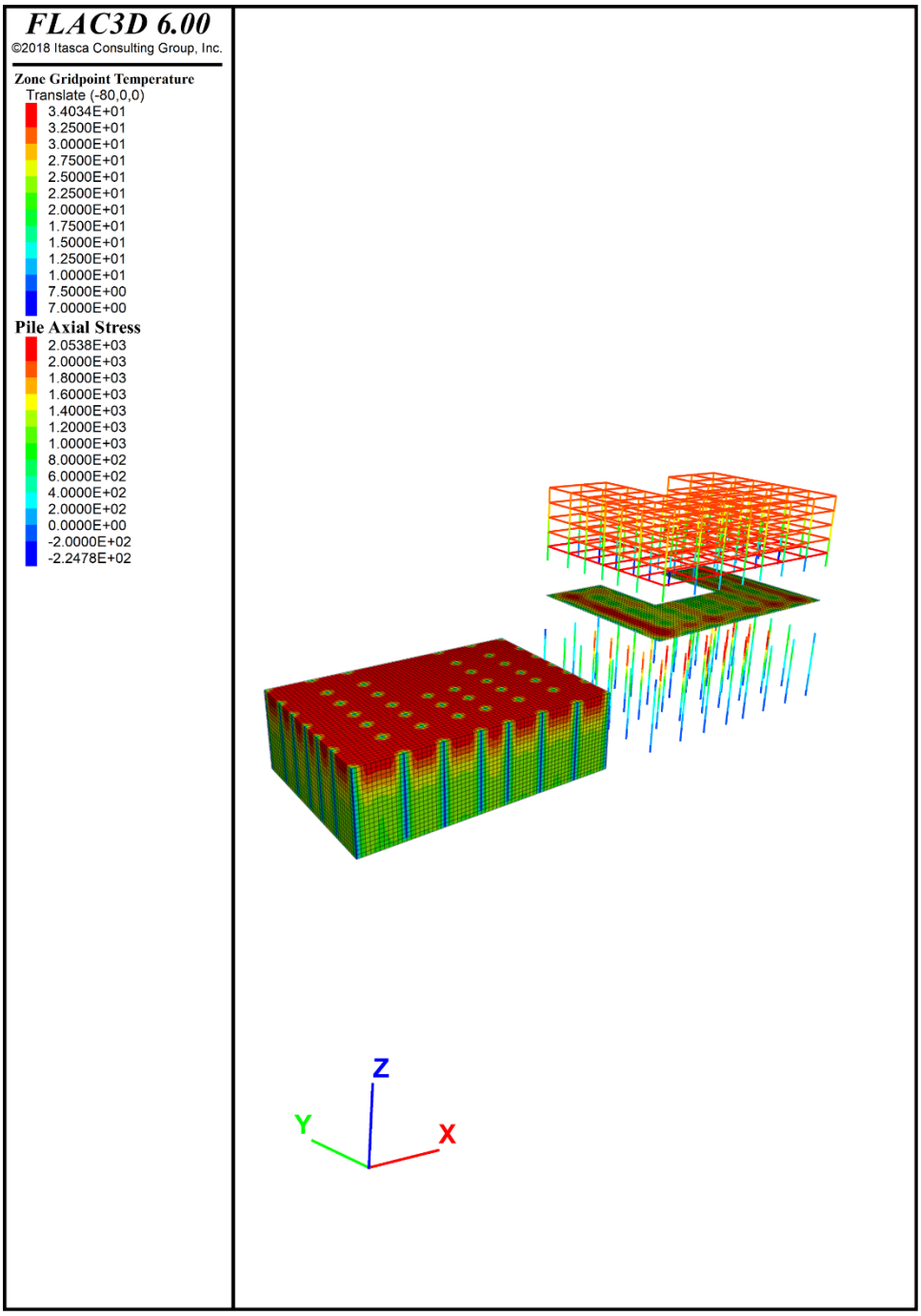

Figure 4.68. Numerical model setup for LAAH building case number 4

4.13.2 Results

The result section is also divided into two part: thermal efficiency and foundation behavior.

4.13.2.1 Thermal Efficiency

The average temperature increases for the LAAH building two-year operation leads to the result presented in Figure 4.69. Since the case number 8 and 13 in the design recommendation study (4.12) represents closely the condition of liberal pile foundation spacing setup, these two average temperature increases are brought for comparison side by side with the analysis of the LAAH full scale simulation.

For the first year of heating, the initial average temperature increases from $23.5°C$ to $25°C$ after 180 days of nonstop operation; leading to the temperature increase of only $2°C$. With the heat source temperature at $51°C$, the residual thermal gradient at the end of the first-year heating process is $26°C$. Starting the cooling process in the first year, the average temperature decreases from $25°C$ to $24°C$ after 90 days of nonstop operation; leading to the temperature decrease of only $1°C$. With the heat source temperature at $7°C$, the residual thermal gradient at the end of the first-year heating process is $17°C$.

For the second year of heating, the initial average temperature increases from $24°C$ to $26°C$ after 180 days of nonstop operation; leading to the temperature increase of only $2°C$. With the heat source temperature at $51°C$, the residual thermal gradient at the end of the first-year heating process is $25°C$. Starting the cooling process in the first year, the average temperature decreases from $26°C$ to $25°C$ after 90 days of nonstop operation; leading to the temperature decrease of only $1°C$. With the heat source temperature at $7°C$, the residual thermal gradient at the end of the first-year heating process is $18°C$. Overall, concerning the thermal pollution issue, the

LAAH building will not have problems such as soil overheating, significant loss in efficiency, or thermal pollution over the years of using geothermal foundation according to this schedule. Of course, the proposed operational schedule is subjected to change for any unseen reasons such as maintenance, demand, etc.

Although, the LAAH building will not have issues regarding the efficiency and thermal pollution of the soil mass underneath, there is still the amount of thermal load produced by the system that needs to be assessed. As mentioned before, having larger spacing will result in better thermal efficiency in avoiding thermal pollution, while the production of the system could be reducing. This is simply due to the fact that there will be less energy pile available to be used when the pile spacing under a building is large. However, one might argue that there could be lesser piles, but by increasing the pile length the thermal load generation can go higher. It is worth mentioning that in cases which the increase in pile length solely for the purpose of geothermal production increase wouldn't lead to more economical design options and might be challenged by the owner.

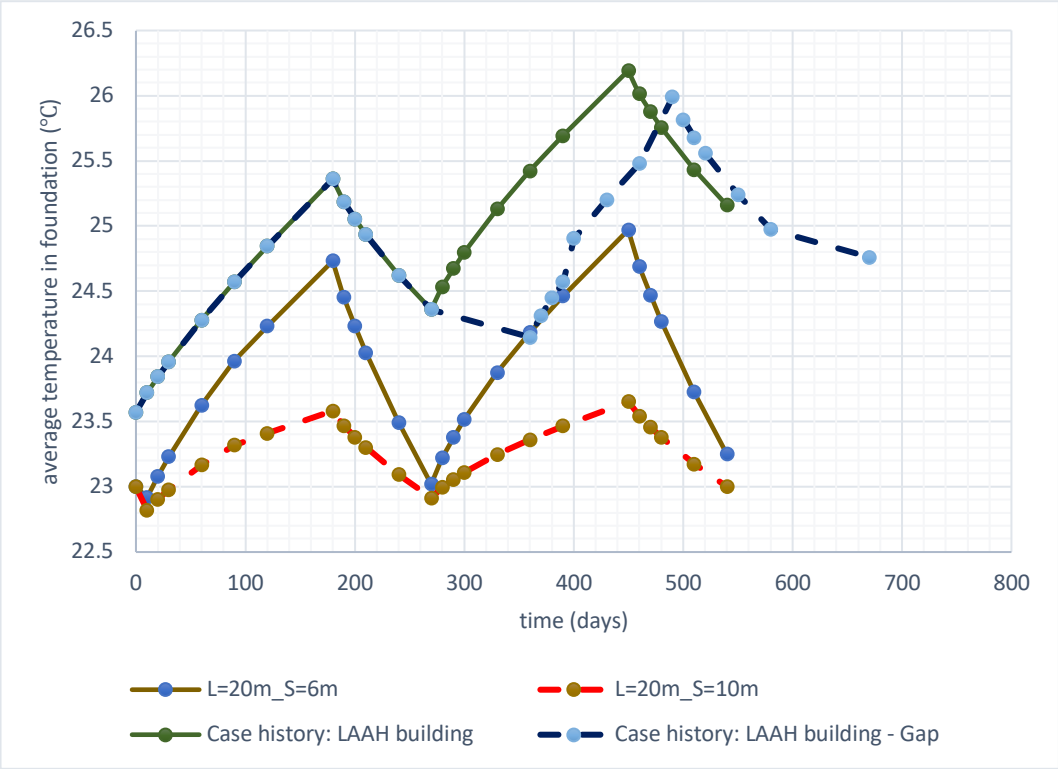

Figure 4.69. LAAH building average temperature increase

4.13.2.2 Foundation Behavior

The case number 1 is the actual representation of LAAH building setup in full scale. It was further investigated the effect of end bearing link on the pile axial load distribution in case number 2. As presented in Figure 4.71, both conditions exert similar behavior with slight differences for cooling in the second year. As for the full contact condition of the slab, Figure 4.74 and Figure 4.77 shows the pile load distribution. The behavior is very similar to the one observed in the design recommendation (Figure 4.60) case number 8 where the pile spacing was $6\text{m} \times 6\text{m}$.

The $0.0762\text{m}(3")$ gap between bottom of the structural slab and soil surface found to be efficient and appropriate. The maximum z-displacement from the numerical analysis in case number 1 after two years of thermal loading was about $0.0116\text{m}(1.16\text{cm})$ according to Figure 4.70. The full-scale application of geothermal foundation under LAAH building simulated in case 1, shows gradual reduction in compression axial load (Figure 4.71). On the contrary, if the foundation design of liberal were to not have any gap between its structural slab and load bearing soil, there were to be significant generation of tension load within the pile when subjected to cyclic thermal loading (Figure 4.74 and Figure 4.77). According to the Figure 4.74 and Figure 4.77, the generated tension load at the pile top link from the heating process is about the mirror value in compression $(\approx -1000kN)$during mechanical loading only step $(\approx 1000kN)$in the first year. For the second year, the situation gets even worse during the heating process, increasing the tension load to about twice at the pile top link.

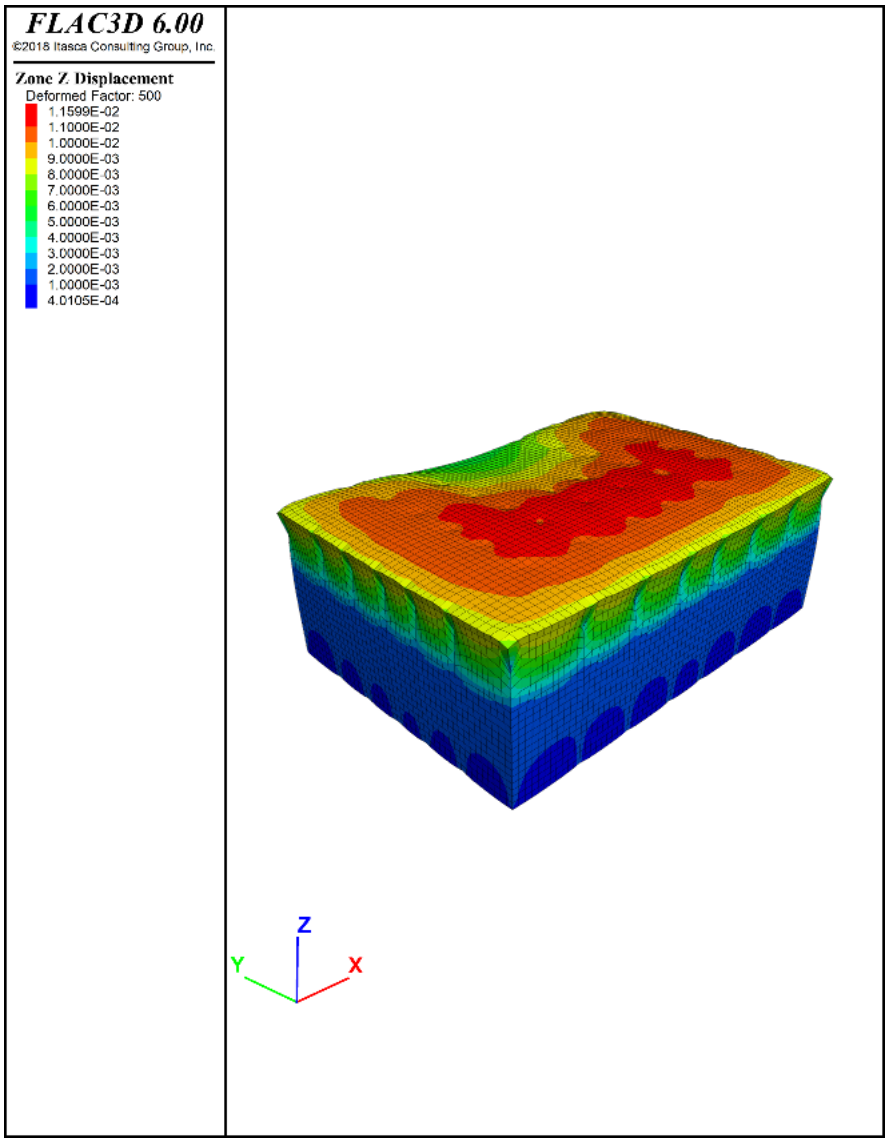

Figure 4.70. Z-displacement contour plot after two years of thermal loading

Furthermore, the cohesion strength of the coupling spring in the pile SEL was changed to different value. This was to study the possibility of mobilization of shaft full friction capacity during the cyclic heating and cooling process. Comparing the Figure 4.74 and Figure 4.77 for pile axial load; Figure 4.75 and Figure 4.76 for the pile and soil z-displacement profile, it can be stated that correction on the CCS didn't induce significant changes to the foundation behavior as far as the pile and soil movement goes.

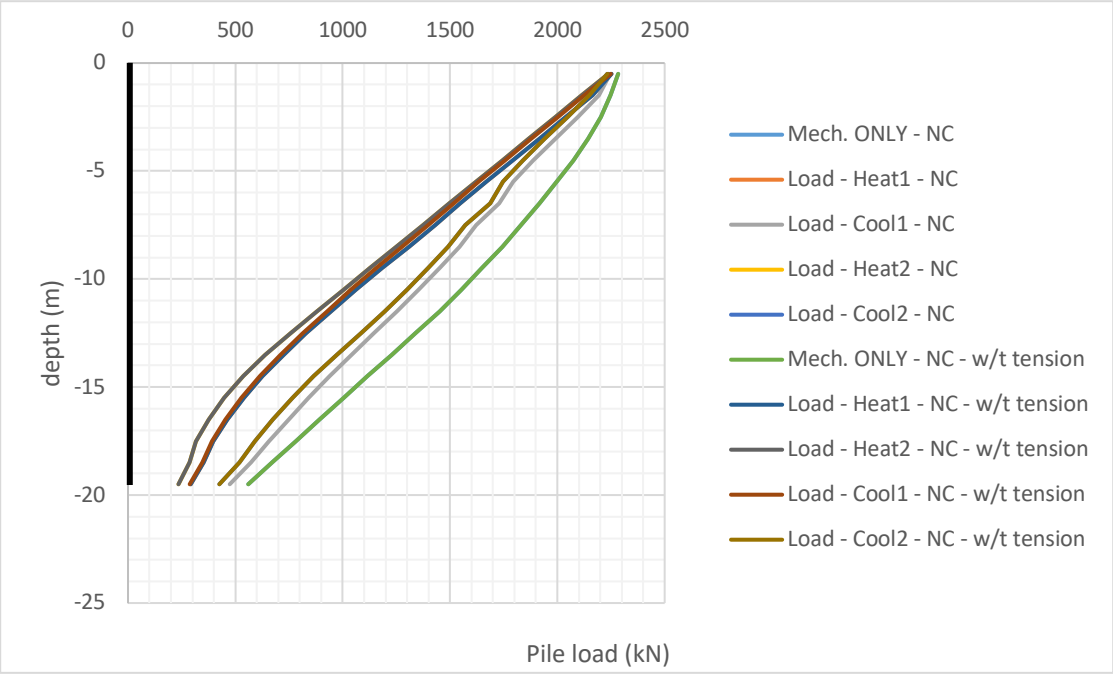

Figure 4.71. LAAH building central pile load distribution for case number 1 and 2

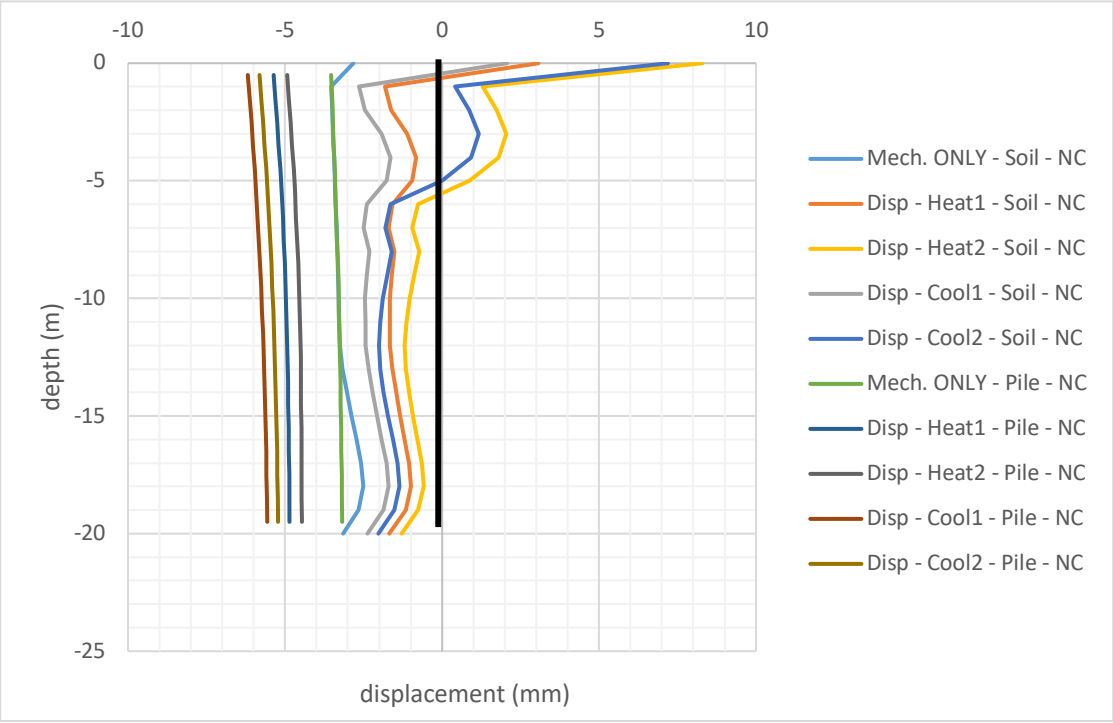

Figure 4.72. LAAH building central pile and soil z-displacement for case number 1

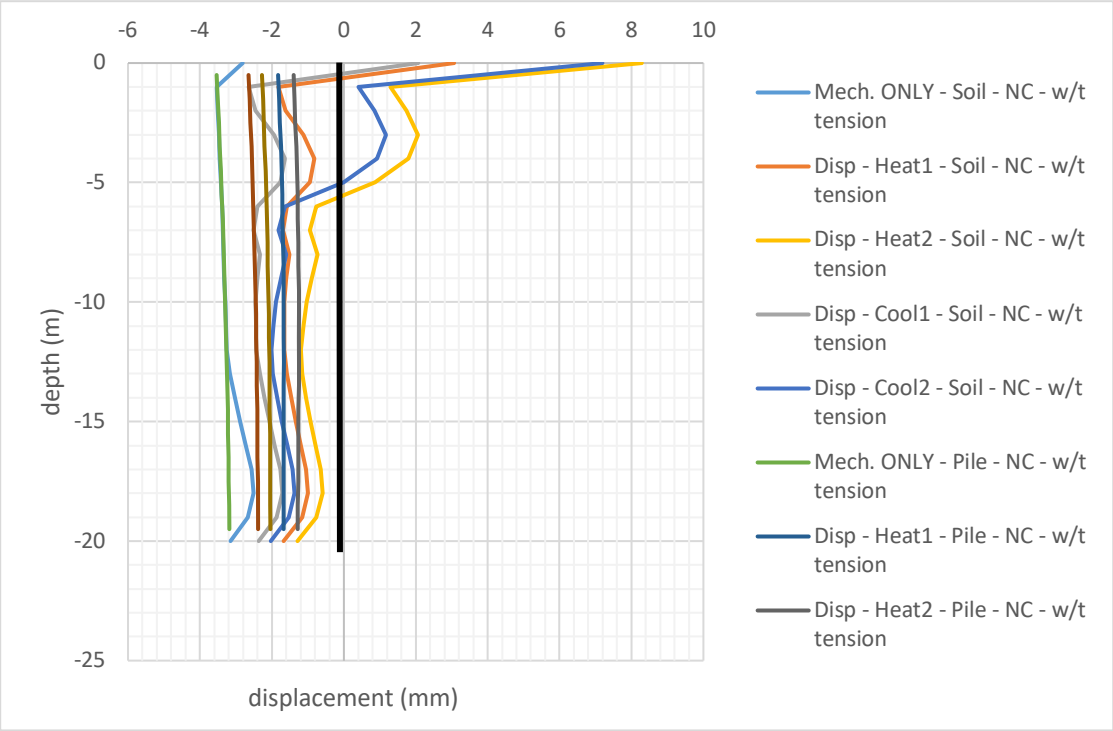

Figure 4.73. LAAH building central pile and soil z-displacement for case number 2

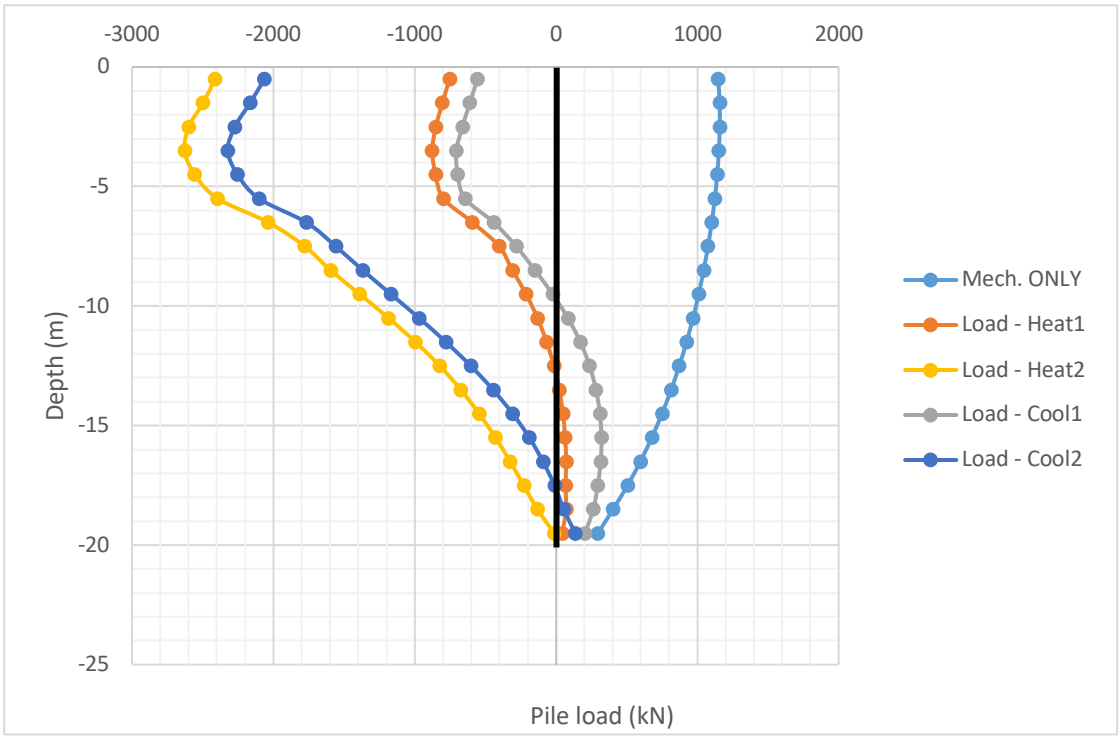

Figure 4.74. LAAH building central pile load distribution for case number 3

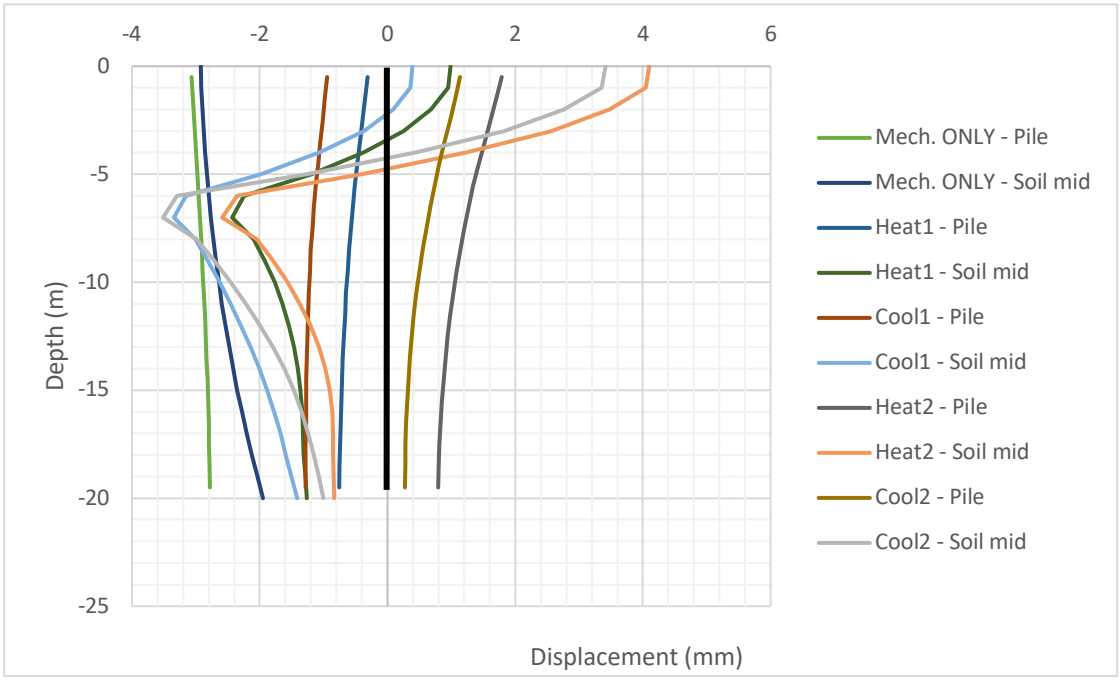

Figure 4.75. LAAH building central pile and midway soil z-displacement for case number 3

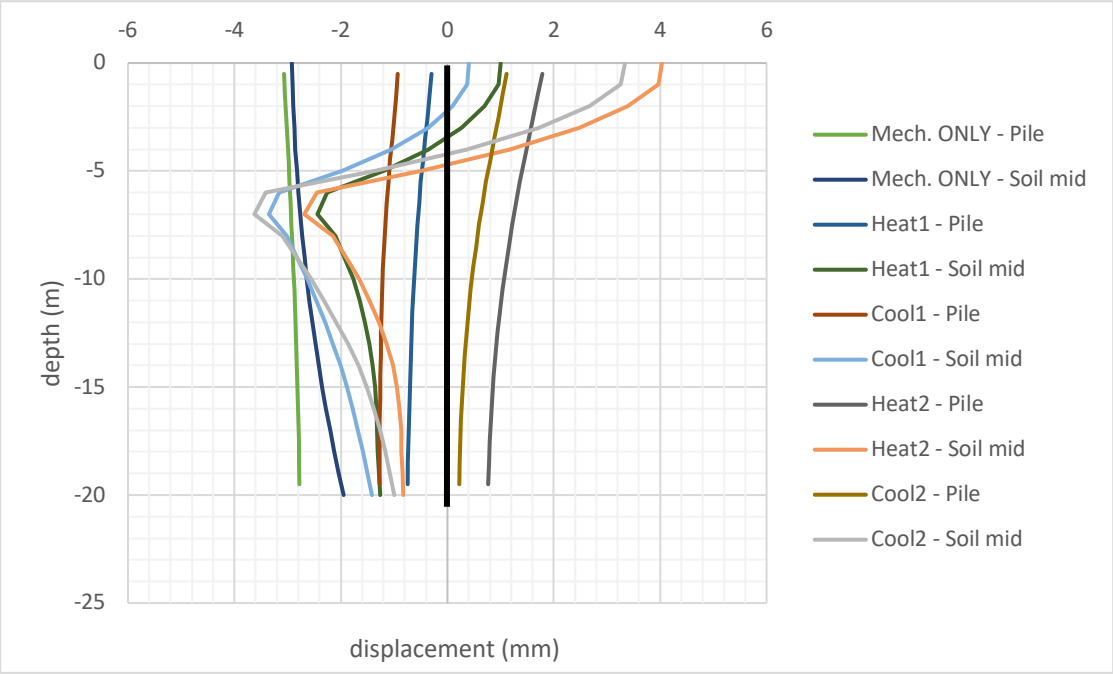

Figure 4.76. LAAH building central pile and midway soil z-displacement for case number 3

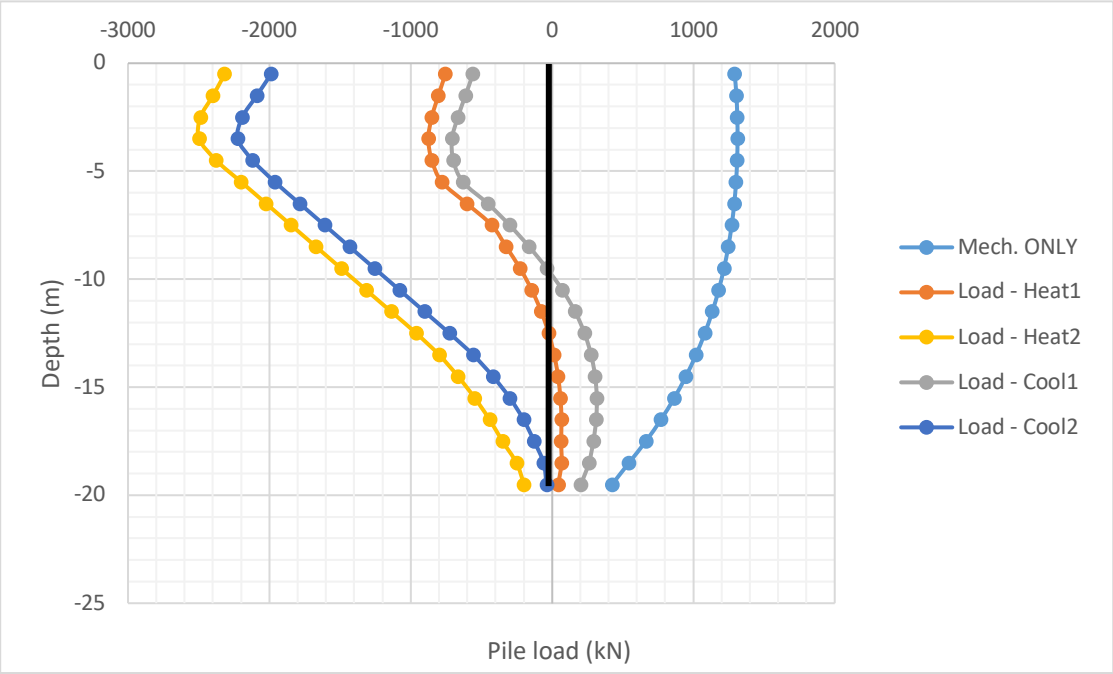

Figure 4.77. LAAH building central pile load distribution for case number 4

5. ECONOMIC ANALYSIS

The reduction in the electricity consumption, the CO_2, and greenhouse gas emission is the common areas that is positively affected by the geothermal foundation usage. The economic benefits toward utilizing geothermal foundation as the main or complementary system for the purpose of HVAC might include tax exemption and incentives, federal and state subsidies, and lower utility bills. There is however an upfront additional cost toward the installation of the geothermal loops in the building's foundation.

There are very few publications available focusing on details of the economic cost, savings, and incentives by using a full-scale geothermal foundation system. In this research study, we were able to acquire one cost breakdown of the full-scale application of geothermal foundation system. This chart only details the upfront installation cost of the system.

A total number of 230 steel piles with $0.4572\text{m}(18")$ in diameter and $45.72\text{m}(150')$of length. From the 230 pile, 105 is equipped with the geothermal loop as energy pile. Total nominal capacity of the geothermal system to provide is $352\text{kW}(100\text{tons})$. The system performs as a complimentary system, in which eliminates 1 cooling tower and 1 boiler. The total upfront cost for the 100-ton energy pile system is estimated as $\$558,219$. The reduction in cost by eliminating some of the traditional system components is estimated to be $\$373,302$. The total cost to install the full-scale geothermal foundation system is $\$184,917$.

Unfortunately, there is no public data available on the operation and the performance details of the system toward saving electricity consumption and reducing utility bill. Based on our findings in this research work, there is not a one size fits all economic analysis available for the full-scale application of geothermal foundation. Partially, this is due to the fact that within U.S. there are numerous deductions and subsidies provided by each state differently. Also, the

operation and maintenance schedule will be different from case to case; in which makes it hard to provide global information for this technology advantages.

Due to the lack of background knowledge on the realistic cost-benefit analysis of a full-scale geothermal foundation system, the following presents some practical recommendations based on the findings so far to maximize the efficiency of the energy pile system:

1. Based on the findings of the pile length effect, the minimum recommended pile length for an efficient geothermal system must be $40\mathrm{m}$. The deeper the pile goes; the more temperature gradient is available in the ground for both heating and cooling cycle. Therefore, during the design phase of such foundations, the length of the pile has to be taken into the account for studying the feasibility and particularly the amount of production expected from the system.
2. In the case of having pile "clear" spacing less than 2m, it is beneficial to use the system partially during certain times of the day; such as during the non-peak hours of electricity consumption. This will allow enough time to recover some of the temperature gradient for the next day. Therefore, during the design phase of such foundations, pile "clear" spacing has to be taken into the account for studying the feasibility and particularly the thermal efficiency expected from the system.
3. According to the recommendation analysis, for cooling dominated climate, the economic justification to use geothermal foundation with spacing less than 3 meters and length of about 20 meters cannot be made. In other words, the use of geothermal loops for cooling dominated climate is not recommended when pile foundation configuration falls within these spacing and length criteria.

4. Partial implementation of the geothermal system is recommended to offset the cost of installation with savings from reduction in electricity consumption. Operation schedule of the system must be closely monitored in the case of partial implementation to avoid soil overheating or disruption in ground's thermal heat gradient potential in long-term.

6. CONCLUSION AND CONTRIBUTION TO NEW KNOWLEDGE

6.1 Conclusions

Based on the previous material including experimental and numerical work on the full-scale application of geothermal foundation system in cooling dominated climate, the following final concluding remarks can be made:

1. The shrink-swell movement in high plastic clays will not be exacerbated by the thermal loading from geothermal foundation application.
2. The creep behavior of the soil will be affected by the cyclic thermal loading, most notably during the soil heating process corresponding to the cooling of the building. On the other hand, the soil cooling process corresponding to the heating of the building can increase the creep movement but not as much as the soil heating process.
3. Creep failure might occur but only for loads approaching the ultimate capacity of the pile.
4. The pile spacing has a direct impact on the long-term variation in soil temperature due to using the geothermal foundation. A clear spacing larger than six meter alleviates this influence. However, this larger spacing means that less piles will be used and thus the thermal load generated by the geothermal system will decrease.
5. The pile length has a considerable impact on the thermal load generated by the geothermal system. The deeper the piles, the more geothermal energy can be exchanged between the building foundation and the surrounding soil.
6. If the pile spacing is less than 3 meters, a geothermal system is likely to overheat the soil mass, thus rendering the geothermal system unlikely to be advantageous.
7. If the pile length is less than 40 meters, a geothermal system is unlikely to generate sufficient thermal load to be advantageous.

8. A geothermal pile foundation under a mat has a considerable effect on the load distribution in the piles. For example, it may be necessary to check the connection between the pile and the slab for large tension loads.
9. To alleviate the vertical expansion of the soil when heated, it may be advisable to create a void equal to twice the amount of the movement allowed for the mechanical loading only.
10. Even if some of the recommendations mentioned above cannot be met, it may still be advantageous to use the geothermal system for part of the time particularly during peak electricity demand when the cost of electricity is high.

6.2 Contribution to New Knowledge

The presented research work has developed and contributed to the new knowledge realm by providing the following points:

1. Developed and verified a fully saturated, fully coupled thermo-hydro-mechanical numerical scheme in FLAC3D for full scale soil-pile-building interaction.
2. Provided answer to the design concerns regarding the thermal pollution issue from the application of geothermal foundation system in cooling dominated climate.
3. Proposed design recommendations and guidelines to optimize the design of a full-scale geothermal foundation system with respect to the pile clear spacing and length variations.
4. Analyzed the possible impacts of cyclic thermal loading on the creep behavior of high plastic clay soil.
5. Provided answer to the issue of accelerating the shrink-swell problem within high plastic clay when subjected to cyclic thermal loading.

6. Developed simplified thermal efficiency design recommendation chart for full scale application of geothermal foundation system vs. pile spacing.
7. Developed average soil temperature increase plot for complex pile spacing and length configuration vs. operation time of the system.

6.3 Future Work

As for the possible future line of work in the full-scale application of geothermal foundation system, the following is highly recommended:

1. Studying the full-scale application of geothermal foundation in high plastic clay soil with the focus on thermal and creep model coupling.
2. Building a prototype actual building fully instrumented to monitor the full-scale impact of geothermal foundation in cooling dominated climate.
3. Work on further improving the fully saturated constitutive models when coupled with thermal module.

REFERENCES

Abdelaziz, S. L. A. M. (2013). Deep energy foundations: geotechnical challenges and design considerations. (Doctor of Philosophy), Virginia Polytechnic Institute and State University, Blacksburg, Virginia.

Abdelaziz, S., Olgun, C., & Martin, J. (2011). Design and operational considerations of geothermal energy piles. Paper presented at the Geo-Frontiers 2011 at Advances in Geotechnical Engineering.

Abuel-Naga, H., et al. (2006). "Experimental evaluation of engineering behavior of soft Bangkok clay under elevated temperature." Journal of Geotechnical and Geoenvironmental Engineering 132(7): 902-910.

Abu-Hamdeh, N. H., & Reeder, R. C. (2000). Soil thermal conductivity effects of density, moisture, salt concentration, and organic matter. Soil science society of America Journal, 64(4), 1285-1290.

Akrouch, G. A., Sánchez, M., & Briaud, J.-L. (2014). Thermo-mechanical behavior of energy piles in high plasticity clays. Acta Geotechnica, 9(3), 399-412.

Akrouch, G. A., Briaud, J.-L., Sanchez, M., & Yilmaz, R. (2015). Thermal Cone Test to Determine Soil Thermal Properties. Journal of Geotechnical and Geoenvironmental Engineering, 142(3), 04015085.

Agar, J., Morgenstern, N., & Scott, J. (1987). Shear strength and stress-strain behaviour of Athabasca oil sand at elevated temperatures and pressures. Canadian Geotechnical Journal, 24(1), 1-10.

Amatya, B., Soga, K., Bourne-Webb, P., Amis, T., & Laloui, L. (2012). Thermo-mechanical behaviour of energy piles. Géotechnique, 62(6), 503-519.

Amis, T., Webb, P., & Amatya, B. (2009). Geothermal business buoyant. Geodrilling International, Aspermont UK, London, UK.

Arson, C., Berns, E., Akrouch, G., Sanchez, M., & Briaud, J. (2013). Heat Propagation around geothermal piles and implications on energy balance. Energy Book Series, 1, 628-635.

Baldi, G., Hueckel, T., & Pellegrini, R. (1988). Thermal volume changes of the mineral-water system in low-porosity clay soils. Canadian geotechnical journal, 25(4), 807-825.

Baldi, G., Hueckel, T., Peano, A., & Pellegrini, R. (1991). Developments in modelling of thermohydro-geomechanical behaviour of Boom clay and clay-based buffer materials (volume 1). Nuclear Science and Technology, EUR 13365/1.

Ballouz, M., Nasr, G., & Briaud, J.-L. (1991). Dynamic and Static Testing of Nine Drilled Shafts at Texas A & M University Geotechnical Research Sites: Geotechnical Engineering, Department of Civil Engineering, and Texas A & M University.

Biot, M. A. (1956). Thermoelasticity and irreversible thermodynamics. Journal of Applied Physics, 27(3), 240-253.

Bourne-Webb, P., Amatya, B., Soga, K., Amis, T., Davidson, C., & Payne, P. (2009). Energy pile test at Lambeth College, London: geotechnical and thermodynamic aspects of pile response to heat cycles. Geotechnique, 59(3), 237-248.

Brandl, H. (2006). Energy foundations and other thermo-active ground structures. Geotechnique, 56(2), 81-122.

Brettmann, T. and T. Amis (2011). Thermal conductivity evaluation of a pile group using geothermal energy piles. Geo-Frontiers 2011: Advances in Geotechnical Engineering**:** 499-508.

Briaud, J.-L. (2000). The national geotechnical experimentation sites at Texas A&M University: clay and sand. Geotechnical Special Publication, 26-51.

Briaud, J.-L. (2000). the national geotechnical experimentation sites at Texas A&M University: clay and sand. A summary. National Geotechnical Experimentation Sites. Geotechnical Special Publication, 93, 26-51.

Briaud, J.-L. (2013). Geotechnical engineering: unsaturated and saturated soils: John Wiley & Sons.

Briaud, J.-L., Ballouz, M., & Nasr, G. (2000). Static capacity prediction by dynamic methods for three bored piles. Journal of Geotechnical and Geoenvironmental engineering, 126(7), 640-649.

Budhu, M. (2008). Soil mechanics and foundations, (With CD): John Wiley & Sons.

Caulk, R., Ghazanfari, E., & McCartney, J. S. (2016). Parameterization of a calibrated geothermal energy pile model. Geomechanics for Energy and the Environment, 5, 1-15.

Cecinato, F., Piglialepre, R., Loveridge, F., & Nicholson, D. (2016). Numerical analysis of thermal cycling during a multi-stage energy pile thermal response test. Paper presented at the Energy Geotechnics, ISBN 978-1-138-03299-6.

Cekerevac, C., Laloui, L., & Vulliet, L. (2003). A new temperature controlled triaxial apparatus. Deformation Characteristics of Geomaterials. Sous la direction de Di Benedetto H. et al, 133-137.

Cekerevac, C., & Laloui, L. (2004). Experimental study of thermal effects on the mechanical behaviour of a clay. International Journal for Numerical and Analytical Methods in Geomechanics, 28(3), 209-228.

Combarnous, M., & Bories, S. (1975). Hydrothermal convection in saturated porous media, & Advances in Hydroscience, v. V. T. Chow, Academic Press, New York.

Cui, Y. J., Sultan, N., & Delage, P. (2000). A thermomechanical model for saturated clays. Canadian Geotechnical Journal, 37(3), 607-620.

Deqi, W., Lin, LU, Aiqiang, PAN. (2017). "Investigating the Impact of Thermo-physical Property Difference between Soil and Pile on the Thermal Performance of Energy Piles." Procedia Engineering 205: 3199-3205.

Di Donna, A., & Laloui, L. (2013). Soil Response under Thermomechanical Conditions Imposed by Energy Geostructures. Energy Geostructures, 3-21.

Di Donna, A., & Laloui, L. (2015). Numerical analysis of the geotechnical behaviour of energy piles. International Journal for Numerical and Analytical Methods in Geomechanics, 39(8), 861-888.

Di Donna, A., Loria, A. F. R., & Laloui, L. (2016). Numerical study of the response of a group of energy piles under different combinations of thermo-mechanical loads. Computers and Geotechnics, 72, 126-142.

Dixon, D., Gray, M., Lingnau, B., Graham, J., & Campbell, S. (1993). Thermal expansion testing to determine the influence of pore water structure on water flow through dense clays. Paper presented at the Proceedings of the 46th Canadian Geotechnical Conference, Saskatoon, Sask.

Duncan, J. M., & Chang, C.-Y. (1970). Nonlinear analysis of stress and strain in soils. Journal of Soil Mechanics & Foundations Division.

Eriksson, L. (1989). Temperature effects on consolidation properties of sulphide clays. Paper presented at the Proceedings of the 12th international conference on soil mechanics and foundation engineering.

Evans, J. C., Chaney, R., & Fang, H. (1981). Influence of Pore Fluid on Clay Behavior. Retrieved from Fritz Engineering Laboratory Report.

Itasca Consulting Group Inc., (2018), FLAC3D 6.0 Documentation. Online version

François, B., & Laloui, L. (2008). ACMEG-TS: A constitutive model for unsaturated soils under non-isothermal conditions. International Journal for Numerical and Analytical Methods in Geomechanics, 32(16), 1955-1988.

Gao, J., Zhang, X., Liu, J., Li, K., & Yang, J. (2008). Numerical and experimental assessment of thermal performance of vertical energy piles: an application. Applied Energy, 85(10), 901-910.

Gazetas, G., & Dobry, R. (1984). Horizontal response of piles in layered soils. Journal of Geotechnical engineering.

Gibert, J. P., & Jaudin, F. (1999). Using geothermal waters in France: The district heating system of Chaudes-Aigues from the middle Ages. Stories from a heated Earth, R. Cataldi, SF Hodgson, JW Lund (eds.), Geothermal Resources Council, Davis, CA/USA, 287-306.

Graham, J., Tanaka, N., Crilly, T., & Alfaro, M. (2001). Modified Cam-Clay modelling of temperature effects in clays. Canadian geotechnical journal, 38(3), 608-621.

Gurpersaud, N., Vanapalli, S. K., & Sivathayalan, S. (2011). Pull-out capacity of soil nails in unsaturated soils. Paper presented at the Communication présentée à Pan-Am CGS Geotechnical conference.

Hamada, Y., Saitoh, H., Nakamura, M., Kubota, H., & Ochifuji, K. (2007). Field performance of an energy pile system for space heating. Energy and Buildings, 39(5), 517-524.

Hassanizadeh, S. M. (1986a). Derivation of basic equations of mass transport in porous media, Part 1. Macroscopic balance laws. Advances in water resources, 9(4), 196-206.

Hassanizadeh, S. M. (1986b). Derivation of basic equations of mass transport in porous media, Part 2. Generalized Darcy's and Fick's laws. Advances in water resources, 9(4), 207-222.

Hokmabadi, A., Fatahi, B., & Samali, B. (2014). Seismic response of mid-rise buildings on shallow and end-bearing pile foundations in soft soil. Soils and Foundations, 54(3), 345-363.

Horne, R., & O'sullivan, M. (1974). Oscillatory convection in a porous medium heated from below. Journal of Fluid Mechanics, 66(02), 339-352.

Hueckel, T., & Baldi, G. (1990). Thermoplasticity of saturated clays: experimental constitutive study. Journal of Geotechnical engineering, 116(12), 1778-1796.

Hueckel, T., & Borsetto, M. (1990). Thermoplasticity of saturated soils and shales: constitutive equations. Journal of Geotechnical engineering, 116(12), 1765-1777.

Hueckel, T. and R. Pellegrini (1992). "Effective stress and water pressure in saturated clays during heating–cooling cycles." Canadian Geotechnical Journal 29(6): 1095-1102.

Imal, M., Yılmaz, K., & Pınarbaşı, A. (2015). Energy Efficiency Evaluation and Economic Feasibility Analysis of a Geothermal Heating and Cooling System with a Vapor-Compression Chiller System. Sustainability, 7(9), 12926-12946.

Johnston, I., Narsilio, G., & Colls, S. (2011). Emerging geothermal energy technologies. KSCE Journal of Civil Engineering, 15(4), 643-653.

Knellwolf, C., Peron, H., & Laloui, L. (2011). Geotechnical analysis of heat exchanger piles. Journal of Geotechnical and Geoenvironmental Engineering.

Kalantidou, A., Tang, A. M., Pereira, J.-M., & Hassen, G. (2012). Preliminary study on the mechanical behaviour of heat exchanger pile in physical model. Géotechnique, 62(11), 1047.

Khalili, N., et al. (2010). "Skeletal thermal expansion coefficient and thermo-hydro-mechanical constitutive relations for saturated homogeneous porous media." Mechanics of materials 42(6): 593-598.

Laloui, L. (2001). Thermo-mechanical behavior of soils. Revue française de génie civil, 5(6), 809-843.

Laloui, L., Nuth, M., & Vulliet, L. (2006). Experimental and numerical investigations of the behaviour of a heat exchanger pile. International Journal for Numerical and Analytical Methods in Geomechanics, 30(8), 763-781.

Lingnau, B., et al. (1996). Effects of temperature on strength and compressibility of sand-bentonite buffer. Engineering Geology 41(1-4): 103-115.

Liu, Y., Vanapalli, S. K., & Amina, W. (2017). Load-deformation Analysis of a Pile in Expansive Soil upon Infiltration. Paper presented at the Proceedings of the 2nd World Congress on Civil, Structural, and Environmental Engineering (CSEE).

Mayne, P. W. "Cone penetration testing state-of-practice. Final Report NCHRP Project 20-05; Task 37-14, Georgia Institute of Technology, Atlanta, GA, February 2007." Transportation Research Board Synthesis Study.

McCartney, J. S., & Murphy, K. D. (2012). Strain Distributions in Full-Scale Energy Foundations (DFI Young Professor Paper Competition 2012). DFI Journal-The Journal of the Deep Foundations Institute, 6(2), 26-38.

McCartney, J. S., LaHaise, D., LaHaise, T., & Rosenberg, J. (2010). Application of geoexchange experience to geothermal foundations. Art of Foundation Engineering Practice (GSP 198), 411-422.

Mimouni, T., & Laloui, L. (2014). Towards a secure basis for the design of geothermal piles. Acta Geotechnica, 9(3), 355-366.

Mita, K., Dasari, G., & Lo, K. (2004). Performance of a three-dimensional Hvorslev-modified Cam Clay model for over consolidated clay. International Journal of Geomechanics, 4(4), 296-309.

Modaressi, H., & Laloui, L. (1997). A thermo-viscoplastic constitutive model for clays. International Journal for Numerical and Analytical Methods in Geomechanics, 21(5), 313-335.

Morrone, B., Coppola, G., & Raucci, V. (2014). Energy and economic savings using geothermal heat pumps in different climates. Energy Conversion and Management, 88, 189-198.

Murphy, K. D., et al. (2015). "Evaluation of thermo-mechanical and thermal behavior of full-scale energy foundations." Acta Geotechnica 10(2): 179-195.

Musson, A., Harrison, B., Gordon, K., Wright, S., & Sandiford, M. (2009). Thermal thinking: Optimal targeting for Australian geothermal explorers. Paper presented at the Proc. Australian Geothermal Energy Conference.

Naik, D. (1986). Effect of Temperature and Pore Fluid on Shear Characteristic of Clay. International Symposium on Environmental Geotechnology, Pennsylvania.

Nguyen, V. T., Tang, A. M., & Pereira, J.-M. (2017). Long-term thermo-mechanical behavior of energy pile in dry sand. Acta Geotechnica, 1-9.

Noble, C. A., & Demirel, T. (1969). Effect of temperature on strength behavior of cohesive soil. Highway Research Board Special Report (103).

Olgun, G., Martin, J., Abdelaziz, S., Iovino, P., Catalbas, F., Elks, C., Gouvin, P. (2012). Field-testing of energy piles at Virginia Tech. Paper presented at the Proc. 37th Annual Conference on Deep Foundations, Houston, TX, USA.

Olivella, S., Carrera, J., Gens, A., & Alonso, E. (1994). Nonisothermal multiphase flow of brine and gas through saline media. Transport in porous media, 15(3), 271-293.

Paaswell, R. E. (1969). Transient temperature influences on soil behavior. Highway Research Board Special Report (103).

Pahud, D., & Hubbuch, M. (2007). Measured thermal performances of the energy pile system of the dock midfield at Zürich Airport.

Palciauskas, V. and P. Domenico (1982). "Characterization of drained and undrained response of thermally loaded repository rocks." Water Resources Research 18(2): 281-290.

Park, J. (2013). Comparative analysis of the VRF system and conventional HVAC systems, focused on life-cycle cost, Georgia Institute of Technology, Department of Architecture.

Philip, J., & De Vries, D. (1957). Moisture movement in porous materials under temperature gradients. Eos, Transactions American Geophysical Union, 38(2), 222-232.

Plum, R. L., & Esrig, M. I. (1969). Some temperature effects on soil compressibility and pore water pressure. Highway Research Board Special Report (103).

Rees, S., Adjali, M., Zhou, Z., Davies, M., & Thomas, H. (2000). Ground heat transfer effects on the thermal performance of earth-contact structures. Renewable and Sustainable Energy Reviews, 4(3), 213-265.

Romero, E., Villar, M., & Lloret, A. (2005). Thermo-hydro-mechanical behavior of two heavily over consolidated clays. Engineering Geology, 81(3), 255-268.

Rouissi, K., Krarti, M., & McCartney, J. S. (2012). Analysis of thermo-active foundations with U-tube heat exchangers. Journal of Solar Energy Engineering, 134(2), 021008.

Ryozo, O., Kentaro, S., Mutsumi, Y., Yoshiro, S., & SuchHO, H. (2006). Development of a ground source heat pump system with Ground heat exchanger utilizing the cast-in-place concrete pile foundations of a building. The 2005 World Sustainable Building Conference, Tokyo, Japan (1059-1066).

Saggu, R., & Chakraborty, T. (2014). Cyclic thermo-mechanical analysis of energy piles in sand. Geotechnical and Geological Engineering, 33(2), 321-342.

Saggu, R., & Chakraborty, T. (2016). Thermomechanical Response of Geothermal Energy Pile Groups in Sand. International Journal of Geomechanics, 04015100.

Salciarini, D., Ronchi, F., Cattoni, E., & Tamagnini, C. (2013). Thermomechanical effects induced by energy piles operation in a small piled raft. International Journal of Geomechanics, 15(2), 04014042.

Schanz, T., Vermeer, P., & Bonnier, P. (1999). The hardening soil model: formulation and verification. Beyond 2000 in Computational Geotechnics, 281-296.

Sorey, M. L. (1975). Numerical modeling of liquid geothermal systems: Geological Survey, Menlo Park, Calif. (USA).

Sultan, N., Delage, P., & Cui, Y. (2002). Temperature effects on the volume change behaviour of Boom clay. Engineering Geology, 64(2), 135-145.

Suryatriyastuti, M., Mroueh, H., & Burlon, S. (2012). Understanding the temperature-induced mechanical behavior of energy pile foundations. Renewable and Sustainable Energy Reviews, 16(5), 3344-3354.

Suryatriyastuti, M., Burlon, S., & Mroueh, H. (2016). On the understanding of cyclic interaction mechanisms in an energy pile group. International Journal for Numerical and Analytical Methods in Geomechanics, 40(1), 3-24.

Sutman, M., Olgun, C. G., & Brettmann, T. (2015). Full-scale field testing of energy piles IFCEE 2015 (pp. 1638-1647).

Sutman, M., Olgun, G., Laloui, L., & Brettmann, T. (2017). Effect of End-Restraint Conditions on Energy Pile Behavior. In Geotechnical Frontiers 2017 (pp. 165-174).

Tsutsumi, A., & Tanaka, H. (2012). Combined effects of strain rate and temperature on consolidation behavior of clayey soils. Soils and Foundations, 52(2), 207-215.

Wang, C.-l., Liu, H.-l., Kong, G.-q., & Wang Wai Ng, C. (2017). Different types of energy piles with heating–cooling cycles. Proceedings of the Institution of Civil Engineers-Geotechnical Engineering, 170(3), 220-231.

Wood, C. J., Liu, H., & Riffat, S. B. (2010). An investigation of the heat pump performance and ground temperature of a piled foundation heat exchanger system for a residential building. The 3rd International Conference on Sustainable Energy and Environmental Protection, SEEP, Elsevier, 35(12), 4932-4940.

Wooding, R. (1957). Steady state free thermal convection of liquid in a saturated permeable medium. Journal of Fluid Mechanics, 2(03), 273-285.

Wu, D., Liu, H.-L., Kong, G.-Q., Ng, C. W. W., & Cheng, X.-H. (2018). Displacement response of an energy pile in saturated clay. Proceedings of the Institution of Civil Engineers-Geotechnical Engineering, 1-44.

Wu, W., Li, X., Charlier, R., & Collin, F. (2004). A thermo-hydro-mechanical constitutive model and its numerical modelling for unsaturated soils. Computers and Geotechnics, 31(2), 155-167.

Yavari, N., Tang, A., Pereira, J., & Hassen, G. (2016). Mechanical behaviour of a small-scale energy pile in saturated clay. Géotechnique, 66(11), 878-887.

Zhang, Q.-q., & Zhang, Z.-m. (2012). A simplified nonlinear approach for single pile settlement analysis. Canadian Geotechnical Journal, 49(11), 1256-1266.